Black Hole Perturbation Theory

International Center for Theoretical Sciences
Summer School on Gravitational-Wave Astronomy

Bangalore (July 25 – August 05, 2016)

Emanuele Berti

(August 26, 2016)

Contents

1 Introduction

These notes are a significantly expanded version of informal lecture notes originally prepared for a lecture on black-hole physics delivered at the DPG Physics School "General Relativity @ 99", organized by Gerhard Schäfer and Clifford M. Will and held on Sep 14–19 2014 at the Physikzentrum in Bad Honnef, Germany. The goal of the notes is to introduce some key ideas in black hole physics that highlight an intimate connection between the dynamics of particles and waves in black-hole spacetimes. More specifically, I will show that the geodesic motion of *particles* is related to the characteristic properties of *wave* scattering in black hole backgrounds. I will introduce the proper oscillation modes of a black hole ("quasinormal modes") and illustrate how they are related with the stability of circular orbits for massless particles in the geometrical optics limit. Finally, I will explain the basic ideas behind superradiance, and I will give a concise introduction to "hot topics" in current research. The prerequisite background is a knowledge of physics at the advanced undergraduate level, namely nonrelativistic quantum mechanics and general relativity at the level of Hartle [112], Schutz [185] or Carroll [63]. In particular, I will assume some familiarity with the Einstein field equations, the Schwarzschild metric and the Kerr metric.

I will focus on the core physics, rather than the mathematics. So – whenever given the choice – I will consider the simplest prototype problem (one that can quickly be solved with pen and paper), providing references to generalizations that involve heavier calculations but no substantial new physics.

In Chapter 2, after a short review of the derivation of the geodesic equations from a variational principle, I will focus on geodesics in spherically symmetric spacetimes (more in particular, the Schwarzschild spacetime). I will discuss orbital stability in terms of Lyapunov exponents, then I will apply the formalism to compute the principal Lyapunov exponent for circular null geodesics in Schwarzschild.

In Chapter 3 I will introduce a simple prototype for black-hole perturbations induced by a "test" field, i.e. a massive scalar field. I will separate variables for the corresponding wave equation (the Klein-Gordon equation), and then I will discuss two techniques to solve the associated eigenvalue problem: Leaver's continued fraction method and the WKB approximation. Last but not least, I will show how the application of the same techniques to rotating (Kerr) black holes leads to the interesting possibility of superradiant amplification.

In Chapter 4 I introduce the basics of perturbation theory for spherically symmetric spacetimes. I show how to decompose the perturbations in terms of scalar, vector and tensor spherical harmonics. Then I derive the "master equations" describing spin-one and spin-two perturbations (including the source terms) and show how to integrate them in special cases (e.g. for particles falling into a Schwarzschild black hole).

In Chapter 5 I introduce some exciting ideas in black hole physics that have been a focus of recent research, in particular: (1) critical phenomena in black-hole binary encounters, and (2) the idea that astrophysical measurements of black-hole spins can constrain the mass of light bosonic fields (via superradiant instabilities).

Chapter 6 is (for the moment) a cut & paste of research papers collecting the basic ideas about ringdown detection, parameter estimation, and expected astrophysical rates with future Earth- and space-based interferometers.

For further reading on black holes I recommend Shapiro and Teukolsky's *Black holes, white dwarfs, and neutron stars* [188], Frolov and Novikov's *Black hole physics: Basic concepts and new developments* [95], Chandrasekhar's *The Mathematical Theory of Black Holes* [65] and a recent overview article by Teukolsky [197]. For reviews of black-hole perturbation theory, see [44, 131, 160]. Throughout these notes, unless otherwise specified, I will use geometrical units ($G = c = 1$) and I will follow the sign conventions of Misner, Thorne and Wheeler [153].

1.1 Newtonian Black Holes?

Popular articles on black holes often mention that a Newtonian analog of the black-hole concept (a "dark star") was first proposed by Michell in 1783. Michell's idea was simple: the escape velocity of an object at the surface R of a star (or planet) with mass M is

$$v_{\rm esc}^2 = \frac{2GM}{R}\,. \tag{1.1.1}$$

If we consider light as a corpuscle traveling at speed c, light can not escape to infinity whenever $v_{\rm esc} > c$. Therefore the condition for the existence of "dark stars" in Newtonian mechanics is

$$\frac{2GM}{c^2 R} \geq 1\,. \tag{1.1.2}$$

Remarkably, a similar situation holds in Einstein's theory. The field equations tell us that there exist vacuum, spherically symmetric solutions of the field equations describing a source of mass M such that the (areal) radius of the horizon – the region from which even light can not escape – corresponds to the equal sign in (1.1.2). They also tell us that the redshift of light emitted from the horizon is infinite: the object is perceived as completely black. A major difference is that in Newtonian gravity particles can cross the surface $r = 2GM/c^2$, while in General Relativity this surface marks a causal boundary in spacetime.

What popular books usually do not address is the following question: can Michell's solutions exist in nature? In general relativity, the most compact stars are made out of incompressible matter and they correspond to the Buchdahl limit $R/M = 9/4$ (see e.g. [185]), but they are not black holes! In Newtonian mechanics,

a naive argument tells us that as we pile up more and more material of constant density ρ_0, the ratio M/R increases:

$$\frac{M}{R} = \frac{4}{3}\pi R^2 \rho_0 \,. \tag{1.1.3}$$

This equation would seem to suggest that Michell's dark stars *could* indeed form. Unfortunately, we forgot to include the binding energy U:

$$U = \int -\frac{GM\,dM}{r} = -\int \frac{G}{r}\left(\frac{4}{3}\pi\, r^3 \rho_0\right) 4\pi r^2 \rho_0 dr = -\frac{16G\pi^2}{15}\rho_0^2 R^5 \,. \tag{1.1.4}$$

Once we do, the total mass M_T of the hypothetical dark star is given by the rest mass M plus the binding energy:

$$\frac{M_T}{R} = \frac{4}{3}\pi R^2 \rho_0 - \frac{16G\pi^2}{15c^2}\rho_0^2 R^4 = \frac{M}{R}\left[1 - \frac{3}{5}\frac{G}{c^2}\frac{M}{R}\right] \leq \frac{5c^2}{12G}\,, \tag{1.1.5}$$

where the upper limit is obtained by maximizing the function in the range (1.1.2). Thus, the "dark star criterion" (1.1.2) is never satisfied, even for the unrealistic case of constant-density matter. In fact, the endpoint of Newtonian gravitational collapse depends very sensitively on the equation of state, even in spherical symmetry [103, 148].

Despite the physical impossibility to construct Newtonian black holes with "ordinary" matter, the genesis of the idea is historically interesting. The email from Steve Detweiler to James Fry reported in Box 1.1 (reproduced here with permission from Steve Detweiler - thanks!) has some amusing remarks on Reverend Michell's contributions to science.

Box 1.1 Steve Detweiler's email to James Fry on Reverend Michell's "black holes" (and other amusing things)

Date: Tue, 25 Aug 98 08:11:25 -0400
From: Steve Detweiler
To: James Fry
Subject: Re: Newtonian black holes

Jim,

The Reverend John Michell in a letter to his good friend Henry Cavendish that was published in Transactions of the Royal Society in 1784. Here is an excerpt of a summary I made in a letter to a friend–I think it's amusing!

The reference is "On the Means of discovering the Distance, Magnitude, etc. of the Fixed Stars, in consequence of the Diminution of the Velocity of their Light, in case such a Diminution should be found to take place in any of them, and such other Data should be procured from Observations, as would be farther necessary for that Purpose", by the Rev. John Michell, B.D.F.R.S., in a letter to Henry Cavendish, Esq. F.R.S. and A.S., Philosophical Transactions of the Royal Society of London, Vol. LXXIV, 35-57 (1784). We sure don't title papers the way they used to.

I was at Yale when I found out about this article, so I called up their rare books library and was informed that 1784 really wasn't so long ago and that the volume I wanted was on the stacks in the main library. I just checked it out, they had to glue in a new due date sticker in back, and I had it on my desk for six months.

Michell's idea is to determine the distance to the stars by measuring the speed of light from the stars–the further away the star is, the slower the light would be moving. He

conceded that there would need to be improvement in prism quality for this to be possible, but he thought it was within reach. It's an interesting paper, the arguments are all geometrical, where there should be an equation he writes it out long hand, all the s's look like f's, and it's fun to read. Somewhere in the middle of the paper (paragraph 16), he notes that if a star were of the same density as the sun but with a radius 500 times larger, then the light would be pulled back to star and not escape. He even surmises that we might be able to detect such an object if it were in a binary system and we observed the motion of the companion. So we should have celebrated the Black Hole Bicentennial back in 1984!

And Michell was an interesting fellow. He wrote 4 papers that I know about, and I think these are in chronological order. In one paper (1760), he notes a correspondence between volcanos and fault lines in the earth's crust and first suggested that earthquakes might be caused by masses of rocks shifting beneath the earth's surface. In another, Michell (1767) estimates that if the stars were just scattered randomly on the celestial sphere then the probability that the Pleiades would be grouped together in the sky is 1 part in 500,000. So he concluded that the Pleiades must be a stellar system in its own right—this is the first known application of statistics to astronomy. In a third paper, he devised a torsion balance and used it to measure the $1/r^2$ dependence of the force between magnetic poles. His fourth paper has the black hole reference. After that work, he started a project to modify his magnetic-force torsion balance to measure the force of gravity between two masses in the laboratory. Unfortunately, he died in the middle of the project. But his good friend, Henry Cavendish, stepped in, made important improvements and completed the experiment! In his own paper, Cavendish gives a footnote reference to Michell.

1.2 Some Basic Definitions

Just for reference (and to facilitate the reading of the MATHEMATICA notebooks), here we list some basic definitions that should be familiar from previous courses in general relativity. Given a metric $g_{\mu\nu}$, we denote its inverse by $g^{\mu\nu}$ and its determinant by g. The Christoffel symbols are defined by

$$\Gamma^{\mu}_{\alpha\beta} = \frac{1}{2} g^{\mu\nu} \left(\partial_\alpha g_{\nu\beta} + \partial_\beta g_{\nu\alpha} - \partial_\nu g_{\alpha\beta} \right) . \tag{1.2.6}$$

Then we define the Riemann tensor, Ricci tensor, Ricci scalar, Einstein tensor, Kretschmann scalar and Gauss-Bonnet invariant in the usual way:

$$R^{\alpha}{}_{\beta\gamma\delta} = \partial_\gamma \Gamma^{\alpha}_{\beta\delta} - \partial_\delta \Gamma^{\alpha}_{\beta\gamma} + \Gamma^{\alpha}_{\mu\gamma} \Gamma^{\mu}_{\beta\delta} - \Gamma^{\alpha}_{\mu\delta} \Gamma^{\mu}_{\beta\gamma} , \tag{1.2.7}$$

$$R_{\alpha\beta} = R^{\mu}{}_{\alpha\mu\beta} , \tag{1.2.8}$$

$$R = g^{\alpha\beta} R_{\alpha\beta} , \tag{1.2.9}$$

$$G_{\alpha\beta} = R_{\alpha\beta} - \frac{1}{2} g_{\alpha\beta} R . \tag{1.2.10}$$

$$K = R_{\alpha\beta\gamma\delta} R^{\alpha\beta\gamma\delta} , \tag{1.2.11}$$

$$R_{\rm GB} = K - 4 R^{\alpha\beta} R_{\alpha\beta} + R^2 , \tag{1.2.12}$$

Covariant derivatives of vectors and tensors are computed as follows:

$$\nabla_\beta A^\mu = \partial_\beta A^\mu + \Gamma^{\mu}_{\alpha\beta} A^\alpha , \tag{1.2.13}$$

$$\nabla_\beta A_\mu = \partial_\beta A_\mu - \Gamma^{\alpha}_{\mu\beta} A_\alpha , \tag{1.2.14}$$

$$\nabla_\beta A^{\mu\nu} = \partial_\beta A^{\mu\nu} + \Gamma^{\mu}_{\alpha\beta} A^{\alpha\nu} + \Gamma^{\nu}_{\alpha\beta} A^{\mu\alpha} , \tag{1.2.15}$$

$$\nabla_\beta A_{\mu\nu} = \partial_\beta A_{\mu\nu} - \Gamma^{\alpha}_{\mu\beta} A_{\alpha\nu} - \Gamma^{\alpha}_{\nu\beta} A_{\mu\alpha} . \tag{1.2.16}$$

Other relations that are useful in simplifying the calculation of the Laplacian of a scalar field Φ in curved spacetime are:

$$\Gamma^{\mu}_{\mu\beta} = \frac{1}{\sqrt{-g}}\partial_\beta\sqrt{-g}\,, \tag{1.2.17}$$

$$\nabla_\alpha A^\alpha = \frac{1}{\sqrt{-g}}\partial_\alpha\left(\sqrt{-g}A^\alpha\right)\,, \tag{1.2.18}$$

$$\Box\Phi = \nabla_\alpha\nabla^\alpha\Phi = \frac{1}{\sqrt{-g}}\partial_\alpha\left(\sqrt{-g}\partial^\alpha\Phi\right)\,. \tag{1.2.19}$$

1.3 The Schwarzschild and Kerr Metrics

I refer to the textbooks by Hartle [112], Schutz [185] or Carroll [63] for introductions to the Schwarzschild and Kerr spacetimes that provide the necessary background for these lecture notes. Here I collect the relevant metrics and a few useful results, mainly to establish notation. The Schwarzschild metric reads

$$ds^2 = -\left(1-\frac{2M}{r}\right)dt^2 + \left(1-\frac{2M}{r}\right)^{-1}dr^2 + r^2(d\theta^2+\sin^2\theta d\phi^2)\,, \tag{1.3.20}$$

where M is the black-hole mass. The Kerr metric for a black hole with mass M and angular momentum J reads:

$$\begin{aligned} ds^2 &= -\left(1-\frac{2Mr}{\Sigma}\right)dt^2 - \frac{4aMr\sin^2\theta}{\Sigma}dtd\phi \\ &+ \frac{\Sigma}{\Delta}dr^2 + \Sigma d\theta^2 + \left(r^2+a^2+\frac{2Mra^2\sin^2\theta}{\Sigma}\right)\sin^2\theta d\phi^2\,. \end{aligned} \tag{1.3.21}$$

where

$$a \equiv \frac{J}{M}\,, \quad \Delta \equiv r^2 - 2Mr + a^2\,, \quad \Sigma \equiv r^2 + a^2\cos^2\theta\,. \tag{1.3.22}$$

The event horizon is located at the larger root of $\Delta = 0$, namely

$$r_+ = M + \sqrt{M^2 - a^2}\,. \tag{1.3.23}$$

Stationary observers at fixed values of r and θ rotate with constant angular velocity

$$\Omega = \frac{d\phi}{dt} = \frac{u^\phi}{u^t}\,. \tag{1.3.24}$$

For timelike observers, the condition $u_\mu u^\mu = -1$ yields

$$-1 = u_t^2\left[g_{tt} + 2\Omega g_{t\phi} + \Omega^2 g_{\phi\phi}\right]\,, \tag{1.3.25}$$

where I have used (1.3.24) to eliminate u^ϕ. The quantity in square brackets must be negative; but since $g_{\phi\phi}$ is positive, this is true only if $\Omega_- < \Omega < \Omega_+$, where $\Omega_\pm$ denotes the two roots of the quadratic, i.e.

$$\Omega_\pm = \frac{-g_{t\phi} \pm \sqrt{g_{t\phi}^2 - g_{tt}g_{\phi\phi}}}{g_{\phi\phi}}\,. \tag{1.3.26}$$

Note that $\Omega_- = 0$ when $g_{tt} = 0$, i.e. $r^2 - 2Mr + a^2\cos^2\theta = 0$, which occurs at

$$r_0 = M + (M^2 - a^2\cos^2\theta)^{1/2}\,. \tag{1.3.27}$$

Observers between r_0 and r_+ must have $\Omega > 0$, i.e. *no static observers exist within* $r_+ < r < r_0$. This is the reason why the surface $r = r_0$ is called the "static limit". The surface r_0 is also called the "boundary of the ergosphere", because this is the region within which energy can be extracted from the black hole via the Penrose process (a close relative of the superradiant amplification that I will discuss in Chapter 3).

1.3.1 *"Rational Polynomial" Coordinates*

A very useful form of the metric for use in algebraic manipulation software like MATHEMATICA or MAPLE makes use of "rational polynomial" coordinates (see e.g. Sec. 6 of [200]). The key trick is to use the variable $\chi \equiv \cos\theta$, so that $\chi \in [-1, 1]$. Then

$$\sin\theta = \sqrt{1-\chi^2}\,, \quad d\chi = -\sin\theta d\theta\,, \quad d\theta = -\frac{d\chi}{\sqrt{1-\chi^2}}\,. \tag{1.3.28}$$

In terms of the (t, r, χ, ϕ) coordinates, the Boyer–Lindquist version of the Kerr spacetime becomes

$$\begin{aligned} ds^2 &= -\left\{1-\frac{2Mr}{r^2+a^2\chi^2}\right\} dt^2 - \frac{4aMr(1-\chi^2)}{r^2+a^2\chi^2}\, d\phi\, dt \\ &\quad + \frac{r^2+a^2\chi^2}{r^2-2Mr+a^2}\, dr^2 + (r^2+a^2\chi^2)\,\frac{d\chi^2}{1-\chi^2} \\ &\quad + (1-\chi^2)\left\{r^2+a^2+\frac{2Ma^2r(1-\chi^2)}{r^2+a^2\chi^2}\right\} d\phi^2. \end{aligned} \tag{1.3.29}$$

Now all metric components are simple rational polynomials of the coordinates, and the elimination of trigonometric functions makes computer-based symbolic manipulations much faster. For instance, the nontrivial Kretschmann scalar

$$K = R_{\alpha\beta\gamma\delta}R^{\alpha\beta\gamma\delta} = \frac{48M^2(r^2-a^2\chi^2)[(r^2+a^2\chi^2)^2-16r^2a^2\chi^2]}{(r^2+a^2\chi^2)^6} \tag{1.3.30}$$

can be computed more rapidly.

We will use a similar trick to speed up and simplify perturbative calculations in the Schwarzschild background. In this context, let us note some identities involving angular functions that will be useful later. The associated Legendre functions $P_{\ell m}(\theta)$ satisfy

$$\frac{1}{\sin\theta}\partial_\theta\left(\sin\theta\partial_\theta P_{\ell m}\right) - \frac{m^2}{\sin^2\theta}P_{\ell m} = -\ell(\ell+1)P_{\ell m}\,. \tag{1.3.31}$$

Using

$$\partial_\theta P_{\ell m} = -(1-\chi^2)^{1/2}\partial_\chi P_{\ell m}\,, \tag{1.3.32}$$

$$\partial_\theta^2 P_{\ell m} = (1-\chi^2)\partial_\chi^2 P_{\ell m} - \chi\partial_\chi P_{\ell m}\,, \tag{1.3.33}$$

we can easily show that, in terms of χ, this differential equation reads

$$(1-\chi^2)P''_{\ell m}(\chi) - 2\chi P'_{\ell m}(\chi) + \left[\ell(\ell+1) - \frac{m^2}{1-\chi^2}\right] P_{\ell m}(\chi) = 0\,, \tag{1.3.34}$$

where primes denote derivatives with respect to χ.

1.4 Conventions

Chandrasekhar uses a "mostly minus" signature and a time dependence $e^{i\omega t}$ for the perturbations [cf. e.g. his Eq. (16), Chapter 4]. We will use a "mostly plus" signature [EB: With the exception of Chapter 4: sorry, I will fix this later] and the following convention on the Fourier transform:

$$f(r,\,t) = \frac{1}{\sqrt{2\pi}}\int e^{-i\omega t} f(r,\,\omega)d\omega\,, \tag{1.4.35}$$

$$f(r,\,\omega) = \frac{1}{\sqrt{2\pi}}\int e^{i\omega t} f(r,\,t)dt\,, \tag{1.4.36}$$

1.5 Mathematica Notebooks and other code

In this section we list supporting Mathematica notebooks or Fortran codes, and the sections they refer to:

- Section 3.1: ScalarVectorPerturbations.nb
- Section 3.2.2: ReggeWheelerBoundaryConditions.nb
- Section 3.3.2: Scattering_Scalars_Book.nb
- Section 3.4.1 continued_fraction_scalar_perturbation_schwarzschild.nb
- Section 3.4.2 quasinormal_modes_wkb.nb
- Section 3.6.1: separation_massive_scalar_kerr.nb
- Section 4.1: GerlachSengupta.nb
- Section 4.2: ScalarVectorPerturbations.nb
- Section 4.4.1: regge_wheeler_schwarschild.nb
- Section 4.4.3: regge_wheeler_schwarschild_with_source_v2.nb
- Section 4.5: zerilli_schwarschild_with_source.nb
- Section 4.5.4: plunge4.tgz **(note: this is a Fortran77 program)**

1.6 Acknowledgments

I am grateful to Vitor Cardoso, Leonardo Gualtieri and Hector Okada da Silva for their help and support in the preparation of these lecture notes and of the accompanying Mathematica notebooks.

This work was supported by NSF CAREER Grant No. PHY-1055103, by FCT contract IF/00797/2014/CP1214/CT0012 under the IF2014 Programme, and by the H2020-MSCA-RISE-2015 Grant No. StronGrHEP-690904.

2 Particles

2.1 Geodesic Equations from a Variational Principle

In Einstein's theory, particles do not fall under the action of a force. Their motion corresponds to the trajectory in space-time that extremizes[1] the proper interval between two events. Mathematically, this means that the equations of motion (or "geodesic equations") can be found by a variational principle, i.e. by extremizing the action

$$\int d\lambda\, 2\mathcal{L} \equiv \int d\lambda \left(g_{\mu\nu} \frac{dx^\mu}{d\lambda} \frac{dx^\nu}{d\lambda} \right) , \tag{2.1.1}$$

where the factor of 2 in the definition of the Lagrangian density $\mathcal{L}$ was inserted for later convenience. Therefore our task is to write down the usual Euler-Lagrange equations

$$\frac{d}{d\lambda} \frac{\partial \mathcal{L}}{\partial \dot{x}^\alpha} = \frac{\partial \mathcal{L}}{\partial x^\alpha} \tag{2.1.2}$$

for the Lagrangian

$$\mathcal{L} = \frac{1}{2} g_{\mu\nu} \frac{dx^\mu}{d\lambda} \frac{dx^\nu}{d\lambda} = \frac{1}{2} g_{\mu\nu} \dot{x}^\mu \dot{x}^\nu \, . \tag{2.1.3}$$

Here I introduced the notation

$$\dot{x}^\mu \equiv \frac{dx^\mu}{d\lambda} = p^\mu \tag{2.1.4}$$

[1] The "principle of least action" is a misnomer, because the action is not always minimized along a geodesic: it can either have a minimum or a saddle point (see [167] for an introduction and [166] for a detailed discussion in general relativity, as well as references to the corresponding problem in classical mechanics).

for the particle's four-momentum, a choice that allows us to consider both massless and massive particles at the same time (cf. [167, 188] for more details). The "affine parameter" λ can be identified with proper time (more precisely, with τ/m_0) along the timelike geodesic of a particle of rest mass m_0. The canonical momenta associated with this Lagrangian are

$$p_\mu = \frac{\partial \mathcal{L}}{\partial \dot{x}^\mu}\,, \tag{2.1.5}$$

and they satisfy

$$p_\mu = g_{\mu\nu}\dot{x}^\nu = g_{\mu\nu}p^\nu\,. \tag{2.1.6}$$

More explicitly, introducing the usual notation $\partial_\mu = \frac{\partial}{\partial x^\mu}$, one has

$$\frac{\partial \mathcal{L}}{\partial \dot{x}^\alpha} = g_{\mu\alpha}\dot{x}^\mu\,, \tag{2.1.7}$$

$$\frac{d}{d\lambda}\frac{\partial \mathcal{L}}{\partial \dot{x}^\alpha} = g_{\mu\alpha}\ddot{x}^\mu + \dot{x}^\mu \frac{dg_{\mu\alpha}}{d\lambda} = g_{\mu\alpha}\ddot{x}^\mu + \dot{x}^\mu\dot{x}^\nu\partial_\nu g_{\mu\alpha}\,, \tag{2.1.8}$$

$$\frac{\partial \mathcal{L}}{\partial x^\alpha} = \frac{1}{2}\partial_\alpha g_{\mu\nu}\dot{x}^\mu\dot{x}^\nu\,, \tag{2.1.9}$$

and therefore

$$g_{\mu\alpha}\ddot{x}^\mu + \dot{x}^\mu\dot{x}^\nu\partial_\nu g_{\mu\alpha} - \frac{1}{2}\dot{x}^\mu\dot{x}^\nu\partial_\alpha g_{\mu\nu} = 0\,. \tag{2.1.10}$$

Now, μ and ν are dummy indices. By symmetrizing one gets $2\dot{x}^\mu\dot{x}^\nu\partial_\nu g_{\mu\alpha} = \dot{x}^\mu\dot{x}^\nu(\partial_\nu g_{\mu\alpha} + \partial_\mu g_{\nu\alpha})$, and finally

$$2g_{\mu\alpha}\ddot{x}^\mu + \dot{x}^\mu\dot{x}^\nu\left(\partial_\nu g_{\mu\alpha} + \partial_\mu g_{\nu\alpha} - \partial_\alpha g_{\mu\nu}\right) = 0\,. \tag{2.1.11}$$

From the definition of the Christoffel symbols

$$\Gamma^\mu_{\ \beta\gamma} = \frac{1}{2}g^{\mu\rho}\left(\partial_\gamma g_{\beta\rho} + \partial_\beta g_{\gamma\rho} - \partial_\rho g_{\beta\gamma}\right) \tag{2.1.12}$$

it follows that

$$\ddot{x}^\mu + \Gamma^\mu_{\ \beta\gamma}\dot{x}^\beta\dot{x}^\gamma = 0\,, \tag{2.1.13}$$

i.e. the usual geodesic equation.

2.2 Geodesics in Static, Spherically Symmetric Spacetimes

In most of these notes I will consider a general static, spherically symmetric metric (not necessarily the Schwarzschild metric) of the form

$$ds^2 = -f(r)dt^2 + \frac{1}{h(r)}dr^2 + r^2(d\theta^2 + \sin^2\theta d\phi^2)\,. \tag{2.2.14}$$

This metric can describe (for example) a spherical star, and it reduces to the Schwarzschild metric (see e.g. [63, 112, 185]) when $f(r) = h(r) = 1 - 2M/r$. For brevity, in the following I will omit the r-dependence of $f(r)$ and $h(r)$. For this metric, the Lagrangian for geodesic motion reduces to

$$2\mathcal{L} = g_{\mu\nu}\dot{x}^\mu\dot{x}^\nu = -f\dot{t}^2 + h^{-1}\dot{r}^2 + r^2\left(\dot{\theta}^2 + \sin^2\theta\dot{\phi}^2\right)\,. \tag{2.2.15}$$

The momenta associated with this Lagrangian are

$$p_t \;=\; \frac{\partial \mathcal{L}}{\partial \dot{t}} = -f\dot{t}\,, \tag{2.2.16}$$

$$p_r = \frac{\partial \mathcal{L}}{\partial \dot{r}} = h^{-1}\dot{r}\,, \tag{2.2.17}$$

$$p_\theta = \frac{\partial \mathcal{L}}{\partial \dot{\theta}} = r^2\dot{\theta}\,, \tag{2.2.18}$$

$$p_\phi = \frac{\partial \mathcal{L}}{\partial \dot{\phi}} = r^2\sin^2\theta\dot{\phi}\,. \tag{2.2.19}$$

The Hamiltonian is related to the Lagrangian by a Legendre transform:

$$\mathcal{H} = p_\mu \dot{x}^\mu - \mathcal{L} = g_{\mu\nu}\dot{x}^\mu\dot{x}^\nu - \mathcal{L} = \mathcal{L} \tag{2.2.20}$$

and it is equal to the Lagrangian, as could be anticipated because the Lagrangian (2.1.3) is "purely kinetic" (there is no potential energy contribution). Therefore $\mathcal{H} = \mathcal{L}$ and they are both constant.

As a consequence of the static, spherically symmetric nature of the metric, the Lagrangian (2.2.15) does not depend on t and ϕ. Therefore the t- and ϕ-components yield two conserved quantities E and L:

$$\frac{dp_t}{d\lambda} = \frac{d}{d\lambda}\left(\frac{\partial \mathcal{L}}{\partial \dot{t}}\right) = \frac{\partial \mathcal{L}}{\partial t} = 0 \Longrightarrow -p_t = f\dot{t} = E\,, \tag{2.2.21}$$

$$\frac{dp_\phi}{d\lambda} = \frac{d}{d\lambda}\left(\frac{\partial \mathcal{L}}{\partial \dot{\phi}}\right) = \frac{\partial \mathcal{L}}{\partial \phi} = 0 \Longrightarrow p_\phi = r^2\sin^2\theta\dot{\phi} = L\,. \tag{2.2.22}$$

The radial equation reads

$$\frac{dp_r}{d\lambda} = \frac{d}{d\lambda}\left(\frac{\partial \mathcal{L}}{\partial \dot{r}}\right) = \frac{\partial \mathcal{L}}{\partial r}\,. \tag{2.2.23}$$

The remaining equation tells us that

$$\frac{dp_\theta}{d\lambda} = \frac{d}{d\lambda}(r^2\dot{\theta}) = \frac{\partial \mathcal{L}}{\partial \theta} = r^2\sin\theta\cos\theta\dot{\phi}^2\,, \tag{2.2.24}$$

so if we choose $\theta = \pi/2$ when $\dot{\theta} = 0$ it follows that $\ddot{\theta} = 0$, and the orbit will be confined to the equatorial plane $\theta = \pi/2$ at all times. In conclusion:

$$f\dot{t} = E\,, \tag{2.2.25}$$

$$r^2\dot{\phi} = L\,, \tag{2.2.26}$$

where E is the particle's energy and L is the orbital angular momentum (in the case of massive particles, these quantities should actually be interpreted as the particle energy and orbital angular momentum *per unit rest mass*: $E = E_{\rm particle}/m_0$ and $L = L_{\rm particle}/m_0$, see [188] for a clear discussion). The constancy of the Lagrangian now implies

$$\frac{E^2}{f} - \frac{\dot{r}^2}{h} - \frac{L^2}{r^2} = -2\mathcal{L} = \delta_1\,, \tag{2.2.27}$$

where the constant $\delta_1 = 0$ for null orbits, and its value can be set to be $\delta_1 = 1$ for timelike orbits by a redefinition of the affine parameter (i.e., a rescaling of "proper time units") along the geodesic. Therefore the conservation of the Lagrangian is equivalent to the normalization condition for the particle's four-velocity: $p_\mu p^\mu = -\delta_1$, where $\delta_1 = 0$ for massless particles and $\delta_1 = 1$ for massive particles, respectively. This is the familiar "effective potential" equation used to study the qualitative features of geodesic motion:

$$\dot{r}^2 = V_r\,, \tag{2.2.28}$$

$$V_r \equiv h\left(\frac{E^2}{f} - \frac{L^2}{r^2} - \delta_1\right)\,, \tag{2.2.29}$$

where $\delta_1 = 0$ (1) for null (timelike) geodesics.

2.3 Schwarzschild Black Holes

In the special case of Schwarzschild black holes, $f(r) = h(r) = 1 - 2M/r$, and the radial equation reduces to

$$\dot{r}^2 = V_r^{\rm Schw} \equiv E^2 - f\left(\frac{L^2}{r^2} + \delta_1\right) . \tag{2.3.30}$$

Carroll [63] rewrites this equation in a form meant to facilitate comparison with the Newtonian limit:

$$\frac{1}{2}\dot{r}^2 = \mathcal{E} - \mathcal{V}_{\delta_1}(r) , \tag{2.3.31}$$

where $\mathcal{E} \equiv E^2/2$ and

$$\mathcal{V}_{\delta_1}(r) = \delta_1\left(\frac{1}{2} - \frac{M}{r}\right) + \frac{L^2}{2r^2} - \frac{ML^2}{r^3} . \tag{2.3.32}$$

A more conventional choice (cf. Shapiro and Teukolsky [188] or Misner-Thorne-Wheeler [153]) is to write

$$\dot{r}^2 = E^2 - 2\mathcal{V}_{\delta_1}(r) \tag{2.3.33}$$

and to define

$$V_{\rm part}(r) = 2\mathcal{V}_{\delta_1=1}(r) = \left(1 - \frac{2M}{r}\right)\left(1 + \frac{L^2}{r^2}\right) , \tag{2.3.34}$$

$$V_{\rm phot}(r) = \frac{2\mathcal{V}_{\delta_1=0}(r)}{L^2} = \frac{1}{r^2}\left(1 - \frac{2M}{r}\right) . \tag{2.3.35}$$

The motion of photons depends only on the impact parameter $b = L/E$ (as it should, by virtue of the equivalence principle; the same result can be obtained by a simple rescaling of the affine parameter $\lambda \to L\lambda$ [188]):

$$\left(\frac{dr}{d\lambda}\right)^2 = \frac{1}{b^2} - V_{\rm phot}(r) . \tag{2.3.36}$$

The potentials (2.3.34) and (2.3.35) are plotted in Figs. 2.1 and 2.2, respectively. The qualitative features of particle motion in these potentials are treated in most books on general relativity (see e.g. [63, 112, 153, 185, 188]), so there is no need to repeat the discussion here, except for some important remarks in the next Section that will be useful below.

Note that, according to the definitions above, the derivatives of the radial particle potential V_r and the derivatives of the potentials ($\mathcal{V}_{\delta_1}$, $V_{\rm part}$, $V_{\rm phot}$) have opposite signs. Therefore unstable orbits (in particular the "light ring", i.e. the unstable photon orbit at $r = 3M$, for which $V''_{\rm phot} < 0$) have $V_r'' > 0$.

2.3.1 Circular Geodesics in the Schwarzschild Metric

By definition, circular geodesics have constant areal radius coordinate r: $\dot{r} = 0$ and $\ddot{r} = 0$, with the second condition ensuring that circular orbits remain circular. From Eq. (2.2.28) it follows that $V_r = V_r' = 0$. The condition $(V_r^{\rm Schw})' = 0$ is equivalent to

$$L^2(r - 3M) = \delta_1 M r^2 . \tag{2.3.37}$$

From this equality one can already draw two conclusions:

(i) Circular geodesics exist only for $r \geq 3M$.

(ii) Null circular geodesics ($\delta_1 = 0$) exist only at $r = 3M$.

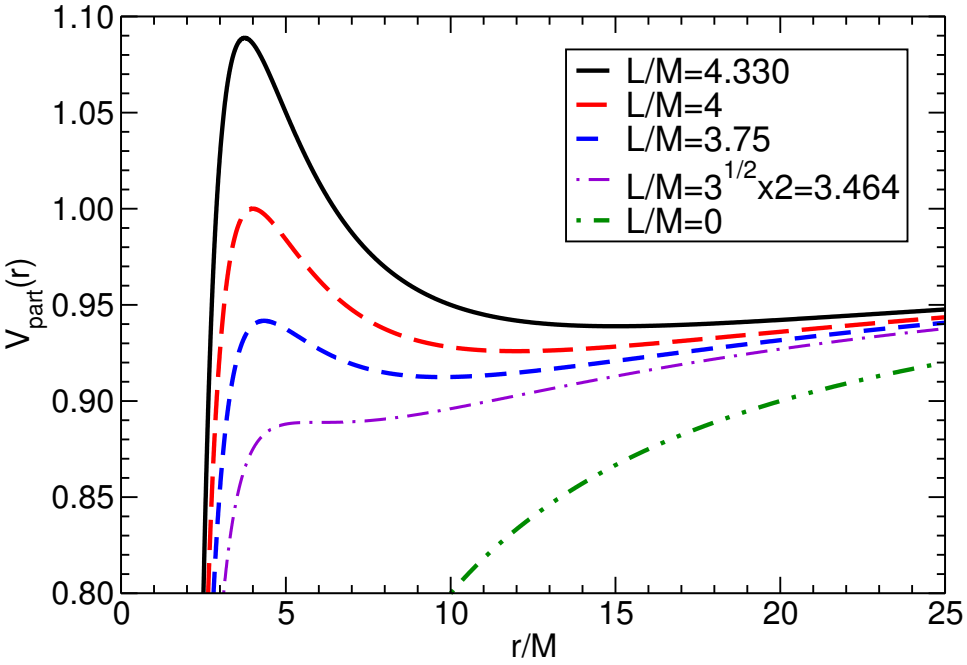

Figure 2.1: Effective potential (2.3.34) for massive particles.

The angular frequency of the circular orbit (as measured at infinity) is

$$\Omega_c \equiv \frac{d\phi}{dt} = \frac{\dot{\phi}}{\dot{t}} = \frac{fL}{r^2 E}\,. \tag{2.3.38}$$

Eq. (2.3.37) implies $L^2 = \delta_1 M r^2/(r-3M)$, and the condition $V_r = 0$ translates to $E^2 = \delta_1 r f^2/(r-3M)$. Therefore we get the relativistic analog of Kepler's law:

$$\Omega_c^2 = \frac{f^2 L^2}{r^4 E^2} = \frac{M}{r^3}\,. \tag{2.3.39}$$

To understand the stability of these geodesics under small perturbations we must look at $(V_r^{\rm Schw})''$. After substituting L^2 from Eq. (2.3.37), we get

$$(V_r^{\rm Schw})'' = -\frac{2\delta_1 M(r-6M)}{r^3(r-3M)}\,. \tag{2.3.40}$$

Thus,

(iii) Circular geodesics with $r \geq 6M$ are stable (this is why $r = 6M$ is referred to as the "innermost stable circular orbit", or ISCO).

(iv) Circular geodesics with $3M \leq r < 6M$ are all unstable.

2.3.2 The Critical Impact Parameter

The effective potential for geodesic motion was given in Eq. (2.3.30). Let us consider two extreme cases: $E = 1$ and the ultrarelativistic limit $E \to \infty$ (where the second case corresponds to massless, ultrarelativistic particles, and therefore it is equivalent to considering $\delta_1 = 0$).

For $E = 1$, i.e., particles dropped from rest at infinity, we have

$$\dot{r}^2 \;=\; 1 - f\left(\frac{L^2}{r^2}+1\right) = \frac{2M^3}{r^3}\left(\frac{r^2}{M^2}+\frac{L^2}{M^2}-\frac{1}{2}\frac{L^2}{M^2}\frac{r}{M}\right) \tag{2.3.41}$$

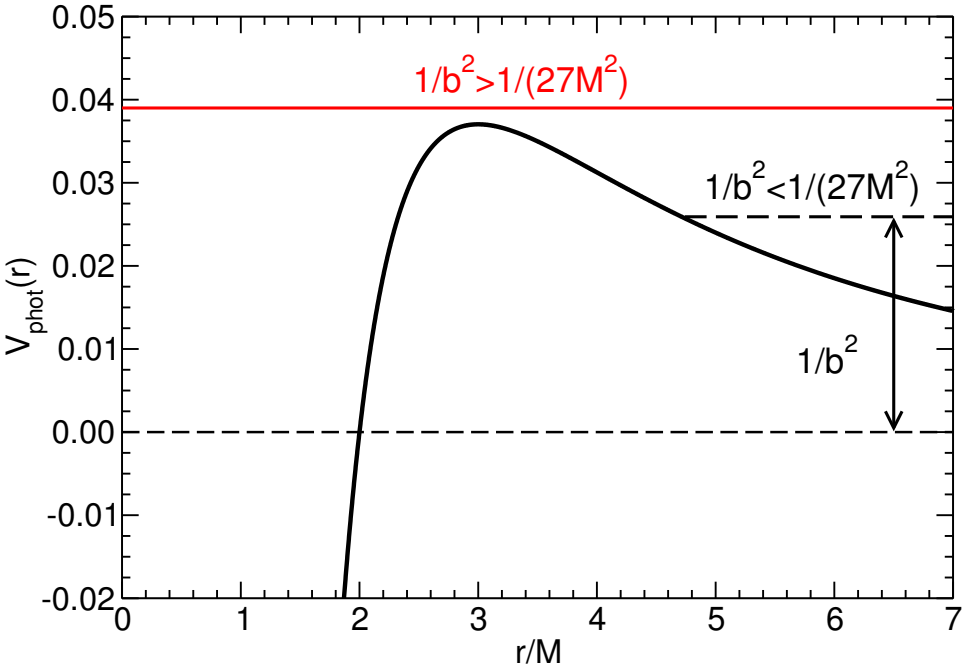

Figure 2.2: Effective potential (2.3.35) for photons. The critical impact parameter (2.3.45), corresponding to the light ring, separates plunging orbits from scattering orbits.

$$= \frac{2M^3}{r^3}\left(\frac{r}{M}-\frac{L}{M}\frac{L/M+\sqrt{(L/M)^2-16}}{4}\right)\left(\frac{r}{M}-\frac{L}{M}\frac{L/M-\sqrt{(L/M)^2-16}}{4}\right) .$$

From this factorization, it is clear that there is a turning point (i.e., a real value of r for which $\dot{r}=0$) if and only if $(L/M)^2-16>0$. Furthermore, all turning points lie outside the horizon (that is located at $r=r_+=2M$). It follows that the critical angular momentum for capture is

$$L_{\rm crit}=4M\,. \tag{2.3.42}$$

When we consider the capture of massless particles ($\delta_1=0$), defining an impact parameter $b=L/E$, we get

$$\dot{r}^2=E^2-f\left(\frac{L^2}{r^2}\right)=\frac{E^2}{r^3}\left(r^3-rfb^2\right)\,. \tag{2.3.43}$$

To find the turning points we must now solve a cubic equation. Following Chandrasekhar [65], we look for the critical b such that the cubic polynomial $r^3-rfb^2=r^3-rb^2+2Mb^2$ has no real positive roots. Now, it is well known that the roots $(r_1,\,r_2,\,r_3)$ of the polynomial ar^3+br^2+cr+d satisfy $r_1+r_2+r_3=-b/a$ and $r_1r_2r_3=-d/a$. We know for sure that there is always one negative root, because the polynomial tends to $-\infty$ as $r\to-\infty$ and it is positive (equal to $2Mb^2$) at $r=0$. Therefore we have two possibilities: (1) one real, negative root and two complex-conjugate roots, or (2) one real, negative root and two distinct, real roots. The critical case is when the two real roots of case (2) degenerate into a single real root. Clearly, at this point one must have

$$(r^3-rfb^2)'=3r^2-b^2=0\quad\text{or}\quad r=b/\sqrt{3}\,. \tag{2.3.44}$$

Substituting back into the polynomial, this will only be a root if

$$b_{\rm crit}\;=\;3\sqrt{3}M\,, \tag{2.3.45}$$

$$r_{\rm crit} \;=\; 3M\,. \tag{2.3.46}$$

The main conclusions of this discussion can be summarized as follows:

(1) Circular null geodesics (the trajectories of massless scalars, photons or gravitons circling the black hole) are located at $r = 3M$, and they are unstable;

(2) The critical impact parameter for capture of light rays (or gravitons, or massless scalars) corresponds precisely to these circular null geodesics.

As we will see in Chapter 3, circular null geodesics are linked (in the geometric-optics limit) to the oscillation modes of black holes. To make this understanding quantitative, we need a measure of the instability rate of circular null geodesics. This measure relies on the classical theory of orbital stability based on Lyapunov exponents, that I review below.

2.4 Order and Chaos in Geodesic Motion

In the theory of dynamical systems, Lyapunov exponents are a measure of the average rate at which nearby trajectories converge or diverge in phase space. A positive Lyapunov exponent indicates a divergence between nearby trajectories, i.e., a high sensitivity to initial conditions. To investigate geodesic stability in terms of Lyapunov exponents, we begin with the equations of motion schematically written as

$$\frac{dX_i}{dt} = H_i(X_j)\,. \tag{2.4.47}$$

We linearize these equations about a certain orbit $X_i(t)$ and we get

$$\frac{d\,\delta X_i(t)}{dt} = K_{ij}(t)\,\delta X_j(t)\,, \tag{2.4.48}$$

where

$$K_{ij}(t) = \left.\frac{\partial H_i}{\partial X_j}\right|_{X_i(t)} \tag{2.4.49}$$

is the linear stability matrix [72]. The solution to the linearized equations can be written as

$$\delta X_i(t) = L_{ij}(t)\,\delta X_j(0) \tag{2.4.50}$$

in terms of the evolution matrix $L_{ij}(t)$, which must obey

$$\dot{L}_{ij}(t) = K_{im}(t) L_{mj}(t) \tag{2.4.51}$$

as well as $L_{ij}(0) = \delta_{ij}$, so that Eq. (2.4.50) is satisfied at $t = 0$. The eigenvalues λ_i of L_{ij} are called "Lyapunov exponents". More precisely, the principal Lyapunov exponent is the largest of these eigenvalues, such that

$$\lambda_0 = \lim_{t\to\infty} \frac{1}{t} \log\left(\frac{L_{jj}(t)}{L_{jj}(0)}\right)\,. \tag{2.4.52}$$

2.4.1 *Lyapunov Exponents for Circular Orbits in Static, Spherically Symmetric Spacetimes*

Let us now restrict attention to a class of problems for which one has a two-dimensional phase space of the form $X_i(t) = (p_r, r)$. Let us focus on circular orbits in static, spherically symmetric metrics[2] and linearize the equations of motion with $X_i(t) = (p_r, r)$ about orbits of constant areal radius r. As pointed out by Cornish and Levin [72], Lyapunov exponents are in general coordinate-dependent. To measure the orbital instability rate through the principal Lyapunov exponent λ_0, a sensible choice is to use Schwarzschild time t, i.e. the time measured by an observer at infinity. The relevant equations of motion are Eqs. (2.2.17) and (2.2.23). Linearizing them about circular orbits of radius r_c yields

$$\dot{\delta r} = [h' p_r]_{r=r_c, p_r=0}\, \delta r + h \delta p_r = h \delta p_r = \frac{1}{g_{rr}} \delta p_r \,, \tag{2.4.53}$$

$$\dot{\delta p_r} = \frac{d}{dr}\left(\frac{\partial \mathcal{L}}{\partial r}\right) \delta r \,, \tag{2.4.54}$$

where dots denote derivatives with respect to λ, and it is understood that the quantities in the linearized equations must be evaluated at $r = r_c$ and $p_r = 0$. Converting from the affine parameter λ to Schwarzschild time (which implies dividing everything through by a factor $\dot{t}$) we get the linear stability matrix

$$K_{ij} = \begin{pmatrix} 0 & K_1 \\ K_2 & 0 \end{pmatrix} \,, \tag{2.4.55}$$

where

$$K_1 = \dot{t}^{-1} \frac{d}{dr}\left(\frac{\partial \mathcal{L}}{\partial r}\right) \,, \tag{2.4.56}$$

$$K_2 = \left(\dot{t}\, g_{rr}\right)^{-1} \,. \tag{2.4.57}$$

Therefore, for circular orbits, the principal Lyapunov exponents can be expressed as

$$\lambda_0 = \pm \sqrt{K_1 K_2} \,. \tag{2.4.58}$$

The fact that eigenvalues come in pairs is a reflection of energy conservation: the volume in phase space is also conserved [72]. From now on I will drop the $\pm$ sign, and simply refer to λ_0 as the "Lyapunov exponent".

From the equations of motion it follows that

$$\frac{\partial \mathcal{L}}{\partial r} = \frac{d}{d\lambda}\frac{\partial \mathcal{L}}{\partial \dot{r}} = \frac{d}{d\lambda}\left(g_{rr}\dot{r}\right) = \dot{r}\frac{d}{dr}(g_{rr}\dot{r}) \,, \tag{2.4.59}$$

where in the second equality I used Eq. (2.2.15). The definition of V_r, Eq. (2.2.28), implies

$$V_r' = \frac{d}{dr}\left(\dot{r}^2\right) = 2\dot{r}\frac{d}{dr}\dot{r} \tag{2.4.60}$$

and

$$\dot{r}\frac{d}{dr}(g_{rr}\dot{r}) = g_{rr}\dot{r}\frac{d}{dr}\dot{r} + \dot{r}^2 g_{rr}' = g_{rr}\frac{1}{2}V_r' + V_r g_{rr}' = \frac{1}{2g_{rr}}\left[g_{rr}^2 V_r\right]' \,, \tag{2.4.61}$$

[2] Our treatment is actually general enough to study circular orbits in stationary spherically symmetric spacetimes, and also equatorial circular orbits in stationary spacetimes (including the higher-dimensional generalization of rotating black holes, known as the Myers-Perry metric): cf. [62] for generalizations to these cases.

so that finally

$$\frac{\partial \mathcal{L}}{\partial r} = \frac{1}{2g_{rr}} \frac{d}{dr} \left(g_{rr}^2 \, V_r \right) \, . \tag{2.4.62}$$

For circular geodesics $V_r = V_r' = 0$ [27], so Eq. (2.4.58) reduces to

$$\lambda_0 = \sqrt{\frac{1}{\dot{t}^2 g_{rr}} \frac{d}{dr} \left(\frac{\partial \mathcal{L}}{\partial r} \right)} = \sqrt{\frac{1}{\dot{t}^2 g_{rr}} \frac{d}{dr} \left[\frac{1}{2g_{rr}} \frac{d}{dr} \left(g_{rr}^2 \, V_r \right) \right]} = \sqrt{\frac{1}{\dot{t}^2 g_{rr}} \left(\frac{g_{rr}}{2} V_r'' \right)} \tag{2.4.63}$$

and finally

$$\lambda_0 = \sqrt{\frac{V_r''}{2\dot{t}^2}} \, . \tag{2.4.64}$$

Recall from our discussion of geodesics that unstable orbits have $V_r'' > 0$, and correspond to real values of the Lyapunov exponent λ_0. Following Pretorius and Khurana [170], we can define a critical exponent

$$\gamma \equiv \frac{\Omega_c}{2\pi\lambda_0} = \frac{T_{\lambda_0}}{T_\Omega} \, , \tag{2.4.65}$$

where Ω_c was given in Eq. (2.3.38); in addition we have introduced a typical orbital timescale $T_\Omega \equiv 2\pi/\Omega_c$ and an instability timescale $T_{\lambda_0} \equiv 1/\lambda_0$ (note that in Ref. [72] the authors use a different definition of the orbital timescale, $T_\Omega \equiv 2\pi/\dot{\phi}$). Then the critical exponent can be written as

$$\gamma = \frac{1}{2\pi} \sqrt{\frac{2\dot{\phi}^2}{V_r''}} \, . \tag{2.4.66}$$

For circular null geodesics in many spacetimes of interest $V_r'' > 0$ [cf. Eq. (2.3.40)], which implies instability.

A quantitative characterization of the instability requires a calculation of the associated timescale λ_0. Let us turn to this calculation for timelike and circular orbits.

Timelike Geodesics

From Eq. (2.2.29), the requirement $V_r = V_r' = 0$ for circular orbits yields

$$E^2 = \frac{2f^2}{2f - r\,f'} \, , \quad L^2 = \frac{r^3 \, f'}{2f - rf'} \, , \tag{2.4.67}$$

where here and below all quantities are evaluated at the radius of a circular timelike orbit. Since the energy must be real, we require

$$2f - rf' \, > \, 0 \, . \tag{2.4.68}$$

The second derivative of the potential is

$$V_r'' = 2\frac{h}{f} \frac{-3ff'/r + 2(f')^2 - ff''}{2f - rf'} \, , \tag{2.4.69}$$

and the orbital angular velocity is given by

$$\Omega = \frac{\dot{\phi}}{\dot{t}} = \sqrt{\frac{f'}{2r}} \, . \tag{2.4.70}$$

Using Eqs. (2.4.64), (2.2.25) and (2.4.69) to evaluate the Lyapunov exponent at the circular timelike geodesics, we get

$$\lambda_0 \quad = \quad \frac{1}{\sqrt{2}} \sqrt{-\frac{h}{f} \left[\frac{3ff'}{r} - 2(f')^2 + ff'' \right]}$$

$$= \frac{1}{2}\sqrt{(2f - rf')\, V_r''(r)}\,. \tag{2.4.71}$$

Bearing in mind that $2f - rf' > 0$ and that unstable orbits are defined by $V_r'' > 0$, we can see that λ_0 will be real whenever the orbit is unstable, as expected.

Null Geodesics

Circular null geodesics satisfy the conditions:

$$V_r = 0 \quad \Longrightarrow \quad \frac{E}{L} = \pm\sqrt{\frac{f_c}{r_c^2}}\,, \tag{2.4.72}$$

$$V_r' = h\left(-\frac{E^2}{f^2}f' + \frac{2L^2}{r^3}\right) = h\frac{L^2}{r^3}\left(-\frac{f'r}{f} + 2\right) = 0\,, \tag{2.4.73}$$

and therefore

$$2f_c = r_c f_c'\,. \tag{2.4.74}$$

Here and below a subscript c means that the quantity in question is evaluated at the radius $r = r_c$ of a circular null geodesic. An inspection of (2.4.74) shows that circular null geodesics can be seen as the innermost circular timelike geodesics. By taking another derivative and using Eq. (2.4.74) we find

$$V_r''(r_c) = \frac{h_c}{f_c}\frac{L^2}{r_c^4}\left[2f_c - r_c^2 f_c''\right]\,, \tag{2.4.75}$$

and the coordinate angular velocity is

$$\Omega_c = \frac{\dot{\phi}}{\dot{t}} = \left(\frac{f_c'}{2r_c}\right)^{1/2} = \frac{f_c^{1/2}}{r_c}\,. \tag{2.4.76}$$

Let us define the "tortoise" coordinate

$$\frac{dr}{dr_*} = (hf)^{1/2}\,. \tag{2.4.77}$$

For circular orbits that satisfy Eq. (2.4.74), a simple calculation shows that

$$\frac{d^2}{dr_*^2}\left(\frac{f}{r^2}\right) = -\frac{hf}{r^4}\left(2f - r^2 f''\right)\,. \tag{2.4.78}$$

Combining this result with Eq. (2.4.75), we finally obtain

$$\lambda_0 = -\frac{1}{\sqrt{2}}\sqrt{\frac{r_c^2 f_c}{L^2}V_r''(r_c)} = \frac{1}{\sqrt{2}}\sqrt{-\frac{r_c^2}{f_c}\left(\frac{d^2}{dr_*^2}\frac{f}{r^2}\right)_{r=r_c}}\,. \tag{2.4.79}$$

This is the main result of this Chapter. In the next Chapter I will show that the rate of divergence of circular null geodesics at the light ring, as measured by the principal Lyapunov exponent, is equal (in the geometrical optics limit) to the damping time of black-hole perturbations induced by any massless bosonic field.

3

Scalar Waves

3.1 Massive Scalar Fields in a Spherically Symmetric Spacetime

Consider now the perturbations induced by a probe *field* (rather than a particle) propagating in a background spacetime, that for the purpose of this section could be either a black hole or a star. In the usual perturbative approach we assume that the scalar field Φ contributes very little to the energy density (i.e. we drop quadratic terms in the field throughout, assuming that the energy-momentum tensor of the scalar field is negligible). Then the problem reduces to that of a scalar field evolving in a fixed background, and the "true" metric can be replaced by a solution to the Einstein equations, that we will assume for simplicity to be spherically symmetric. Let us therefore start from the metric (2.2.14), which reduces to the Schwarzschild metric when $f = h = 1 - 2M/r$. The Klein-Gordon equation in this background reads

$$\left(\Box - \mu^2\right) \Phi = 0 \,. \tag{3.1.1}$$

Here the mass μ has dimensions of an inverse length, $m = \mu\hbar$ (with $G = c = 1$). The necessary conversions can be performed recalling that the Compton wavelength $\lambda_C = h/(mc)$ of a particle (in km) is related to its mass (in eV) by

$$\lambda_C[\text{km}] \times m[\text{eV}] = 1.24 \times 10^{-9} \,. \tag{3.1.2}$$

Note also that a ten-Solar Mass black hole has a Schwarzschild radius of ~ 30 km. Compton wavelengths comparable to the size of astrophysical black holes correspond

to very light particles of mass $\approx 10^{-10}$ eV (this observation will be useful in Chapter 5). Using a standard identity from tensor analysis, the Klein-Gordon equation can be written

$$\frac{1}{\sqrt{-g}}\partial_\mu\left(\sqrt{-g}g^{\mu\nu}\partial_\nu\Phi\right)-\mu^2\Phi=0\,, \tag{3.1.3}$$

where all quantities refer to the metric (2.2.14). Since the metric is spherically symmetric, the field evolution should be independent of rotations: this suggests that the angular variables θ and ϕ should factor out of the problem. The field can be decomposed as

$$\Phi(t,r,\theta,\phi)=\sum_{\ell=0}^{\infty}\sum_{m=-\ell}^{\ell}\frac{\Psi^{s=0}_{\ell m}(r)}{r}P_{\ell m}(\theta)\,e^{-i\omega t}\,e^{im\phi}\,, \tag{3.1.4}$$

where the superscript "$s=0$" is a reminder that these are spin-zero perturbations, $Y_{\ell m}(\theta,\phi)=P_{\ell m}(\theta)\,e^{im\phi}$ are the usual scalar spherical harmonics, and the associated Legendre functions $P_{\ell m}(\theta)$ satisfy Eq. (1.3.31), that we rewrite here for convenience:

$$\frac{1}{\sin\theta}\partial_\theta\left(\sin\theta\partial_\theta P_{\ell m}\right)-\frac{m^2}{\sin^2\theta}P_{\ell m}=-\ell(\ell+1)P_{\ell m}\,. \tag{3.1.5}$$

Note that this decomposition is the most general possible, because the spherical harmonics are a complete orthonormal set of functions. Inserting (3.1.4) into equation (3.1.3) and using (1.3.31), we get the following radial wave equation for $\Psi^{s=0}_{\ell m}(r)$:

$$fh\frac{d^2\Psi^{s=0}_l}{dr^2}+\frac{1}{2}(fh)'\frac{d\Psi^{s=0}_l}{dr}+\left[\omega^2-\left(\mu^2 f+\frac{\ell(\ell+1)}{r^2}f+\frac{(fh)'}{2r}\right)\right]\Psi^{s=0}_l=0\,, \tag{3.1.6}$$

where we can write $\Psi^{s=0}_l(r)$ rather than $\Psi^{s=0}_{\ell m}(r)$ because the differential equation does not depend on m (the background is spherically symmetric). In analogy with (2.4.77), we can introduce the "generalized tortoise coordinate"

$$\frac{dr}{dr_*}\equiv(fh)^{1/2} \tag{3.1.7}$$

to eliminate the first-order derivative and obtain the following radial equation:

$$\frac{d^2\Psi^{s=0}_l}{dr_*^2}+\left[\omega^2-V_0(\mu)\right]\Psi^{s=0}_l=0\,, \tag{3.1.8}$$

where the mass-dependent scalar potential reads

$$V_0(\mu)\equiv f\mu^2+f\frac{\ell(\ell+1)}{r^2}+\frac{(fh)'}{2r}\,. \tag{3.1.9}$$

The tortoise coordinate will turn out to be useful because, in the Schwarzschild metric, the location of the horizon ($r=2M$) corresponds to $r_*\to-\infty$, as can be seen e.g. from Eq. (3.1.12) below: the problem of black-hole perturbations can be formulated as a one-dimensional scattering problem over the real axis.

For most black-hole metrics in four and higher dimensions, $f=h$. In particular, for the Schwarzschild metric the potential reads

$$V_0^{\rm Schw}(\mu)=\left(1-\frac{2M}{r}\right)\left(\mu^2+\frac{\ell(\ell+1)}{r^2}+\frac{2M}{r^3}\right)\,, \tag{3.1.10}$$

and the tortoise coordinate satisfies

$$\frac{dr_*}{dr}=\left(1-\frac{2M}{r}\right)^{-1}=1+\frac{2M}{r-2M}\,, \tag{3.1.11}$$

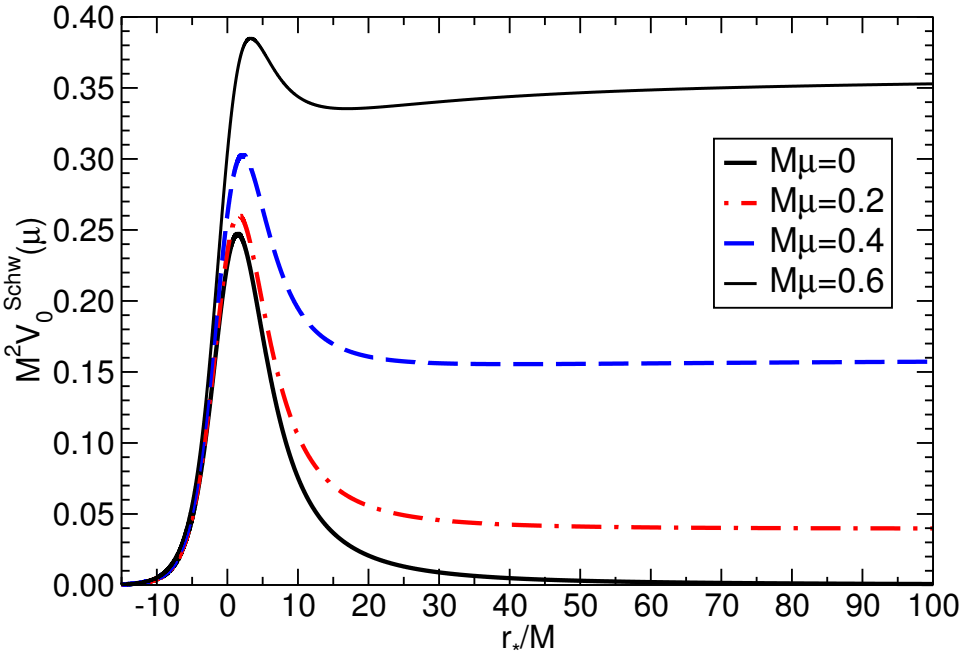

Figure 3.1: Schwarzschild potential (3.1.10) for massive scalar perturbations with $\ell = 2$ and different values of the scalar mass ($\mu = 0, 0.2, 0.4, 0.6$). The mass term acts as a confining potential: it gives rise to a local minimum and allows for the existence of quasi-bound states.

which is easily integrated to give

$$r_* = r + 2M \ln\left(\frac{r}{2M} - 1\right) , \tag{3.1.12}$$

where the integration constant has been fixed using a common choice in the literature. These calculations are simple enough to be done by hand. However, to illustrate some basic techniques that we will need later, the scalar wave equation for a massive field in the Schwarzschild background is also derived in the Notebook ScalarVectorPerturbations.nb.

The potential (3.1.10) has some crucial properties that are illustrated in Fig. 3.1: (i) it tends to zero as $r \to 2M$ ($r_*/M \to -\infty$), where $f = 1-2M/r \to 0$; (ii) it tends to μ^2 as $r/M \to \infty$ ($r_*/M \to \infty$), so whenever $\mu \neq 0$ there is a "reflective potential barrier" at infinity; (iii) when the mass term is nonzero there is a local minimum outside the peak of the potential, that allows for the existence of quasi-bound states (that slowly leak out to infinity because of dissipation).

Box 3.1 Master Equation for Massless Bosonic Fields, and the Peak of the Potential

Separating the equations describing massless spin-one and spin-two (i.e., electromagnetic and gravitational) perturbations in the Schwarzschild background is not as easy as separating the angular dependence for the scalar field (things get even harder for massive fields: see references in Section 5.2 below). The angular separation can be performed using vector and tensor spherical harmonics (see Chapter 4). As we will see, this leads to a remarkable result: perturbations induced by any of these bosonic fields satisfy a

single "master equation",

$$\frac{d^2\Psi^s_\ell}{dr_*^2} + \left[\omega^2 - V_s\right]\Psi^s_\ell = 0\,, \tag{3.1.13}$$

where

$$\begin{aligned} V_s &= f\left(\frac{\ell(\ell+1)}{r^2} + \frac{2M(1-s^2)}{r^3}\right) \\ &= f\left(\frac{\Lambda}{r^2} + \frac{2\beta}{r^3}\right). \end{aligned} \tag{3.1.14}$$

In the last line we set $M = 1$ to simplify the algebra. We also introduced $\beta \equiv 1 - s^2$ and $\Lambda = \ell(\ell+1)$, where $s = 0,\ 1,\ 2$ is the spin of the perturbing field. Then Eq. (3.1.10) is just a special case, corresponding to $s = 0$ and $\mu = 0$. Let us look for the extrema of the function $Q(r_*) = \omega^2 - V_s(r)$. It is easy to show that

$$Q'(r_*) = \left(1 - \frac{2}{r}\right)\left\{\frac{\Lambda}{r^3}\left(2 - \frac{6}{r}\right) + \frac{2\beta}{r^4}\left(3 - \frac{8}{r}\right)\right\} \tag{3.1.15}$$

Besides the asymptote as $r \to 2$, the only zero occurs when the curly brace vanishes. Multiplying the curly brace by r^5 one gets a quadratic equation, that is easily solved for the location of the extremum:

$$r_0 = \frac{3}{2\Lambda}\left\{\Lambda - \beta + \sqrt{\Lambda^2 + \beta^2 + \frac{14}{9}\Lambda\beta}\right\}. \tag{3.1.16}$$

It is readily seen that $r_0 \to 3$ when $\Lambda \to \infty$ (i.e. in the eikonal, or geometrical optics, limit). Even for small l's the location of the peak is very close to the marginal photon orbit: for $\ell = 2$, $s = (0,\ 1,\ 2)$ one gets $r_0 = (2.95171,\ 3,\ 3.28078)$; for $\ell = 3$, $s = (0,\ 1,\ 2)$ one gets $r_0 = (2.97415,\ 3,\ 3.0001)$.

3.2 Some Properties of the Master Equation

It is useful at this point to pause and review some basic properties of second-order ordinary differential equations similar to the "master equation" (3.1.13).

3.2.1 Wronskian

Consider the second-order ordinary differential equation

$$\frac{d^2\Psi}{dx^2} + p(x)\frac{d\Psi}{dx} + q(x)\Psi = 0\,. \tag{3.2.17}$$

In general, this equation admits two linearly independent solutions $\Psi_1,\ \Psi_2$. The Wronskian $\mathcal{W}$ is defined as $\mathcal{W}(\Psi_1,\ \Psi_2,\ x) \equiv \Psi_1\Psi_2' - \Psi_2\Psi_1'$, and it has the property

$$\begin{aligned} \frac{d}{dx}\mathcal{W} &= \Psi_1\Psi_2'' - \Psi_2\Psi_1'' = \Psi_1(-p\Psi_2' - q\Psi_2) - \Psi_2(-p\Psi_1' - q\Psi_1) \\ &= -\Psi_1 p\Psi_2' + p\Psi_2\Psi_1' = -p\mathcal{W}\,. \end{aligned} \tag{3.2.18}$$

This equation is easily integrated:

$$\mathcal{W}(\Psi_1,\ \Psi_2,\ x) = \mathcal{W}(\Psi_1,\ \Psi_2,\ x_0)\exp\left(-\int_{x_0}^{x} p(x')dx'\right), \tag{3.2.19}$$

and we see that the Wronskian is *constant* whenever $p(x) = 0$, as in the case of the master equation (3.1.13).

3.2.2 Boundary conditions

Horizon

For most spacetimes of interest the potential $V_s \to 0$ as $r \to 2M$ ($r_* \to -\infty$), and in this limit solutions to the wave equation behave as $\Psi \sim e^{-i\omega(t\pm r_*)}$. Classically nothing should leave the horizon: only ingoing modes (corresponding to a plus sign) should be present, and therefore

$$\Psi \sim e^{-i\omega(t+r_*)}\,, \quad r_* \to -\infty \ \ (r \to r_+)\,. \tag{3.2.20}$$

This boundary condition at the horizon can also be seen to follow from regularity requirements. For non-extremal spacetimes, the tortoise coordinate tends to

$$r_* = \int f^{-1}\, dr \sim [f'(r_+)]^{-1} \log(r - r_+)\,, \quad r \sim r_+\,, \tag{3.2.21}$$

with $f'(r_+) > 0$. Near the horizon, outgoing modes behave as

$$e^{-i\omega(t-r_*)} = e^{-i\omega v} e^{2i\omega r_*} \sim e^{-i\omega v}(r - r_+)^{2i\omega/f'(r_+)}\,, \tag{3.2.22}$$

where $v = t + r_*$. Therefore, unless $2i\omega/f'(r_+)$ is a positive integer, the outgoing modes cannot be smooth, i.e. of class $\mathcal{C}^\infty$, and they must be discarded.

Numerical integrations often start at some finite radius $r = 2M + \epsilon$ outside the horizon. Therefore it is useful to compute subleading corrections to the pure ingoing-wave behavior for the homogeneous equation (3.1.13), of the form

$$\Psi \sim e^{-i\omega r_*}\left[1 + a(r-2M) + b(r-2M)^2 + \dots\right]\,. \tag{3.2.23}$$

In the Notebook ReggeWheelerBoundaryConditions.nb we obtain these corrections (extensions of this sort of calculations to the Zerilli equation are simple). The first two coefficients in this expansion are

$$a = \frac{i\left(\ell^2+\ell+1\right)}{2(4\omega+i)}\,, \tag{3.2.24}$$

$$b = -\frac{\ell(\ell+1)\left(\ell^2+\ell+8i\omega+2\right)+12i\omega}{16\left(8\omega^2+6i\omega-1\right)}\,. \tag{3.2.25}$$

Infinity

For asymptotically flat spacetimes, the metric at spatial infinity tends to the Minkowski metric, and therefore the potential for wave propagation is zero there. By requiring

$$\Psi \sim e^{-i\omega(t-r_*)}, \quad r \to \infty\,, \tag{3.2.26}$$

we discard unphysical waves "entering the spacetime from infinity".

However, in scattering experiments one is *interested* in having waves coming in from infinity. In this case all we can say is that near infinity ($r \to \infty$) the solution is a superposition of ingoing and outgoing waves:

$$\Psi \sim e^{-i\omega r_*}\left(1 + \frac{a_{\rm in}}{r} + \frac{b_{\rm in}}{r^2} + \dots\right) + e^{i\omega r_*}\left(1 + \frac{a_{\rm out}}{r} + \frac{b_{\rm bout}}{r^2} + \dots\right)\,. \tag{3.2.27}$$

As shown in the Notebook, the first few coefficients in this large–r expansion read

$$a_{\rm in} = \frac{-i\ell(\ell+1)}{2\omega}\,, \tag{3.2.28}$$

$$b_{\rm in} = -\frac{(\ell-1)\ell(\ell+1)(\ell+2)+4i\omega}{8\omega^2}\,, \tag{3.2.29}$$

$$a_{\rm out} = \frac{i\ell(\ell+1)}{2\omega}\,, \tag{3.2.30}$$

$$b_{\rm out} = \frac{-(\ell-1)\ell(\ell+1)(\ell+2)+4i\omega}{8\omega^2}\,. \tag{3.2.31}$$

3.3 Quasinormal Modes and Their Excitation

Unlike most idealized macroscopic physical systems, perturbed black-hole spacetimes are intrinsically dissipative due to the presence of the event horizon, which acts as a one-way membrane. In fact, the system is "leaky" both at the horizon and at infinity, where energy is dissipated in the form of gravitational radiation. This precludes a standard normal-mode analysis: dissipation means that the system is not time-symmetric, and that the associated boundary-value problem is non-Hermitian. In general, after a transient that depends on the source of the perturbation, the response of a black hole is dominated by characteristic complex frequencies (the "quasinormal modes", henceforth QNMs). The imaginary part is nonzero because of dissipation, and its inverse is the decay timescale of the perturbation. The corresponding eigenfunctions are usually not normalizable, and, in general, they do not form a complete set (cf. [68,162] for more extensive discussions). Almost any real-world physical system is dissipative, so one might reasonably expect QNMs to be ubiquitous in physics. QNMs are indeed useful in the treatment of many dissipative systems, e.g. in the context of atmospheric science and leaky resonant cavities. Extensive reviews on black-hole QNMs and their role in various fields of physics (including gravitational-wave astronomy, the gauge-gravity duality and high-energy physics) can be found in [44, 131, 132, 160].

Black-hole QNMs were initially studied to assess the stability of the Schwarzschild metric [168, 199]. Goebel [104] was the first to realize that they can be thought of as waves traveling around the black hole: more precisely, they can be interpreted as waves *trapped at the unstable circular null geodesic* (the "light ring") and slowly leaking out. This qualitative picture was refined by several authors over the years [62,78,79,83,90,147,194]. It will be shown below that the instability timescale of the geodesics is the decay timescale of the QNM, and the oscillation frequency $\omega \sim c/r_{\rm mb}$, with c the speed of light and $r_{\rm mb}$ the light-ring radius (see [62] for generalizations of these arguments to rotating and higher-dimensional black holes).

3.3.1 A Pedagogical Example: A Vibrating String

Some key features of the black-hole perturbation problem are exemplified by a very simple system: a vibrating string with fixed ends. To simplify the mathematics we choose units such that the velocity of the waves in the string $c = 1$, and we consider a string of length π. Then any disturbance of the string obeys the wave equation

$$\frac{\partial^2 u}{\partial t^2} = \frac{\partial^2 u}{\partial x^2} \quad \text{on} \quad 0 \leq x \leq \pi \,, \tag{3.3.32}$$

with $u(t, 0) = u(t, \pi) = 0$. The general solution of this problem is easily verified to be

$$u(t, x) = \sum_{n=1}^{\infty} \left(\bar{C}_n \cos nt + \bar{C}'_n \sin nt\right) \sin\left(nx\right) , \tag{3.3.33}$$

where we used an overbar to avoid confusion with the *quasinormal* excitation coefficients C_n, as defined in Eq. (3.3.62) below. In Fourier language we say the general solution is a superposition of normal modes with sinusoidal dependence on x and t, labeled by an integer n. Each mode has frequency $\omega = n$.

For the general solution to be useful we must determine the constants $\bar{C}_n$ and $\bar{C}'_n$, that is, we must determine the *contribution of each individual mode*. This contribution can easily be computed once we are given *initial data*, namely the initial configuration $u(0, x) \equiv u_0(x)$ and velocity profile $\partial_t u(0, x) \equiv v_0(x)$ of the string. Indeed, consider (3.3.33) and its first derivative, both evaluated at $t = 0$.

Multiplying both sides by $\sin nx$ and integrating on $(0\,,\pi)$ we get

$$\bar{C}_n = \frac{2}{\pi}\int_0^\pi u_0(x)\,\sin nx\,dx\,, \qquad \bar{C}'_n = \frac{2}{n\pi}\int_0^\pi v_0(x)\,\sin nx\,dx\,, \tag{3.3.34}$$

which completely specifies the solution.

In more general situations it is not possible to find closed-form elementary solutions satisfying some given boundary conditions (in our vibrating string example, the "fixed ends" condition). However, an elegant formal solution can be obtained using Green's functions. Let us consider a slight generalization of Eq. (3.3.32):

$$\frac{\partial^2 u}{\partial x^2} - \frac{\partial^2 u}{\partial t^2} - V(x)\,u = \mathcal{S}\,, \tag{3.3.35}$$

where we introduced a potential $V(x)$ and a source $\mathcal{S}$ representing, say, external forces acting on the system (for a free vibrating string $V(x) = \mathcal{S} = 0$). We define the Laplace transform of $u(t,x)$ as[1]

$$\mathcal{L}u(t,x) \equiv \hat{u}(\omega\,,x) = \int_{t_0}^\infty u(t,x)e^{i\omega t}dt\,, \tag{3.3.36}$$

In terms of the Laplace transform, the original field can be written as

$$u(t,x) = \frac{1}{2\pi}\int_{-\infty+ic}^{\infty+ic} \hat{u}(\omega\,,x)e^{-i\omega t}d\omega\,. \tag{3.3.37}$$

Using the elementary property $\mathcal{L}\left[\frac{\partial u(t,x)}{\partial t}\right] = -i\omega\mathcal{L}u - e^{i\omega t_0}u(x,t_0)$, the Laplace transformation of (3.3.35) leads to

$$\frac{\partial^2 \hat{u}}{\partial x^2} + \left[\omega^2 - V(x)\right]\hat{u} = I(\omega\,,x)\,, \tag{3.3.38}$$

where

$$I(\omega\,,x) = e^{i\omega t_0}\left[i\omega u(t,x) - \frac{\partial u(t,x)}{\partial t}\right]_{t=t_0} + \hat{\mathcal{S}}\,. \tag{3.3.39}$$

This equation is formally solved with the use of a Green's function $G(x,x')$ such that

$$\frac{\partial^2 \hat{u}}{\partial x^2} + \left[\omega^2 - V(x)\right]G(x\,,x') = \delta(x-x')\,. \tag{3.3.40}$$

In terms of the Green's function the solution is simply given by

$$\hat{u} = \int I(\omega\,,x')G(x\,,x')dx'\,. \tag{3.3.41}$$

Suppose we know the Green's function. Then the previous equation shows that, given $I(\omega\,,x')$ (which means, in the absence of external forces, given initial data) we can determine, at least in principle, the solution.

There is a general prescription to construct the Green's function [155]. Find two linearly independent solutions of the homogeneous equation, say $\hat{u}_1(\omega\,,x)$ and $\hat{u}_2(\omega\,,x)$, each satisfying one of the required boundary conditions: for the vibrating string these solutions would be such that $\hat{u}_1(\omega\,,0) = 0$, $\hat{u}_2(\omega\,,\pi) = 0$. The Green's function is then

$$G(x\,,x') = \frac{1}{W}\begin{cases} \hat{u}_1(x)\hat{u}_2(x') & \text{if } x \le x'\,, \\ \\ \hat{u}_1(x')\hat{u}_2(x) & \text{if } x' \le x\,, \end{cases} \tag{3.3.42}$$

[1]The usual Laplace variable $s = -i\omega$. We prefer to use ω for notational consistency with previous work by Leaver [137] and Andersson [16]. Our transform is well defined as long as $\mathrm{Im}(\omega) \ge c$.

where we defined the Wronskian between the two solutions

$$W = \frac{\partial \hat{u}_1}{\partial x}\hat{u}_2 - \hat{u}_1\frac{\partial \hat{u}_2}{\partial x}\,, \tag{3.3.43}$$

which for equations of the type (3.3.38) is a constant. For the vibrating string the homogeneous solutions are elementary functions: $\hat{u}_1 = \sin\omega x$, $\hat{u}_2 = \sin\omega(x-\pi)$, and the Green's function

$$G(x\,,x') = \begin{cases} -\frac{\sin\omega x \sin\omega(x'-\pi)}{\omega\sin\omega\pi} & \text{if } x \le x'\,, \\ -\frac{\sin\omega x' \sin\omega(x-\pi)}{\omega\sin\omega\pi} & \text{if } x' \le x\,. \end{cases} \tag{3.3.44}$$

Notice that the Wronskian $W = -\omega\sin\omega\pi$ is zero at $\omega = n$ with n integer, that is, at the *normal frequencies* of the system. Near the zeros of the Wronskian (which are also *poles of the Green's function*: see below), located at $\omega = n$, we have $W \simeq -[n\pi\cos(n\pi)]\,(\omega - n)$. At the zeros of the Wronskian, the two solutions $\hat{u}_1$ and $\hat{u}_2$ are no longer independent: they satisfy both boundary conditions simultaneously. In fact, setting $\omega = n$ in (3.3.44) we can see that $\hat{u}_1$ and $\hat{u}_2$ coincide, and correspond to the normal modes of the system. Using (3.3.37), (3.3.39) and (3.3.41) and setting for simplicity $t_0 = \mathcal{S} = 0$ we get

$$u(t\,,x) = \frac{1}{2\pi}\int dx' d\omega\,[i\omega u_0(x') - v_0(x')]\,G(x\,,x')e^{-i\omega t}\,. \tag{3.3.45}$$

The $\omega-$integral can be performed by closing the contour of integration. We choose the contour depicted in Fig. 3.2.

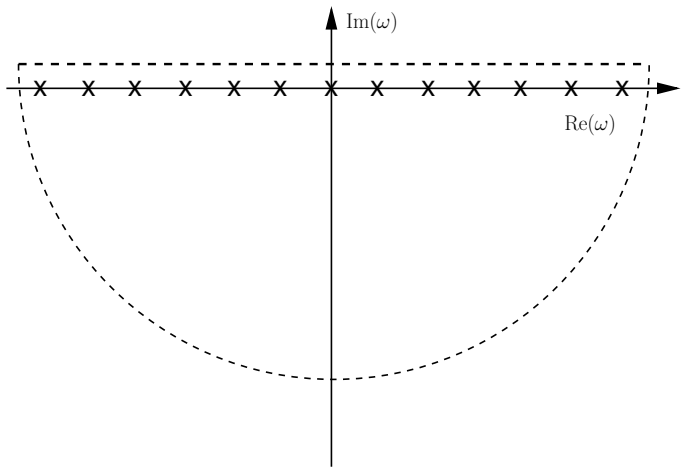

Figure 3.2: Integration contour for the vibrating string problem. Crosses mark zeros of the Wronskian W, corresponding to the normal frequencies of the system.

If $\hat{u}_1(x)\,,\hat{u}_2(x)$ are analytic and have no essential singularities inside the contour[2], the poles of the Green's function are all due to zeros of the Wronskian. In this way we get for the integral in (3.3.45),

$$u(t\,,x) \quad = \quad \frac{1}{2\pi}\int dx' d\omega\,[i\omega u_0(x') - v_0(x')]\,G(x\,,x')e^{-i\omega t}$$

[2]Both conditions are met in the case of a vibrating string, but both are *violated* when we deal with black hole QNMs. For black holes, the Green's function essential singularity at the origin gives rise to tails, and the integral over the half-circle at infinity is responsible for the early-time response of the black hole. See discussion after Eq. (3.3.59).

$$= -i\sum_n \frac{1}{n\pi}\left\{\int dx' \sin nx' \left[inu_0(x') - v_0(x')\right]\right\} e^{-int}\sin nx$$
$$+\frac{1}{2\pi}\int_{HC} d\omega \int dx' \left[i\omega u_0(x') - v_0(x')\right] G(x\,,x')e^{-i\omega t}\,, \quad (3.3.46)$$

where "HC" in the second term means that the integration should be performed along the half-circle. Not surprisingly, taking the real part of the right hand side we recover the result (3.3.33) with expansion coefficients given by (3.3.34).

The bottom line of this discussion is that the general solution depends crucially on two elements: (i) the residues of the Green's function evaluated at the poles (that is, at the normal frequencies); (ii) the function $I(\omega\,,x)$, which (in the absence of initial forces) is nothing but the initial data. By inspection, the net result for the field can be expressed as a sum of the form

$$u(t\,,x) \propto \sum_n \frac{J_n(t\,,x)}{\partial_\omega W} u_n(\omega_n\,,x)e^{-i\omega_n t}\,, \quad (3.3.47)$$

where $\omega_n = n$ is a normal frequency, $J_n(t\,,x) = \int dx' I(\omega_n\,,x')\, u_n(\omega_n\,,x')$ and $u_n(\omega_n\,,x) = \sin nx$ is a normal mode wavefunction (that is, any of the homogeneous solutions evaluated at the normal frequency $\omega_n = n$). We will see below that a similar result holds for black hole ringdown.

Effect of Initial Data

In the previous section we pointed out that initial data play a crucial role to determine the excitation of the normal modes of a system. For illustration, below we consider three simple examples that will be useful in the following to understand, by analogy, the initial-data dependence of the excitation of a Kerr black hole.

Suppose first that we have an (initially stationary) plucked string: the string's initial profile is a triangle of height h with a vertex at x^S, i.e. $v_0(x) = 0$ and

$$u_0(x) = \begin{cases} \frac{xh}{x^S} & \text{if } 0 \le x \le x^S\,, \\ \\ \frac{h(\pi - x)}{\pi - x^S} & \text{if } x^S \le x \le \pi\,. \end{cases} \quad (3.3.48)$$

Stationarity of the initial data implies that $\bar{C}'_n = 0$, so that

$$u(t,x) = \sum_{n=1}^{\infty} \bar{C}_n \cos nt \sin nx\,, \quad \bar{C}_n = \frac{2h}{n^2}\frac{\sin nx^S}{x^S(\pi - x^S)} \quad (3.3.49)$$

Notice that modes having a node at x^S, where the string is plucked, are not excited ($\bar{C}_n = 0$). Notice also that the "excitation factors" $\bar{C}_n$ decrease as $1/n^2$.

As a second example take stationary, localized "δ-function" initial data of the form

$$u_0(x) = \delta(x - x^S)\,, \quad v_0(x) = 0\,. \quad (3.3.50)$$

The excitation factors are trivially computed:

$$\bar{C}_n = \frac{2}{\pi}\sin\left(nx^S\right). \quad (3.3.51)$$

It is apparent that all modes are excited to a comparable amplitude except for modes with a node at the plucking point, which are not excited at all.

Our third and last example are stationary, gaussian initial data:

$$u_0(x) = e^{-b(x-x^S)^2}\,, \quad v_0(x) = 0\,. \quad (3.3.52)$$

For large b the gaussian is strongly peaked at $x = x^S$, in which case the contribution to the integral outside of $(0, \pi)$ can be ignored and we have

$$\begin{aligned} \bar{C}_n &= \frac{2}{\pi}\int_0^\pi u_0(x)\,\sin nx\,dx \simeq \frac{2}{\pi}\int_{-\infty}^{\infty} e^{-b(x-x^S)^2}\sin nx\,dx \\ &= \frac{2\sin(nx^S)}{\sqrt{\pi b}}e^{-n^2/(4b)}\,. \end{aligned} \tag{3.3.53}$$

Therefore a mode with given n is maximally excited when the width of the gaussian satisfies the condition $b = n^2/2$. The basic lesson we learn from these examples is that the excitation of a system is very sensitive to the initial data. More specifically, whether a given mode is excited or not depends strongly on the point where we excite the system ("pluck the string").

3.3.2 Oscillating Black Holes

[EB: This is a placeholder to discuss the Notebook SCATTERING_SCALARS_BOOK.NB]

In the Sasaki-Nakamura (SN) formalism [118,180–182], perturbations of a Kerr black hole induced by a spin-s field are described by a single function $X^{(s)}(t, r)$ whose Laplace transform satisfies

$$\frac{d^2\hat{X}^{(s)}(\omega\,,r)}{dr_*^2} + V_{SN}\hat{X}^{(s)}(\omega\,,r) = I(\omega\,,r)\,, \tag{3.3.54}$$

where the effective potential V_{SN} depends both on the radial coordinate and on the frequency. The function $I(\omega\,,r)$ is a linear combination of the SN function $X^{(s)}(t_0\,,r)$ and its time derivative $\dot{X}^{(s)}(t_0\,,r)$ at time t_0 (see below for the explicit expression for scalar perturbations). The tortoise coordinate r_* is defined by the condition

$$\frac{dr_*}{dr} = \frac{r^2+a^2}{\Delta}\,, \tag{3.3.55}$$

ranging from $-\infty$ (the location of the event horizon) to $+\infty$ (spatial infinity). We use Boyer-Lindquist coordinates and follow Leaver's choice of units, setting $G = c = 2M = 1$. In Leaver's units the angular momentum per unit mass a is such that $0 \le a \le M = 1/2$, and the horizon function $\Delta = r^2 - r + a^2$. Sometimes we will present our results in terms of the more familiar dimensionless angular momentum $j = 2a$, such that $0 \le j \le 1$. The class of problems that fit in this description include any massless field in the Kerr geometry, including gravitational, electromagnetic and scalar fields [3].

The main difference with the vibrating string example is that our system is not conservative: waves can escape to infinity. For this reason an expansion in normal modes is not possible (see [131, 137, 160] for extensive discussions of this point). Wave propagation is also complicated by backscattering off the background

[3] In Eq. (3.3.35), the potential $V(x)$ and the source $\mathcal{S}$ were introduced to reproduce the structure of Eq. (3.3.54). In general, in the SN formalism the wave equation contains a first derivative of the wavefunction:

$$\frac{d^2X}{dr_*^2} - \mathcal{F}\frac{dX}{dr_*} - \mathcal{U}X = S\,,$$

where we also allow for the presence of a source term S. This is no restriction, since a trivial change of variable of the form

$$X = \exp\left[\int \frac{\mathcal{F}}{2}dr_*\right] X_2$$

eliminates the first derivative, yielding

$$\frac{d^2X_2}{dr_*^2} + \left(\frac{\mathcal{F}'}{2} - \frac{\mathcal{F}^2}{4} - \mathcal{U}\right)X_2 = S\exp\left[-\int\frac{\mathcal{F}}{2}dr_*\right]\,.$$

curvature, which is responsible for tail effects [171]. Despite these complications it can be shown that the poles of the Green's function (now located at complex frequencies corresponding to the QNMs) still play an important role in the evolution.

The QNM contribution can be isolated from other features of the signal, such as the late-time tail, using the Green's function technique [16, 137]. First one defines a solution of the homogeneous equation having the correct behavior at the horizon (only ingoing waves),

$$\lim_{r\to r_+} \hat{X}^{(s)}_{r_+} \sim e^{-i(\omega-m\Omega)r_*}\,, \tag{3.3.56}$$

$$\lim_{r\to\infty} \hat{X}^{(s)}_{r_+} \sim A_{\rm in}(\omega)e^{-i\omega r_*} + A_{\rm out}(\omega)e^{i\omega r_*}\,, \tag{3.3.57}$$

where $r_\pm = [1\pm(1-4a^2)^{1/2}]/2$, and a second solution $\hat{X}^{(s)}_{\infty_+}$ behaving as $e^{i\omega r_*}$ for large values of r. Since the Wronskian $W = 2i\omega A_{\rm in}$ we can express the general solution as [16]

$$\hat{X}^{(s)}(\omega\,,r) = \hat{X}^{(s)}_{\infty_+}\int_{-\infty}^{r_*}\frac{I(\omega\,,r)\hat{X}^{(s)}_{r_+}}{2i\omega A_{\rm in}}dr'_* + \hat{X}^{(s)}_{r_+}\int_{r_*}^{\infty}\frac{I(\omega\,,r)\hat{X}^{(s)}_{\infty_+}}{2i\omega A_{\rm in}}dr'_*\,. \tag{3.3.58}$$

To proceed we make the astrophysically reasonable assumption that the observer is located far away from the black hole. If the initial data have compact support and this support is entirely located closer to the black hole with respect to the observer (this is basically a "no-incoming radiation from infinity" condition), a good approximation will be

$$\hat{X}^{(s)}(\omega\,,r) \simeq \frac{e^{i\omega r_*}}{2i\omega A_{\rm in}}\int_{-\infty}^{\infty} I(\omega\,,r)\hat{X}^{(s)}_{r_+}dr'_*\,. \tag{3.3.59}$$

As explained in [16, 137, 161], when we invert this expression to get the solution in the time domain we get (as in the vibrating string case) a contribution from the poles of the Green's function. This contribution can again be isolated by closing the path of integration, as was done in Eq. (3.3.46). An important difference that distinguishes black hole spacetimes is that there is now an essential singularity at $\omega = 0$ and a branch cut extending from the singularity to $-i\infty$ [69, 70, 124, 161]. To prevent the essential singularity from lying inside the integration contour we must modify slightly the contour of Fig. 3.2. We place a branch cut along the negative imaginary-ω axis and split the half circle at $|\omega|\to\infty$ into two quarter circles. The new contour is shown in Fig. 3.3. The poles in the complex frequency plane are the zeros of $A_{\rm in}$: they correspond to perturbations satisfying *both* ingoing wave conditions at the horizon and outgoing wave conditions at infinity, i.e. (by definition) to QNMs. QNM frequencies have negative imaginary part. Since we assume a Fourier dependence of the form $X^{(s)}(t,r)\sim e^{-i\omega t}$ this means that there are no exponentially growing modes. There is an infinity of QNMs, usually sorted by the magnitude of their imaginary part and labelled by an integer n.

Extracting the QNM contribution[4] to the radiated wave we get

$$X^{(s)}(t\,,r) = -{\rm Re}\left[\sum_n B_n e^{-i\omega_n(t-r_*)}\int_{-\infty}^{\infty}\frac{I(\omega\,,r)\hat{X}^{(s)}_{r_+}}{A_{\rm out}}dr'_*\right] \tag{3.3.60a}$$

$$= -{\rm Re}\left[\sum_n C_n e^{-i\omega_n(t-r_*)}\right]\,, \tag{3.3.60b}$$

[4]There are also other contributions to the signal. The essential singularity at the origin ($\omega = 0$) gives rise to the tail of the time evolved wavefunction; the integral over the quarter circles at infinite frequency produces the early time response of the black hole. Since our main focus is the QNM contribution we discard these two terms in the integral. For more details we refer the reader to [69, 70, 137, 161].

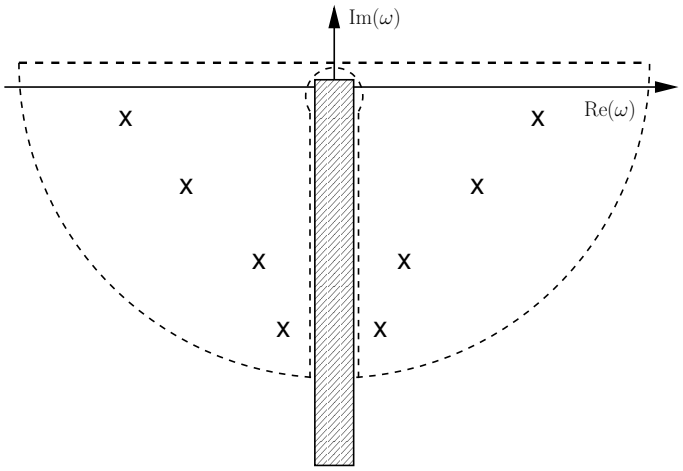

Figure 3.3: Integration contour to invert Eq. (3.3.59). The shaded area is the branch cut and crosses mark zeros of the Wronskian W (the QNM frequencies).

where the sum is over all poles in the complex plane and the *quasinormal excitation factors* (QNEFs) B_n are defined as

$$B_n = \frac{A_{\rm out}}{2\omega\alpha_n} \equiv \frac{A_{\rm out}}{2\omega}\left(\frac{dA_{\rm in}}{d\omega}\right)^{-1}\Bigg|_{\omega=\omega_n} . \tag{3.3.61}$$

Here α_n is a commonly used notation for the derivative of $A_{\rm in}$ at the QNM frequency. The *quasinormal excitation coefficients* C_n can be computed as

$$C_n = B_n \int_{-\infty}^{\infty} \frac{I(\omega\,,r)\hat{X}^{(s)}_{r_+}}{A_{\rm out}} dr'_* \tag{3.3.62}$$

whenever the integral on the right hand side, which must be evaluated at the QNM frequency $\omega=\omega_n$, is convergent. In general the QNM frequencies ω_n, the B_n's and the C_n's (as well as the wavefunction) depend on (l,m) and the spin of the perturbing field s, but to simplify the notation we will omit this dependence whenever there is no risk of confusion.

By definition of the QNM frequencies, $\hat{X}^{(s)}_{r_+} \sim A_{\rm out}e^{i\omega r_*}$ as $r_*\to\infty$ at $\omega=\omega_n$: in this sense the above integral is "normalized". For source terms $I(\omega\,,r)$ that are zero outside some finite range of r, or have sufficiently rapid exponential decay as $|r_*|\to\infty$, the integral is also convergent. For other classes of initial data the integral as evaluated on the real line is, in general, divergent. This is a major difference with respect to ordinary normal mode expansions. The normal modes of closed mechanical systems are Sturm-Liouville eigenfunctions of the wave equation, and their excitation coefficients are weighted integrals of the source term over the mode. Since the Sturm-Liouville eigenfunctions are always bounded, the integrals always converge. For QNM expansions a meaningful definition of the integral for general source terms requires more care, and the introduction of an analytical continuation procedure [137,195].

Equation (3.3.60) is one of the main results we will use throughout the rest of the paper. Once we specify initial data, the QNEFs allow the determination of the QNM content of a signal. QNEFs have long been known for scalar, electromagnetic and gravitational perturbations of Schwarzschild black holes [16,137,195]. More recently there have been attempts to extend those calculations to scalar perturbations of Kerr

black holes [101, 102]. Electromagnetic and (most importantly for gravitational-wave phenomenology) gravitational perturbations of Kerr black holes have not been dealt with so far. One purpose of the present work is to fill this gap. Before turning to an explicit calculation of the B_n's we will provide the explicit form of the function $I(\omega\,, r)$ for $s = 0$. We will also address two important conceptual issues: the time-shift problem and the convergence of the QNM expansion.

3.4 Solution of the Scattering Problem

One of the most fascinating aspects of black-hole physics is that the master equation (3.1.13) can be solved using methods familiar from nonrelativistic quantum mechanics, in particular from scattering theory. We will first review a method developed by Leaver [135] to compute QNM frequencies "exactly" (within the limits of a computer's numerical accuracy). Leaver's method follows quite closely techniques that were developed to deal with the hydrogen ion in quantum mechanics as early as 1934 [123]. Then we will confirm the intuitive picture of black-hole QNMs as light-ring perturbations using one of the simplest "textbook" approximation technique to solve scattering problems: the Wentzel-Kramers-Brillouin (WKB) approximation. In the black-hole perturbation theory context, the WKB approximation was first investigated by Mashhoon [146], Schutz and Will [186].

3.4.1 Leaver's Solution

Leaver's solution of the wave equation is based on a classic 1934 paper by Jaffé on the electronic spectra of the hydrogen molecular ion [123] – quantum mechanics comes to the rescue again! The wave equation is found to be a special case of the so-called "generalized spheroidal wave equation" [136], for which the solution can be written as a series expansion. By replacing the series expansion into the differential equations and imposing QNM boundary conditions, one finds recursion relations for the expansion coefficients. The series solution converges only when a certain continued fraction relation involving the mode frequency and the black hole parameters holds. The evaluation of continued fractions amounts to elementary algebraic operations, and the convergence of the method is excellent, even at high damping. In the Schwarzschild case, in particular, the method can be tweaked to allow for the determination of modes of order up to $\sim 100,000$ [159].

As stated (without proof) in Box 3.1, the angular dependence of the metric perturbations of a Schwarzschild black hole can be separated using tensorial spherical harmonics [206]. Depending on their behavior under parity transformations, the perturbation variables are classified as *polar* (even) or *axial* (odd). The resulting differential equations can be manipulated to yield two wave equations, one for the polar perturbations (that we shall denote by a "plus" superscript) and one for the axial perturbations ("minus" superscript):

$$\left(\frac{d^2}{dr_*^2} + \omega^2\right) Z_l^{\pm} = V_l^{\pm} Z_l^{\pm}\,. \tag{3.4.63}$$

We are interested in solutions of equation (3.4.63) that are purely outgoing at spatial infinity ($r \to \infty$) and purely ingoing at the black hole horizon ($r \to 1$). These boundary conditions are satisfied by an infinite, discrete set of complex frequencies $\omega = \omega_R + \mathrm{i}\omega_I$ (the QNM frequencies). For the Schwarzschild solution the two potentials $V^{\pm}$ are quite different, yet the QNMs for polar and axial perturbations are the same. The proof of this surprising fact can be found in [65]. The underlying reason is that polar and axial perturbations are related by a differential transformation discovered by Chandrasekhar [65], and both potentials can be seen to emerge from

a single "superpotential". In fancier language, the axial and polar potentials are related by a supersymmetry transformation (where "supersymmetry" is to be understood in the sense of nonrelativistic quantum mechanics): cf. [138]. Since polar and axial perturbations are isospectral and V^- has an analytic expression which is simpler to handle, we can focus on the axial equation for $Z_l^- = \Psi_l^{s=2}$, i.e. the master equation (3.1.13) with $s = 2$.

We will now find an algebraic relation that can be solved (numerically) to determine the eigenfrequencies of scalar, electromagnetic and gravitational perturbations of a Schwarzschild black hole. For a study of the differential equation it is convenient to use units where $2M = 1$, so that the horizon is located at $r = 1$ (the use of these units will be limited to this section). In these units, Eq. (3.1.11) relating the tortoise coordinate and the usual Schwarzschild coordinate radius r simplifies to

$$\frac{dr}{dr_*} = \frac{\Delta}{r^2}\,, \tag{3.4.64}$$

with $\Delta = r(r-1)$. When written in terms of the "standard" radial coordinate r and in units $2M = 1$, the master equation (3.1.13) reads:

$$r(r-1)\frac{d^2\Psi_l^s}{dr^2} + \frac{d\Psi_l^s}{dr} - \left[\ell(\ell+1) - \frac{s^2-1}{r} - \frac{\omega^2 r^3}{r-1}\right]\Psi_l^s = 0\,, \tag{3.4.65}$$

where s is the spin of the perturbing field ($s = 0,\ 1,\ 2$ for scalar, electromagnetic and gravitational perturbations, respectively) and l is the angular index of the perturbation. Perturbations of a Schwarzschild background are independent of the azimuthal quantum number m, because of spherical symmetry (this is not true for Kerr black holes). Equation (3.4.65) can be solved using a series expansion of the form:

$$\Psi_l^s = (r-1)^{-\mathrm{i}\omega} r^{2\mathrm{i}\omega} e^{\mathrm{i}\omega(r-1)} \sum_{j=0}^{\infty} a_j \left(\frac{r-1}{r}\right)^j\,, \tag{3.4.66}$$

where the prefactor is chosen to incorporate the QNM boundary conditions at the horizon and at infinity:

$$\Psi_l^s \sim e^{\mathrm{i}\omega r_*} \sim e^{\mathrm{i}\omega(r+\ln r)} \sim r^{\mathrm{i}\omega} e^{\mathrm{i}\omega r} \quad \text{as} \quad r \to \infty\,, \tag{3.4.67}$$

$$\Psi_l^s \sim e^{-\mathrm{i}\omega r_*} \sim e^{-\mathrm{i}\omega \ln(r-1)} \sim (r-1)^{-\mathrm{i}\omega} \quad \text{as} \quad r \to 1\,. \tag{3.4.68}$$

Substituting the series expansion (3.4.66) in (3.4.65) we get a three-term recursion relation for the expansion coefficients a_j:

$$\begin{aligned} &\alpha_0 a_1 + \beta_0 a_0 = 0, \\ &\alpha_n a_{n+1} + \beta_n a_n + \gamma_n a_{n-1} = 0, \qquad n = 1, 2, \ldots \end{aligned} \tag{3.4.69}$$

where α_j, β_j and γ_j are simple functions of the frequency ω, l and s [135]:

$$\alpha_n = n^2 + (2 - 2\mathrm{i}\omega)n + 1 - 2\mathrm{i}\omega\,, \tag{3.4.70}$$

$$\beta_n = -\left[2n^2 + (2 - 8\mathrm{i}\omega)n - 8\omega^2 - 4\mathrm{i}\omega + \ell(\ell+1) + 1 - s^2\right]\,, \tag{3.4.71}$$

$$\gamma_n = n^2 - 4\mathrm{i}\omega n - 4\omega^2 - s^2\,. \tag{3.4.72}$$

A mathematical theorem due to Pincherle guarantees that the series is convergent (and the QNM boundary conditions are satisfied) when the following continued fraction condition on the recursion coefficients holds:

$$0 = \beta_0 - \frac{\alpha_0\gamma_1}{\beta_1 -}\,\frac{\alpha_1\gamma_2}{\beta_2 -}\ldots \tag{3.4.73}$$

The n–th QNM frequency is (numerically) the most stable root of the n–th inversion of the continued-fraction relation (3.4.73), i.e., it is a solution of

$$\beta_n - \frac{\alpha_{n-1}\gamma_n}{\beta_{n-1}-}\frac{\alpha_{n-2}\gamma_{n-1}}{\beta_{n-2}-}\cdots\frac{\alpha_0\gamma_1}{\beta_0} = \frac{\alpha_n\gamma_{n+1}}{\beta_{n+1}-}\frac{\alpha_{n+1}\gamma_{n+2}}{\beta_{n+2}-}\cdots \qquad (n=1,2,\dots).$$

The infinite continued fraction appearing in equation (3.4.74) can be summed "bottom to top" starting from some large truncation index N. Nollert [159] has shown that the convergence of the procedure improves if the sum is started using a wise choice for the value of the "rest" of the continued fraction, R_N, defined by the relation

$$R_N = \frac{\gamma_{N+1}}{\beta_{N+1} - \alpha_{N+1}R_{N+1}}\,. \tag{3.4.74}$$

Assuming that the rest can be expanded in a series of the form

$$R_N = \sum_{k=0}^{\infty} C_k N^{-k/2}\,, \tag{3.4.75}$$

it turns out that the first few coefficients in the series are $C_0 = -1$, $C_1 = \pm\sqrt{-2\mathrm{i}\omega}$, $C_2 = (3/4 + 2\mathrm{i}\omega)$ and $C_3 = \left[\ell(\ell+1)/2 + 2\omega^2 + 3\mathrm{i}\omega/2 + 3/32\right]/C_1$ (the latter coefficient contains a typo in [159], but this is irrelevant for numerical calculations).

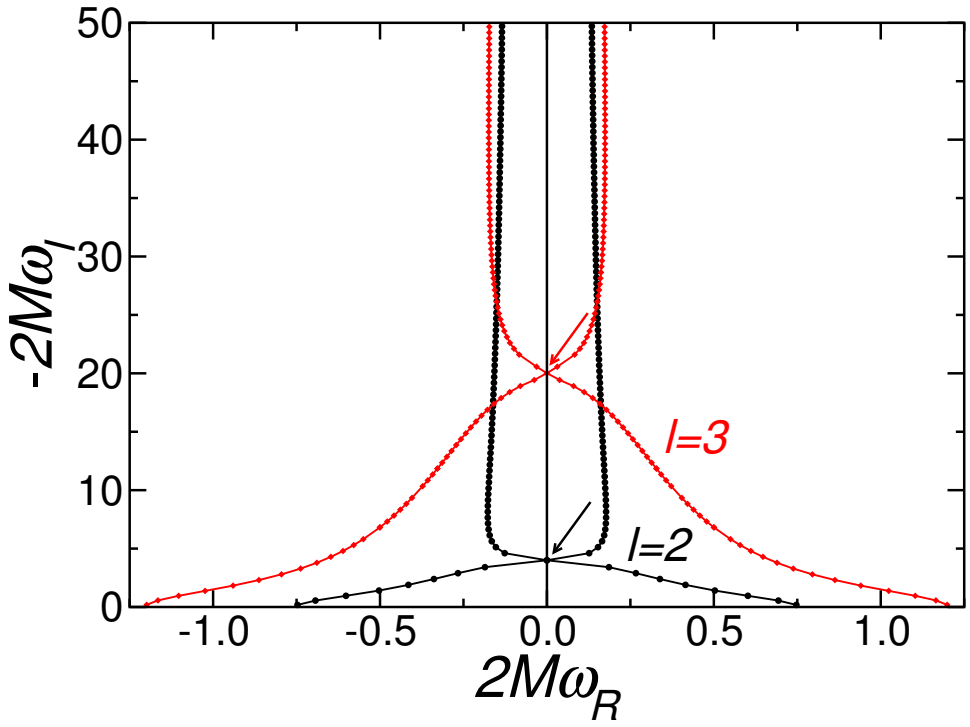

Figure 3.4: Quasinormal frequencies for gravitational perturbations with $\ell = 2$ (blue circles) and $\ell = 3$ (red diamonds). Compare eg. Figure 1 in [159]. In both cases we mark by an arrow the algebraically special mode, that is given analytically by Equation (3.4.77). Notice that as the imaginary part of the frequency tends to infinity the real part tends to a finite, *l-independent* limit. (From Ref. [44].)

The dominant QNM frequencies with $\ell = 2$ and $\ell = 3$ resulting from this procedure are shown in Table 3.1 and Figure 3.4. Reintroducing physical units, the

fundamental oscillation frequency $f = \omega_R/(2\pi)$ and the damping time $\tau = 1/|\omega_I|$ of an astrophysical black hole scale with mass according to the relation

$$f = 1.207 \left(\frac{10\ M_\odot}{M}\right) \text{kHz}\,, \qquad \tau = 0.5537 \left(\frac{M}{10\ M_\odot}\right) \text{ms}\,. \tag{3.4.76}$$

An "algebraically special" mode, whose frequency is (almost) purely imaginary, separates the lower QNM branch from the upper branch [66]. This algebraically special mode is located at

$$\tilde{\Omega}_\ell = \pm \mathrm{i} \frac{(\ell-1)\ell(\ell+1)(l+2)}{6}\,, \tag{3.4.77}$$

and it can be taken as roughly marking the onset of the asymptotic high-damping regime. The algebraically special mode quickly moves downwards in the complex plane (i.e., upwards in the figure) as ℓ increases: from Table 3.1 we see that it corresponds to an overtone index $n = 9$ when $\ell = 2$, and to an overtone index $n = 41$ when $\ell = 3$. This means that for high values of ℓ the asymptotic high-damping regime sets in later, becoming harder to probe using numerical methods. The algebraically special modes are a fascinating technical subject: they can be shown to be related to the instability properties of naked singularities [58], and (strictly speaking) they are not even QNMs, because they do not satisify QNM boundary conditions: see e.g. [33] and references therein.

Table 3.1: Representative Schwarzschild quasinormal frequencies for $\ell = 2$ and $\ell = 3$ (from [135]).

	$\ell = 2$	$\ell = 3$
n	$2M\omega_n$	$2M\omega_n$
1	(0.747343,-0.177925)	(1.198887,-0.185406)
2	(0.693422,-0.547830)	(1.165288,-0.562596)
3	(0.602107,-0.956554)	(1.103370,-0.958186)
4	(0.503010,-1.410296)	(1.023924,-1.380674)
5	(0.415029,-1.893690)	(0.940348,-1.831299)
6	(0.338599,-2.391216)	(0.862773,-2.304303)
7	(0.266505,-2.895822)	(0.795319,-2.791824)
8	(0.185617,-3.407676)	(0.737985,-3.287689)
9	(0.000000,-3.998000)	(0.689237,-3.788066)
10	(0.126527,-4.605289)	(0.647366,-4.290798)
11	(0.153107,-5.121653)	(0.610922,-4.794709)
12	(0.165196,-5.630885)	(0.578768,-5.299159)
20	(0.175608,-9.660879)	(0.404157,-9.333121)
30	(0.165814,-14.677118)	(0.257431,-14.363580)
40	(0.156368,-19.684873)	(0.075298,-19.415545)
41	(0.154912,-20.188298)	(-0.000259,-20.015653)
42	(0.156392,-20.685630)	(0.017662,-20.566075)
50	(0.151216,-24.693716)	(0.134153,-24.119329)
60	(0.148484,-29.696417)	(0.163614,-29.135345)

Nollert was the first to compute highly damped quasinormal frequencies corresponding to *gravitational* perturbations [159]. His main result was that the real parts of the quasinormal frequencies are well fitted, for large n, by a relation of the form

$$\omega_R = \omega_\infty + \frac{\lambda_{s,l}}{\sqrt{n}}\,. \tag{3.4.78}$$

These numerical results are perfectly consistent with analytical calculations [47]. Motl [156] analyzed the continued fraction condition (3.4.73) to find that highly damped quasinormal frequencies satisfy the relation

$$\omega \sim T_H \ln 3 + (2n+1)\pi \mathrm{i} T_H + \mathcal{O}(n^{-1/2})\,. \tag{3.4.79}$$

(in units $2M = 1$, the Hawking temperature of a Schwarzschild black hole $T_H = 1/4\pi$). This conclusion was later confirmed by complex-integration techniques [157] and phase-integral methods [17], and it may have a connection with Bekenstein's ideas on black-hole area quantization [116].

3.4.2 The WKB Approximation

While Leaver's method provides the most accurate numerical solution of the scattering problem, the WKB approximation is useful to develop physical intuition on the meaning of QNMs. The derivation below follows quite closely the paper by Schutz and Will [186], which in turn is based on the excellent treatment in the book by Bender and Orszag [32]. Consider the equation[5]

$$\frac{d^2\Psi}{dx^2} + Q(x)\Psi = 0\,, \tag{3.4.82}$$

where Ψ is the radial part of the perturbation variable (the time dependence has been separated by Fourier decomposition, and the angular dependence is separated using the scalar, vector or tensor spherical harmonics appropriate to the problem at hand). The coordinate x is a tortoise coordinate such that $x \to -\infty$ at the horizon and $x \to \infty$ at spatial infinity. The function $-Q(x)$ is constant in both limits ($x \to \pm\infty$) but not necessarily the same at both ends, and it rises to a maximum in the vicinity of $x = 0$ (more specifically, as we have seen above, at $r \simeq 3M$). Since $Q(x)$ tends to a constant at large $|x|$, we have

$$\Psi \sim e^{\pm \mathrm{i}\alpha x} \quad \text{as} \quad x \to \pm\infty \tag{3.4.83}$$

with $\mathrm{Re}(\alpha) > 0$. If $Q(x) \to 0$, $\omega = \alpha$. With our convention on the Fourier decomposition ($\Psi \sim e^{-\mathrm{i}\omega t}$), outgoing waves at $x \to \infty$ correspond to the positive sign in the equation above, and waves going into the horizon as $x \to -\infty$ correspond to the negative sign in the equation above (cf. Fig. 3.1).

The domain of definition of $Q(x)$ can be split in three regions: a region I to the left of the turning point where $Q(x_{\rm I}) = 0$, a "matching region" II with $x_{\rm I} < x < x_{\rm II}$, and a region III to the right of the turning point where $Q(x_{\rm II}) = 0$. As shown in Box 3.2, in regions I and III we can write the solution in the "physical optics" WKB approximation:

$$\Psi_{\rm I} \sim Q^{-1/4} \exp\left\{\pm \mathrm{i}\int_{x_2}^{x} [Q(t)]^{1/2} dt\right\}\,, \tag{3.4.84}$$

$$\Psi_{\rm III} \sim Q^{-1/4} \exp\left\{\pm \mathrm{i}\int_{x}^{x_1} [Q(t)]^{1/2} dt\right\}\,, \tag{3.4.85}$$

[5] In quantum mechanics, the Schrödinger equation for a particle of mass m and energy E moving in a one-dimensional potential $V(x)$

$$\left[-\frac{\hbar^2}{2m}\frac{d^2}{dx^2} + V(x)\right]\Psi = E\Psi \tag{3.4.80}$$

can be rewritten in the previous form with

$$-Q(x) = \frac{2m}{\hbar^2}\left[V(x) - E\right]\,. \tag{3.4.81}$$

Box 3.2 WKB Approximation: "Physical Optics"

Introduce a perturbative parameter ϵ (proportional to $\hbar$ in quantum mechanics) and write the ODE as

$$\epsilon^2 \Psi'' = Q(x)\Psi \,. \tag{3.4.86}$$

Note the sign difference with respect to Eq. (3.4.80). Now write the solution in the form

$$\Psi(x) \sim \exp\left[\frac{1}{\epsilon}\sum_{n=0}^{\infty}\epsilon^n S_n(x)\right] \,, \tag{3.4.87}$$

and compute the derivatives:

$$\Psi' \sim \left(\frac{1}{\epsilon}\sum_{n=0}^{\infty}\epsilon^n S_n'\right)\exp\left[\frac{1}{\epsilon}\sum_{n=0}^{\infty}\epsilon^n S_n\right] \,, \tag{3.4.88}$$

$$\Psi'' \sim \left[\frac{1}{\epsilon^2}\left(\sum_{n=0}^{\infty}\epsilon^n S_n'\right)^2 + \frac{1}{\epsilon}\sum_{n=0}^{\infty}\epsilon^n S_n''\right]\exp\left[\frac{1}{\epsilon}\sum_{n=0}^{\infty}\epsilon^n S_n\right] \,, \tag{3.4.89}$$

$$\tag{3.4.90}$$

Substituting into the ODE and dividing by the common exponential factors we get

$$(S_0')^2 + 2\epsilon S_0' S_1' + \epsilon S_0'' + \cdots = Q(x) \,. \tag{3.4.91}$$

The first two terms in the expansion yield the so-called "eikonal equation" and "transport equation":

$$(S_0')^2 = Q(x) \,, \tag{3.4.92}$$

$$2S_0' S_1' + S_0'' = 0 \,. \tag{3.4.93}$$

The solution to the eikonal equation is

$$S_0(x) = \int^x \sqrt{Q(t)}dt \,, \tag{3.4.94}$$

while the solution to the transport equation is

$$S_1(x) = -\frac{1}{4}\ln Q(x) + \text{constant} \,. \tag{3.4.95}$$

The leading-order solution is called the "geometrical optics" approximation. The next-to-leading order solution (including $S_1(x)$) is called the "physical optics" approximation. For higher-order solutions, cf. [32, 121, 133].

The idea is now to find the equivalent of the Bohr-Sommerfeld quantization rule from quantum mechanics. We want to relate two WKB solutions across the "matching region" whose limits are the classical turning points, where $\omega^2 = V(r)$. The technique works best when the classical turning points are close, i.e. when $\omega^2 \sim V_{\max}$, where $V_{\max}$ is the peak of the potential. In region II, we expand

$$Q(x) = Q_0 + \frac{1}{2}Q_0''(x - x_0)^2 + \mathcal{O}(x - x_0)^3 \,. \tag{3.4.96}$$

If we set $k \equiv Q_0''/2$ and we make the change of variables $t = (4k)^{1/4}e^{\mathrm{i}\pi/4}(x - x_0)$, we find that the equation reduces to

$$\frac{d^2\Psi}{dt^2} + \left[-\frac{\mathrm{i}Q_0}{(2Q_0'')^{1/2}} - \frac{1}{4}t^2\right]\Psi = 0 \,. \tag{3.4.97}$$

We now define a parameter ν such that

$$\nu + \frac{1}{2} = -\frac{\mathrm{i}Q_0}{(2Q_0'')^{1/2}}\,. \tag{3.4.98}$$

Then the differential equation takes the form

$$\frac{d^2\Psi}{dt^2} + \left[\nu + \frac{1}{2} - \frac{1}{4}t^2\right]\Psi = 0\,, \tag{3.4.99}$$

whose solutions are parabolic cylinder functions, commonly denoted by $D_\nu(z)$ [11, 32]. These special functions are close relatives of Hermite polynomials (this makes sense, because the quadratic approximation means that we locally approximate the potential as a quantum harmonic oscillator problem, and Hermite polynomials are well known to be the radial solutions of the quantum harmonic oscillator). The solution in region II is therefore a superposition of parabolic cylinder functions:

$$\Psi = AD_\nu(z) + BD_{-\nu-1}(\mathrm{i}z)\,, \quad z \equiv (2Q_0'')^{\frac{1}{4}} e^{\mathrm{i}\frac{\pi}{4}}(r_* - \bar{r}_*)\,. \tag{3.4.100}$$

Using the asymptotic behavior of parabolic cylinder functions [11,32] and imposing the outgoing-wave condition at spatial infinity we get, near the horizon,

$$\Psi \sim Ae^{-\mathrm{i}\pi\nu}z^\nu e^{-z^2/4} - \mathrm{i}\sqrt{2\pi}A\left[\Gamma(-\nu)\right]^{-1} e^{5i\pi/4}z^{-\nu-1}e^{z^2/4}\,. \tag{3.4.101}$$

QNM boundary conditions imply that the outgoing term, proportional to $e^{z^2/4}$, should be absent, so $1/\Gamma(-\nu) = 0$, or $\nu = n(= 0\,, 1\,, 2\,, ...)$. Therefore the leading-order WKB approximation yields a "Bohr-Sommerfeld quantization rule" defining the QNM frequencies:

$$Q_0/\sqrt{2Q_0''} = \mathrm{i}(n + 1/2)\,, \quad n = 0\,, 1\,, 2\,, ... \tag{3.4.102}$$

Higher-order corrections to this parabolic approximation have been computed [168]. Iyer and Will [120,121] carried out a third-order WKB expansion. If for brevity we define $\alpha = n + 1/2$, their result reads:

$$\omega^2 = \left[V_0 + (-2V_0'')^{1/2}\,\tilde{\Lambda}(n)\right] - \mathrm{i}\alpha\,(-2V_0'')^{1/2}\left[1 + \tilde{\Omega}(n)\right]\,, \tag{3.4.103}$$

where

$$\tilde{\Lambda}(n) = \frac{1}{(-2V_0'')^{1/2}}\left[\frac{1}{8}\left(\frac{V_0^{(4)}}{V_0''}\right)\left(\frac{1}{4} + \alpha^2\right) - \frac{1}{288}\left(\frac{V_0'''}{V_0''}\right)^2\left(7 + 60\alpha^2\right)\right]\,, \tag{3.4.104}$$

$$\begin{aligned}\tilde{\Omega}(n) &= \frac{1}{(-2V_0'')}\left[\frac{5}{6912}\left(\frac{V_0'''}{V_0''}\right)^4(77 + 188\alpha^2) - \frac{1}{384}\frac{V_0'''^2 V_0^{(4)}}{V_0''^3}(51 + 100\alpha^2)\right.\\ &+ \frac{1}{2304}\left(\frac{V_0^{(4)}}{V_0''}\right)^2(67 + 68\alpha^2) + \frac{1}{288}\frac{V_0'''V_0^{(5)}}{V_0''^2}\left(19 + 28\alpha^2\right)\\ &- \left.\frac{1}{288}\frac{V_0^{(6)}}{V_0''}\left(5 + 4\alpha^2\right)\right]\,.\end{aligned} \tag{3.4.105}$$

In the equations above, the overtone number is non-negative ($n = 0$, 1, 2, ...) for $\mathrm{Re}(\omega) > 0$, and negative ($n = -1$, -2, ...) for $\mathrm{Re}(\omega) < 0$. A subscript 0 on a variable means that it is evaluated at the value of r_* that corresponds to the maximum of the potential. For generic-spin perturbations of the Schwarzschild metric,

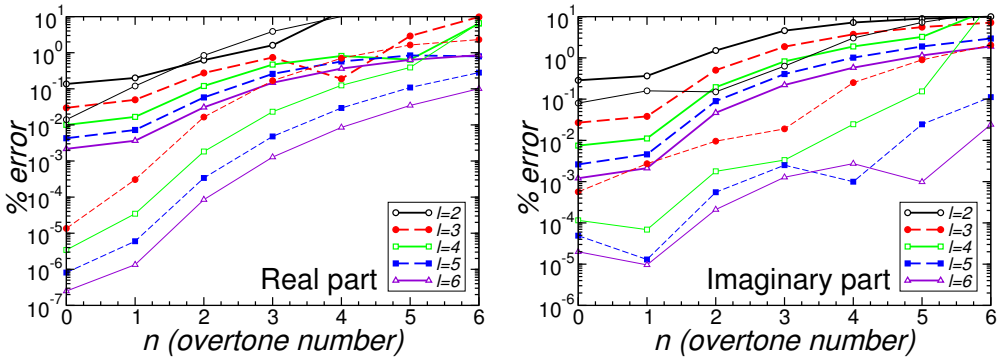

Figure 3.5: Accuracy of the WKB approximation for the real part (left panel) and imaginary part (right panel) of the QNM frequencies. (From Ref. [44].)

the potential is given by Eq. (3.1.14) and the location of the maximum is given by Eq. (3.1.16). In the Notebook QUASINORMAL_MODES_WKB.NB we implement these results and, as an application, we recover the Schwarzschild QNM frequencies reported by Iyer [120]. Konoplya [133] pushed the expansion up to sixth order. There is no rigorous proof of convergence, but the results do improve for higher WKB orders. Fig. 3.5 compares numerical results for the QNMs of Schwarzschild black holes from Leaver's continued fraction method against third-order (thick lines) and sixth-order (thin lines) WKB predictions. The WKB approximation works best for low overtones, i.e. modes with a small imaginary part, and in the eikonal limit of large ℓ (which corresponds to large quality factors, or large ω_R/ω_I). The method assumes that the potential has a single extremum, which is the case for most (but not all) black-hole potentials: see e.g. [119] for counterexamples.

3.5 Geodesic Stability and Black-Hole Quasinormal Modes

Let us reconsider the Bohr-Sommerfeld quantization condition (3.4.102). In a spherically symmetric, asymptotically flat spacetime of the form (2.2.14), the Klein-Gordon equation can be written as in Eq. (3.4.82) with the tortoise coordinate (2.4.77). In the eikonal limit ($\ell \to \infty$) we get

$$Q \simeq \omega^2 - f\frac{\ell^2}{r^2}\,. \tag{3.5.106}$$

It is easy to check that scalar, electromagnetic and gravitational perturbations of static black holes have the same behavior in the eikonal limit (in fact, the same conclusion applies to higher-dimensional spacetimes [119,126,127]). In other words, there is a well-defined geometrical optics (eikonal) limit where the potential for a wide class of massless perturbations is "universal". For Q in Eq. (3.5.106) above we find that the extremum r_0 of Q satisfies $2f(r_0) = r_0 f'(r_0)$, i.e. r_0 coincides with the location of the null circular geodesic r_c, as given by Eq. (2.4.74). Furthermore, the WKB formula (3.4.102) implies that, in the large-ℓ limit,

$$\omega_{\rm QNM} = \ell\frac{\sqrt{f_c}}{r_c} - i\frac{(n+1/2)}{\sqrt{2}}\sqrt{-\frac{r_c^2}{f_c}\left(\frac{d^2}{dr_*^2}\frac{f}{r^2}\right)_{r=r_c}}\,. \tag{3.5.107}$$

Comparing this result with Eqs. (2.4.76) and (2.4.79), it follows that

$$\omega_{\rm QNM} = \Omega_c\,\ell - i(n+1/2)\,|\lambda_0|\,. \tag{3.5.108}$$

This is one of the punchlines of these notes: **in the eikonal approximation, the real and imaginary parts of the QNMs of any spherically symmetric, asymptotically flat spacetime are given by (multiples of) the frequency and instability timescale of the unstable circular null geodesics.**

Dolan and Ottewill [83] have introduced a WKB-inspired asymptotic expansion of QNM frequencies and eigenfunctions in powers of the angular momentum parameter $l + 1/2$. Their asymptotic expansion technique is easily iterated to high orders, and it is very accurate (at least for spherically symmetric spacetimes). The asymptotic expansion also provides physical insight into the nature of QNMs, nicely connecting the geometrical understanding of QNMs as perturbations of unstable null geodesics with the singularity structure of the Green's function.

3.6 Superradiant Amplification

The discussion so far was limited to uncharged and/or nonrotating black holes. The inclusion of charge and rotation leads to the interesting possibility of superradiant amplification. I will first explain the conceptual foundations of superradiance, and then look at the astrophysically most interesting case of rotational superradiance in the Kerr spacetime. For a stationary, asymptotically flat black hole, the equations describing spin-s fields can be written in the form

$$\frac{d^2\Psi}{dr_*^2} + V(\omega, r)\Psi = 0\,, \tag{3.6.109}$$

where as usual ω is the frequency in a Fourier transform with respect to the asymptotic time coordinate: $\Psi(t) = e^{-i\omega t}\Psi(\omega)$, and the radius r_* is a convenient tortoise coordinate. As it turns out, the tortoise coordinate and the radial potential at the horizon ($r \to r_+$) and at infinity ($r \to \infty$) behave as follows:

$$\begin{cases} r_* \sim r\,, & V \sim \omega^2 & \text{as } r \to \infty\,, \\ e^{r_*} \sim (r - r_+)^\alpha\,, & V \sim (\omega - \varpi)^2 & \text{as } r \to r_+\,, \end{cases} \tag{3.6.110}$$

where α is a positive constant. The function ϖ can be related to rotation (in the Kerr geometry $\varpi = m\Omega$, with m an azimuthal number and $\Omega = a/(2Mr_+)$ the angular velocity of the horizon) or it can be a "chemical potential" (in the Reissner-Nordström geometry $\varpi = qQ$, where q is the charge of the perturbing field and Q the charge of the black hole).

Waves scattering in this background have the following asymptotic behavior:[6]

$$\Psi_1 \sim \begin{cases} \mathcal{T}_{\rm in}\,(r - r_+)^{-{\rm i}\alpha(\omega-\varpi)} + \mathcal{T}_{\rm out}\,(r - r_+)^{{\rm i}\alpha(\omega-\varpi)} & \text{as } r \to r_+\,, \\ \mathcal{R}\,{\rm e}^{{\rm i}\omega r} + {\rm e}^{-{\rm i}\omega r} & \text{as } r \to \infty\,. \end{cases} \tag{3.6.111}$$

These boundary conditions correspond to an incident wave of unit amplitude coming from infinity, giving rise to a reflected wave of amplitude $\mathcal{R}$ going back to infinity. At the horizon there is a transmitted wave of amplitude $\mathcal{T}_{\rm in}$ going into the horizon, and a wave of amplitude $\mathcal{T}_{\rm out}$ going out of the horizon.

Assuming a real potential (this is true for massive scalar fields and in most other cases), the complex conjugate of the solution Ψ_1 satisfying the boundary conditions (3.6.111) will satisfy the complex-conjugate boundary conditions:

$$\Psi_2 \sim \begin{cases} \mathcal{T}^*_{\rm in}(r - r_+)^{{\rm i}\alpha(\omega-\varpi)} + \mathcal{T}^*_{\rm out}(r - r_+)^{-{\rm i}\alpha(\omega-\varpi)} & \text{as } r \to r_+\,, \\ \mathcal{R}^*{\rm e}^{-{\rm i}\omega r} + {\rm e}^{{\rm i}\omega r} & \text{as } r \to \infty\,. \end{cases} \tag{3.6.112}$$

[6] For simplicity, here we consider a massless field, but the discussion is generalized to massive fields in a straightforward way.

These two solutions are linearly independent, and the standard theory of ODEs implies that their Wronskian $W \equiv \Psi_1 \partial_{r_*} \Psi_2 - \Psi_2 \partial_{r_*} \Psi_1$ is a constant (independent of r). If we evaluate the Wronskian near the horizon, we get

$$W = 2\mathrm{i}(\omega - \varpi) \left(|\mathcal{T}_{\rm in}|^2 - |\mathcal{T}_{\rm out}|^2 \right) , \tag{3.6.113}$$

and near infinity we find

$$W = -2\mathrm{i}\omega (|\mathcal{R}|^2 - 1) , \tag{3.6.114}$$

where we used $dr_*/dr = \frac{\alpha}{r - r_+}$. Equating the two yields

$$|\mathcal{R}|^2 = 1 - \frac{\omega - \varpi}{\omega} \left(|\mathcal{T}_{\rm in}|^2 - |\mathcal{T}_{\rm out}|^2 \right) . \tag{3.6.115}$$

The reflection coefficient $|\mathcal{R}|^2$ is usually less than unity, but there are some notable exceptions:

- If $|\mathcal{T}_{\rm in}| = |\mathcal{T}_{\rm out}|$, i.e., if there is no absorption by the black hole, then $|\mathcal{R}| = 1$.
- If $|\mathcal{T}_{\rm in}| > |\mathcal{T}_{\rm out}|$, i.e., if the hole absorbs more than what it gives away, there is superradiance in the regime $\omega < \varpi$. Indeed, for $\omega - \varpi < 0$ we have that $|\mathcal{R}|^2 > 1$. Such a scattering process, where the reflected wave has actually been amplified, is known as superradiance. Of course the excess energy in the reflected wave must come from energy "stored in the black hole", which therefore decreases.
- If $|\mathcal{T}_{\rm in}| < |\mathcal{T}_{\rm out}|$, there is superradiance in the opposite regime $\omega > \varpi$, but this condition also means that there is energy coming out of the black hole, so it is not surprising to see superradiance.

For the Schwarzschild spacetime $\varpi = 0$, and only waves going into the horizon are allowed ($\mathcal{T}_{\rm out} = 0$). Therefore

$$|\mathcal{R}|^2 = 1 - |\mathcal{T}_{\rm in}|^2 . \tag{3.6.116}$$

This is simply stating that energy is conserved.

If we impose the physical requirement that no waves should come out of the horizon ($\mathcal{T}_{\rm out} = 0$) and we set $\varpi = m\Omega$, as appropriate for superradiance in the Kerr metric, we get

$$|\mathcal{R}|^2 = 1 - \left(1 - \frac{m\Omega}{\omega} \right) |\mathcal{T}_{\rm in}|^2 . \tag{3.6.117}$$

Therefore superradiance in the Kerr spacetime will occur whenever

$$0 < \omega < m\Omega . \tag{3.6.118}$$

The amount of superradiant amplification depends on the specific field perturbing the black hole, and it must be obtained by direct integration of the wave equation.

There is no superradiance for fermions: can you tell why?

3.6.1 Massive Scalar Fields in the Kerr Metric

As a prototype of the general treatment of superradiance provided above, consider the Klein-Gordon equation (3.1.1) describing massive scalar field perturbations in the Kerr metric. In Boyer-Lindquist coordinates, the equation reads (see e.g. [82])

$$\left[\frac{(r^2 + a^2)^2}{\Delta} - a^2 \sin^2\theta \right] \frac{\partial^2 \Phi}{\partial t^2} + \frac{4iMamr}{\Delta} \frac{\partial \Phi}{\partial t} \tag{3.6.119}$$

$$-\frac{\partial}{\partial r}\left(\Delta\frac{\partial\Phi}{\partial r}\right)-\frac{1}{\sin\theta}\frac{\partial}{\partial\theta}\left(\sin\theta\frac{\partial\Phi}{\partial\theta}\right)-m^2\left[\frac{a^2}{\Delta}-\frac{1}{\sin^2\theta}\right]\Phi+\mu^2\Sigma\Phi=0\,,$$

where $a=J/M$, $\Delta\equiv r^2-2Mr+a^2$ and we assumed an azimuthal dependence $\Phi\sim e^{im\phi}$. The black-hole inner and outer horizons are located at the zeros of Δ, namely $r_\pm=M\pm\sqrt{M^2-a^2}$. Focus for simplicity on the case $\mu=0$. Assuming a harmonic time dependence and using spheroidal wave functions [38, 93], defined as

$$\frac{d}{dx}\left[(1-x^2)\frac{dS_{\ell m}}{dx}\right]+\left[(cx)^2+E_{\ell m}-\frac{m^2}{1-x^2}\right]S_{\ell m}=0 \tag{3.6.120}$$

(where $x=\cos\theta$ and $c=a\omega$) to separate the angular dependence, we write [53]:

$$\Phi=\int d\omega e^{-i\omega t}\sum_{\ell,m}e^{im\phi}\frac{R_{\ell m}(r,\omega)}{(r^2+a^2)^{1/2}}S_{\ell m}(\theta,\omega)\,. \tag{3.6.121}$$

As shown in the Notebook SEPARATION_MASSIVE_SCALAR_KERR.NB, this leads to the radial wave equation

$$\frac{d^2R_{\ell m}}{dr_*^2}+\left[\frac{K^2+(2am\omega-a^2\omega^2-E_{\ell m})\Delta}{(r^2+a^2)^2}-\frac{dG}{dr_*}-G^2\right]R_{\ell m}=0\,, \tag{3.6.122}$$

where

$$K=(r^2+a^2)\omega-am\,, \tag{3.6.123}$$

$$G=\frac{r\Delta}{(r^2+a^2)^2}\,, \tag{3.6.124}$$

$$\frac{dr_*}{dr}=\frac{r^2+a^2}{\Delta}\,. \tag{3.6.125}$$

$E_{\ell m}$ is an angular separation constant, equal to $\ell(\ell+1)$ when $a=0$ and obtained in more complicated ways when $a\neq0$ [38].

We can easily see that this potential satisfies the boundary conditions (3.6.110) for superradiance. As $r\to\infty$, $\Delta\sim r^2$, $K\sim\omega r^2$, $G\sim r^{-1}$, $dr_*/dr\sim1$, $dG/dr_*\sim dG/dr\sim r^{-2}$, and therefore the potential $V\sim K^2/(r^2+a^2)^2\sim(\omega r^2)^2/r^4\sim\omega^2$.

As $r\to r_+$, $\Delta=(r-r_+)(r-r_-)\to0$, $(r^2+a^2)\to2Mr_+$. Therefore $G\to0$, $dG/dr_*\sim\left[\Delta/(r^2+a^2)\right]dG/dr\to0$, and the dominant term is

$$\left(\frac{K}{r^2+a^2}\right)^2\sim\left[\frac{2Mr_+\omega-am}{2Mr_+}\right]^2=\left(\omega-m\frac{a}{2Mr_+}\right)^2=(\omega-m\Omega)^2\,. \tag{3.6.126}$$

Now, the previous treatment implies that

$$R_{\ell m}\sim\begin{cases}\mathcal{T}e^{-\mathrm{i}(\omega-m\Omega)r_*} & \text{as } r\to r_+\,,\\ \mathcal{R}\mathrm{e}^{\mathrm{i}\omega r_*}+\mathrm{e}^{-\mathrm{i}\omega r_*} & \text{as } r\to\infty\,.\end{cases} \tag{3.6.127}$$

The superradiant amplification for scalar perturbations with $\ell=m=2$ is shown in Fig. 3.6 (where I reproduce the results obtained in [18] by an independent frequency-domain numerical code). As a general rule, superradiant instabilities get stronger as the spin of the perturbing field increases.

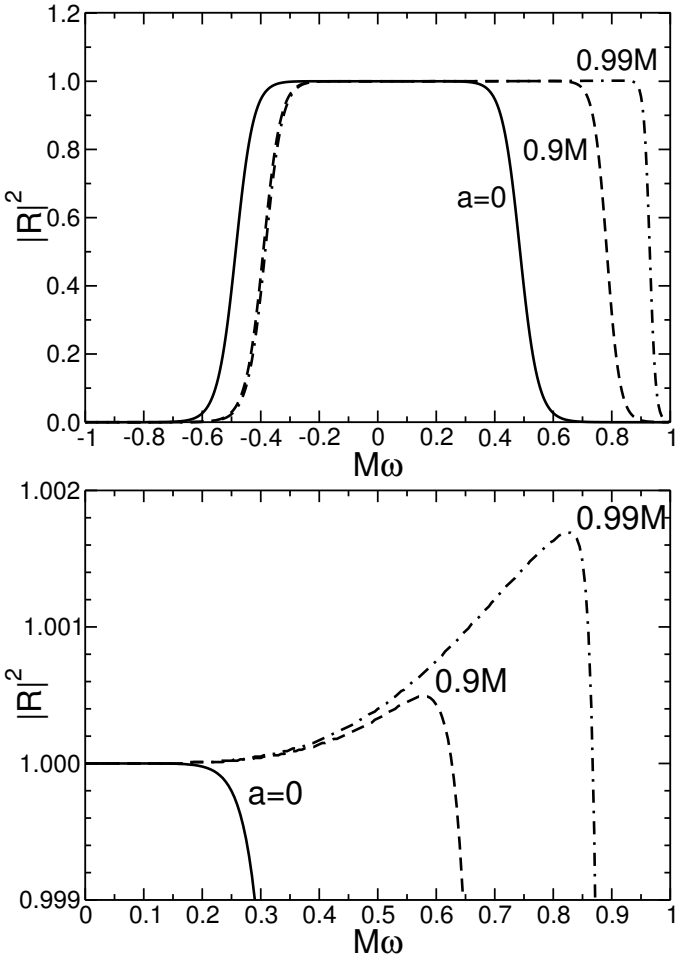

Figure 3.6: Superradiant amplification of scalar waves with $\ell = m = 2$ in Kerr black holes (cf. Fig. 1 of [18]). Superradiant amplification occurs when $M\omega \leq m(M\Omega)$. The bottom panel shows a close-up of the superradiant regime ($M\omega \leq 0.627$ for $a/M = 0.9$, and $M\omega \leq 0.868$ for $a/M = 0.99$).

4

Electromagnetic and gravitational perturbations

4.1 Vector and Tensor Spherical Harmonics

As a preliminary step to study perturbations induced by electromagnetic (vector) and gravitational (tensor) fields, we are interested in introducing a formalism to decompose the perturbations in appropriate (vector and tensor) generalizations of the spherical harmonics. The classic notation by Regge-Wheeler, Zerilli and Mathews [149,172,206] is not very transparent, and there are many different conventions in the gravitational-wave literature (see e.g. the classic review by Thorne [198], or Maggiore's book [141] for a more pedagogical account). Here we follow the notation first introduced by Gerlach and Sengupta [98–100], which has recently been revived in studies of stellar collapse [110,144,145], perturbations of higher-dimensional black holes [119, 126–128] and wave extraction in numerical relativity [49, 158].

Let us first "split" the spacetime coordinates as follows:

$$x^\mu = (z^A, y^a) \tag{4.1.1}$$

where

$$z^A = (\theta,\, \phi)\,, \quad y^a = (t,\, r)\,. \tag{4.1.2}$$

We introduce the metric on the sphere $ds^2 = \gamma_{AB} dz^A dz^B = (d\theta^2 + \sin^2\theta d\phi^2)$, i.e.

$$\gamma_{AB} \equiv \begin{pmatrix} 1 & 0 \\ 0 & \sin^2\theta \end{pmatrix} \tag{4.1.3}$$

and we denote the covariant derivative with respect to the metric γ_{AB} by ∇_A.

In Cartesian coordinates, the usual definition of the Levi-Civita symbol ϵ_{AB} can be written in matrix form:

$$\varepsilon_{AB} \equiv \begin{pmatrix} 0 & 1 \\ -1 & 0 \end{pmatrix} \tag{4.1.4}$$

This is not a tensor, but a tensor density of weight one[1]. It can be turned into a tensor if we multiply it by the Jacobian [2] $\sqrt{|\gamma|} = \sin\theta$. This yields the Levi-Civita tensor in spherical coordinates:

$$\varepsilon_{AB} \equiv \begin{pmatrix} 0 & \sin\theta \\ -\sin\theta & 0 \end{pmatrix}. \tag{4.1.5}$$

The spherical harmonics are eigenvectors of the Laplacian operator on the sphere. In other words, the associated Legendre equation (1.3.31) can be written in the elegant form

$$\gamma^{AB} \nabla_A \nabla_B Y^{\ell m} = -\ell(\ell+1) Y^{\ell m} \tag{4.1.6}$$

As stressed by Regge and Wheeler [172], under a rotation of the frame around the origin, the ten components of the perturbation tensor $h_{\mu\nu}$ transform as three SO(2) scalars h_{ab}, two SO(2) vectors h_{Aa} and one SO(2) second-order tensor h_{AB}, when considered as covariant quantities on the sphere. A parity transformation is a simultaneous inversion of all cartesian axes, which corresponds to the angular transformation $(\theta, \phi) \to (\pi - \theta, \pi + \phi)$. The spherical harmonics have parity $(-1)^\ell$, since $Y^{\ell m}(\pi - \theta, \pi + \phi) = (-1)^\ell Y^{\ell m}(\theta, \phi)$. The perturbations can be expanded in a complete basis using scalar, vector and tensor spherical harmonics with either the same parity as the spherical harmonics ("even" or "polar" quantities) or the opposite parity ("odd" or "axial" quantities). As shown in the Notebook GERLACH-SENGUPTA.NB, we can construct vector and tensor harmonics of a given parity by taking covariant derivatives on the sphere as follows:

- the polar vector harmonics

$$Y^{\ell m}_A \equiv \nabla_A Y^{\ell m} = (Y^{\ell m}_{,\theta}, Y^{\ell m}_{,\phi}); \tag{4.1.7}$$

- the axial vector harmonics

$$S^{\ell m}_A \equiv \varepsilon_{AC} \gamma^{BC} \nabla_B Y^{\ell m} = \varepsilon_A{}^B \nabla_B Y^{\ell m} = \left(\frac{1}{\sin\theta} Y^{\ell m}_{,\phi}, -\sin\theta Y^{\ell m}_{,\theta} \right); \tag{4.1.8}$$

- the polar rank-two tensor harmonics

$$Z^{\ell m}_{AB} \equiv \nabla_A \nabla_B Y^{\ell m} + \frac{\ell(\ell+1)}{2} \gamma_{AB} Y^{\ell m} = \frac{1}{2} \begin{pmatrix} W^{\ell m} & X^{\ell m} \\ X^{\ell m} & -\sin^2\theta W^{\ell m} \end{pmatrix}; \tag{4.1.9}$$

- the axial rank-two tensor harmonics

$$S^{\ell m}_{AB} \equiv \frac{1}{2}(\nabla_B S^{\ell m}_A + \nabla_A S^{\ell m}_B) = \frac{1}{2} \begin{pmatrix} \frac{1}{\sin\theta} X^{\ell m} & -\sin\theta W^{\ell m} \\ -\sin\theta W^{\ell m} & -\sin\theta X^{\ell m} \end{pmatrix}. \tag{4.1.10}$$

[1] See e.g. `http://www.physics.ucc.ie/apeer/PY4112/Tensors.pdf`.
[2] See e.g. Problem 3.20 in [139].

Here we have defined the following combinations, which will appear very often:

$$X^{\ell m} \equiv 2(Y^{\ell m}_{,\theta\phi} - \cot\theta Y^{\ell m}_{,\phi}) \tag{4.1.11}$$

$$W^{\ell m} \equiv Y^{\ell m}_{,\theta\theta} - \cot\theta Y^{\ell m}_{,\theta} - \frac{1}{\sin^2\theta} Y^{\ell m}_{,\phi\phi}\,. \tag{4.1.12}$$

In summary, the metric perturbation $h_{\mu\nu}$ can be decomposed in SO(2)-irreducible representations, which can be expanded in terms of the corresponding spherical harmonics. Leaving aside normalization issues, we can write, schematically:

$$\begin{aligned} h_{ab}(t,r,\theta,\phi) &= \bar{h}_{ab,\ell m}(t,r) Y^{\ell m}(\theta,\phi) \\ h_{aA}(t,r,\theta,\phi) &= h^{\rm pol}_{a,\ell m}(t,r) Y^{\ell m}_A(\theta,\phi) + h^{\rm ax}_{a,\ell m}(t,r) S^{\ell m}_A(\theta,\phi) \\ h_{AB}(t,r,\theta,\phi) &= r^2\left[K_{\ell m}(t,r)\gamma_{AB} Y^{\ell m}(\theta,\phi) + G_{\ell m}(t,r)\nabla_A\nabla_B Y^{\ell m}(\theta,\phi)\right] \\ &\quad + 2h_{\ell m}(t,r) S^{\ell m}_{AB}(\theta,\phi)\,. \end{aligned} \tag{4.1.13}$$

4.1.1 Orthogonality and Normalization Properties

We now want to fix the normalization of these harmonics. We define the scalar product on the two-sphere as

$$\langle f, g\rangle \equiv \int d\Omega f^* g = \int \sin\theta\, d\theta d\phi f^* g\,. \tag{4.1.14}$$

the scalar product between two SO(2) vectors as

$$\langle f_A,\, g_A\rangle \equiv \int d\Omega\, \gamma^{AB} f_A{}^*\, g_B\,, \tag{4.1.15}$$

and the scalar product between two SO(2) tensors as

$$\langle f_{AB},\, g_{AB}\rangle \equiv \int d\Omega\, \gamma^{AC}\gamma^{BD} f_{AB}{}^*\, g_{CD}\,. \tag{4.1.16}$$

Using the associated Legendre equation (1.3.31) and the orthogonality property for the scalar spherical harmonics

$$\langle Y^{\ell m}, Y^{\ell' m'}\rangle = \delta^{\ell\ell'}\delta^{mm'} \tag{4.1.17}$$

we have

$$\begin{aligned} \langle Y^{\ell m}_A, Y^{\ell m}_A\rangle = \langle S^{\ell m}_A, S^{\ell m}_A\rangle &= \int d\theta d\phi \sin\theta \left(Y^{*\ell m}_{,\theta} Y^{\ell m}_{,\theta} + \frac{1}{\sin^2\theta} Y^{*\ell m}_{,\phi} Y^{\ell m}_{,\phi}\right) \\ &= -\int d\theta d\phi \sin\theta Y^{*\ell m}\left(Y^{\ell m}_{,\theta\theta} + \cot\theta Y^{\ell m}_{,\theta} + \frac{Y^{\ell m}_{,\phi\phi}}{\sin^2\theta}\right) \\ &= \ell(\ell+1)\int d\theta d\phi \sin\theta Y^{*\ell m} Y^{\ell m} \\ &= \ell(\ell+1) = 2(n+1) \end{aligned} \tag{4.1.18}$$

where

$$n \equiv \frac{1}{2}(\ell-1)(\ell+2)\,. \tag{4.1.19}$$

The spin-two spin-weighted spherical harmonics can be shown to be given by

$${}_{-2}S^{\ell m}(\theta,\phi) \equiv \frac{1}{\sqrt{(\ell-1)\ell(\ell+1)(\ell+2)}}\left(W^{\ell m}(\theta,\phi) - \frac{i}{\sin\theta} X^{\ell m}(\theta,\phi)\right)\,, \tag{4.1.20}$$

and their orthogonality property

$$\langle {}_{-2}S^{\ell m},\, {}_{-2}S^{\ell' m'} \rangle = \delta^{\ell\ell'}\delta^{mm'} \tag{4.1.21}$$

implies

$$\begin{aligned}
&\langle Z^{\ell m}_{AB}, Z^{\ell' m'}_{AB} \rangle = \langle S^{\ell m}_{AB}, S^{\ell' m'}_{AB} \rangle \\
&= \frac{1}{2}\int d\theta d\phi \sin\theta \left(W^{*\ell m} W^{\ell' m'} + \frac{1}{\sin^2\theta} X^{*\ell m} X^{\ell' m'} \right) \\
&= \frac{1}{2}(\ell-1)\ell(\ell+1)(\ell+2)\delta^{\ell\ell'}\delta^{mm'} \\
&= 2n(n+1)\delta^{\ell\ell'}\delta^{mm'} \,.
\end{aligned} \tag{4.1.22}$$

In general, in the following we will consider the *inner product* $(\mathbf{R},\, \mathbf{T})$ of two tensors $\mathbf{T}$ and $\mathbf{R}$ on the two-sphere as

$$(\mathbf{R},\, \mathbf{T}) \equiv \int R_{\mu\nu} T_{\lambda\rho} \eta^{\mu\lambda} \eta^{\nu\rho} d\Omega \,, \tag{4.1.23}$$

where the integral is evaluated on a hypersurface with constant t and r, and

$$\eta^{\mu\nu} = \mathrm{diag}\left(-1, 1, \frac{1}{r^2}, \frac{1}{r^2 \sin^2\theta} \right) . \tag{4.1.24}$$

These considerations justify the normalization of the "standard" harmonics used by Zerilli and Regge-Wheeler, that we list below for reference.

4.1.2 Polar Spherical Harmonics

$$\mathbf{a}^{(0)}_{\ell m} = \begin{pmatrix} Y^{\ell m} & 0 & 0 & 0 \\ 0 & 0 & 0 & 0 \\ 0 & 0 & 0 & 0 \\ 0 & 0 & 0 & 0 \end{pmatrix} \tag{4.1.25}$$

$$\mathbf{a}^{(1)}_{\ell m} = -i\mathbf{a}^{(1),Z}_{\ell m} = \frac{1}{\sqrt{2}} \begin{pmatrix} 0 & Y^{\ell m} & 0 & 0 \\ Y^{\ell m} & 0 & 0 & 0 \\ 0 & 0 & 0 & 0 \\ 0 & 0 & 0 & 0 \end{pmatrix} \tag{4.1.26}$$

$$\mathbf{a}_{\ell m} = \begin{pmatrix} 0 & 0 & 0 & 0 \\ 0 & Y^{\ell m} & 0 & 0 \\ 0 & 0 & 0 & 0 \\ 0 & 0 & 0 & 0 \end{pmatrix} \tag{4.1.27}$$

$$\mathbf{b}^{(0)}_{\ell m} = -i\mathbf{b}^{(0),Z}_{\ell m} = \frac{n_\ell r}{\sqrt{2}} \begin{pmatrix} 0 & 0 & Y^{\ell m}_{,\theta} & Y^{\ell m}_{,\phi} \\ 0 & 0 & 0 & 0 \\ Y^{\ell m}_{,\theta} & 0 & 0 & 0 \\ Y^{\ell m}_{,\phi} & 0 & 0 & 0 \end{pmatrix} \tag{4.1.28}$$

$$\mathbf{b}_{\ell m} = \frac{n_\ell r}{\sqrt{2}} \begin{pmatrix} 0 & 0 & 0 & 0 \\ 0 & 0 & Y^{\ell m}_{,\theta} & Y^{\ell m}_{,\phi} \\ 0 & Y^{\ell m}_{,\theta} & 0 & 0 \\ 0 & Y^{\ell m}_{,\phi} & 0 & 0 \end{pmatrix} \tag{4.1.29}$$

$$\mathbf{f}_{\ell m} = \frac{m_\ell r^2}{\sqrt{2}} \begin{pmatrix} 0 & 0 & 0 & 0 \\ 0 & 0 & 0 & 0 \\ 0 & 0 & W^{\ell m} & X^{\ell m} \\ 0 & 0 & X^{\ell m} & -\sin^2\theta W^{\ell m} \end{pmatrix} \tag{4.1.30}$$

$$\mathbf{g}_{\ell m} = \frac{r^2}{\sqrt{2}} \begin{pmatrix} 0 & 0 & 0 & 0 \\ 0 & 0 & 0 & 0 \\ 0 & 0 & Y^{\ell m} & 0 \\ 0 & 0 & 0 & \sin^2\theta Y^{\ell m} \end{pmatrix} \tag{4.1.31}$$

4.1.3 Axial Spherical Harmonics

$$\mathbf{c}^{(0)}_{\ell m} = i\mathbf{c}^{(0),Z}_{\ell m} = \frac{in_\ell r}{\sqrt{2}} \begin{pmatrix} 0 & 0 & \frac{1}{\sin\theta}Y^{\ell m}_{,\phi} & -\sin\theta Y^{\ell m}_{,\theta} \\ 0 & 0 & 0 & 0 \\ \frac{1}{\sin\theta}Y^{\ell m}_{,\phi} & 0 & 0 & 0 \\ -\sin\theta Y^{\ell m}_{,\theta} & 0 & 0 & 0 \end{pmatrix} \tag{4.1.32}$$

$$\mathbf{c}_{\ell m} = \frac{in_\ell r}{\sqrt{2}} \begin{pmatrix} 0 & 0 & 0 & 0 \\ 0 & 0 & \frac{1}{\sin\theta}Y^{\ell m}_{,\phi} & -\sin\theta Y^{\ell m}_{,\theta} \\ 0 & \frac{1}{\sin\theta}Y^{\ell m}_{,\phi} & 0 & 0 \\ 0 & -\sin\theta Y^{\ell m}_{,\theta} & 0 & 0 \end{pmatrix} \tag{4.1.33}$$

$$\mathbf{d}_{\ell m} = \frac{im_\ell r^2}{\sqrt{2}} \begin{pmatrix} 0 & 0 & 0 & 0 \\ 0 & 0 & 0 & 0 \\ 0 & 0 & \frac{1}{\sin\theta}X^{\ell m} & -\sin\theta W^{\ell m} \\ 0 & 0 & -\sin\theta W^{\ell m} & -\sin\theta X^{\ell m} \end{pmatrix} \tag{4.1.34}$$

The following coefficients appear repeatedly in the normalization factors:

$$n_\ell = \frac{1}{\sqrt{\ell(\ell+1)}}\,, \qquad m_\ell = \frac{1}{\sqrt{\ell(\ell+1)(\ell-1)(\ell+2)}}\,. \tag{4.1.35}$$

Note that, schematically, these harmonics can be written in terms of the previous combinations as follows (a dagger † means that the corresponding elements of the matrix are obtained by symmetry):

$$\begin{aligned}
\mathbf{a}^{(0)}_{\ell m} &= \left(\begin{array}{cc|c} Y^{\ell m} & 0 & 0 \\ 0 & 0 & \\ \hline & 0 & 0 \end{array}\right) \\
\mathbf{a}^{(1)}_{\ell m} &= \frac{1}{\sqrt{2}}\left(\begin{array}{cc|c} 0 & Y^{\ell m} & 0 \\ \dagger & 0 & \\ \hline & 0 & 0 \end{array}\right) \\
\mathbf{a}_{\ell m} &= \left(\begin{array}{cc|c} 0 & 0 & 0 \\ 0 & Y^{\ell m} & \\ \hline & 0 & 0 \end{array}\right) \\
\mathbf{b}^{(0)}_{\ell m} &= \frac{n_\ell r}{\sqrt{2}}\left(\begin{array}{c|c} 0 & Y^{\ell m}_A \\ & 0 \\ \hline \dagger & 0 \end{array}\right) \\
\mathbf{b}_{\ell m} &= \frac{n_\ell r}{\sqrt{2}}\left(\begin{array}{c|c} 0 & 0 \\ & Y^{\ell m}_A \\ \hline \dagger & 0 \end{array}\right)
\end{aligned}$$

$$
\begin{aligned}
\mathbf{f}_{\ell m} &= m_\ell r^2 \sqrt{2} \left(\begin{array}{c|c} 0 & 0 \\ \hline 0 & Z^{\ell m}_{AB} \end{array} \right) \\
\mathbf{g}_{\ell m} &= \frac{r^2}{\sqrt{2}} \left(\begin{array}{c|c} 0 & 0 \\ \hline 0 & \gamma_{AB} Y^{\ell m} \end{array} \right) \\
\mathbf{c}^{(0)}_{\ell m} &= \frac{\mathrm{i} n_\ell r}{\sqrt{2}} \left(\begin{array}{c|c} 0 & S^{\ell m}_A \\ & 0 \\ \hline \dagger & 0 \end{array} \right) \\
\mathbf{c}_{\ell m} &= \frac{\mathrm{i} n_\ell r}{\sqrt{2}} \left(\begin{array}{c|c} 0 & 0 \\ & S^{\ell m}_A \\ \hline \dagger & 0 \end{array} \right) \\
\mathbf{d}_{\ell m} &= \mathrm{i} m_\ell r^2 \sqrt{2} \left(\begin{array}{c|c} 0 & 0 \\ \hline 0 & S^{\ell m}_{AB} \end{array} \right)
\end{aligned}
$$

4.1.4 *Normalization of the t–k Spherical Harmonics*

$$
\begin{aligned}
(\mathbf{a}^{(1)}_{\ell m}, \mathbf{a}^{(1)}_{\ell m}) &= \int a^{(1)*}_{\ell m \mu\nu} a^{(1)}_{\ell m \lambda\rho} \eta^{\mu\lambda} \eta^{\nu\rho} d\Omega \\
&= 2 \int \eta^{tt} \eta^{rr} \frac{(-i)i}{2} Y^\star_{\ell m} Y_{\ell m} d\Omega = - \int Y^\star_{\ell m} Y_{\ell m} d\Omega = -1
\end{aligned}
$$

$$
\begin{aligned}
(\mathbf{b}^{(0)}_{\ell m}, \mathbf{b}^{(0)}_{\ell m}) &= \int b^{(0)*}_{\ell m \mu\nu} b^{(0)}_{\ell m \lambda\rho} \eta^{\mu\lambda} \eta^{\nu\rho} d\Omega \\
&= 2 \int \frac{(-ir)ir}{2\ell(\ell+1)} \left\{ \eta^{tt} \eta^{\phi\phi} Y^\star_{\ell m,\phi} Y_{\ell m,\phi} + \eta^{tt} \eta^{\theta\theta} Y^\star_{\ell m,\theta} Y_{\ell m,\theta} \right\} d\Omega \\
&= -\frac{1}{\ell(\ell+1)} \int \left\{ \frac{Y^\star_{\ell m,\phi} Y_{\ell m,\phi}}{\sin^2\theta} + Y^\star_{\ell m,\theta} Y_{\ell m,\theta} \right\} \sin\theta d\theta d\phi \\
&= -\frac{1}{\ell(\ell+1)} \int Y^\star_{\ell m} \left\{ -Y_{\ell m,\theta\theta} - \cot\theta Y_{\ell m,\theta} + \frac{m^2 Y_{\ell m}}{\sin^2\theta} \right\} d\Omega \\
&= -\frac{1}{\ell(\ell+1)} \int Y^\star_{\ell m} \left\{ \ell(\ell+1) Y_{\ell m} \right\} d\Omega = -1
\end{aligned}
$$

$$
\begin{aligned}
(\mathbf{c}^{(0)}_{\ell m}, \mathbf{c}^{(0)}_{\ell m}) &= \int c^{(0)*}_{\ell m \mu\nu} c^{(0)}_{\ell m \lambda\rho} \eta^{\mu\lambda} \eta^{\nu\rho} d\Omega \\
&= 2 \int \frac{r^2}{2\ell(\ell+1)} \left\{ \eta^{tt} \eta^{\phi\phi} \sin^2\theta Y^\star_{\ell m,\theta} Y_{\ell m,\theta} + \eta^{tt} \eta^{\theta\theta} \frac{Y^\star_{\ell m,\phi} Y_{\ell m,\phi}}{\sin^2\theta} \right\} d\Omega \\
&= -\frac{1}{\ell(\ell+1)} \int \left\{ \frac{Y^\star_{\ell m,\phi} Y_{\ell m,\phi}}{\sin^2\theta} + Y^\star_{\ell m,\theta} Y_{\ell m,\theta} \right\} \sin\theta d\theta d\phi \\
&= -\frac{1}{\ell(\ell+1)} \int Y^\star_{\ell m} \left\{ -Y_{\ell m,\theta\theta} - \cot\theta Y_{\ell m,\theta} + \frac{m^2 Y_{\ell m}}{\sin^2\theta} \right\} d\Omega \\
&= -\frac{1}{\ell(\ell+1)} \int Y^\star_{\ell m} \left\{ \ell(\ell+1) Y_{\ell m} \right\} d\Omega = -1
\end{aligned}
$$

4.2 Electromagnetic Perturbations

As a warm-up problem in writing down perturbation equations using vector and tensor harmonics, consider a black hole perturbed by a test vector field (e.g. the electromagnetic vector potential A_μ). In spherical polar coordinates (t, r, θ, ϕ) we

can construct a basis of vector harmonics to expand the vector field by augmenting the vector harmonics on the sphere to include t and r components, as follows:

$$\begin{aligned}
\left[e_t Y^{\ell m}\right] &= (Y^{\ell m},\, 0,\, 0,\, 0)\,. && (4.2.36)\\
\left[e_r Y^{\ell m}\right] &= (0,\, Y^{\ell m},\, 0,\, 0)\,, && (4.2.37)\\
\left[\nabla Y^{\ell m}\right] &= (0,\, 0,\, Y^{\ell m}_{,\theta},\, Y^{\ell m}_{,\phi})\,, && (4.2.38)\\
\left[L Y^{\ell m}\right] &= (0,\, 0,\, ir\frac{1}{\sin\theta} Y^{\ell m}_{,\phi},\, -ir\sin\theta Y^{\ell m}_{,\theta})\,. && (4.2.39)
\end{aligned}$$

In the last two harmonics we recognize the covariant derivatives on the sphere, $Y^{\ell m}_{\rm A}$ and $irS^{\ell m}_{\rm A}$. We can now study Maxwell's equations in a Schwarzschild background:

$$\nabla_\nu F^{\mu\nu} = F^{\mu\nu}{}_{;\nu} = \frac{1}{\sqrt{-g}}\partial_\nu\left(\sqrt{-g}F^{\mu\nu}\right) = 0\,, \tag{4.2.40}$$

where the field tensor

$$F_{\mu\nu} \equiv A_{\nu;\mu} - A_{\mu;\nu} = A_{\nu,\mu} - A_{\mu,\nu}\,, \tag{4.2.41}$$

a comma stands for an ordinary derivative, and a semi-colon for a covariant derivative (the last equality above follows, of course, from the symmetry of the Christoffel symbols). As the background is spherically symmetric, we can expand $A_\mu(t,r,\theta,\phi)$ in 4-dimensional vector spherical harmonics [177]. Reabsorbing a factor of ir in the definition of $a^{\ell m}(t,r)$ below, we get:

$$A_\mu = \sum_{\ell,m}\left(\begin{bmatrix} 0 \\ 0 \\ \frac{a^{\ell m}(t,r)}{\sin\theta}Y^{\ell m}_{,\phi} \\ -a^{\ell m}(t,r)\sin\theta Y^{\ell m}_{,\theta}\end{bmatrix} + \begin{bmatrix} f^{\ell m}(t,r)Y^{\ell m} \\ h^{\ell m}(t,r)Y^{\ell m} \\ k^{\ell m}(t,r)Y^{\ell m}_{,\theta} \\ k^{\ell m}(t,r)Y^{\ell m}_{,\phi}\end{bmatrix}\right)\,, \tag{4.2.42}$$

where the first term on the right-hand side has parity $(-1)^{l+1}$ and the second term has parity $(-1)^l$, m is the azimuthal number and l the angular quantum number.

By plugging this expansion into Maxwell's equations (4.2.40) and using the ODE (1.3.31) (as well as its derivatives), we get the following system of equations (see the Notebook ScalarVectorPerturbations.nb):

$$\ell(\ell+1)[f^{\ell m} - \partial_t k^{\ell m}] - rf\left(2\partial_r f^{\ell m} + r\partial_r^2 f^{\ell m} - 2\partial_t h^{\ell m} - r\partial_t\partial_r h^{\ell m}\right) = 0\,, \tag{4.2.43}$$

$$\ell(\ell+1)[h^{\ell m} - \partial_r k^{\ell m}] + \frac{r^2}{f}\left(-\partial_r\partial_t f^{\ell m} + \partial_t^2 h^{\ell m}\right) = 0\,, \tag{4.2.44}$$

$$f\partial_r f[h^{\ell m} - \partial_r k^{\ell m}] + f^2[\partial_r h^{\ell m} - \partial_r^2 k^{\ell m}] - \partial_t f^{\ell m} + \partial_t^2 k^{\ell m} = 0 \tag{4.2.45}$$

$$\frac{\ell(\ell+1)f}{r^2}a^{\ell m} - f\partial_r f\partial_r a^{\ell m} - f^2\partial_r^2 a^{\ell m} + \partial_t^2 a^{\ell m} = 0\,. \tag{4.2.46}$$

The first and second equation are just the t and r components of Maxwell's equations (4.2.40); the third and fourth can be obtained from linear combinations of the θ and ϕ components. The last equation for $a^{\ell m}$ is already decoupled. We introduce the "tortoise coordinate" r_* defined by the relation

$$\frac{dr}{dr_*} = f\,, \tag{4.2.47}$$

so that

$$\partial_r a^{\ell m} = \frac{1}{f}\partial_{r_*} a^{\ell m}\,, \quad \partial_r^2 a^{\ell m} = -\frac{1}{f^2}\partial_r f\partial_{r_*} a^{\ell m} + \frac{1}{f^2}\partial_{r_*}^2 a^{\ell m}\,, \tag{4.2.48}$$

and the last equation can be recast in the Schrödinger form

$$\frac{\partial^2 a^{\ell m}}{\partial r_*^2} - \frac{\partial^2 a^{\ell m}}{\partial t^2} - V_{s=1}(r) a^{\ell m} = 0\,, \tag{4.2.49}$$

with

$$V_{s=1}(r) \equiv f \frac{\ell(\ell+1)}{r^2}\,. \tag{4.2.50}$$

We can eliminate $k^{\ell m}$ by taking a derivative of (4.2.43) with respect to r, a derivative of (4.2.44) with respect to t, and subtracting. We also define

$$\Upsilon^{\ell m} = \frac{r^2}{\ell(\ell+1)} \left(\partial_t h^{\ell m} - \partial_r f^{\ell m}\right)\,, \tag{4.2.51}$$

and use the definition of the tortoise coordinate to get:

$$\frac{\partial^2 \Upsilon^{\ell m}}{\partial r_*^2} - \frac{\partial^2 \Upsilon^{\ell m}}{\partial t^2} - V_{s=1}(r) \Upsilon^{\ell m} = 0\,, \tag{4.2.52}$$

where the potential V is the same as in Eq. (4.2.50). If we now assume a time dependence $a^{\ell m}(t,r) \propto e^{-\mathrm{i}\omega t}$, $\Upsilon^{\ell m} \propto e^{-\mathrm{i}\omega t}$, we conclude - as anticipated in Eq. (3.1.13) – that *both* equations for electromagnetic perturbations of the Schwarzschild geometry take the form

$$\frac{\partial^2 \Psi_\ell^{s=1}}{\partial r_*^2} + \left[\omega^2 - V_{s=1}\right] \Psi_\ell^{s=1} = 0\,, \tag{4.2.53}$$

where $\Psi_\ell^{s=1} = a^{\ell m}$ for odd-parity perturbations and $\Psi_\ell^{s=1} = \Upsilon^{\ell m}$ for even-parity perturbations.

4.3 Gravitational Perturbations

Gravitational perturbations are the most important, since they convey information about the structure of the gravitational field equations, but are also the most difficult to handle. The problem can be stated as follows: given a solution of Einstein's field equations, for instance the Minkowski or Schwarzschild geometry, how does a small perturbation *in the metric* evolve? A "small perturbation" here means anything – a wave, a falling particle, a celestial body – that disturbs slightly the background metric. To be more specific, suppose that, at least in some restricted region of spacetime, the metric functions can be written as

$$g_{\mu\nu}(x^\nu) = {}^{(0)}g_{\mu\nu}(x^\nu) + h_{\mu\nu}(x^\nu)\,, \tag{4.3.54}$$

where the metric ${}^{(0)}g_{\mu\nu}(x^\nu)$ is the background metric, given by some known solution of Einstein's equations, and $h_{\mu\nu}(x^\nu)$ is a small perturbation. The quantity $\mathbf{x}$ is a vector of spacetime coordinates. If we expand all quantities to first order in $h_{\mu\nu}$, we get to first order in $h_{\mu\nu}$

$$g^{\mu\nu} = {}^{(0)}g^{\mu\nu} - h^{\mu\nu}\,, \tag{4.3.55}$$

where we have to remember that indices are lowered and raised with the help of the background geometry. We also have

$$\Gamma^\mu_{\nu\lambda} = {}^{(0)}\Gamma^\mu_{\nu\lambda} + \delta\Gamma^\mu_{\nu\lambda}\,, \tag{4.3.56}$$

with

$$\delta\Gamma^\mu_{\nu\lambda} = \frac{1}{2}\, {}^{(0)}g^{\mu\rho} \left(h_{\rho\lambda;\,\nu} + h_{\rho\nu;\,\lambda} - h_{\nu\lambda;\,\rho}\right)\,, \tag{4.3.57}$$

and

$$R_{\mu\nu} = {}^{(0)}R_{\mu\nu} + \delta R_{\mu\nu}\,, \tag{4.3.58}$$

with

$$\delta R_{\mu\nu} = \delta\Gamma^{\rho}_{\mu\rho;\,\nu} - \delta\Gamma^{\rho}_{\mu\nu;\,\rho}\,. \tag{4.3.59}$$

The ten independent metric perturbations can be expanded in terms of the tensor spherical harmonics introduced in Section 4.1.

4.3.1 Gauge Fixing: the Regge-Wheeler Gauge

Our main conclusion in that section – Eq. ((4.1.13), that we reproduce here for convenience – was that the metric perturbation $h_{\mu\nu}$ can be decomposed as follows:

$$\begin{aligned}
h_{ab}(t,r,\theta,\phi) &= \bar{h}_{ab,\ell m}(t,r)Y^{\ell m}(\theta,\phi)\\
h_{aA}(t,r,\theta,\phi) &= h^{\rm pol}_{a,\ell m}(t,r)Y^{\ell m}_{A}(\theta,\phi) + h^{\rm ax}_{a,\ell m}(t,r)S^{\ell m}_{A}(\theta,\phi)\\
h_{AB}(t,r,\theta,\phi) &= r^2\left[K_{\ell m}(t,r)\gamma_{AB}Y^{\ell m}(\theta,\phi) + G_{\ell m}(t,r)\nabla_A\nabla_B Y^{\ell m}(\theta,\phi)\right]\\
&\quad +2h_{\ell m}(t,r)S^{\ell m}_{AB}(\theta,\phi)\,.
\end{aligned} \tag{4.3.60}$$

It is always possible to perform a gauge transformation to set certain coefficients to zero. [EB: Expand discussion] The choice of gauge made by Regge and Wheeler corresponds to setting

$$h^{\rm pol}_{a,\ell m}(t,r) = G_{\ell m}(t,r) = h_{\ell m}(t,r) = 0\,, \tag{4.3.61}$$

so (calling $h^{\rm ax}_a$ simply h_a)

$$h_{\mu\nu}(t,r,\theta,\phi) = \begin{pmatrix} \bar{h}_{ab,\ell m}(t,r)Y^{\ell m}(\theta,\phi) & h_{a,\ell m}(t,r)S^{\ell m}_{A}(\theta,\phi) \\ h_{a,\ell m}(t,r)S^{\ell m}_{A}(\theta,\phi) & r^2K_{\ell m}(t,r)\gamma_{AB}Y^{\ell m}(\theta,\phi) \end{pmatrix}\,, \tag{4.3.62}$$

where

$$\bar{h}_{ab,\ell m}(t,r) = \begin{pmatrix} H_{0,\ell m}(t,r) & H_{1,\ell m}(t,r) \\ H_{1,\ell m}(t,r) & H_{2,\ell m}(t,r) \end{pmatrix}\,, \tag{4.3.63}$$

and

$$\bar{h}_{a,\ell m}(t,r) = \begin{pmatrix} h_{0,\ell m}(t,r) \\ h_{1,\ell m}(t,r) \end{pmatrix}\,. \tag{4.3.64}$$

With this decomposition, the perturbations are described by two axial ($h_{0,\ell m}$, $h_{1,\ell m}$) and four polar ($H_{0,\ell m}$, $H_{1,\ell m}$, $H_{2,\ell m}$, $K_{\ell m}$) scalar functions. Omitting for brevity the ℓm subscript on the various coefficients, our starting point will be the axial (or odd) metric perturbation

$$h^{\rm ax}_{\mu\nu} = \begin{pmatrix} 0 & 0 & \frac{h_0}{\sin\theta}Y^{\ell m}_{,\phi} & -h_0\sin\theta Y^{\ell m}_{,\theta} \\ 0 & 0 & \frac{h_1}{\sin\theta}Y^{\ell m}_{,\phi} & -h_1\sin\theta Y^{\ell m}_{,\theta} \\ \frac{h_0}{\sin\theta}Y^{\ell m}_{,\phi} & \frac{h_1}{\sin\theta}Y^{\ell m}_{,\phi} & 0 & 0 \\ -h_0\sin\theta Y^{\ell m}_{,\theta} & -h_1\sin\theta Y^{\ell m}_{,\theta} & 0 & 0 \end{pmatrix} \tag{4.3.65}$$

and the polar (or even) metric perturbation

$$h^{\rm pol}_{\mu\nu} = \begin{pmatrix} -f(r)\,H_0Y_{\ell m} & -H_1Y_{\ell m} & 0 & 0 \\ -H_1Y_{\ell m} & -\frac{1}{f(r)}H_2Y_{\ell m} & 0 & 0 \\ 0 & 0 & -r^2KY_{\ell m} & 0 \\ 0 & 0 & 0 & -r^2\sin^2\theta KY_{\ell m} \end{pmatrix} \tag{4.3.66}$$

Recalling that spherical harmonics depend on ϕ through the combination $e^{im\phi}$, the line elements for axial and polar perturbations (that can be considered separately) can also be written as

$$ds^2 = -f(r)dt^2 + \frac{1}{f(r)}dr^2 + r^2d\theta^2 + r^2\sin^2\theta d\phi^2$$

$$
\begin{aligned}
&+ \quad im2h^0_{\ell m}\frac{1}{\sin\theta}Y_{\ell m}dtd\theta - 2h^0_{\ell m}\sin\theta Y^{\ell m}_{,\theta}dtd\phi \\
&+ \quad im2h^1_{\ell m}\frac{1}{\sin\theta}Y_{\ell m}drd\theta - 2h^1_{\ell m}\sin\theta Y^{\ell m}_{,\theta}drd\phi
\end{aligned} \tag{4.3.67}
$$

and

$$
\begin{aligned}
ds^2 &= -f(r)\left[1+H_0Y_{\ell m}\right]dt^2 + \frac{1}{f(r)}\left[1-H_2Y_{\ell m}\right]dr^2 \\
&+ r^2\left[1-KY_{\ell m}\right]d\theta^2 + r^2\sin^2\theta\left[1-KY_{\ell m}\right]d\phi^2 \\
&- 2H_1Y_{\ell m}dtdr\,.
\end{aligned} \tag{4.3.68}
$$

4.4 The Regge-Wheeler Equation

4.4.1 Vacuum Case

Calculations in perturbation theory are usually very lengthy, and it is convenient to use a symbolic manipulation package like Mathematica. The calculations in this section are performed in the Notebook REGGE_WHEELER_SCHWARSCHILD.NB.

If we insert decomposition (4.3.67) into the $t\phi$, $r\phi$ and $\theta\phi$ components of Einstein's equations and expand at first order in the metric perturbations we get the following system of equations [89, 199]:

$$
\left[4M-\ell(\ell+1)r\right]h_0 + ir(r-2M)\left(2\omega h_1 + \omega r h_1' - irh_0''\right) = 0\,, \tag{4.4.69}
$$

$$
2ir^2\omega h_0 + \left[(r-2M)(2-\ell-\ell^2)+r^3\omega^2\right]h_1 - ir^3\omega h_0' = 0\,, \tag{4.4.70}
$$

$$
ir^3\omega h_0 + (r-2M)\left[2Mh_1 + r(r-2M)h_1'\right] = 0\,, \tag{4.4.71}
$$

where primes denote derivatives with respect to r.

Equation (4.4.69) is redundant[3]. We can solve Eq. (4.4.71) for h_0:

$$
h_0 = \frac{i}{\omega r^2}\left(1-\frac{2M}{r}\right)\left[2Mh_1 + r(r-2M)h_1'\right] \tag{4.4.72}
$$

and substitute in Eq. (4.4.70) to get

$$
\begin{aligned}
&h_1\left[-(r-2M)(\ell^2+\ell-2)+r^3\omega^2-8M+\frac{20M^2}{r}\right] \\
&+(r-2M)\left[-2(r-5M)h_1' + r(r-2M)h_1''\right] = 0\,.
\end{aligned} \tag{4.4.73}
$$

If we define a new wavefunction $Z^{(-)}$ as

$$
Z^{(-)}(r) = \frac{1}{r}\left(1-\frac{2M}{r}\right)h_1(r) \tag{4.4.74}
$$

and substitute in (4.4.73), we get

$$
\frac{\partial^2 Z^{(-)}}{\partial r_*^2} + \left[\omega^2 - V^{(-)}_{s=-2}\right]Z^{(-)} = 0\,, \tag{4.4.75}
$$

where the potential $V^{(-)}_{s=-2}$ is

$$
V^{(-)}_{s=-2} = \left(1-\frac{2M}{r}\right)\left(\frac{\ell(\ell+1)}{r^2}-\frac{6M}{r^3}\right)\,. \tag{4.4.76}
$$

Note that $Z^{(-)}$ determines both h_1 and h_0, since

$$
h_0 = \frac{i}{\omega}\partial_{r_*}\left(rZ^{(-)}\right)\,. \tag{4.4.77}
$$

[3] In fact, if we evaluate the expression $\frac{if}{\omega}\partial_r R_{r\phi} - R_{t\phi}$ and we substitute h_0' using (4.4.70), we get Eq. (4.4.71).

4.4.2 Point-Particle Source Term

One of the simplest situation we can conceive is that of perturbations induced by a point particle of rest mass $m_0 \ll M$. As derived in detail in [167] [Eq. (5.108)], the stress-energy tensor for a point particle moving on a geodesic with world line $z^\mu(\tau)$ and four-velocity $u^\mu(\tau) = \frac{dz^\mu}{d\tau}$ (where τ denotes proper time) is given by

$$T^{\mu\nu} = m_0 c \int u^\mu u^\nu \frac{\delta(x^\mu - z^\mu(\tau))}{\sqrt{-g}} d\tau \,. \tag{4.4.78}$$

By setting $c = 1$, writing $d\tau = \frac{d\tau}{dT} dt$ – where in $\frac{dT}{d\tau}$ we can recognize the relativistic γ factor – and integrating in t, we can rewrite this as:

$$\begin{aligned} T^{\mu\nu} &= \frac{m_0}{\sqrt{-g}} \frac{dT}{d\tau} \frac{dz^\mu}{dt} \frac{dz^\nu}{dt} \delta(r - R(t)) \delta(\theta - \Theta(t)) \delta(\phi - \Phi(t)) \\ &= \frac{m_0}{r^2 |\sin\Theta|} \frac{dT}{d\tau} \frac{dz^\mu}{dt} \frac{dz^\nu}{dt} \delta(r - R(t)) \delta(\theta - \Theta(t)) \delta(\phi - \Phi(t)) \\ &= \frac{m_0}{r^2} \frac{dT}{d\tau} \frac{dz^\mu}{dt} \frac{dz^\nu}{dt} \delta(r - R(t)) \delta(\cos\theta - \cos\Theta(t)) \delta(\phi - \Phi(t)) \\ &= \frac{m_0}{r^2} \frac{dT}{d\tau} \frac{dz^\mu}{dt} \frac{dz^\nu}{dt} \delta(r - R(t)) \delta^{(2)}(\Omega - \Omega(t)) \,. \end{aligned} \tag{4.4.79}$$

In going from the second to the third line we used the well-known property of the delta function

$$\delta(f(x)) = \sum_{x = x_i} \frac{\delta(x - x_i)}{|f'(x_i)|} \,, \tag{4.4.80}$$

where the x_i's are the roots of $f(x) = 0$. We also introduced the definition

$$\delta^{(2)}(\Omega - \Omega(t)) = \delta(\phi - \Phi(t)) \delta(\cos\theta - \cos\Theta(t)) \,. \tag{4.4.81}$$

Of course this implies that

$$T_{\mu\nu} = g_{\mu\lambda} g_{\nu\rho} \frac{m_0}{r^2} \frac{dT}{d\tau} \frac{dz^\lambda}{dt} \frac{dz^\rho}{dt} \delta(r - R(t)) \delta^{(2)}(\Omega - \Omega(t)) \,. \tag{4.4.82}$$

The odd (axial) metric perturbations are sourced by the axial part of the particle's stress-energy tensor, which can be decomposed on the basis of the axial tensor spherical harmonics defined in Section 4.1.3:

$$\mathbf{T}^{\rm ax} = \sum_{\ell m} (Q_{\ell m}{}^{(0)} \mathbf{c}^{(0)}_{\ell m} + Q_{\ell m} \mathbf{c}_{\ell m} + D_{\ell m} \mathbf{d}_{\ell m}) \,. \tag{4.4.83}$$

The coefficients of the expansion are obtained by taking the *inner product* $(\mathbf{R}, \mathbf{T})$ of the tensor $\mathbf{T}$ with the corresponding harmonic $\mathbf{R}$, as defined in Eq. (4.1.23). So, for example, the coefficient $Q_{\ell m}$ can be obtained as:

$$\begin{aligned} Q_{\ell m} &= (\mathbf{c}_{\ell m}, \mathbf{T}) = \int c^*_{\ell m \mu\nu} T_{\lambda\rho} \eta^{\mu\lambda} \eta^{\nu\rho} d\Omega \\ &= \int_0^{2\pi} d\phi \int_{-1}^{1} d\cos\theta \eta^{\mu\lambda} \eta^{\nu\rho} c^*_{\ell m \mu\nu} T_{\lambda\rho} \,. \end{aligned} \tag{4.4.84}$$

Note however that, as shown in Section 4.1.4, the harmonics containing $t - k$ terms have negative norm, and therefore the corresponding coefficients (i.e., $A^{(1)}_{\ell m}$, $B^{(0)}_{\ell m}$, $Q^{(0)}_{\ell m}$) are defined with a minus sign. For example

$$\begin{aligned} Q^{(0)}_{\ell m} &= -(\mathbf{c}^{(0)}_{\ell m}, \mathbf{T}) = -\int c^{(0)*}_{\ell m \mu\nu} T_{\lambda\rho} \eta^{\mu\lambda} \eta^{\nu\rho} d\Omega = \\ &= -\int_0^{2\pi} d\phi \int_{-1}^{1} d\cos\theta \eta^{\mu\lambda} \eta^{\nu\rho} c^{(0)*}_{\ell m \mu\nu} T_{\lambda\rho} \,, \end{aligned}$$

and similarly for the other coefficients.

4.4.3 The Regge-Wheeler Equation with Source

As we saw earlier, the Regge-Wheeler equation only involves the $r\phi$ and $\theta\phi$ components of the Einstein equations, so in practice we only need to compute $Q_{\ell m}$ and $D_{\ell m}$.

The $r\phi$ and $\theta\phi$ components of the Einstein equations $\delta G_{\mu\nu} = 8\pi T_{\mu\nu}$ read:

$$\frac{1}{2}\frac{1}{f}\left\{\ddot{h_1} - \dot{h_0}' + \frac{2}{r}\dot{h_0} + \frac{2n}{r^2}fh_1\right\} = 8\pi\frac{in_\ell r}{\sqrt{2}}Q_{\ell m}\,,$$
$$\frac{1}{2}\left\{fh_1' + \frac{2M}{r^2}h_1 - \frac{1}{f}\dot{h_0}\right\} = 8\pi\frac{im_\ell r^2}{\sqrt{2}}D_{\ell m}\,,$$

or

$$\ddot{h_1} - \dot{h_0}' + \frac{2}{r}\dot{h_0} + \frac{2nf}{r^2}h_1 = A\,, \tag{4.4.85}$$
$$fh_1' + \frac{2M}{r^2}h_1 - \frac{1}{f}\dot{h_0} = B\,, \tag{4.4.86}$$

where

$$A \equiv 16\pi\frac{in_\ell rf}{\sqrt{2}}Q_{\ell m}\,, \tag{4.4.87}$$
$$B \equiv 16\pi\frac{im_\ell}{\sqrt{2}}r^2D_{\ell m}\,. \tag{4.4.88}$$

From Eq. (4.4.86) we get

$$\dot{h_0} = f^2h_1' + \frac{2Mf}{r^2}h_1 - fB \tag{4.4.89}$$

and

$$\dot{h_0}' = f^2h_1'' + \left(f^2\right)_{,r}h_1' + \left(\frac{2Mf}{r^2}\right)_{,r}h_1 + \frac{2Mf}{r^2}h_1' - (fB)_{,r} \tag{4.4.90}$$

and since

$$\left(f^2\right)_{,r} = \frac{4Mf}{r^2} \tag{4.4.91}$$

we find

$$\dot{h_0}' = f^2h_1'' + \frac{6Mf}{r^2}h_1' + \left(\frac{2Mf}{r^2}\right)_{,r}h_1 - (fB)_{,r}\,. \tag{4.4.92}$$

By replacing Eqs. (4.4.89) and (4.4.92) in Eq. (4.4.85) we get

$$\ddot{h_1} - f^2h_1'' - \frac{6Mf}{r^2}h_1' - \left(\frac{2Mf}{r^2}\right)_{,r}h_1 + (fB)_{,r} + \frac{2f^2}{r}h_1' + \frac{4Mf}{r^3}h_1 - \frac{2f}{r}B + \frac{2nf}{r^2}h_1 = A\,. \tag{4.4.93}$$

We now make the following substitution:

$$h_1 = \tfrac{r}{f}Z, \qquad \ddot{h_1} = \frac{r}{f}\ddot{Z} \tag{4.4.94}$$
$$h_1' = \left(\tfrac{r}{f}\right)_{,r}Z + \tfrac{r}{f}Z', \quad h_1'' = \left(\frac{r}{f}\right)_{,rr}Z + 2\left(\frac{r}{f}\right)_{,r}Z' + \frac{r}{f}Z'',$$

and consequently

$$f^2 h_1'' = f^2 \left(\frac{r}{f}\right)_{,rr} Z + 2f^2 \left(\frac{r}{f}\right)_{,r} Z' + rfZ''. \tag{4.4.95}$$

and Eq. (4.4.93) becomes

$$\begin{aligned}
&\frac{r}{f}\ddot{Z} - f^2 \left(\frac{r}{f}\right)_{,rr} Z - 2f^2 \left(\frac{r}{f}\right)_{,r} Z' - \frac{r}{f} Z'' \\
&+ \left[\frac{2}{r} f^2 - \frac{6M}{r^2} f\right] \left[\left(\frac{r}{f}\right)_{,r} Z + \frac{r}{f} Z'\right] \\
&+ \left[\frac{4M}{r^3} f - \left(\frac{2M}{r^2} f\right)_{,r} + \frac{2n}{r^2} f\right] \frac{r}{f} Z \\
&= A + \frac{2}{r} fB - (Bf)_{,r}
\end{aligned}$$

i.e.

$$\begin{aligned}
&\frac{r}{f}\ddot{Z} - f^2 \left(\frac{r}{f}\right)_{,rr} Z \\
&+ Z' \left\{-2f^2 \left(\frac{r}{f}\right)_{,r} + \left(\frac{2}{r} f^2 - \frac{6M}{r^2} f\right) \frac{r}{f}\right\} \\
&+ Z \left\{-f^2 \left(\frac{r}{f}\right)_{,rr} + \left(\frac{2}{r} f^2 - \frac{6M}{r^2} f\right) \left(\frac{r}{f}\right)_{,r} \right. \\
&\left. + \left[\frac{4M}{r^3} f - \left(\frac{2M}{r^2} f\right)_{,r} + \frac{2n}{r^2} f\right] \frac{r}{f}\right\} = A + \frac{2}{r} fB - (Bf)_{,r}
\end{aligned} \tag{4.4.96}$$

By explicitly computing the coefficients of Eq. (4.4.96) we find

$$\ddot{Z} - f^2 Z'' - \frac{2M}{r^2} fZ' - \frac{2f}{r^3} (3M - r - nr) Z = \frac{f}{r} \left[A + \frac{2}{r} fB - (Bf)_{,r}\right] \tag{4.4.97}$$

In addition, since

$$\frac{d}{dr_*} = f \frac{d}{dr} \quad \rightarrow \quad \frac{d^2}{dr_*^2} = f \frac{d}{dr} f \frac{d}{dr} = f^2 \frac{d^2}{dr^2} + \frac{2M}{r^2} f \frac{d}{dr}, \tag{4.4.98}$$

$$f^2 Z'' = \frac{d^2 Z}{dr_*^2} - \frac{2M}{r^2} fZ', \tag{4.4.99}$$

Eq. (4.4.97) yields

$$\begin{aligned}
&\ddot{Z} - \frac{d^2 Z}{dr_*^2} + \left[\frac{2M}{r^2} f - \frac{2M}{r^2} f\right] Z' - \frac{f}{r^3} \left[-2(n+1)r + 6M\right] Z \\
&= \frac{2^{2\nu}}{r} \left[A + \frac{2}{r} fB - (Bf)_{,r}\right].
\end{aligned} \tag{4.4.100}$$

The source term can be written as

$$\begin{aligned}
&\frac{f}{r} \left[A + \frac{2}{r} fB - (Bf)_{,r}\right] = \\
&\frac{16\pi\imath}{\sqrt{2}} \frac{f}{r} \left[n_\ell r f Q_{\ell m} + \frac{2}{r} m_\ell f r^2 D_{\ell m} - \left(m_\ell r^2 f D_{\ell m}\right)_{,r}\right] =
\end{aligned}$$

$$\frac{16\pi\imath}{\sqrt{2}}\frac{f}{r}\left[n_\ell r f Q_{\ell m}+2m_\ell f r D_{\ell m}-2m_\ell f r D_{\ell m}-m_\ell r^2\left(f D_{\ell m}\right)_{,r}\right]=$$
$$-\frac{16\pi\imath}{\sqrt{2}}\frac{f}{r}\left[m_\ell r^2\left(f D_{\ell m}\right)_{,r}-n_\ell r f Q_{\ell m}\right]$$
$$=-\frac{16\pi\imath}{\sqrt{2}\sqrt{\ell(\ell-1)(\ell+1)(\ell+2)}}\frac{f}{r}\left[r^2\left(f D_{\ell m}\right)_{,r}-\sqrt{(\ell-1)(\ell+2)}r f Q_{\ell m}\right].$$

Now recall that $2(n+1)=\ell(\ell+1)$, so we get our final result:

$$\ddot{Z}-\frac{d^2Z}{dr_*^2}+\frac{f}{r^3}\left[\ell(\ell+1)r-6M\right]Z \tag{4.4.101}$$
$$=-\frac{16\pi\imath}{\sqrt{2}\sqrt{\ell(\ell-1)(\ell+1)(\ell+2)}}\frac{f}{r}\left[r^2\left(f D_{\ell m}\right)_{,r}-\sqrt{(\ell-1)(\ell+2)}r f Q_{\ell m}\right].$$

This equation formally[4] coincides with that given by Zerilli in the erratum of [206] – see also Eqs. (A35) and (A36) of [178]) – after a Fourier transform ($\ddot{Z}\to-\omega^2 Z$).

4.4.4 *Calculation of $Q_{\ell m}$ and $D_{\ell m}$ for Equatorial Orbits*

Let us first consider

$$Q_{\ell m}=\int_0^{2\pi}d\phi\int_{-1}^{1}d\cos\theta\,\eta^{\mu\lambda}\eta^{\nu\rho}c^*_{\ell m\mu\nu}T_{\lambda\rho}\,. \tag{4.4.102}$$

The integrand is

$$\begin{aligned}\eta^{\mu\lambda}\eta^{\nu\rho}c^*_{\ell m\mu\nu}T_{\lambda\rho} &= 2\eta^{rr}\eta^{\phi\phi}c^*_{\ell mr\phi}T_{r\phi}+2\eta^{rr}\eta^{\theta\theta}c^*_{\ell mr\theta}T_{r\theta}\\ &= \frac{2c^*_{\ell mr\phi}T_{r\phi}}{r^2\sin^2\theta}+\frac{2}{r^2}c^*_{\ell mr\theta}T_{r\theta}\\ &= \frac{in_\ell\sqrt{2}}{r\sin\theta}\left(T_{r\phi}\frac{\partial Y^*_{\ell m}}{\partial\theta}-T_{r\theta}\frac{\partial Y^*_{\ell m}}{\partial\phi}\right).\end{aligned}$$

Let us evaluate separately $T_{r\phi}$ and $T_{r\theta}$:

$$\begin{aligned}T_{r\phi} &= \frac{m_0}{r^2}\frac{dT}{d\tau}g_{r\mu}\frac{dz^\mu}{dt}g_{\phi\nu}\frac{dz^\nu}{dt}\delta(r-R(t))\delta^{(2)}(\Omega-\Omega(t))\\ &= \frac{m_0}{r^2}\frac{dT}{d\tau}\frac{1}{f}\frac{dR}{dt}\left(g_{\phi\phi}\frac{d\Phi}{dt}\right)\delta(r-R(t))\delta^{(2)}(\Omega-\Omega(t))\\ &= \frac{m_0}{r^2}\frac{dT}{d\tau}\frac{1}{f}\frac{dR}{dt}\left(r^2\sin^2\theta\frac{d\Phi}{dt}\right)\delta(r-R(t))\delta^{(2)}(\Omega-\Omega(t))\\ &= m_0\frac{dT}{d\tau}\frac{1}{f}\frac{dR}{dt}\left(\frac{d\Phi}{dt}\right)\sin^2\theta\delta(r-R(t))\delta^{(2)}(\Omega-\Omega(t)),\end{aligned}$$

$$\begin{aligned}T_{r\theta} &= \frac{m_0}{r^2}\frac{dT}{d\tau}\frac{dR}{dt}\frac{1}{f}g_{\theta\theta}\frac{d\Theta}{dt}\delta(r-R(t))\delta^{(2)}(\Omega-\Omega(t))\\ &= m_0\frac{dT}{d\tau}\frac{dR}{dt}\frac{1}{f}\frac{d\Theta}{dt}\delta(r-R(t))\delta^{(2)}(\Omega-\Omega(t)).\end{aligned}$$

Therefore

$$\eta^{\mu\lambda}\eta^{\nu\rho}c^*_{\ell m\mu\nu}T_{\lambda\rho}=\frac{in_\ell\sqrt{2}}{r\sin\theta}m_0\frac{1}{f}\frac{dT}{d\tau}\frac{dR}{dt}\delta(r-R(t))\left\{\frac{d\Phi}{dt}\sin^2\theta\delta^{(2)}(\Omega-\Omega(t))\frac{\partial {Y_{\ell m}}^*}{\partial\theta}\right.$$

[4] However note that our expressions for $Q_{\ell m}$ and $D_{\ell m}$ differ from those given by Zerilli by a sign, because according to our choice of the metric $h_0^{ours}=-h_0^{Zer}$, and similarly for h_1.

$$-\frac{d\Theta}{dt}\delta^{(2)}(\Omega-\Omega(t))\frac{\partial {Y_{\ell m}}^*}{\partial\phi}\Bigg\}\,,$$

$$Q_{\ell m}=\frac{in_\ell\sqrt{2}}{r}m_0\frac{1}{f}\frac{dT}{d\tau}\frac{dR}{dt}\delta(r-R(t))\Bigg\{\frac{d\Phi}{dt}\int_0^{2\pi}d\phi$$
$$\int_{-1}^{1}d\cos\theta\,\sin\theta\frac{\partial {Y_{\ell m}}^*}{\partial\theta}\delta(\phi-\Phi(t))\delta(\cos\theta-\cos\Theta(t))$$
$$-\frac{d\Theta}{dt}\int_0^{2\pi}d\phi\int_{-1}^{1}d\cos\theta\,\frac{1}{\sin\theta}\frac{\partial {Y_{\ell m}}^*}{\partial\phi}\delta(\phi-\Phi(t))\delta(\cos\theta-\cos\Theta(t))\Bigg\}\,,$$

and consequently

$$Q_{\ell m}=\frac{in_\ell\sqrt{2}}{r}m_0\frac{1}{f}\frac{dR}{d\tau}\delta(r-R(t))\Bigg\{\frac{d\Phi}{dt}\sin\Theta(t)\,\frac{\partial {Y_{\ell m}}^*}{\partial\theta}\Big|_{(\Theta(t),\Phi(t))}$$
$$-\frac{1}{\sin\Theta(t)}\frac{\partial {Y_{\ell m}}^*}{\partial\phi}\Big|_{(\Theta(t),\Phi(t))}\Bigg\}\,.$$

For equatorial orbits ($\Theta(t)=\frac{\pi}{2}$) we get our final result:

$$Q_{\ell m}(r,t)=\frac{in_\ell\sqrt{2}}{r}m_0\frac{1}{f}\frac{dR}{d\tau}\delta(r-R(t))\left(\frac{d\Phi}{dt}Y^*_{\ell m,\theta}\Big|_{(\theta=\frac{\pi}{2},\Phi(t))}\right)\,. \tag{4.4.103}$$

Now let us compute

$$D_{\ell m}=\int_0^{2\pi}d\phi\int_{-1}^{1}d\cos\theta\eta^{\mu\lambda}\eta^{\nu\rho}d^*_{\ell m\mu\nu}T_{\lambda\rho}\,. \tag{4.4.104}$$

We find

$$\eta^{\mu\lambda}\eta^{\nu\rho}d^*_{\ell m\mu\nu}T_{\lambda\rho}=\eta^{\phi\lambda}\eta^{\phi\rho}d^*_{\ell m\phi\phi}T_{\lambda\rho}+\eta^{\theta\lambda}\eta^{\theta\rho}d^*_{\ell m\theta\theta}T_{\lambda\rho}+2\eta^{\theta\lambda}\eta^{\phi\rho}d^*_{\ell m\theta\phi}T_{\lambda\rho}=$$
$$=\frac{1}{r^4\sin^4\theta}T_{\phi\phi}d^*_{\ell m\phi\phi}+\frac{1}{r^4}d^*_{\ell m\theta\theta}T_{\theta\theta}+\frac{2}{r^4\sin^2\theta}d^*_{\ell m\theta\phi}T_{\theta\phi}=$$
$$=-\frac{im_\ell r^2}{\sqrt{2}}\left\{\frac{1}{r^4\sin^4\theta}(-\sin\theta X^*_{\ell m}T_{\phi\phi})+\frac{1}{r^4\sin\theta}X^*_{\ell m}T_{\theta\theta}+\frac{2}{r^4\sin^2\theta}(-\sin\theta W^*_{\ell m})T_{\theta\phi}\right\}=$$
$$=\frac{im_\ell}{\sqrt{2}}\left\{\frac{X^*_{\ell m}T_{\phi\phi}}{r^2\sin^3\theta}-\frac{X^*_{\ell m}T_{\theta\theta}}{r^2\sin\theta}+\frac{2W^*_{\ell m}T_{\theta\phi}}{r^2\sin\theta}\right\}\,.$$

For the quantities $T_{\phi\phi}$, $T_{\theta\theta}$ and $T_{\theta\phi}$ we have

$$\begin{aligned}T_{\phi\phi}&=\frac{m_0}{r^2}\frac{dT}{d\tau}\left(g_{\phi\mu}\frac{dz^\mu}{dt}\right)^2\delta(r-R(t))\delta^{(2)}(\Omega-\Omega(t))\\&=\frac{m_0}{r^2}\frac{dT}{d\tau}\left(r^2\sin^2\theta\frac{d\Phi}{dt}\right)^2\delta(r-R(t))\delta^{(2)}(\Omega-\Omega(t))\\&=m_0\frac{dT}{d\tau}r^2\sin^4\theta\left(\frac{d\Phi}{dt}\right)^2\delta(r-R(t))\delta^{(2)}(\Omega-\Omega(t))\end{aligned}$$

$$\begin{aligned}T_{\theta\theta}&=\frac{m_0}{r^2}\frac{dT}{d\tau}\left(g_{\theta\theta}\frac{d\Theta}{dt}\right)^2\delta(r-R(t))\delta^{(2)}(\Omega-\Omega(t))\\&=m_0r^2\frac{dT}{d\tau}\left(\frac{d\Theta}{dt}\right)^2\delta(r-R(t))\delta^{(2)}(\Omega-\Omega(t))\end{aligned}$$

$$\begin{aligned} T_{\theta\phi} &= \frac{m_0}{r^2}\frac{dT}{d\tau}g_{\theta\mu}\frac{dz^\mu}{dt}g_{\phi\nu}\frac{dz^\nu}{dt}\delta(r-R(t))\delta^{(2)}(\Omega-\Omega(t)) \\ &= \frac{m_0}{r^2}\frac{dT}{d\tau}r^2\frac{d\Theta}{dt}r^2\sin^2\theta\frac{d\Phi}{dt}\delta(r-R(t))\delta^{(2)}(\Omega-\Omega(t)) \\ &= m_0\frac{dT}{d\tau}r^2\sin^2\theta\frac{d\Theta}{dt}\frac{d\Phi}{dt}\delta(r-R(t))\delta^{(2)}(\Omega-\Omega(t)) \end{aligned}$$

Putting everything together:

$$\begin{aligned} \eta^{\mu\lambda}\eta^{\nu\rho}d^*_{\ell m\mu\nu}T_{\lambda\rho} &= \frac{im_\ell}{\sqrt{2}}m_0\frac{dT}{d\tau}\delta(r-R(t))\,\delta^{(2)}(\Omega-\Omega(t))\ \times \\ \times\left\{X^*_{\ell m}\left[\frac{1}{r^2\sin^3\theta}r^2\sin^4\theta\left(\frac{d\Phi}{dt}\right)^2-\frac{1}{r^2\sin\theta}r^2\left(\frac{d\Theta}{dt}\right)^2\right]+\right. \\ \left.+2W^*_{\ell m}\cdot\frac{1}{r^2\sin\theta}r^2\sin^2\theta\left(\frac{d\Theta}{dt}\right)\left(\frac{d\Phi}{dt}\right)\right\} &= \\ = \frac{im_\ell}{\sqrt{2}}m_0\frac{dT}{d\tau}\delta(r-R(t))\,\delta^{(2)}(\Omega-\Omega(t))\ \times \\ \times\left\{\frac{X^*_{\ell m}}{\sin\theta}\left[\sin^2\theta\left(\frac{d\Phi}{dt}\right)^2-\left(\frac{d\Theta}{dt}\right)^2\right]+2W^*_{\ell m}\sin\theta\left(\frac{d\Theta}{dt}\right)\left(\frac{d\Phi}{dt}\right)\right\}. \end{aligned}$$

For equatorial orbits $\Theta=\pi/2$ and $\frac{d\Theta}{dt}=0$, so our final result is:

$$D_{\ell m}=m_0\ \frac{im_\ell}{\sqrt{2}}\ \frac{dT}{d\tau}\ \delta(r-R(t))\left(\frac{d\Phi}{dt}\right)^2 X^*_{\ell m}\Big|_{\Theta=\frac{\pi}{2},\Phi(t)}\ . \tag{4.4.105}$$

4.4.5 Planar Geodesics

We can now use the geodesic equations

$$\frac{dT}{d\tau}=\frac{E}{1-\frac{2M}{r}},\qquad\text{and}\qquad\frac{d\Phi}{d\tau}=\frac{L_z}{r^2}. \tag{4.4.106}$$

to further simplify $Q_{\ell m}$ and $D_{\ell m}$. From the geodesic equations we have

$$\frac{d\Phi}{dt}=\frac{L_z}{r^2}\cdot\frac{1-2M/r}{E}\qquad\rightarrow\qquad\frac{1}{f}\frac{d\Phi}{dt}=\frac{L_z}{Er^2}$$

and $Q_{\ell m}$ becomes

$$\begin{aligned} Q_{\ell m}(r,t) &= m_0\ \frac{in_\ell\sqrt{2}}{E}\ \frac{L_z}{r^3}\frac{dR}{d\tau}\ \delta(r-R(t))\cdot Y^*_{\ell m,\theta}\Big|_{\theta=\frac{\pi}{2},\Phi(t)} \\ &= m_0\ in_\ell\sqrt{2}\frac{L_z}{r^3}\frac{1}{f}\frac{dR}{dt}\ \delta(r-R(t))\cdot Y^*_{\ell m,\theta}\Big|_{\theta=\frac{\pi}{2},\Phi(t)} \end{aligned} \tag{4.4.107}$$

In addition

$$X^*_{\ell m}=2\frac{\partial}{\partial\phi}\left[\frac{\partial}{\partial\theta}-\cot\theta\right]Y^*_{\ell m}=-2im\left[\frac{\partial}{\partial\theta}-\cot\theta\right]Y^*_{\ell m}$$

when evaluated at $\Theta=\pi/2$ becomes

$$X^*_{\ell m}\Big|_{\theta=\frac{\pi}{2},\Phi(t)}=-2im\frac{\partial}{\partial\theta}Y^*_{\ell m}\Big|_{\theta=\frac{\pi}{2},\Phi(t)}$$

Moreover

$$\frac{dT}{d\tau}\cdot\left(\frac{d\Phi}{dt}\right)^2=\frac{L_z^2}{E}\frac{f}{r^4}$$

and therefore $D_{\ell m}$ can be rewritten as follows:

$$D_{\ell m}=m_0\,\frac{im_\ell}{\sqrt{2}}\,\frac{L_z^2}{E}\,\frac{f}{r^4}\,\delta(r-R(t))\cdot(-2im)\frac{\partial}{\partial\theta}Y^*_{\ell m}\Big|_{\theta=\frac{\pi}{2},\Phi(t)}\ ,$$

and finally

$$D_{\ell m}=m_0\,\frac{2mm_\ell}{\sqrt{2}}\,\frac{L_z^2}{E}\,\frac{f}{r^4}\,\delta(r-R(t))\cdot\frac{\partial}{\partial\theta}Y^*_{\ell m}\Big|_{\theta=\frac{\pi}{2},\Phi(t)}\tag{4.4.108}$$

Summarizing: the stress-energy tensor components of interest for axial perturbations are

$$T_{r\phi} = -\frac{in_\ell r}{\sqrt{2}}Q_{\ell m}\ \sin\theta\ Y^{\ell m}_{,\theta}\,,\tag{4.4.109}$$

$$T_{\phi\theta} = -\frac{im_\ell r^2}{\sqrt{2}}D_{\ell m}\ \sin\theta\ W_{\ell m}\,,\tag{4.4.110}$$

where

$$Q_{\ell m}(r,t) = m_0\ in_\ell\sqrt{2}\frac{L_z}{r^3}\frac{1}{f}\frac{dR}{dt}\ \delta(r-R(t))\cdot Y^*_{\ell m,\theta}\Big|_{\theta=\frac{\pi}{2},\Phi(t)}\ ,\tag{4.4.111}$$

$$D_{\ell m}(r,t) = m_0\ \sqrt{2}mm_\ell\ \frac{L_z^2}{E}\frac{f}{r^4}\ \delta(r-R(t))\cdot Y^*_{\ell m,\theta}\Big|_{\theta=\frac{\pi}{2},\Phi(t)}\ .\tag{4.4.112}$$

4.5 The Zerilli Equation with Source

Let us now turn to the polar part of the perturbed metric (4.3.68), or (4.3.66) in matrix form. The relevant components of Einstein's equations, obtained from the Mathematica Notebook ZERILLI_SCHWARSCHILD_WITH_SOURCE.NB or Maple, are:

$$\delta G_{tt}=\left\{\left(1-\frac{2M}{r}\right)^2\frac{\partial^2K}{\partial r^2}+\frac{1}{r}\left(1-\frac{2M}{r}\right)\left(3-\frac{5M}{r}\right)\frac{\partial K}{\partial r}-\frac{1}{r}\left(1-\frac{2M}{r}\right)^2\frac{\partial H_2}{\partial r}\right.$$
$$\left.-\frac{1}{r^2}\left(1-\frac{2M}{r}\right)(H_2-K)-\frac{\ell(\ell+1)}{2r^2}\left(1-\frac{2M}{r}\right)(H_2+K)\right\}Y_{\ell m}\,,\tag{4.5.113}$$

$$\begin{aligned}\delta G_{tr} &= -\frac{Y_{\ell m}}{r^2(r-2M)}\left\{\frac{\partial}{\partial t}\left[\frac{\partial K}{\partial r}(2Mr^2-r^3)+H_2(r^2-2Mr)\right.\right.\\ &- \left.\left.K(r^2-3Mr)\right]+H_1(n+1)(r-2M)\right\}=\\ &= \left\{\frac{\partial}{\partial t}\left[\frac{\partial K}{\partial r}+\frac{K-H_2}{r}-\frac{M}{r(r-2M)}K\right]-\frac{\ell(\ell+1)}{2r^2}H_1\right\}Y_{\ell m}\,,\end{aligned}\tag{4.5.114}$$

$$\delta G_{t\phi}=-\frac{imY_{\ell m}}{2}\left\{\left(1-\frac{2M}{r}\right)\frac{\partial H_1}{\partial r}+\frac{2M}{r^2}H_1-\frac{\partial(H_2+K)}{\partial t}\right\}\,,\tag{4.5.115}$$

$$\begin{aligned}
\delta G_{rr} &= \frac{Y_{\ell m}}{r(r-2M)^2}\left\{r^3\frac{\partial^2 K}{\partial t^2}+(3Mr^2-r^2-2M^2)\frac{\partial K}{\partial r}\right.\\
&+ (4Mr-2r^2)\frac{\partial H_1}{\partial r}+(r^2-4Mr+4M^2)\frac{\partial H_0}{\partial r}\\
&+ \left.(r-2M)H_2+n(r-2M)K-H_0(n+1)(r-2M)\right\}\\
&= \left\{\left(1-\frac{2M}{r}\right)^{-2}\frac{\partial^2 K}{\partial t^2}-\frac{1-M/r}{r-2M}\frac{\partial K}{\partial r}-\frac{2}{r-2M}\frac{\partial H_1}{\partial t}+\frac{1}{r}\frac{\partial H_0}{\partial r}\right.\\
&+ \left.\frac{1}{r(r-2M)}(H_2-K)+\frac{\ell(\ell+1)}{2r(r-2M)}(K-H_0)\right\}Y_{\ell m}\,, \qquad (4.5.116)
\end{aligned}$$

$$\begin{aligned}
\delta G_{r\theta} &= -\frac{Y^{\ell m}_{,\theta}}{2(1-2M/r)}\left\{-\frac{\partial H_1}{\partial t}+\left(1-\frac{2M}{r}\right)\frac{\partial(H_0-K)}{\partial r}\right.\\
&+ \left.\frac{2M}{r^2}H_0+\frac{1-M/r}{r}(H_2-H_0)\right\}. \qquad (4.5.117)
\end{aligned}$$

To separate the angular part in $\delta G_{\phi\phi}$ and $\delta G_{\theta\theta}$ we take the following combinations of the perturbed Einstein's equations:

$$\begin{aligned}
&\frac{\delta G_{\theta\theta}}{\sin^2\theta}-\delta G_{\phi\phi}=\\
&= \frac{1}{2\sin^2\theta}\left\{\left[(\sin^2\theta)Y^{\ell m}_{,\theta\theta}-\sin\theta\cos\theta Y^{\ell m}_{,\theta}+m^2 Y_{\ell m}\right](H_0-H_2)\right\}\\
&= \left\{\frac{H_0-H_2}{2}\right\}W_{\ell m}\,, \qquad (4.5.118)
\end{aligned}$$

$$\begin{aligned}
&\frac{\delta G_{\theta\theta}}{\sin^2\theta}+\delta G_{\phi\phi}=\\
&= -r^2 Y_{\ell m}\left\{-\left(1-\frac{2M}{r}\right)^{-1}\frac{\partial^2 K}{\partial t^2}+\left(1-\frac{2M}{r}\right)\frac{\partial^2 K}{\partial r^2}\right.\\
&+ \left(1-\frac{M}{r}\right)\frac{2}{r}\frac{\partial K}{\partial r}-\left(1-\frac{2M}{r}\right)^{-1}\frac{\partial^2 H_2}{\partial t^2}+2\frac{\partial^2 H_1}{\partial r\partial t}-\left(1-\frac{2M}{r}\right)\frac{\partial^2 H_0}{\partial r^2}\\
&+ \frac{2(1-M/r)}{r-2M}\frac{\partial H_1}{\partial t}-\frac{1-M/r}{r}\frac{\partial H_2}{\partial r}-\frac{1+M/r}{r}\frac{\partial H_0}{\partial r}\\
&- \left.\frac{\ell(\ell+1)}{2r^2}(H_2-H_0)\right\}. \qquad (4.5.119)
\end{aligned}$$

The corresponding components of the stress-energy tensor can easily be obtained by inspection of the polar spherical harmonics:

$$T_{tt} = Y_{\ell m}A^{(0)}_{\ell m}\,, \qquad (4.5.120)$$

$$T_{tr} = \frac{Y_{\ell m}}{\sqrt{2}}A^{(1)}_{\ell m}\,, \qquad (4.5.121)$$

$$T_{rr} = Y_{\ell m}A_{\ell m}\,, \qquad (4.5.122)$$

$$T_{t\phi} = \frac{imn_\ell r Y_{\ell m}}{\sqrt{2}}B^{(0)}_{\ell m}\,, \qquad (4.5.123)$$

$$T_{r\theta} = \frac{n_\ell r Y^{\ell m}_{,\theta}}{\sqrt{2}} B_{\ell m}\,, \tag{4.5.124}$$

$$T_{\phi\phi} = \frac{r^2 \sin^2\theta}{\sqrt{2}} \left(Y_{\ell m} G_{\ell m} - m_\ell W_{\ell m} F_{\ell m}\right)\,, \tag{4.5.125}$$

$$T_{\theta\theta} = \frac{r^2}{\sqrt{2}} \left(Y_{\ell m} G_{\ell m} + m_\ell W_{\ell m} F_{\ell m}\right)\,. \tag{4.5.126}$$

We thus find our basic equations in the form[5]:

$$\begin{aligned}\delta G_{tt} \;\Rightarrow\; 8\pi A^{(0)}_{\ell m} = \Bigg\{ & \left(1-\frac{2M}{r}\right)^2 \frac{\partial^2 K}{\partial r^2} + \frac{1}{r}\left(1-\frac{2M}{r}\right)\left(3-\frac{5M}{r}\right)\frac{\partial K}{\partial r} \\ - \;& \frac{1}{r}\left(1-\frac{2M}{r}\right)^2 \frac{\partial H_2}{\partial r} - \frac{1}{r^2}\left(1-\frac{2M}{r}\right)(H_2 - K) \\ - \;& \frac{\ell(\ell+1)}{2r^2}\left(1-\frac{2M}{r}\right)(H_2+K)\Bigg\}\,,\end{aligned} \tag{4.5.129}$$

$$\begin{aligned}\delta G_{tr} \;\Rightarrow\; & \frac{8\pi i A^{(1),Z}_{\ell m}}{\sqrt{2}} = \frac{8\pi A^{(1)}_{\ell m}}{\sqrt{2}} = \\ = \;& \left\{\frac{\partial}{\partial t}\left[\frac{\partial K}{\partial r} + \frac{K-H_2}{r} - \frac{M}{r(r-2M)}K\right] - \frac{\ell(\ell+1)}{2r^2}H_1\right\}\,,\end{aligned} \tag{4.5.130}$$

$$\begin{aligned}\delta G_{rr} \;\Rightarrow\; & 8\pi A_{\ell m} = \\ = \;& \Bigg\{\left(1-\frac{2M}{r}\right)^{-2}\frac{\partial^2 K}{\partial t^2} - \frac{1-M/r}{r-2M}\frac{\partial K}{\partial r} - \frac{2}{r-2M}\frac{\partial H_1}{\partial t} + \frac{1}{r}\frac{\partial H_0}{\partial r} \\ + \;& \frac{1}{r(r-2M)}(H_2 - K) + \frac{\ell(\ell+1)}{2r(r-2M)}(K - H_0)\Bigg\}\,,\end{aligned} \tag{4.5.131}$$

$$\begin{aligned}\delta G_{t\phi} \;\Rightarrow\; & -8\pi\sqrt{2} r n_\ell i B^{(0),Z}_{\ell m} = -8\pi\sqrt{2} r n_\ell B^{(0)}_{\ell m} = \\ = \;& \left\{\left(1-\frac{2M}{r}\right)\frac{\partial H_1}{\partial r} + \frac{2M}{r^2}H_1 - \frac{\partial(H_2+K)}{\partial t}\right\}\,,\end{aligned} \tag{4.5.132}$$

$$\begin{aligned}\delta G_{r\theta} \;\Rightarrow\; & -8\pi\sqrt{2} n_\ell (r-2M) B_{\ell m} = \\ = \;& \Bigg\{-\frac{\partial H_1}{\partial t} + \left(1-\frac{2M}{r}\right)\frac{\partial(H_0 - K)}{\partial r} \\ + \;& \frac{2M}{r^2}H_0 + \frac{1-M/r}{r}(H_2 - H_0)\Bigg\}\,,\end{aligned} \tag{4.5.133}$$

[5]Our definition of the tensor spherical harmonics is slightly different from the one used by Zerilli. In writing Einstein's equations with source we must remember that our coefficients and Zerilli's coefficients are related by:

$$A^{(1)}_{\ell m} = i A^{(1),Z}_{\ell m}\,, \tag{4.5.127}$$

$$B^{(0)}_{\ell m} = i B^{(0),Z}_{\ell m}\,. \tag{4.5.128}$$

All other coefficients are equal.

$$\frac{\delta G_{\theta\theta}}{\sin^2(\theta)} - \delta G_{\phi\phi} \Rightarrow -8\pi\sqrt{2} m_\ell r^2 F_{\ell m} = \left\{ \frac{H_0 - H_2}{2} \right\}, \tag{4.5.134}$$

$$\begin{aligned}
&\frac{\delta G_{\theta\theta}}{\sin^2(\theta)} + \delta G_{\phi\phi} \Rightarrow -8\pi\sqrt{2} G_{\ell m} = \\
= \quad & \left\{ -\left(1 - \frac{2M}{r}\right)^{-1} \frac{\partial^2 K}{\partial t^2} + \left(1 - \frac{2M}{r}\right) \frac{\partial^2 K}{\partial r^2} \right. \\
+ \quad & \left(1 - \frac{M}{r}\right) \frac{2}{r} \frac{\partial K}{\partial r} - \left(1 - \frac{2M}{r}\right)^{-1} \frac{\partial^2 H_2}{\partial t^2} + 2 \frac{\partial^2 H_1}{\partial r \partial t} - \left(1 - \frac{2M}{r}\right) \frac{\partial^2 H_0}{\partial r^2} \\
+ \quad & \frac{2(1 - M/r)}{r - 2M} \frac{\partial H_1}{\partial t} - \frac{1 - M/r}{r} \frac{\partial H_2}{\partial r} - \frac{1 + M/r}{r} \frac{\partial H_0}{\partial r} \\
- \quad & \left. \frac{\ell(\ell+1)}{2r^2} (H_2 - H_0) \right\}.
\end{aligned} \tag{4.5.135}$$

These equations coincide those given by Zerilli [206], taking into account the relations (4.5.127) and (4.5.128).

4.5.1 Reducing the System to a Second-order Equation

Consider now the Fourier transform of the equations listed in the previous paragraph. Adopting the convention (1.4.35) on the Fourier transform of the perturbed quantities, the equations in the Fourier domain are simply obtained by replacing all time derivatives by the product $(-\mathrm{i}\omega)$. Solving the Fourier transforms of Eq. (4.5.130) for $\frac{dK}{dr}$ and the Fourier transform of Eq. (4.5.132) for $\frac{dH_1}{dr}$, we get:

$$\frac{dK}{dr} + \frac{1}{r} \frac{1 - \frac{3M}{r}}{1 - \frac{2M}{r}} K - \frac{H_2}{r} + \frac{\ell(\ell+1)}{2\mathrm{i}\omega r^2} H_1 = -\frac{4\pi\sqrt{2}}{\omega} A^{(1),Z}_{\ell m}, \tag{4.5.136}$$

$$\frac{dH_1}{dr} + \frac{\mathrm{i}\omega}{1 - \frac{2M}{r}} (K + H_2) + \frac{2M}{r^2} \left(1 - \frac{2M}{r}\right)^{-1} H_1 = -\frac{8\pi i\sqrt{2} n_\ell r^2}{r - 2M} B^{(0),Z}_{\ell m}. \tag{4.5.137}$$

Differentiating the Fourier transform of Eq. (4.5.134) with respect to r we find

$$\frac{dH_0}{dr} = \frac{dH_2}{dr} - 16\pi\sqrt{2} m_\ell \frac{d}{dr} \left(r^2 F_{\ell m}\right). \tag{4.5.138}$$

Substituting Eqs. (4.5.138) and (4.5.136) in (4.5.133) we get

$$\begin{aligned}
\frac{dH_2}{dr} \quad + \quad & \frac{1}{r} \frac{1 - \frac{3M}{r}}{1 - \frac{2M}{r}} K - \frac{1}{r} \frac{1 - \frac{4M}{r}}{1 - \frac{2M}{r}} H_2 + \left[\frac{\mathrm{i}\omega}{1 - \frac{2M}{r}} + \frac{\ell(\ell+1)}{2\mathrm{i}\omega r^2} \right] H_1 \\
= \quad & -\frac{4\pi\sqrt{2}}{\omega} A^{(1),Z}_{\ell m} - 8\pi\sqrt{2} n_\ell r B_{\ell m} \\
+ \quad & 16\pi\sqrt{2} m_\ell \left[\frac{d}{dr} \left(r^2 F_{\ell m}\right) - \frac{r(r - 3M)}{r - 2M} F_{\ell m} \right].
\end{aligned} \tag{4.5.139}$$

Substituting Eqs. (4.5.136), (4.5.137) and (4.5.139) in Eq. (4.5.131) we obtain an algebraic relation between H_2, H_1 and K:

$$- \quad \left[\frac{6M}{r} + (\ell - 1)(\ell + 2) \right] H_2 + \left[(\ell - 1)(\ell + 2) - \frac{2\omega^2 r^2}{1 - \frac{2M}{r}} + \frac{2M}{r} \frac{1 - \frac{3M}{r}}{1 - \frac{2M}{r}} \right] K$$

$$+ \quad \left[2\mathrm{i}\omega r + \frac{\ell(\ell+1)M}{\mathrm{i}\omega r^2}\right] H_1 = F(r)\,, \tag{4.5.140}$$

where the source-term contribution on the right-hand side is given by:

$$\begin{aligned} F(r) &= 16\pi r(r-2M)A_{\ell m} - \frac{8\pi\sqrt{2}M}{\omega}A^{(1),Z}_{\ell m} + 16\pi\sqrt{2}r(r-2M)n_\ell B_{\ell m} \\ &- 16\pi\sqrt{2}\left[(\ell-1)(\ell+2) + \frac{6M}{r}\right] m_\ell r^2 F_{\ell m}\,. \end{aligned}$$

To simplify the algebra, we will write the system of ordinary differential equations (4.5.136), (4.5.139) and (4.5.137), complemented by the algebraic relation (4.5.140), in the schematic form:

$$K' + \alpha K + \beta H_2 + \gamma H_1 = S_1\,, \tag{4.5.141}$$
$$H_2' + \alpha K + \delta H_2 + \epsilon H_1 = S_2\,, \tag{4.5.142}$$
$$H_1' + \xi K + \xi H_2 + \rho H_1 = S_3\,, \tag{4.5.143}$$
$$\theta H_2 + \lambda K + \mu H_1 = F\,. \tag{4.5.144}$$

Now we define the Zerilli function Z as the following linear combination of K and H_1:

$$Z \equiv \zeta K + \eta H_1\,, \tag{4.5.145}$$

where:

$$\begin{aligned} \zeta &= \frac{r^2}{nr+3M}\,, \\ \eta &= \frac{r-2M}{\mathrm{i}\omega(nr+3M)}\,. \end{aligned}$$

Taking the derivative of this relation, using the equations for K' and H_1' and eliminating H_2 by virtue of the algebraic relation (4.5.144) we find

$$Z' = C_K K + C_{H_1} H_1 + \Sigma\,, \tag{4.5.146}$$

where:

$$\begin{aligned} C_K &= \zeta' - \zeta(\alpha - \beta\lambda/\theta) - \eta(\xi - \xi\lambda/\theta)\,, \\ C_{H_1} &= \eta' - \zeta(\gamma - \beta\mu/\theta) - \eta(\rho - \xi\mu/\theta)\,, \\ \Sigma &= \zeta(S_1 - \beta F/\theta) + \eta(S_3 - \xi F/\theta)\,. \end{aligned}$$

Differentiating again and following the same procedure we have

$$\frac{d^2Z}{dr_*^2} = \left(1-\frac{2M}{r}\right)\frac{d}{dr}\left[\left(1-\frac{2M}{r}\right)Z'\right] = \tilde{C}_K K + \tilde{C}_{H_1} H_1 + \tilde{\Sigma}\,, \tag{4.5.147}$$

where now

$$\begin{aligned} \tilde{C}_K &= \left(1-\frac{2M}{r}\right)^2 \left[C_K' - C_K(\alpha - \beta\lambda/\theta) - C_{H_1}(\xi - \xi\lambda/\theta)\right] \\ &+ \left(1-\frac{2M}{r}\right)\frac{2M}{r^2}C_K\,, \\ \tilde{C}_{H_1} &= \left(1-\frac{2M}{r}\right)^2 \left[C_{H_1}' - C_{H_1}(\rho - \xi\mu/\theta) - C_K(\gamma - \beta\mu/\theta)\right] \end{aligned}$$

$$+ \quad \left(1-\frac{2M}{r}\right)\frac{2M}{r^2}C_{H_1}\,,$$

and the source term is given by:

$$\begin{aligned}\tilde{\Sigma} &= \left(1-\frac{2M}{r}\right)^2\left[\Sigma' + C_K(S_1-\beta F/\theta) + C_{H_1}(S_3-\xi F/\theta)\right]\\ &+ \left(1-\frac{2M}{r}\right)\frac{2M}{r^2}\Sigma\,. \end{aligned} \tag{4.5.148}$$

The linear system of Eqs. (4.5.145) and (4.5.146) can be solved to yield [cf. Eqs. (A37) and (A38) in [178], which correct typos in Zerilli's paper]:

$$\begin{aligned}K &= \frac{n(n+1)r^2+3nMr+6M^2}{r^2(nr+3M)}Z + \left(1-\frac{2M}{r}\right)Z'\\ &+ \frac{4\pi r(r-2M)}{\sqrt{n+1}(nr+3M)\omega}\left(\sqrt{2(n+1)}A^{(1),Z}_{\ell m}+2B^{(0),Z}_{\ell m}\right)\,,\end{aligned} \tag{4.5.149}$$

$$\begin{aligned}H_1 &= -\mathrm{i}\omega\frac{nr^2-3nMr-3M^2}{(r-2M)(nr+3M)}Z - \mathrm{i}\omega r Z'\\ &- \frac{8\sqrt{2}\pi i r^3}{\sqrt{2}(nr+3M)}\left(A^{(1),Z}_{\ell m}+\frac{2B^{(0),Z}_{\ell m}}{\sqrt{2(n+1)}}\right)\,.\end{aligned} \tag{4.5.150}$$

Backsubstituting these relations in Eq. (4.5.147) we finally get the Zerilli equation with source:

$$\frac{d^2Z}{dr_*^2}+\left[\omega^2-V_{\rm even}\right]Z = S\,, \tag{4.5.151}$$

where the potential is given by

$$V_{\rm even} = \left(1-\frac{2M}{r}\right)\frac{2n^2(n+1)r^3+6n^2Mr^2+18nM^2r+18M^3}{r^3(nr+3M)^2}\,. \tag{4.5.152}$$

Recall that $n\equiv(\ell-1)(\ell+2)/2$ [Eq. (4.1.19)]. In Zerilli's notation, and correcting several typos in the original paper, the source $S=S_{\ell m}$ is given by

$$\begin{aligned}S_{\ell m} &= -i\frac{r-2M}{r}\frac{d}{dr}\left[\frac{(r-2M)^2}{r(nr+3M)}\left(\frac{ir^2}{r-2M}\tilde{C}_{1\ell m}+\tilde{C}_{2\ell m}\right)\right]\\ &+ i\frac{(r-2M)^2}{r(nr+3M)^2}\left[\frac{n(n+1)r^2+3nMr+6M^2}{r^2}\tilde{C}_{2\ell m}\right.\\ &+ \left. i\frac{nr^2-3nMr-3M^2}{r-2M}\tilde{C}_{1\ell m}\right]\,,\end{aligned} \tag{4.5.153}$$

with[6]

$$\begin{aligned}\tilde{C}_{1\ell m} &= -\frac{8\pi}{\sqrt{2}\omega}A^{(1),Z}_{\ell m}-\frac{\tilde{B}_{\ell m}}{r}+16\pi\sqrt{2}rm_\ell F_{\ell m}\,,\\ \tilde{C}_{2\ell m} &= \frac{8\pi\sqrt{2}n_\ell r^2}{\mathrm{i}\omega(r-2M)}B^{(0),Z}_{\ell m}+\frac{ir}{r-2M}\tilde{B}_{\ell m}-\frac{16\pi i\sqrt{2}r^3m_\ell}{r-2M}F_{\ell m}\,,\\ \tilde{B}_{\ell m} &= \frac{8\pi r^2(r-2M)}{nr+3M}\left[A_{\ell m}+\sqrt{2}n_\ell B_{\ell m}\right]-\frac{4\pi\sqrt{2}Mr}{(nr+3M)\omega}A^{(1),Z}_{\ell m}\,.\end{aligned}$$

[6]Note that there is a typo in the definition of $\tilde{B}_{\ell m}$, Eq. (A42) in [178]: in their notation ($n\to\lambda$), the factor $\sqrt{\frac{2}{\lambda r+3M}}$ should read $\frac{\sqrt{2}}{(\lambda r+3M)}$.

The correct form of Zerilli's source term is given, e.g., in Eqs. (A45), (A46) and (A47) of [178]. The source $S_{\ell m}$ can be written in a more transparent way by factoring out the terms with different spherical harmonic coefficients:

$$\begin{aligned} S_{\ell m} = & - \frac{8\pi(r-2M)^2}{nr+3M} A_{\ell m} \\ & - \frac{8\pi\sqrt{2}(r-2M)M(nr+3r-3M)}{\omega r(nr+3M)^2} A^{(1),Z}_{\ell m} - \frac{4\pi\sqrt{2}(r-2M)^2}{\omega(nr+3M)} A^{(1),Z}_{\ell m\ ,r} \\ & - \frac{8\pi(r-2M)^2}{\sqrt{n+1}(nr+3M)} B_{\ell m} \\ & + \frac{8\pi(r-2M)(12M^2+r^2n^2+3nrM-6rM)}{\omega\sqrt{n+1}r(nr+3M)^2} B^{(0),Z}_{\ell m} \\ & - \frac{8\pi(r-2M)^2}{\omega\sqrt{n+1}(nr+3M)} B^{(0),Z}_{\ell m\ ,r} + \frac{8\pi\sqrt{2}(r-2M)}{\sqrt{n(n+1)}} F_{\ell m}\,. \end{aligned} \tag{4.5.154}$$

4.5.2 Point-Particle Source Term

We now turn to the computation of the functions we still need, that is, $A_{\ell m}$, $A^{(1)}_{\ell m}$, $B^{(0)}_{\ell m}$, $B_{\ell m}$ and $F_{\ell m}$. Let us first compute some more components of the stress-energy tensor, Eq. (4.4.82). We have:

$$T_{rr} = \frac{m_0}{r^2}\frac{dT}{d\tau}\frac{1}{f^2}\left(\frac{dR}{dt}\right)^2 \delta(r-R(t))\delta^{(2)}(\Omega-\Omega(t))\,, \tag{4.5.155}$$

$$\begin{aligned} T_{tr} &= \frac{m_0}{r^2}\frac{dT}{d\tau}(-f)\frac{1}{f}\frac{dR}{dt}\delta(r-R(t))\delta^{(2)}(\Omega-\Omega(t)) \\ &= -\frac{m_0}{r^2}\frac{dT}{d\tau}\frac{dR}{dt}\delta(r-R(t))\delta^{(2)}(\Omega-\Omega(t))\,, \end{aligned} \tag{4.5.156}$$

$$\begin{aligned} T_{r\theta} &= \frac{m_0}{r^2}\frac{dT}{d\tau}\frac{1}{f}\frac{dR}{dt}r^2\frac{d\Theta}{dt}\delta(r-R(t))\delta^{(2)}(\Omega-\Omega(t)) \\ &= m_0\frac{1}{f}\frac{dT}{d\tau}\frac{dR}{dt}\frac{d\Theta}{dt}\delta(r-R(t))\delta^{(2)}(\Omega-\Omega(t))\,, \end{aligned} \tag{4.5.157}$$

$$\begin{aligned} T_{t\phi} &= \frac{m_0}{r^2}\frac{dT}{d\tau}(-f)r^2\sin^2\theta\frac{d\Phi}{dt}\delta(r-R(t))\delta^{(2)}(\Omega-\Omega(t)) \\ &= -m_0 f\frac{dT}{d\tau}\frac{d\Phi}{dt}\sin^2\theta\delta(r-R(t))\delta^{(2)}(\Omega-\Omega(t))\,, \end{aligned} \tag{4.5.158}$$

$$\begin{aligned} T_{t\theta} &= \frac{m_0}{r^2}\frac{dT}{d\tau}(-f)r^2\frac{d\Theta}{dt}\delta(r-R(t))\delta^{(2)}(\Omega-\Omega(t)) \\ &= -m_0 f\frac{dT}{d\tau}\frac{d\Theta}{dt}\delta(r-R(t))\delta^{(2)}(\Omega-\Omega(t))\,. \end{aligned} \tag{4.5.159}$$

The components $T_{r\phi}$, $T_{r\theta}$, $T_{\theta\phi}$, $T_{\theta\theta}$ and $T_{\phi\phi}$ were computed when we evaluated the axial source terms.

Taking into account these results and the expressions for the polar spherical harmonics (Section 4.1.2) we find:

$$A_{\ell m} = \int d\Omega\ \left(\eta^{rr}\right)^2 a^*_{\ell mrr} T_{rr}$$

$$= \frac{m_0}{r^2}\frac{dT}{d\tau}\frac{1}{f^2}\left(\frac{dR}{dt}\right)^2 \delta(r-R(t))Y^*_{\ell m}\,\big|_{(\Theta(t),\Phi(t))}\ , \qquad (4.5.160)$$

$$\begin{aligned} A^{(1)}_{\ell m} &= iA^{(1),Z}_{\ell m} = -\int d\Omega\ 2\eta^{tt}\eta^{rr}\frac{1}{\sqrt{2}}Y^*_{\ell m}T_{tr} \\ &= -\frac{\sqrt{2}m_0}{r^2}\frac{dT}{d\tau}\frac{dR}{dt}\delta(r-R(t))Y^*_{\ell m}\,\big|_{(\Theta(t),\Phi(t))}\ , \end{aligned} \qquad (4.5.161)$$

$$\begin{aligned} B_{\ell m} &= \int d\Omega\ 2\left[\eta^{\phi\phi}\eta^{rr}b^*_{\ell m\phi r}T_{\phi r}+\eta^{\theta\theta}\eta^{rr}b^*_{\ell mr\theta}T_{r\theta}\right] \\ &= \int d\Omega\ 2\left[\frac{1}{r^2\sin^2\theta}\frac{n_\ell r}{\sqrt{2}}Y^*_{\ell m}m_0\frac{1}{f}\sin^2\theta\frac{dT}{d\tau}\frac{dR}{dt}\frac{d\Phi}{dt}\delta(r-R(t))\delta^{(2)}(\Omega-\Omega(t))\right. \\ &+ \left.\frac{1}{r^2}\frac{n_\ell r}{\sqrt{2}}Y^{\ell m*}_{,\theta}m_0\frac{1}{f}\frac{dT}{d\tau}\frac{dR}{dt}\frac{d\Theta}{dt}\delta(r-R(t))\delta^{(2)}(\Omega-\Omega(t))\right] = \\ &= \sqrt{\frac{2}{\ell(\ell+1)}}m_0\frac{dT}{d\tau}\frac{1}{r-2M}\frac{dR}{dt}\delta(r-R(t))\left[Y^*_{\ell m,\phi}\,\big|_{(\Theta(t),\Phi(t))}\frac{d\Phi}{dt}+Y^{\ell m*}_{,\theta}\,\big|_{(\Theta(t),\Phi(t))}\frac{d\Theta}{dt}\right] \\ &= \sqrt{\frac{2}{\ell(\ell+1)}}m_0\frac{dT}{d\tau}\frac{1}{r-2M}\frac{dR}{dt}\delta(r-R(t))\frac{dY^*_{\ell m}}{dt}\,\big|_{(\Theta(t),\Phi(t))}\ , \end{aligned} \qquad (4.5.162)$$

$$\begin{aligned} B^{(0)}_{\ell m} &= iB^{(0),Z}_{\ell m} = -\int d\Omega\ 2\left[\eta^{tt}\eta^{\phi\phi}b^{(0),*}_{\ell mt\phi}T_{t\phi}+\eta^{tt}\eta^{\theta\theta}b^{(0),*}_{\ell mt\theta}T_{t\theta}\right] \\ &= -\int d\Omega\ 2\left[-\frac{1}{r^2\sin^2\theta}\frac{n_\ell r}{\sqrt{2}}Y^*_{\ell m,\phi}m_0 f\sin^2\theta\frac{dT}{d\tau}\frac{d\Phi}{dt}\delta(r-R(t))\delta^{(2)}(\Omega-\Omega(t))\right. \\ &- \left.\frac{1}{r^2}\frac{n_\ell r}{\sqrt{2}}Y^{\ell m*}_{,\theta}m_0 f\frac{dT}{d\tau}\frac{d\Theta}{dt}\delta(r-R(t))\delta^{(2)}(\Omega-\Omega(t))\right] = \\ &= -\sqrt{\frac{2}{\ell(\ell+1)}}m_0\frac{dT}{d\tau}\frac{1-\frac{2M}{r}}{r}\delta(r-R(t))\left[Y^*_{\ell m,\phi}\,\big|_{(\Theta(t),\Phi(t))}\frac{d\Phi}{dt}+Y^{\ell m*}_{,\theta}\,\big|_{(\Theta(t),\Phi(t))}\frac{d\Theta}{dt}\right] \\ &= -\sqrt{\frac{2}{\ell(\ell+1)}}m_0\frac{dT}{d\tau}\frac{1-\frac{2M}{r}}{r}\delta(r-R(t))\frac{dY^*_{\ell m}}{dt}\,\big|_{(\Theta(t),\Phi(t))}\ , \end{aligned} \qquad (4.5.163)$$

$$\begin{aligned} F_{\ell m} &= \int d\Omega\ \left[\left(\eta^{\theta\theta}\right)^2 f^*_{\ell m\theta\theta}T_{\theta\theta}+\left(\eta^{\phi\phi}\right)^2 f^*_{\ell m\phi\phi}T_{\phi\phi}+2\eta^{\theta\theta}\eta^{\phi\phi}f^*_{\ell m\theta\phi}T_{\theta\phi}\right] \\ &= \int d\Omega\ \left[\frac{1}{r^4}\frac{m_\ell r^2}{\sqrt{2}}W^*_{\ell m}m_0\frac{dT}{d\tau}r^2\left(\frac{d\Theta}{dt}\right)^2\delta(r-R(t))\delta^{(2)}(\Omega-\Omega(t))\right. \\ &- \frac{1}{r^4\sin^4\theta}\frac{m_\ell r^2}{\sqrt{2}}\sin^2\theta W^*_{\ell m}m_0\frac{dT}{d\tau}r^2\sin^4\theta\left(\frac{d\Phi}{dt}\right)^2\delta(r-R(t))\delta^{(2)}(\Omega-\Omega(t)) \\ &+ \left.\frac{2}{r^4\sin^2\theta}\frac{m_\ell r^2}{\sqrt{2}}X^*_{\ell m}m_0\frac{dT}{d\tau}r^2\sin^2\theta\frac{d\Theta}{dt}\frac{d\Phi}{dt}\delta(r-R(t))\delta^{(2)}(\Omega-\Omega(t))\right] \\ &= \sqrt{2}m_\ell m_0\frac{dT}{d\tau}\delta(r-R(t))\left\{\frac{d\Theta}{dt}\frac{d\Phi}{dt}X^*_{\ell m}\,\big|_{(\Theta(t),\Phi(t))}\right. \\ &+ \left.\frac{1}{2}\left[\left(\frac{d\Theta}{dt}\right)^2-\sin^2\theta\left(\frac{d\Phi}{dt}\right)^2\right]W^*_{\ell m}\,\big|_{(\Theta(t),\Phi(t))}\right\}\ . \end{aligned} \qquad (4.5.164)$$

In computing $A^{(1)}_{\ell m}$ and $B^{(0)}_{\ell m}$ we have taken into account the minus sign due to the normalization of the harmonics: cf. the discussion following Eq. (4.1.23).

4.5.3 Circular Orbits

Let us consider the special case of circular orbits ($r = R_0$ =const). The geodesic equations become:

$$\frac{d\Phi}{d\tau} = \frac{L_z}{r^2} = \frac{L_z}{R_0^2}\,, \tag{4.5.165}$$

$$\frac{dT}{d\tau} = E\left(1-\frac{2M}{r}\right)^{-1} = E\left(1-\frac{2M}{R_0}\right)^{-1}\,, \tag{4.5.166}$$

$$\frac{dR}{d\tau} = 0\,. \tag{4.5.167}$$

In this case the particle's energy and angular momentum are given by:

$$E = \left(1-\frac{2M}{R_0}\right)\left(1-\frac{3M}{R_0}\right)^{-1/2}\,, \tag{4.5.168}$$

$$L_z = \sqrt{\frac{MR_0}{1-3M/R_0}}\,. \tag{4.5.169}$$

By inspection we can see that, using Eq. (4.5.167), the only non-zero functions appearing in the source term (4.5.154) are:

$$B^{(0),Z}_{\ell m} = i\sqrt{\frac{2}{\ell(\ell+1)}}m_0\frac{dT}{d\tau}\frac{1-\frac{2M}{r}}{r}\delta(r-R(t))\frac{dY^*_{\ell m}}{dt}\Big|_{(\Theta(t),\Phi(t))} \tag{4.5.170}$$

$$F_{\ell m} = \sqrt{2}m_\ell m_0\frac{dT}{d\tau}\delta(r-R(t))\left\{\frac{d\Theta}{dt}\frac{d\Phi}{dt}X^*_{\ell m}\Big|_{(\Theta(t),\Phi(t))}\right. \tag{4.5.171}$$

$$+ \left.\frac{1}{2}\left[\left(\frac{d\Theta}{dt}\right)^2 - \sin^2\theta\left(\frac{d\Phi}{dt}\right)^2\right]W^*_{\ell m}\Big|_{(\Theta(t),\Phi(t))}\right.\,.$$

Specializing to the equatorial plane ($\Theta(t)=\pi/2$, $\frac{d\Theta}{dt}=0$) we can also write:

$$\frac{dY^*_{\ell m}}{dt}\Big|_{(\pi/2,\Phi(t))} = \frac{d\Phi}{dt}Y^*_{\ell m,\phi}\Big|_{(\pi/2,\Phi(t))} + \frac{d\Theta}{dt}Y^*_{\ell m,\theta}\Big|_{(\pi/2,\Phi(t))} = \tag{4.5.172}$$

$$= \frac{d\Phi}{dt}Y^*_{\ell m,\phi}\Big|_{(\pi/2,\Phi(t))} = -im\frac{d\Phi}{d\tau}\frac{1}{\left(\frac{dT}{d\tau}\right)}Y^*_{\ell m}\Big|_{(\pi/2,\Phi(t))} =$$

$$= -im\frac{L_z}{R_0^2}\frac{1-2M/R_0}{E}Y^*_{\ell m}\Big|_{(\pi/2,\Phi(t))} = -im\sqrt{\frac{M}{R_0^3}}Y^*_{\ell m}\Big|_{(\pi/2,\Phi(t))}$$

where we have used Eqs. (4.5.168) and (4.5.169). So we have:

$$\frac{dY^*_{\ell m}}{dt}\Big|_{(\pi/2,\Phi(t))} = -im\omega_k Y^*_{\ell m}\Big|_{(\pi/2,\Phi(t))}\,, \tag{4.5.173}$$

where $\omega_k = \sqrt{M/R_0^3}$ is the Keplerian frequency. For a particle in an equatorial orbit $\phi = m\omega_k t$, and

$$Y^*_{\ell m}\Big|_{(\pi/2,\Phi(t))} = \sqrt{\frac{2\ell+1}{4\pi}}P_{\ell m}(\pi/2)e^{-im\omega_k t}, \tag{4.5.174}$$

se Eq. (4.5.170) yields:

$$B^{(0),Z}_{\ell m} = i\sqrt{\frac{2}{\ell(\ell+1)}}m_0\frac{dT}{d\tau}\frac{1-\frac{2M}{r}}{r}\delta(r-R(t))\frac{dY^*_{\ell m}}{dt}\Big|_{(\pi/2,\Phi(t))} \tag{4.5.175}$$

$$= i\sqrt{\frac{2}{\ell(\ell+1)}}\frac{m_0}{\sqrt{1-3M/R_0}}\frac{1-\frac{2M}{r}}{r}\delta(r-R_0)(-im\omega_k)Y^*_{\ell m}\big|_{(\pi/2,\Phi(t))} =$$
$$= \sqrt{\frac{2}{\ell(\ell+1)}}\frac{mm_0\omega_k}{\sqrt{1-3M/R_0}}\frac{1-\frac{2M}{r}}{r}\delta(r-R_0)\sqrt{\frac{2\ell+1}{4\pi}}P_{\ell m}(\pi/2)e^{-im\omega_k t}\,.$$

If we define the Fourier transform as: [EB: Careful with conventions!]

$$\tilde{B}^{(0),Z}_{\ell m} = \frac{1}{\sqrt{2\pi}}\int_{-\infty}^{+\infty} B^{(0),Z}_{\ell m}e^{\mathrm{i}\omega t}dt \tag{4.5.176}$$

and use the relation

$$\int_{-\infty}^{+\infty} e^{i(\omega-m\omega_k)t}dt = 2\pi\delta(\omega-m\omega_k) \tag{4.5.177}$$

we find:

$$\tilde{B}^{(0),Z}_{\ell m} = \sqrt{\frac{2}{\ell(\ell+1)}}\frac{mm_0\omega_k}{\sqrt{1-3M/R_0}}\frac{1-\frac{2M}{r}}{r}\sqrt{\frac{2\ell+1}{2}}P_{\ell m}(\pi/2)\delta(r-R_0)\delta(\omega-m\omega_k)\,. \tag{4.5.178}$$

For $F_{\ell m}$ we proceed in the same way. For equatorial orbits with $\Theta(t)=\pi/2$ and $\frac{d\Theta}{dt}=0$ the angular dependence reads

$$- \left\{\frac{\sin^2\theta}{2}\left(\frac{d\Phi}{dt}\right)^2\left[\frac{\partial^2}{\partial\theta^2}-\cot\theta\frac{\partial}{\partial\theta}-\frac{1}{\sin^2\theta}\frac{\partial^2}{\partial\phi^2}\right]Y^*_{\ell m}\right\}\big|_{(\pi/2,\Phi(t))} =$$
$$= -\left\{\frac{1}{2}\left(\frac{d\Phi}{dt}\right)^2\left[Y^*_{\ell m,\theta\theta}-Y^*_{\ell m,\phi\phi}\right]\right\}\big|_{(\pi/2,\Phi(t))}\,, \tag{4.5.179}$$

where we have used the definition of $W_{\ell m}$, Eq. (4.1.12). The Legendre equation implies

$$\left[Y^*_{\ell m,\theta\theta}+Y^*_{\ell m,\phi\phi}\right]\big|_{(\pi/2,\Phi(t))} = -\ell(\ell+1)Y^*_{\ell m}\big|_{(\pi/2,\Phi(t))}\,, \tag{4.5.180}$$

so we obtain:

$$\left[Y^*_{\ell m,\theta\theta}-Y^*_{\ell m,\phi\phi}\right]\big|_{(\pi/2,\Phi(t))} = \left[2m^2-\ell(\ell+1)\right]Y^*_{\ell m}\big|_{(\pi/2,\Phi(t))}\,. \tag{4.5.181}$$

Now we can proceed as before. Substituting the geodesic equations in Eq. (4.5.171) yields

$$F_{\ell m} = \frac{m_0\left[\ell(\ell+1)-2m^2\right]}{\sqrt{2(\ell-1)\ell(\ell+1)(\ell+2)}}\frac{M/R_0^3}{\sqrt{1-3M/R_0}}\delta(r-R_0)Y^*_{\ell m}\big|_{(\pi/2,\Phi(t))}\,. \tag{4.5.182}$$

Thus, the Fourier transform of $F_{\ell m}$ is:

$$\tilde{F}_{\ell m} = \frac{m_0\left[\ell(\ell+1)-2m^2\right]}{\sqrt{2(\ell-1)\ell(\ell+1)(\ell+2)}}\frac{M/R_0^3}{\sqrt{1-3M/R_0}}\times \tag{4.5.183}$$
$$\times \sqrt{\frac{2\ell+1}{2}}P_{\ell m}(\pi/2)\delta(r-R_0)\delta(\omega-m\omega_k)\,.$$

4.5.4 Radial Infall

Let us compute the source term for radial infalls with finite energy [43, 91]. In this case the only nonzero components of the four-velocity are u^r and u^t.

By looking at the expression (4.4.82) of the stress-energy tensor, we see that in principle there are three nonzero polar components: $A_{\ell m}$, $A^{(0)}_{\ell m}$ and $A^{(1)}_{\ell m}$. Only two of these components, namely $A_{\ell m}$ [Eq. (4.5.160)] and $A^{(1)}_{\ell m}$ [Eq. (4.5.161)], contribute to the source (4.5.154) of the Zerilli equation, that we rewrite here specializing to the case of radial infalls:

$$\begin{aligned} S_{\ell m} &= -\frac{8\pi(r-2M)^2}{nr+3M}A_{\ell m} - \frac{8\pi\sqrt{2}(r-2M)M(nr+3r-3M)}{\omega r(nr+3M)^2}A^{(1),Z}_{\ell m} \\ &- \frac{4\pi\sqrt{2}(r-2M)^2}{\omega(nr+3M)}A^{(1),Z}_{\ell m\ ,r}\,. \end{aligned} \tag{4.5.184}$$

From Eqs. (2.2.25) and (2.2.28) with $L=0$ we get (we now denote the coordinates along the particle's trajectory by capital letters):

$$\dot{T} \equiv \frac{dT}{d\tau} = \frac{E}{f}\,, \tag{4.5.185}$$

$$\dot{R} \equiv= -\left(E^2-f\right)^{1/2}\,. \tag{4.5.186}$$

Using the property of the δ function

$$\delta(r-R(t)) = \frac{\delta(t-T(r))}{|dR/dt|} = -\frac{\delta(t-T(r))}{dR/dt}\,, \tag{4.5.187}$$

considering orbits with $\Theta(t)\equiv 0$ and recalling the normalization of spherical harmonics we can rewrite

$$\begin{aligned} A_{\ell m}(t) &= \frac{m_0}{r^2}\frac{dT}{d\tau}\frac{1}{f^2}\left(\frac{dR}{dt}\right)^2\delta(r-R(t))Y^*_{\ell m}\left|_{(0,\Phi(t))}\right. \\ &= \frac{m_0}{r^2}\frac{1}{f^2}\left[-\dot{T}\frac{dR}{dt}\right]\delta(t-T(r))\sqrt{\frac{2\ell+1}{4\pi}} \\ &= \frac{m_0}{r^2}\frac{1}{f^2}\left[-\dot{R}\right]\delta(t-T(r))\sqrt{\frac{2\ell+1}{4\pi}} \\ &= \frac{m_0}{r^2}\frac{1}{f^2}\left[E^2-f(r)\right]^{1/2}\delta(t-T(r))\sqrt{\frac{2\ell+1}{4\pi}}\,, \end{aligned} \tag{4.5.188}$$

and by taking the Fourier transform [EB: Convention...]

$$\begin{aligned} A_{\ell m}(\omega) &= \frac{1}{\sqrt{2\pi}}\int\frac{m_0}{r^2}\frac{1}{f^2}\left[E^2-f(r)\right]^{1/2}\delta(t-T(r))\sqrt{\frac{2\ell+1}{4\pi}}\,e^{\mathrm{i}\omega t}dt \\ &= \frac{m_0}{r^2}\frac{1}{f^2}\left[E^2-f(r)\right]^{1/2}\sqrt{\frac{2\ell+1}{2}}\frac{1}{2\pi}e^{\mathrm{i}\omega T(r)}\,, \end{aligned} \tag{4.5.189}$$

Similarly:

$$\begin{aligned} A^{(1)}_{\ell m} &= -\frac{\sqrt{2}m_0}{r^2}\frac{dT}{d\tau}\frac{dR}{dt}\delta(r-R(t))Y^*_{\ell m}\left|_{(0,\Phi(t))}\right.\,, \\ &= \frac{\sqrt{2}m_0}{r^2}\frac{dT}{d\tau}\delta(t-T(r))Y^*_{\ell m}\left|_{(0,\Phi(t))}\right.\,, \\ &= \frac{\sqrt{2}m_0}{r^2}\frac{E}{f}\delta(t-T(r))\sqrt{\frac{2\ell+1}{4\pi}}\,, \end{aligned} \tag{4.5.190}$$

and by taking the Fourier transform [EB: Convention...]

$$A^{(1)}_{\ell m}(\omega) = \frac{1}{\sqrt{2\pi}}\int\frac{\sqrt{2}m_0}{r^2}\frac{E}{f}\delta(t-T(r))\sqrt{\frac{2\ell+1}{4\pi}}\,e^{\mathrm{i}\omega t}dt$$

$$= \frac{\sqrt{2}m_0}{r^2}\frac{E}{f}\sqrt{\frac{2\ell+1}{2}}\frac{1}{2\pi}e^{\mathrm{i}\omega T(r)}\,. \tag{4.5.191}$$

We also need

$$\begin{aligned} A^{(1),Z}_{\ell m\ ,r} &= -\sqrt{2}m_0\sqrt{\frac{2\ell+1}{2}}\frac{1}{2\pi}E\frac{1}{r^2}\frac{1}{f}\left[\frac{2}{r}+\frac{f'}{f}-\mathrm{i}\omega\frac{dT}{dr}\right]e^{\mathrm{i}\omega T(r)} \\ &= -\frac{\sqrt{2}m_0}{r^2 f}\sqrt{\frac{2\ell+1}{2}}\frac{E}{2\pi}\left[\frac{2}{r}+\frac{f'}{f}+\mathrm{i}\omega\frac{E}{f}\left[E^2-f\right]^{-1/2}\right]e^{\mathrm{i}\omega T(r)}\,. \end{aligned} \tag{4.5.192}$$

Plugging these results into Eq. (4.5.184) and simplifying we get

$$S_l(r) = \frac{4m_0 e^{\mathrm{i}\omega T(r)}}{nr+3M}\left(\ell+\frac{1}{2}\right)^{1/2} f(r)\left\{\left[E^2-f(r)\right]^{-1/2}-\frac{2\mathrm{i}nE}{\omega(nr+3M)}\right\}. \tag{4.5.193}$$

where we recall that $f(r) = 1-2M/r$. For a radial infall from rest the previous expression reduces to

$$S_l(r) = \frac{4m_0 e^{\mathrm{i}\omega T(r)}}{nr+3M}\left(\ell+\frac{1}{2}\right)^{1/2}\left(1-\frac{2M}{r}\right)\left[\left(\frac{r}{2M}\right)^{1/2}-\frac{2\mathrm{i}n}{\omega(nr+3M)}\right]. \tag{4.5.194}$$

The particle trajectory is usually obtained numerically, but in this case it can even be written down analytically with the result

$$\begin{aligned} \frac{T(r)}{M} &= -\frac{\gamma}{\gamma^2-1}\left[\left(\gamma^2-1\right)r^2+2r\right]^{1/2} \\ &- 2\gamma\frac{2\gamma^2-3}{(\gamma^2-1)^{3/2}}\ln\left\{\left[\left(\gamma^2-1\right)r\right]^{1/2}+\left[\left(\gamma^2-1\right)r+2\right]^{1/2}\right\} \\ &- \frac{2\ln 2}{r-2}\left\{\left(2\gamma^2-1\right)r+2-2\gamma\left[\left(\gamma^2-1\right)r^2+2r\right]^{1/2}\right\} \end{aligned} \tag{4.5.195}$$

for infalls with finite energy [91], and

$$\frac{T(r)}{M} = -\frac{4}{3}\left(\frac{r}{2M}\right)^{3/2}-4\left(\frac{r}{2M}\right)^{1/2}+2\log\left\{\left[\left(\frac{r}{2M}\right)^{1/2}+1\right]\left[\left(\frac{r}{2M}\right)^{1/2}-1\right]^{-1}\right\} \tag{4.5.196}$$

for infalls from rest [75].

[EB: Work out problem 15.4 on p. 406 of Lightman et al. [139].]

4.6 Isospectrality of Odd and Even Parity Perturbations

It is very remarkable that both the odd (axial) and even (polar) perturbation problems can be reduced to the solution of relatively simple ordinary wave equations with source. It is even more remarkable that the potentials in these two wave equations are intimately related, and that – as a consequence – the two wave equations have the same spectra!

Let us introduce the notation $V^{(+)} = V_{\rm even}$, $V^{(-)} = V_{\rm odd}$. Then it can be easily verified that

$$V^{(\pm)} = \pm\beta\frac{dW}{dr_*}+\beta^2W^2+\kappa W \tag{4.6.197}$$

where $\beta = 6M$, $\kappa = 4n(n+1)$ and

$$W \equiv \frac{r(r-2M)}{2r^3(nr+3M)}\,. \tag{4.6.198}$$

This fact seems to have been discovered by Chandrasekhar [64–67]. Potentials related in this manner are sometimes called super-partner potentials.

Using Eq. (4.6.197), it can be shown (cf. p. 161 of [65]) that the two solutions of the homogeneous wave equations are related as follows:

$$(\kappa + 2\mathrm{i}\omega\beta)Z^{(+)} = (\kappa + 2\beta^2 W)Z^{(-)} + 2\beta\frac{dZ^{(-)}}{dr_*}\,, \tag{4.6.199}$$

$$(\kappa - 2\mathrm{i}\omega\beta)Z^{(-)} = (\kappa + 2\beta^2 W)Z^{(+)} - 2\beta\frac{dZ^{(+)}}{dr_*}\,. \tag{4.6.200}$$

4.6.1 Reflection and Transmission

From the form of the potentials we see that

$$V^{\pm} \to \tfrac{2(n+1)}{r^2} \quad r \to r_* \to \infty\,, \quad V^{\pm} \to c_{\pm}e^{r_*/2M} \quad r_* \to -\infty\,. \tag{4.6.201}$$

Since the potentials fall off more rapidly than $1/r_*$ for $r_* \to \pm\infty$, the asymptotic behavior of both even- and odd- parity solutions is given by

$$Z \sim e^{\pm\mathrm{i}\omega r_*}\,, \quad r_* \to \pm\infty\,. \tag{4.6.202}$$

So we have a problem of reflection and transmission by the one-dimensional potential barrier $V^{(\pm)}$. For real ω we can impose boundary conditions corresponding to an incident wave of unit amplitude from infinity giving rise to a reflected wave of amplitude $R^{(\pm)}(\omega)$ at infinity, and a transmitted wave of amplitude $T^{(\pm)}(\omega)$ at the horizon:

$$Z^{(\pm)} \sim e^{\mathrm{i}\omega r_*} + R^{(\pm)}(\omega)e^{-\mathrm{i}\omega r_*} \quad r_* \to \infty\,, \tag{4.6.203}$$

$$Z^{(\pm)} \sim T^{(\pm)}(\omega)e^{\mathrm{i}\omega r_*} \quad r_* \to -\infty\,. \tag{4.6.204}$$

Because the potential is real we can also write the complex-conjugate boundary conditions

$${Z^{(\pm)}}^* \sim e^{-\mathrm{i}\omega r_*} + {R^{(\pm)}}^*(\omega)e^{\mathrm{i}\omega r_*} \quad r_* \to \infty\,, \tag{4.6.205}$$

$${Z^{(\pm)}}^* \sim {T^{(\pm)}}^*(\omega)e^{-\mathrm{i}\omega r_*} \quad r_* \to -\infty\,. \tag{4.6.206}$$

The Wronskian of the two independent solutions $Z^{(\pm)}$ and ${Z^{(\pm)}}^*$,

$$[Z^{(\pm)}, {Z^{(\pm)}}^*] = \frac{dZ^{(\pm)}}{dr_*}{Z^{(\pm)}}^* - \frac{d{Z^{(\pm)}}^*}{dr_*}Z^{(\pm)}\,, \tag{4.6.207}$$

must be a constant. By evaluating the Wronskian at $r_* = \pm\infty$ we get

$$-2\mathrm{i}\omega(|R^{(\pm)}(\omega)|^2 - 1) = 2\mathrm{i}\omega|T^{(\pm)}(\omega)|^2\,, \tag{4.6.208}$$

which corresponds to conservation of energy:

$$|R^{(\pm)}(\omega)|^2 + |T^{(\pm)}(\omega)|^2 = 1\,. \tag{4.6.209}$$

Now we can show that the reflection and transmission coefficients for even and odd perturbations are *equal*. Consider the two wave equations

$$\frac{d^2Z^{(+)}}{dr_*^2} + \left[\omega^2 - V^{(+)}\right]Z^{(+)} = 0\,, \tag{4.6.210}$$

$$\frac{d^2Z^{(-)}}{dr_*^2} + \left[\omega^2 - V^{(-)}\right] Z^{(-)} = 0\,, \tag{4.6.211}$$

Since $W \to 0$ as $r_* \to \pm\infty$, if we have solutions of (say) the equation for $Z^{(-)}$ such that

$$Z^{(-)} \sim e^{\mathrm{i}\omega r_*} \quad r_* \to \infty\,, \tag{4.6.212}$$
$$Z^{(-)} \sim e^{-\mathrm{i}\omega r_*} \quad r_* \to -\infty\,, \tag{4.6.213}$$

from Eqs. (4.6.199) and (4.6.200) we obtain

$$Z^{(+)} \sim e^{\mathrm{i}\omega r_*} \quad r_* \to \infty\,, \tag{4.6.214}$$
$$Z^{(+)} \sim \frac{\kappa - 2\mathrm{i}\omega\beta}{\kappa + 2\mathrm{i}\omega\beta} e^{-\mathrm{i}\omega r_*} \quad r_* \to -\infty\,, \tag{4.6.215}$$

Therefore

$$T^{(+)} = T^{(-)}\,, \tag{4.6.216}$$
$$R^{(+)} = \frac{\kappa - 2\mathrm{i}\omega\beta}{\kappa + 2\mathrm{i}\omega\beta} R^{(-)}\,. \tag{4.6.217}$$

i.e. the amplitudes of the transmitted waves are identical, and the reflected waves differ only by a phase factor: $R^{(+)} = e^{\mathrm{i}\delta} R^{(-)}$, where

$$e^{\mathrm{i}\delta} = \frac{\kappa - 2\mathrm{i}\omega\beta}{\kappa + 2\mathrm{i}\omega\beta} = \frac{n(n+1) - 3\mathrm{i}\omega M}{n(n+1) + 3\mathrm{i}\omega M}\,. \tag{4.6.218}$$

4.6.2 Stability of Schwarzschild Black Holes

The main motivation to study black hole perturbation theory was to assess linear stability of the perturbations. More specifically: given any initial perturbation of compact support (i.e., confined to a finite interval in r_*), will the perturbation remain bounded at all times? Both axial and polar perturbations satisfy a wave equation of the form

$$\frac{d^2Z}{dr_*^2} + \left[\omega^2 - V\right] Z = 0\,, \tag{4.6.219}$$

where the potentials are smooth, real, independent of ω, and of short range (i.e., their integral is bounded). Then standard quantum mechanics arguments guarantee that the functions Z satisfying the boundary conditions (4.6.203) form a complete set, and any initial perturbation can be expressed as an integral of the form

$$\psi(r_*,\,0) = \frac{1}{\sqrt{2\pi}} \int_{-\infty}^{\infty} \hat{\psi}(\omega,\,0) Z(r_*,\,\omega) d\omega\,. \tag{4.6.220}$$

At time t we will have

$$\psi(r_*,\,t) = \frac{1}{\sqrt{2\pi}} \int_{-\infty}^{\infty} \hat{\psi}(\omega,\,0) e^{\mathrm{i}\omega t} Z(r_*,\,\omega) d\omega\,. \tag{4.6.221}$$

We are guaranteed that

$$\int_{-\infty}^{\infty} |\psi(r_*,\,0)|^2 dr_* = \int_{-\infty}^{\infty} |\hat{\psi}(\omega,\,0)|^2 d\omega = \int_{-\infty}^{\infty} |\psi(r_*,\,t)|^2 dr_*\,, \tag{4.6.222}$$

and therefore $\psi(r_*,\,t)$ is bounded for all $t > 0$. Multiplying the time-domain version of the ODE by $\partial Z^*/\partial t$ and integrating by parts we get the equation

$$\int_{-\infty}^{\infty} \left(\frac{\partial Z^*}{\partial t} \frac{\partial^2 Z}{\partial t^2} + \frac{\partial Z}{\partial r_*} \frac{\partial^2 Z^*}{\partial t \partial r_*} + V Z \frac{\partial Z^*}{\partial t} \right) dr_* = 0\,. \tag{4.6.223}$$

Adding to this equation its complex conjugate, we get the "energy integral"

$$\int_{-\infty}^{\infty}\left(\left|\frac{\partial Z}{\partial t}\right|^2+\left|\frac{\partial Z}{\partial r_*}\right|^2+V|Z|^2\right)dr_*=\text{constant}. \tag{4.6.224}$$

which implies that $|\partial Z/\partial t|^2$ must stay bounded. This excludes the exponential growth of any bounded solution.

4.6.3 *Isospectrality*

Quasinormal modes are defined as solutions with the boundary conditions

$$Z^{(\pm)}\sim A^{(\pm)}e^{-\mathrm{i}\omega r_*}\quad r_*\to\infty\,, \tag{4.6.225}$$
$$Z^{(\pm)}\sim e^{\mathrm{i}\omega r_*}\quad r_*\to-\infty\,, \tag{4.6.226}$$

where now ω is complex. This is an eigenvalue problem. The existence of the energy integral excludes any exponentially growing solutions. If ω is a quasinormal mode and $Z^{(-)}(\omega)$ is a solution, then $Z^{(+)}(\omega)$ will be a solution with the same eigenfrequency and amplitude

$$A^{(+)}=\frac{\kappa-2\mathrm{i}\omega\beta}{\kappa+2\mathrm{i}\omega\beta}A^{(-)}\,. \tag{4.6.227}$$

This is the reason why we can limit attention to the quasinormal mode frequencies of the odd (Regge-Wheeler) potential, which has a simpler analytical form.

4.7 Gravitational Waves from Radial Infalls

The Zerilli equation (4.5.151) can be solved using standard Green's function techniques. We must impose boundary conditions corresponding to ingoing waves at the horizon ($r_*\to-\infty$) and outgoing waves at infinity ($r_*\to\infty$), i.e. [EB: Fix convention!]

$$Z_\ell(r,\omega)\sim A_\ell^{\text{out}}(\omega)e^{\mathrm{i}\omega r_*}\quad(r_*\to-\infty)\,, \tag{4.7.228}$$
$$Z_\ell(r,\omega)\sim A_\ell^{\text{in}}(\omega)e^{-\mathrm{i}\omega r_*}\quad(r_*\to\infty)\,. \tag{4.7.229}$$

The amplitudes of ingoing and outgoing waves can be obtained from numerical solutions of the homogeneous equations $u_\ell(r_*,\omega)$ and $v_\ell(r_*,\omega)$ corresponding to purely outgoing waves at infinity ($r_*\to\infty$) and purely ingoing waves at the horizon ($r_*\to-\infty$), respectively, as follows:

$$A_\ell^{\text{out}}(\omega)\propto\int_{-\infty}^{\infty}u_\ell(r_*,\omega)S_\ell(r_*,\omega)dr_*\,, \tag{4.7.230}$$
$$A_\ell^{\text{in}}(\omega)\propto\int_{-\infty}^{\infty}v_\ell(r_*,\omega)S_\ell(r_*,\omega)dr_*\,, \tag{4.7.231}$$

Then the radiated energy in the ℓth multipole is given by

$$\frac{dE_\ell}{d\omega}=\frac{1}{32\pi}\frac{(\ell+2)!}{(\ell-2)!}\omega^2\left|A_\ell^{\text{out}}(\omega)\right|^2\,. \tag{4.7.232}$$

Restoring physical units, and for infalls from rest, numerical integrations by Davis et al. [75] demonstrated some key results. First, the energy radiated in each multipole decays like

$$E_\ell\sim 0.44\frac{(mc)^2}{M}e^{-2\ell}\,; \tag{4.7.233}$$

second, the frequency spectrum for each multipole decays sharply at frequencies larger than the quasinormal mode frequency, which for large ℓ is well approximated by the eikonal limit

$$\omega \sim \left[c^2 V_\ell^{\max}(r)\right]^{1/2} \sim \frac{\ell c^3}{\sqrt{27}GM}\,; \tag{4.7.234}$$

third, the total energy radiated is approximately

$$E_{\rm total} = 0.0104 mc^2 \left(\frac{m}{M}\right)\,. \tag{4.7.235}$$

For finite-energy infalls...

[EB: Complete; add discussion of circular and eccentric orbits, maybe also scattering.]

5

The Unreasonable Power of Perturbation Theory: Two Examples

5.1 Critical Phenomena in Binary Mergers

The theory of Lyapunov exponents (Section 2.4) has fascinating applications in the study of critical phenomena in black-hole binaries. In the encounter of two black holes, three outcomes are possible: *scattering* for large values of the impact parameter of the collision; *merger* for small values of the impact parameter; and a *delayed merger* in an intermediate regime, where the black holes can revolve around each other (in principle) an infinite number of times N by fine-tuning the impact parameter around some critical value $b = b_*$.

I will illustrate this possibility by first considering the simple case of extreme mass-ratio binaries (i.e., to a first level of approximation, point particles moving along geodesics in a black-hole spacetime), and then by reporting results from numerical simulations of comparable-mass black hole binary encounters.

5.1.1 Extreme-Mass-Ratio Binaries

Consider equatorial ($\theta = \pi/2$) timelike geodesics in the Schwarzschild background. From Eqs. (2.2.25), (2.2.26) and (2.3.30) with $\delta_1 = 1$ we have

$$\dot{t} = \frac{E}{f}\,, \tag{5.1.1}$$

$$\dot{\phi} = \frac{L}{r^2}\,, \tag{5.1.2}$$

$$\dot{r}^2 \quad = \quad E^2 - f\left(1 + \frac{L^2}{r^2}\right) \equiv E^2 - V_{\rm part}(r)\,. \tag{5.1.3}$$

where $f(r) = 1 - 2M/r$, we used the definition (2.3.34) for timelike particles, and (as usual) dots stand for derivatives with respect to proper time τ. Recall that E is the particle's energy at infinity *per unit mass* μ, so $E = 1$ corresponds to an infall from rest and the limit $E \gg 1$ corresponds to ultrarelativistic motion.

Geodesics can be classified according to how their energy compares to the maximum value of the effective potential (2.3.34). A simple calculation shows that the maximum is located at

$$r = \frac{L^2 - \sqrt{L^4 - 12L^2M^2}}{2M}\,, \tag{5.1.4}$$

and that the potential at the maximum has the value

$$V_{\rm part}^{\rm max}(L) = \frac{1}{54}\left[\frac{L^2}{M^2} + 36 + \left(\frac{L^2}{M^2} - 12\right)\sqrt{1 - \frac{12M^2}{L^2}}\right]. \tag{5.1.5}$$

The scattering threshold is then defined by the condition $E^2 = V_{\rm part}^{\rm max}$: orbits with $E^2 > V_{\rm part}^{\rm max}$ are captured, while those with $E^2 < V_{\rm part}^{\rm max}$ are scattered. Given some E, the critical radius or impact parameter $b_{\rm crit}$ that defines the scattering threshold is obtained by solving the scattering threshold condition $E^2 = V_{\rm part}^{\rm max}(L_{\rm crit})$ (in general, numerically) to obtain $L_{\rm crit}(E)$, and then using the following definition of the impact parameter b

$$b = \frac{L}{\sqrt{E^2 - 1}}\,, \tag{5.1.6}$$

to obtain $b_{\rm crit}$.

The geodesic equations listed above can be integrated numerically for chosen values of E and L. For $L > L_{\rm crit}$ the particle does not plunge, but rather scatters to infinity. Examples of plunging orbits for $E = 3$ and different angular momenta $L < L_{\rm crit}$ (i.e., different impact parameters) are shown in Fig. 5.1 in Cartesian-like coordinates $x = r\cos\phi$, $y = r\sin\phi$. The number of revolutions around the black hole before plunge increases as $L \to L_{\rm crit}$.

Using black-hole perturbation theory, it is possible to compute the energy radiated by particles falling into the black hole with different values of (E, L). The details of the calculation can be found in [42] and references therein. In the frequency domain, the radiated energy can be decomposed as a sum

$$E = \sum_{l=2}^{\infty}\sum_{m=-l}^{l}\int_0^{\infty} d\omega \frac{dE_{lm}}{d\omega}\,, \tag{5.1.7}$$

where the indices (l, m) refer to the angular functions used to separate variables (here spin-weighted spherical harmonics of spin weight two). The dominant contribution to the radiation comes from modes with $l = m = 2$. Figure 5.2 shows the energy spectrum of the $l = m = 2$ mode for a particle with $E = 1$ (infall from rest) and different values of the orbital angular momentum $L/L_{\rm crit}$. For $L \ll L_{\rm crit}$ the energy spectra show a simple structure, first identified for radial infalls ($L = 0$) in [75]: the spectrum vanishes at low frequencies, it has a peak, and then an exponential decay at frequencies larger than the black hole's fundamental QNM frequency for the given l. However, additional features appear when L grows, and the nature of the spectra changes quite significantly as $L/L_{\rm crit} \to 1$. As shown in Fig. 5.2, as we fine-tune the angular momentum to the critical value separating plunge and scattering the energy spectra with $L/L_{\rm crit} = 0.99, \ldots, 0.9999$ clearly display a second peak, which is related to the orbital motion of the particle. This very distinctive

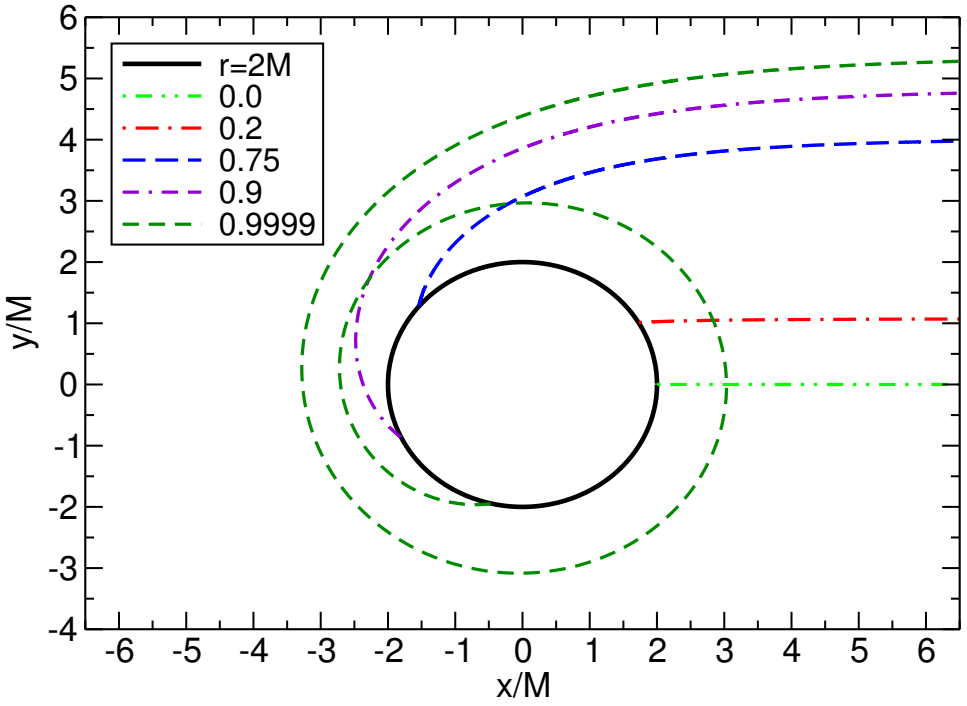

Figure 5.1: Trajectories for different values of $L/L_{\rm crit}$ (as indicated in the legend) and $E = 3$. The black circle of radius 2 marks the location of the horizon. (From Ref. [42].)

"bump" appears at a frequency slightly *lower* than the QNM frequency, significantly enhancing the radiated energy. The location of the "bump" corresponds to (twice) the orbital frequency of the particle at the marginally bound orbit, i.e. $\omega = 2\Omega_{\rm mb} = (4M)^{-1}$. The reason for this local maximum in the spectrum is that when $L \to L_{\rm crit}$ the particle orbits a large number of times close to the circular marginally bound orbit with radius $r = r_{\rm mb}$ (here $r = 4M$ because $E = 1$), eventually taking an infinite amount of proper time to reach the horizon. The proximity of the orbit to criticality is conveniently described by a small dimensionless "criticality parameter"

$$\delta \equiv 1 - \frac{L}{L_{\rm crit}}\,. \tag{5.1.8}$$

In the limit $\delta \to 0$, how many times does the particle hover at the marginally bound circular geodesics before plunging? The answer is given by the Lyapunov exponent calculation of Chapter 2 (see e.g. [170]). To linear order, the growth of the perturbation around the marginally bound orbit is described by

$$\delta r(t) = \delta r_{\rm mb} e^{\lambda_0 t}\,, \tag{5.1.9}$$

so $\ln|\delta r(t)| = \ln|\delta r_{\rm mb}| + \lambda_0 t$. Perturbation theory breaks down when $\delta r(t) \approx 1$, and by that time the number of orbits that have been completed is $N \simeq \Omega_{\rm mb} t/(2\pi)$. Furthermore, $\delta r_{\rm mb} = k\delta$ (with k some constant) for geodesics approaching the marginally bound orbit. Taking the natural logarithm of (5.1.9) and substituting these relations yields

$$0 = \ln|\delta r_{\rm mb}| + \lambda_0 \frac{2\pi N}{\Omega_{\rm mb}} = \ln|k\delta| + \lambda_0 \frac{2\pi N}{\Omega_{\rm mb}}\,. \tag{5.1.10}$$

Now recall our result (2.4.64) for the Lyapunov exponent to get:

$$0 = \ln|k\delta| + \sqrt{\frac{V''_{\rm part}}{2\dot{t}^2_{\rm mb}}}\,\frac{2\pi N}{\Omega_{\rm mb}}\,. \tag{5.1.11}$$

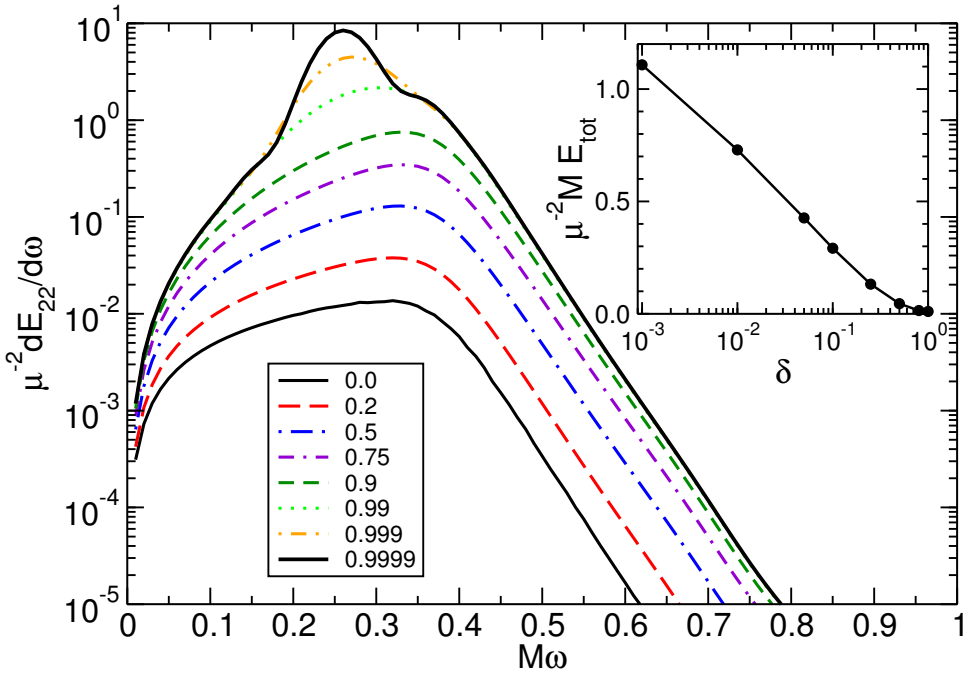

Figure 5.2: Infall from rest: spectra for $l = m = 2$ as $L/L_{\rm crit} \to 1$. In the inset: logarithmic divergence of the total radiated energy in the same limit. (From Ref. [42].)

Therefore the particle orbits the black hole

$$N \simeq -\frac{\Omega_{\rm mb}\dot{t}_{\rm mb}\,\ln|k\delta|}{\pi\sqrt{2V''_{\rm part}}} \tag{5.1.12}$$

times before plunging [41] (recall that dots stand for derivatives with respect to proper time). This logarithmic scaling with the "criticality parameter" δ is typical of many phenomena in physics (see e.g. [71] for the discovery that critical phenomena occur in gravitational collapse, and [111] for a review of subsequent work in the field).

For the Schwarzschild effective potential, $r^5 V''_{\rm part} = 24ML^2 - 6rL^2 + 4Mr^2$, and the angular velocity $\Omega_{\rm mb}$ is nothing but $d\phi/dt$ evaluated at the marginally bound orbit $r = r_{\rm mb}$. When $E = 1$ the marginally bound orbit is located at $r_{\rm mb} = 4M$, $M\Omega_{\rm mb} = 8^{-1}$ and

$$N \sim -\frac{1}{\pi\sqrt{2}}\ln|\delta|\,. \tag{5.1.13}$$

The inset of Fig. 5.2 shows that the *total* radiated energy in the limit $L \to L_{\rm crit}$ does indeed scale logarithmically with δ, and hence linearly with the number of orbits N, as expected from Eq. (5.1.13) for radiation from a particle in circular orbit at the marginally bound geodesic.

In the ultrarelativistic limit $E \to \infty$ the marginally bound orbit is located at the light ring $r_{\rm mb} = 3M$, the corresponding orbital frequency $M\Omega_{\rm mb} = (3\sqrt{3})^{-1}$ and

$$N \sim -\frac{1}{2\pi}\ln|2\delta|\,. \tag{5.1.14}$$

As argued in Chapter 3, the orbital frequency at the light ring is intimately related with the eikonal (long-wavelength) approximation of the fundamental QNM

frequency of a black hole (see also [48, 62, 147, 168]). This implies that ultrarelativistic infalls with near-critical impact parameter are in a sense the most "natural" and efficient "hammer" to resonantly excite the ringdown dynamics of a black hole. The proper oscillation modes of a Schwarzschild black hole cannot be excited by particles on *stable* circular orbits (i.e. particles with orbital radii $r > 6M$ in Schwarzschild coordinates), but near-critical ultrarelativistic infalls are such that the orbital "bump" visible in Figure 5.2 moves just slightly to the right to overlap with the "knee" due to quasinormal ringing. So ultrarelativistic infalls have just the right orbital frequency to excite black hole oscillations.

5.1.2 Comparable-Mass Binaries

Pretorius and Khurana [170] demonstrated that critical behavior of the kind shown above, where the number of orbits scales logarithmically with some criticality parameter δ, occurs also in the encounters of comparable-mass black hole mergers. Now the question is: suppose that two comparable-mass black holes collide close to the speed of light, so that all the center-of-mass energy of the system is kinetic energy. Is it possible to radiate all the kinetic energy of the system by fine-tuning the impact parameter near threshold? And if so, what is the final state of the collision? As demonstrated by numerical relativity simulations in a series of papers [190–192], the answer to this question is "no," and the reason is that the black holes absorb a significant fraction of the energy during a close encounter.

The encounter of two equal-mass black holes is illustrated in Fig. 5.3 (from [190]). The plot shows the trajectory of one of the two black holes (the trajectory of the other hole is reflection-symmetric with respect to that of the first hole). In the numerical simulations we monitor the apparent horizon dynamics of the individual holes by measuring the equatorial circumference $C_{\rm e} = 4\pi M$ and the irreducible mass $M_{\rm irr}$ of each black hole before and after the encounter. The inset of the right panel of Fig. 5.3 shows the variation of these quantities with time: absorption occurs over a short timescale $\approx 10M$. Since the apparent horizon area $A_{\rm AH} = 16\pi M_{\rm irr}^2 = [C_{\rm e}^2/(2\pi)](1+\sqrt{1-\chi^2})$, in this way we can estimate the rest mass and dimensionless spin $\chi = a/M$ of each hole before ($M_{\rm i}$, $\chi_{\rm i}$) and after ($M_{\rm s}$, $\chi_{\rm s}$) the first encounter. We define the absorbed energy $E_{\rm abs} = 2(M_s - M_i)$. It turns out that $(E_{\rm rad}+E_{\rm abs})/M$ accounts for most of the total available kinetic energy in the system, and therefore the system is no longer kinetic-energy dominated after the encounter. A fit of the data yields $E_{\rm rad}/K = 0.46(1 + 1.4/\gamma^2)$ and $E_{\rm abs}/K = 0.55(1 - 1/\gamma)$, where γ is the Lorentz boost parameter, suggesting that radiation and absorption contribute about equally in the ultrarelativistic limit, and therefore that absorption sets an upper bound $\approx 50\%$ on the maximum energy that can be radiated.

The fact that absorption and emission are comparable in the ultrarelativistic limit is supported by point-particle calculations in black hole perturbation theory. For example, Misner et al. [152] studied the radiation from ultrarelativistic particles in circular orbits near the Schwarzschild light ring, i.e. at $r = 3M(1 + \epsilon)$. Using a scalar-field model they found that 50% of the radiation is absorbed and 50% is radiated as $\epsilon \to 0$. The same conclusion applies to *gravitational* perturbations of Schwarzschild black holes when one ignores radiation reaction (self-force) effects, and a recent analysis including self-force effects finds that 42% of the energy should be absorbed by nonrotating black holes as $\epsilon \to 0$ (cf. Fig. 4 of [109]).

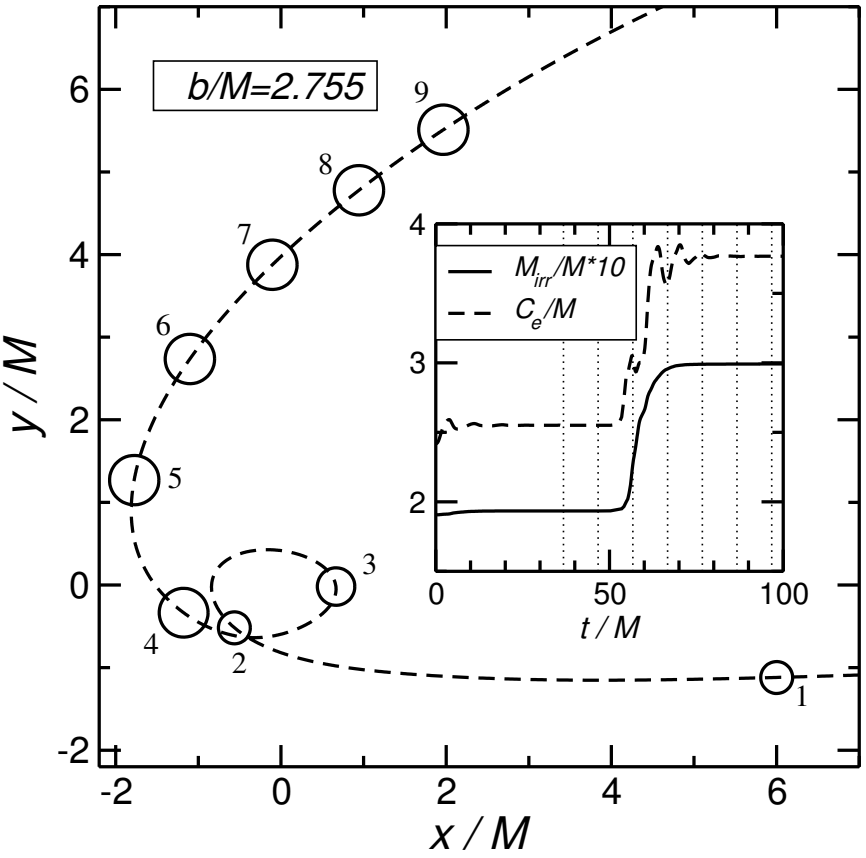

Figure 5.3: Trajectory of one black hole from numerical simulations of equal-mass ultrarelativistic black-hole encounters with a "near-critical" impact parameter $b/M = 2.755$. Inset: time evolution of the irreducible mass $M_{\rm irr}$ and of the circumferential radius $C_{\rm e}$ of each hole. The circles represent the black hole location at intervals $\Delta t = 10\ M$ (corresponding to vertical lines in the inset) and have radius equal to $M_{\rm irr}$. (From Ref. [190].)

5.2 Black-Hole Bombs

The superradiant amplification mechanism discussed in Section 3.6 has a rather dramatic consequence for astrophysics and particle physics: measurements of the spin of massive black holes, the largest and simplest macroscopic objects in the Universe, can be used to set upper bounds on the mass of light bosonic particles. The reason behind this striking connection between the smallest and largest objects in our physical world is the so-called "black-hole bomb" instability first investigated by Press and Teukolsky [169] (see also [60], and [189] for a recent rigorous proof for scalar perturbations).

The idea is the following. Imagine surrounding a rotating black hole by a perfectly reflecting mirror. An ingoing monochromatic wave with frequency in the superradiant regime defined by Eq. (3.6.118) will be reflected and amplified at the expense of the rotational energy of the black hole, then it will be reflected again by the mirror and amplified once more. The process keeps repeating and triggers a runaway growth of the perturbation – a "black-hole bomb". The end state cannot be predicted in linearized perturbation theory, but it is reasonable to expect that we will be left with a slowly rotating (or nonrotating) black hole, transferring the whole rotational energy of the hole (a huge amount compared to nuclear physics standards!) to the field.

The original Press-Teukolsky mechanism is of mostly speculative interest: for example, one could imagine a very advanced civilization building perfectly reflective mirrors around rotating black holes to solve their energy problems. Luckily, nature gives us actual "mirrors" in the form of massive bosonic fields. As shown in Fig. 3.1 for massive scalars, whenever the field has mass the effective potential for wave propagation tends to a nonzero value at infinity. This potential barrier is the particle-physics analog of Press and Teukolsky's perfectly reflecting mirror.

This simple consideration has immediate implications for fundamental physics. Many proposed extensions of the Standard Model predicted the existence of ultralight bosons, such as the light scalars with 10^{-33} eV $< m < 10^{-18}$ eV of the "string axiverse" scenario [21], "hidden photons" [56, 105, 107, 122] and massive gravitons [77, 105, 114]. Explicit calculations of the instability timescales have been performed for massive scalar [59, 73, 81, 82, 169, 176, 208], vector (Proca) [163, 164] and tensor (massive graviton) [54] perturbations of a Kerr black hole. In all cases the instability is regulated by the dimensionless parameter $M\mu$ (in units $G = c = 1$), where M is the BH mass and $m = \mu\hbar$ is the bosonic field mass, and it is strongest for maximally spinning BHs when $M\mu \sim 1$. As discussed around Eq. (3.1.2), for a solar-mass black hole and a field of mass $m \sim 1$ eV the parameter $M\mu \sim 10^{10}$. In this case the instability is exponentially suppressed [208], and the instability timescale would be larger than the age of the Universe. The strongest superradiant instabilities develop when $M\mu \sim 1$, i.e. when the Compton wavelength of the perturbing field is comparable to the "size" of the black hole's event horizon. This can occur for light primordial BHs that may have been produced in the early Universe, or for the ultralight exotic particles proposed in some extensions of the Standard Model. In particular, fields of mass $m \sim 10^{-20}$ eV around the heaviest supermassive black holes ($M \sim 10^{10} M_\odot$) are ideal candidates.

This yields stringent constraints on the mass m of the perturbing field. If there were fields of mass m around a supermassive rotating black hole, the superradiant instability would reduce their spin on a timescale that can be computed using black-hole perturbation theory (this timescale is shortest when $M\mu \sim 1$). We can exclude the existence of a field of mass m whenever the superradiant instability timescale is smaller than the Salpeter time, i.e. the typical time over which accretion could potentially spin up the hole [179]. By setting the Salpeter timescale equal to the instability timescale we can draw "instability windows" such as those shown

in Fig. 5.4; these are sometimes called gaps in the mass-spin black-hole "Regge spectrum" [21]. Any measurement of a black-hole spin with value above one of the instability windows excludes a whole range of masses for the perturbing field.

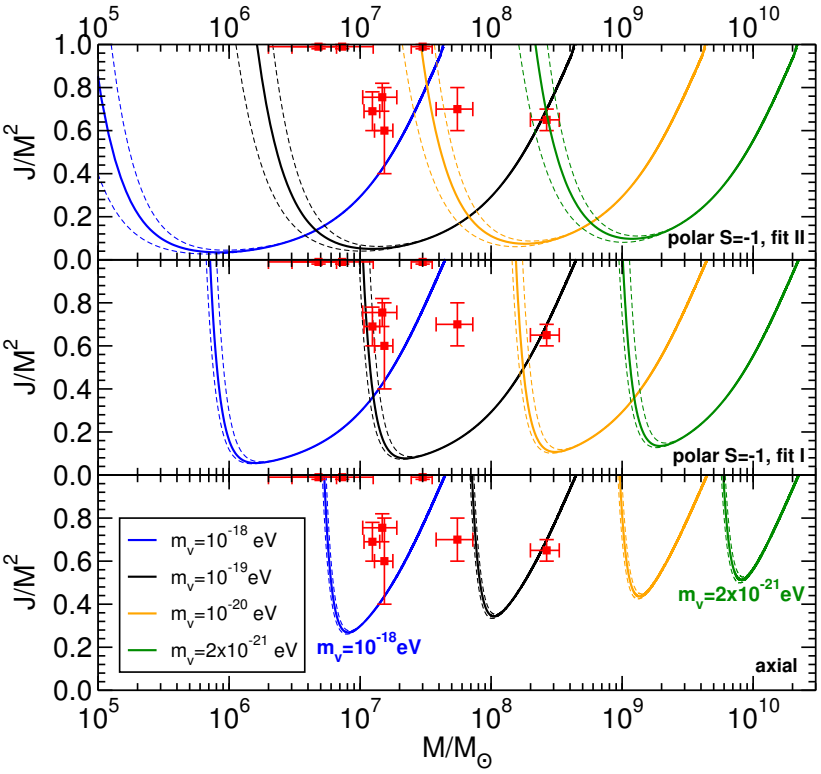

Figure 5.4: Contour plots in the "BH Regge plane" [21] corresponding to an instability timescale shorter than a typical accretion timescale, $\tau_{\rm Salpeter} = 4.5 \times 10^7$ yr, for different values of the vector (Proca) field mass $m_v = \mu\hbar$ (from left to right: $m_v = 10^{-18}$eV, 10^{-19}eV, 10^{-20}eV, 2×10^{-21}eV). The instability operates for both polar (even parity) and axial (odd parity) modes. For polar modes in the $S = -1$ polarization, which provides the strongest instability, we use two different fits (top and middle panel) to numerical calculations of the instability (see [163, 164] for details); axial mode instability windows are shown in the bottom panel. Dashed lines bracket our estimated numerical errors. The experimental points (with error bars) refer to the mass and spin estimates of supermassive BHs listed in Table 2 of [52]. The rightmost point corresponds to the supermassive BH in Fairall 9 [184]. Supermassive BHs lying above each of these curves would be unstable on an observable timescale, and therefore they exclude a whole range of Proca field masses.

It is worth mentioning that massive fields can have other potentially observable signatures. They can modify the inspiral dynamics of compact binaries [13] and even freeze the inspiral of compact objects into massive black holes, creating "floating orbits" that produce stimulated emission of radiation by extracting the hole's rotational energy (the gravitational-wave equivalent of a laser!) [59, 203]. Another potentially observable event is a "bosenova", i.e. a collapse of the axion cloud producing a relatively large emission of scalar radiation (see e.g. [129, 154, 201, 202]).

6

Ringdown Detection and Parameter Estimation

6.1 Optimal Mass Range for Ringdown Detection by (e)LISA

During the ringdown phase, perturbations of a Kerr black hole die away as exponentially damped sinusoids, whose frequencies and damping times are given by (complex) QNM frequencies. We decompose the perturbations in spheroidal harmonics $S_{lm}(\iota, \beta)$ of "spin weight" 2 [38,196], where l and m are indices analogous to those for standard spherical harmonics, and ι and β are angular variables such that the azimuthal, or β dependence goes like $e^{\mathrm{i}\beta}$. For each (l, m) there is an infinity of resonant quasi-normal frequencies, which control the intermediate time behavior of the signal. We label each of these frequencies by an overtone index n such that the mode with $n = 0$ has the longest damping time, followed by $n = 1$ and so on. Thus, in the end QNM frequencies are parameterized by three numbers: $l\,, m$ and n. Now, the time dependence of the signal during ringdown is of the form $e^{\mathrm{i}\omega t}$, but since $\omega = \omega_{lmn} + \mathrm{i}/\tau_{lmn}$ is in general a complex number, we will follow the usual conventions and write this as $e^{-t/\tau_{lmn}} \sin(\omega_{lmn} t + \varphi_{lmn})$, or $e^{-t/\tau_{lmn}} \cos(\omega_{lmn} t + \varphi_{lmn})$, where $\omega_{lmn} = 2\pi f_{lmn}$ is the mode's real part and τ_{lmn} is the damping time of the oscillation. We will also define the quality factor of a QNM as

$$Q_{lmn} \equiv \pi f_{lmn} \tau_{lmn} = \omega_{lmn} \tau_{lmn}/2\,. \tag{6.1.1}$$

In our analysis of the detectability of ringdown radiation, we will assume that the signal lasts for at least one light-propagation time corresponding to the LISA arm length $L \simeq 5 \cdot 10^9$ m, or $T_{\mathrm{light}} = L/c \simeq 16.68$ s (shorter-lived signals may require specialized detection techniques). This places a rough lower limit on the black hole masses that are relevant. To see this, we note that the fundamental mode of a Schwarzschild black hole corresponds to an axially symmetric ($m = 0$), quadrupolar ($l = 2$) perturbation with frequency

$$f_{200} = \pm 1.207 \cdot 10^{-2} (10^6 M_\odot / M)\ \mathrm{Hz}\,, \tag{6.1.2}$$

and damping time

$$\tau_{200} = 55.37 (M/10^6 M_\odot)\ \mathrm{s}\,. \tag{6.1.3}$$

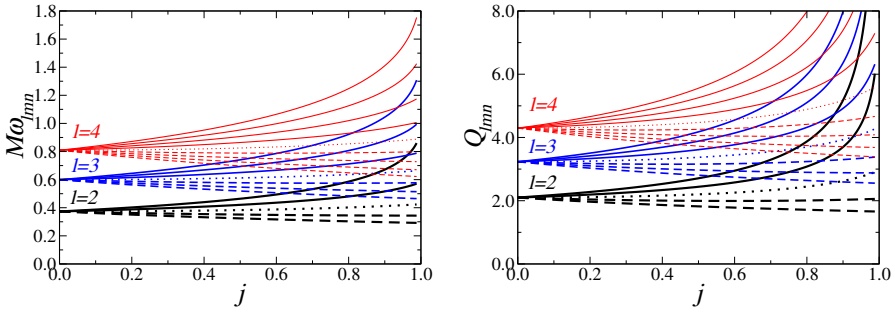

Figure 6.1: Frequency f_{lmn} (left) and quality factor Q_{lmn} (right) for the fundamental modes with $l = 2,\ 3,\ 4$ and different values of m. Solid lines refer to $m = l, .., 1$ (from top to bottom), the dotted line to $m = 0$, and dashed lines refer to $m = -1, .., -l$ (from top to bottom). Quality factors for the higher overtones are lower than the ones we display here.

For rotating holes, the dimensionless frequencies ($M\omega_{lmn}$) and quality factors for the fundamental modes for $l = 2, 3, 4$ are shown as a function of j in Fig. 6.1. Although the quality factors and damping times for corotating ($m > 0$) modes may be larger for rapidly rotating holes, the effects are not dramatic: for $j = 0.80$ the damping time $\tau_{220} = 65.18\left(M/10^6 M_\odot\right)$ s, and for $j = 0.98$ the damping time $\tau_{220} = 127.7\left(M/10^6 M_\odot\right)$ s. Accordingly we will restrict our attention to masses larger than 10^6 or a few times $10^5 M_\odot$.

We can also estimate an upper limit for masses to be considered by noting that LISA's low frequency noise may provide a lower cutoff at 10^{-4} Hz. Equation (6.1.2) then gives a mass upper limit of around $10^8 M_\odot$; if the LISA performance can be extended down to 10^{-5} Hz, then masses as large as $10^9 M_\odot$ may be detectable. Again, these rough bounds are not terribly dependent on the black hole spin or the mode.

6.2 Quasinormal Mode Decomposition and Polarization of the Waveform

The plus and cross components of the gravitational waveform emitted by a perturbed Kerr black hole can be written in terms of the radial Teukolsky function $R_{lm\omega}$ as [196]

$$h_+ + \mathrm{i}h_\times = -\frac{2}{r^4}\int_{-\infty}^{+\infty}\frac{d\omega}{\omega^2}e^{\mathrm{i}\omega t}\sum_{lm}S_{lm}\left(\iota,\beta\right)R_{lm\omega}(r)\,. \tag{6.2.4}$$

The radial Teukolsky function $R_{lm\omega} \sim r^3 Z^{\rm out}_{lm\omega} e^{-\mathrm{i}\omega r}$ as $r \to \infty$, where $Z^{\rm out}_{lm\omega}$ is a complex amplitude.

We assume that the gravitational wave signal during the ringdown phase can be expressed as a linear superposition of exponentially decaying sinusoids. QNMs are known not to be a complete set, and thus such an expansion is not well defined mathematically. However numerical simulations of a variety of (perturbative and non-perturbative) dynamical processes involving black holes show that, at intermediate times, the response of a black hole *is* indeed well described by a linear superposition of damped exponentials. For the time being, we just *assume* that we can write the gravitational waveform as a formal QNM expansion (rather than as a standard Fourier expansion in the real frequency ω) of the Teukolsky function, so

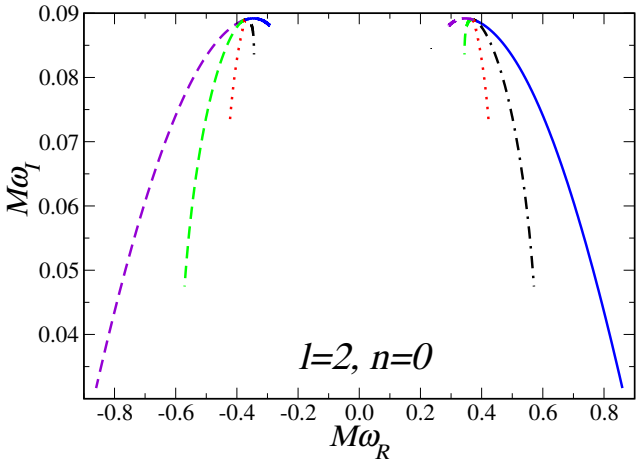

Figure 6.2: Fundamental $l = 2$ QNM frequencies of the Kerr black hole in the range $j \in [0, 0.99]$. Solid (blue) lines correspond to $m = 2$, dot-dashed (black) lines to $m = 1$, dotted (red) lines to $m = 0$, dashed (green) lines to $m = -1$, and short dashed (violet) lines to $m = -2$.

that we can replace Eq. (6.2.4) by

$$h_+ + \mathrm{i}h_\times = \frac{1}{r}\sum_{lmn} e^{\mathrm{i}\omega_{lmn}t} e^{-t/\tau_{lmn}} S_{lmn}\,(\iota,\beta)\, Z^{\rm out}_{lmn}\,, \tag{6.2.5}$$

where n denotes the overtone index and from here on the coordinate t stands for the retarded time $t - r$. We write the complex wave amplitude $Z^{\rm out}_{lmn}$ in terms of a real amplitude $\mathcal{A}_{lmn}$ and a real phase ϕ_{lmn}, and to follow the FH convention we factor out the black hole mass M: $Z^{\rm out}_{lmn} = M\mathcal{A}_{lmn}e^{\mathrm{i}\phi_{lmn}}$. In this way we get

$$h_+ + \mathrm{i}h_\times = \frac{M}{r}\sum_{lmn} \mathcal{A}_{lmn} e^{\mathrm{i}(\omega_{lmn}t+\phi_{lmn})} e^{-t/\tau_{lmn}} S_{lmn}\,. \tag{6.2.6}$$

In this expansion the spheroidal functions $S_{lmn} = S_{lm}(a\omega_{lmn})$ are evaluated at the (complex) QNM frequencies, so they are complex numbers (henceforth we drop the (ι, β) angular dependence on the S_{lmn}).

One frequently finds in the literature the astrophysically reasonable assumption that only the $l = m = 2$ mode is present in the waveform. This viewpoint has two conceptual flaws.

First, QNMs of Schwarzschild and Kerr black holes always come "in pairs". In the Kerr case, for a given (l, m) and a given value of $a = jM$ the eigenvalue problem admits *two* solutions: one with positive (real part of) the frequency, the other with negative real part of the frequency and different damping time. To illustrate this property, in Fig. 6.2 we show the fundamental Kerr QNM with $l = 2$ and different values of m. Positive-m frequencies are related to negative-m frequencies by a simple symmetry property: one can easily see from the perturbation equations that to any QNM frequency characterized by (l, m, n) there corresponds a QNM frequency characterized by $(l, -m, n)$ such that

$$-\omega_{lmn} = \omega_{l-mn}\,, \qquad 1/\tau_{lmn} = 1/\tau_{l-mn}\,, \qquad A^*_{lmn} = A_{l-mn}\,, \tag{6.2.7}$$

(here A_{lmn} is the angular separation constant, not to be confused with the mode amplitude $\mathcal{A}_{lmn}$). In this sense, any solution with positive m is nothing but the "mirror image" of a solution with negative real part and negative m. For $m = 0$ (and, of course, in the Schwarzschild case) the two "mirror solutions" are degenerate

in modulus of the frequency and damping time. However, in general, *a "mode with a given (l,m)" will always contain a superposition of two different damped exponentials.* One of these exponentials could be invisible in the actual waveform because its damping time is shorter, or perhaps because it is less excited in the given physical situation, but formally one can never have anything like an isolated "$l = m = 2$ frequency" with a positive real part. This excitation of both modes is actually observed in time-evolutions of perturbative fields in Kerr backgrounds [85, 134].

Second, a single-mode expansion automatically restricts attention to circularly polarized gravitational waves; more generally one cannot specify the polarization state of the waveform by assuming that it is described by a single QNM frequency. This problem has been overlooked in all previous treatments of the gravitational radiation emitted during ringdown. This omission has no serious consequences for nonrotating holes, but it is conceptually inconsistent when $j \neq 0$. Consider, for example, the starting point of the analysis in FH. They assume that the waveform can be written as [Eq. (3.15) in FH]

$$h_+ + \mathrm{i}h_\times = \frac{M\mathcal{A}_{lmn}}{r} e^{\mathrm{i}(\omega_{lmn}t+\phi_{lmn})} e^{-t/\tau_{lmn}} S_{lmn}\,, \tag{6.2.8}$$

with $l = m = 2$. This is not a general assumption: it implies that the waves are circularly polarized. A more general and consistent approach to ringdown waveforms begins with a general superposition of modes, including the "twin" modes with frequency $\omega'_{lmn} = -\omega_{l-mn}$ and a different damping $\tau'_{lmn} = \tau_{l-mn}$. Then, using the symmetry property (6.2.7) we can easily see that:

$$\begin{aligned}
h_+ + \mathrm{i}h_\times &= \frac{M}{r}\sum_{lmn}\left\{\mathcal{A}_{lmn}e^{\mathrm{i}(\omega_{lmn}t+\phi_{lmn})}e^{-t/\tau_{lmn}}S_{lmn} + \mathcal{A}'_{lmn}e^{\mathrm{i}(\omega'_{lmn}t+\phi'_{lmn})}e^{-t/\tau'_{lmn}}S'_{lmn}\right\} \\
&= \frac{M}{r}\sum_{lmn}\left\{\mathcal{A}_{lmn}e^{\mathrm{i}(\omega_{lmn}t+\phi_{lmn})}e^{-t/\tau_{lmn}}S_{lmn} + \mathcal{A}'_{lmn}e^{\mathrm{i}(-\omega_{l-mn}t+\phi'_{lmn})}e^{-t/\tau_{l-mn}}S^*_{l-mn}\right\} \\
&= \frac{M}{r}\sum_{lmn}\left\{\mathcal{A}_{lmn}e^{\mathrm{i}(\omega_{lmn}t+\phi_{lmn})}e^{-t/\tau_{lmn}}S_{lmn} + \mathcal{A}'_{l-mn}e^{\mathrm{i}(-\omega_{lmn}t+\phi'_{l-mn})}e^{-t/\tau_{lmn}}S^*_{lmn}\right\} \\
&= \frac{M}{r}\sum_{lmn}\left\{\mathcal{A}_{lmn}e^{\mathrm{i}(\omega_{lmn}t+\phi_{lmn})}e^{-t/\tau_{lmn}}S_{lmn} + \mathcal{A}'_{lmn}e^{\mathrm{i}(-\omega_{lmn}t+\phi'_{lmn})}e^{-t/\tau_{lmn}}S^*_{lmn}\right\}.
\end{aligned} \tag{6.2.9}$$

In going from the second to the third line we relabeled $m \to -m$ in the second term, and in going from the third to the fourth line we changed the labeling of the (arbitrary) constants, replacing $\mathcal{A}'_{l-mn}$ by $\mathcal{A}'_{lmn}$ and ϕ'_{l-mn} by ϕ'_{lmn}. So the general waveform depends on four arbitrary, real constants: $\mathcal{A}_{lmn}$, $\mathcal{A}'_{lmn}$, ϕ_{lmn} and ϕ'_{lmn} for each $(l,\ m,\ n)$.

Thus it is clear that only by combining positive and negative values of m can we require the waveform to have any given polarization state. In particular, if $\mathcal{A}_{lmn}e^{\mathrm{i}\phi_{lmn}}S_{lmn} = \mathcal{A}'_{lmn}e^{\mathrm{i}\phi'_{lmn}}S^*_{lmn}$ the waveform becomes pure real (we have a "plus" state); if instead $\mathcal{A}_{lmn}e^{\mathrm{i}\phi_{lmn}}S_{lmn} = -\mathcal{A}'_{lmn}e^{\mathrm{i}\phi'_{lmn}}S^*_{lmn}$ it becomes pure imaginary (we have a "cross" state). In our single-mode analysis we will usually write the (real) plus and cross components measured at the detector as damped sinusoids, specifying arbitrarily their amplitude and relative phase. More rigorously, when we write the waveform as a damped sinusoid we really mean that we have performed a sum of the appropriate QNM components, as described above.

6.3 Including Cosmological Redshift

The general waveform (6.2.9) is written in the rest frame of the black hole, and thus all the quantities appearing there (M, ω_{lmn} and τ_{lmn}) are measured in that

frame. However, because of cosmological effects, in the detector's frame all dimensionful quantities should be interpreted as redshifted. The prescription to include cosmological effects is very simple [94, 143]: r should be replaced by the luminosity distance $D_L(z)$, and all quantities with dimensions $[\text{mass}]^p$ should enter the waveforms at the detector multiplied by the factor $(1+z)^p$. So, whenever the source is at cosmological distance, our r should be replaced by $D_L(z)$, M by the redshifted mass $(1+z)M^0$, f_{lmn} by the redshifted frequency $f^0_{lmn}/(1+z)$, and τ_{lmn} by $(1+z)\tau^0_{lmn}$ (where all quantities marked by a superscript 0 are measured in the source frame).

6.4 Signal-to-Noise Ratio for a Single-Mode Waveform

6.4.1 Analytic Results

We begin by studying the SNR for detection of a single QNM. From Eq. (6.2.9), we can express the (real) waveform measured at the detector as a linear superposition of h_+ and $h_\times$, where, for the given mode $(l,\ m,\ n)$,

$$h_+ = \frac{M}{r}\Re\left[\mathcal{A}^+_{lmn}e^{\mathrm{i}(\omega_{lmn}t+\phi^+_{lmn})}e^{-t/\tau_{lmn}}S_{lmn}(\iota,\beta)\right], \tag{6.4.10a}$$

$$h_\times = \frac{M}{r}\Im\left[\mathcal{A}^\times_{lmn}e^{\mathrm{i}(\omega_{lmn}t+\phi^\times_{lmn})}e^{-t/\tau_{lmn}}S_{lmn}(\iota,\beta)\right], \tag{6.4.10b}$$

where $\mathcal{A}^{+,\times}_{lmn}$ and $\phi^{+,\times}_{lmn}$ are real, and are related to the quantities $\mathcal{A}_{lmn}$, $\mathcal{A}'_{lmn}$, ϕ_{lmn}, and ϕ'_{lmn} of Eq. (6.2.9) by $\mathcal{A}^{+,\times}_{lmn}e^{\mathrm{i}\phi^{+,\times}_{lmn}} = \mathcal{A}_{lmn}e^{\mathrm{i}\phi_{lmn}} \pm \mathcal{A}'_{lmn}e^{-\mathrm{i}\phi'_{lmn}}$, where the $+(-)$ signs correspond to the $+(\times)$ polarizations, respectively. The waveform measured at a detector is given by

$$h = h_+F_+(\theta_S,\phi_S,\psi_S) + h_\times F_\times(\theta_S,\phi_S,\psi_S), \tag{6.4.11}$$

where $F_{+,\times}$ are pattern functions that depend on the orientation of the detector and the direction of the source, given by

$$F_+(\theta_S,\phi_S,\psi_S) = \frac{1}{2}(1+\cos^2\theta_S)\cos 2\phi_S\cos 2\psi_S - \cos\theta_S\sin 2\phi_S\sin 2\psi_S, \tag{6.4.12a}$$

$$F_\times(\theta_S,\phi_S,\psi_S) = \frac{1}{2}(1+\cos^2\theta_S)\cos 2\phi_S\sin 2\psi_S + \cos\theta_S\sin 2\phi_S\cos 2\psi_S. \tag{6.4.12b}$$

To compute the SNR we will usually follow the prescription described in Appendix A of FH (henceforth the *FH convention* or *FH doubling prescription*) as follows: (1) Assume that the waveform for $t<0$ is identical to the waveform for $t>0$ except for the sign of t/τ_{lmn}, i.e. that we replace the decay factor $e^{-t/\tau_{lmn}}$ with $e^{-|t|/\tau_{lmn}}$. (2) Compute the SNR using the standard expression,

$$\rho^2 = 4\int_0^\infty \frac{\tilde{h}^*(f)\tilde{h}(f)}{S_h(f)}df, \tag{6.4.13}$$

where $\tilde{h}(f)$ is the Fourier transform of the waveform, and $S_h(f)$ is the noise spectral density of the detector. (3) Divide by a correction factor of $\sqrt{2}$ in amplitude to compensate for the doubling-up in step (1).

In calculating the SNR, we will average over source directions and over detector and black-hole orientations, making use of the angle averages: $\langle F_+^2\rangle = \langle F_\times^2\rangle = 1/5$,

$\langle F_+ F_\times \rangle = 0$, and $\langle |S_{lmn}|^2 \rangle = 1/4\pi$. This simple averaging is feasible because the mode damping time is short compared to the orbital period of LISA.

Sometimes, for comparison, we will not follow the three steps we just described, but will calculate the Fourier transform of the waveform by integrating only over the range $t > 0$. Since this was the method used by Echeverria [88] and Finn [92], we will refer to this procedure as *the Echeverria-Finn (EF) convention.*

In the rest of this Section we will follow the FH prescription. The Fourier transform of the waveform can be computed using the elementary relation

$$\int_{-\infty}^{\infty} e^{\mathrm{i}\omega t} \left(e^{\pm \mathrm{i}\omega_{lmn} t - |t|/\tau_{lmn}} \right) dt = \frac{2/\tau_{lmn}}{(1/\tau_{lmn})^2 + (\omega \pm \omega_{lmn})^2} \equiv 2 b_\pm \,. \tag{6.4.14}$$

Then the Fourier transforms of the plus and cross components become:

$$\tilde{h}_+ = \frac{M}{r} \mathcal{A}^+_{lmn} \left[e^{\mathrm{i}\phi^+_{lmn}} S_{lmn} b_+ + e^{-\mathrm{i}\phi^+_{lmn}} S^*_{lmn} b_- \right] , \tag{6.4.15a}$$

$$\tilde{h}_\times = -\mathrm{i} \frac{M}{r} \mathcal{A}^\times_{lmn} \left[e^{\mathrm{i}\phi^\times_{lmn}} S_{lmn} b_+ - e^{-\mathrm{i}\phi^\times_{lmn}} S^*_{lmn} b_- \right] . \tag{6.4.15b}$$

We can directly plug these Fourier transforms into the definition (6.4.13) of the SNR to get

$$\begin{aligned} \rho^2(\theta_S, \phi_S, \psi_S, \iota, \beta) = \; & 2 \left(\frac{M}{r} \right)^2 \int_0^\infty \frac{df}{S_h(f)} \times \\ & \times \Big\{ \left(b_+^2 + b_-^2 \right) \left[\mathcal{A}^{+\,2}_{lmn} F_+^2 + \mathcal{A}^{\times\,2}_{lmn} F_\times^2 - 2 \mathcal{A}^+_{lmn} \mathcal{A}^\times_{lmn} F_+ F_\times \sin(\phi^+_{lmn} - \phi^\times_{lmn}) \right] |S_{lmn}|^2 \\ & + 2 b_+ b_- \Big[\Re \left[\left(\mathcal{A}^{+\,2}_{lmn} F_+^2 e^{2\mathrm{i}\phi^+_{lmn}} - \mathcal{A}^{\times\,2}_{lmn} F_\times^2 e^{2\mathrm{i}\phi^\times_{lmn}} \right) S^2_{lmn} \right] \\ & + 2 \mathcal{A}^+_{lmn} \mathcal{A}^\times_{lmn} F_+ F_\times \Im \left(e^{\mathrm{i}(\phi^+_{lmn} + \phi^\times_{lmn})} S^2_{lmn} \right) \Big] \Big\} . \end{aligned} \tag{6.4.16}$$

The terms proportional to S^2_{lmn} cannot be angle-averaged analytically in the usual way, so to deal with this general expression one must perform a Monte Carlo simulation. Given randomly generated values of the angles we can compute numerically the spin-weighted spheroidal harmonics at the QNM frequencies, plug the harmonics into the integrals, and finally average the resulting SNRs. We leave this for future work.

However, especially for slowly-damped modes with $m \geq 0$, the imaginary part of S_{lmn} is typically smaller than the real part:

$$S_{lmn} \simeq \Re(S_{lmn}) \,, \qquad \Re(S_{lmn}) \gg \Im(S_{lmn}) \,. \tag{6.4.17}$$

We give a quantitative discussion of the validity of this approximation elsewhere [38]. We will henceforth assume that the S_{lmn} are real, so that $S^2_{lmn} = |S^2_{lmn}|$, and we can complete the angle averaging analytically to obtain

$$\begin{aligned} \rho^2 = \; & \frac{1}{10\pi} \left(\frac{M}{r} \right)^2 \int_0^\infty \frac{df}{S_h(f)} \times \\ \times \; & \left\{ \left(b_+^2 + b_-^2 \right) \left[\mathcal{A}^{+\,2}_{lmn} + \mathcal{A}^{\times\,2}_{lmn} \right] + 2 b_+ b_- \left[\mathcal{A}^{+\,2}_{lmn} \cos(2\phi^+_{lmn}) - \mathcal{A}^{\times\,2}_{lmn} \cos(2\phi^\times_{lmn}) \right] \right\} . \end{aligned} \tag{6.4.18}$$

We expect that the resulting SNR should be reasonably close to the true angle-averaged result as long as the imaginary part of the harmonics is not too large.

We make the further approximation that the damping time is sufficiently long that the frequency-dependent functions $b_+^2 + b_-^2$ and $b_+ b_-$ may be replaced by suitable δ-functions, namely in the large Q_{lmn} or large τ_{lmn} limit,

$$\begin{aligned} b_+^2 + b_-^2 &\rightarrow \frac{\tau_{lmn}}{4}\left[\delta(f - f_{lmn}) + \delta(f + f_{lmn})\right] , \\ b_+ b_- &\rightarrow \frac{\tau_{lmn}}{8}\frac{1}{1+4Q_{lmn}^2}\left[\delta(f - f_{lmn}) + \delta(f + f_{lmn})\right] , \end{aligned} \tag{6.4.19}$$

where the normalizations are obtained by integrating over positive frequencies only. This approximation is mathematically, though not physically equivalent to assuming that the noise density $S_h(f)$ is strictly constant. We then obtain the angle-averaged SNR,

$$\begin{aligned} \rho^2 = \frac{Q_{lmn}}{40\pi^2 f_{lmn}(1+4Q_{lmn}^2) S_h(f_{lmn})} \quad \times \quad & \left\{ \left(\frac{M\mathcal{A}^+_{lmn}}{r}\right)^2 \left[1 + \cos(2\phi^+_{lmn}) + 4Q_{lmn}^2\right] \right. \\ + \quad & \left. \left(\frac{M\mathcal{A}^\times_{lmn}}{r}\right)^2 \left[1 - \cos(2\phi^\times_{lmn}) + 4Q_{lmn}^2\right] \right\} . \end{aligned} \tag{6.4.20}$$

For simplicity, FH also make an assumption about the relative amplitudes and phases of the waves, taking a pure cosine for the +-polarization ($\phi^+_{lmn} = 0$), a pure sine for the $\times$-polarization ($\phi^\times_{lmn} = 0$), and assuming $\mathcal{A}^+_{lmn} = \mathcal{A}^\times_{lmn} = \mathcal{A}_{lmn}$. With these assumptions, the SNR takes the form,

$$\rho^2_{\rm FH} = \left(\frac{M}{r}\right)^2 \frac{\mathcal{A}^2_{lmn}}{80\pi^5\tau^2_{lmn}} \int_0^\infty \frac{df}{S_h(f)} \left\{ \frac{1}{\left[(f+f_{lmn})^2 + (2\pi\tau_{lmn})^{-2}\right]^2} + \frac{1}{\left[(f-f_{lmn})^2 + (2\pi\tau_{lmn})^{-2}\right]^2} \right\} \tag{6.4.21a}$$

$$\simeq \left(\frac{M}{r}\right)^2 \frac{Q_{lmn}\mathcal{A}^2_{lmn}}{20\pi^2 f_{lmn} S_h(f_{lmn})} , \tag{6.4.21b}$$

where the second expression corresponds to the δ-function limit.

It is now useful, following FH, to define an energy spectrum through the relation

$$\rho^2 = \frac{2}{5\pi^2 r^2} \int_0^\infty \frac{1}{f^2 S_h(f)} \frac{dE}{df} df . \tag{6.4.22}$$

From Eq. (6.4.18), we obtain

$$\frac{dE}{df} = \frac{\pi M^2 f^2}{4} \left\{ \left(b_+^2 + b_-^2\right) \left[\mathcal{A}^{+\,2}_{lmn} + \mathcal{A}^{\times\,2}_{lmn}\right] + 2 b_+ b_- \left[\mathcal{A}^{+\,2}_{lmn} \cos(2\phi^+_{lmn}) - \mathcal{A}^{\times\,2}_{lmn} \cos(2\phi^\times_{lmn})\right] \right\} .$$

We then define the "radiation efficiency" $\epsilon_{\rm rd}$, by

$$\epsilon_{\rm rd} \equiv \frac{E_{\rm GW}}{M} = \frac{1}{M} \int_0^\infty \frac{dE}{df} df . \tag{6.4.23}$$

Substituting Eq. (6.4.23) into (6.4.23) and integrating, and comparing the result with Eq. (6.4.20), we find a relation between SNR and radiation efficiency for a given mode, in the δ-function or constant-noise limit,

$$\rho_{\rm FH} = \left(\frac{2}{5}\right)^{1/2} \left(\frac{1}{\pi f_{lmn} r}\right) \left(\frac{\epsilon_{\rm rd} M}{S_h(f_{lmn})}\right)^{1/2} \frac{2Q_{lmn}}{\sqrt{1+4Q^2_{lmn}}} . \tag{6.4.24}$$

independently of any condition on the relative amplitudes or phases.

With the FH choice of phases and amplitudes, the resulting energy spectrum is their formula (3.18):

$$\left(\frac{dE}{df}\right)_{\rm FH} = \frac{\mathcal{A}_{lmn}^2 M^2 f^2}{32\pi^3 \tau_{lmn}^2}\left\{\frac{1}{[(f+f_{lmn})^2+(2\pi\tau_{lmn})^{-2}]^2}+\frac{1}{[(f-f_{lmn})^2+(2\pi\tau_{lmn})^{-2}]^2}\right\}$$
$$\simeq \frac{\mathcal{A}_{lmn}^2 Q_{lmn} M^2 f_{lmn}}{8}\delta(f-f_{lmn})\,. \qquad (6.4.25)$$

where the second expression corresponds to the δ-function limit. Integrating the FH energy spectrum (6.4.25) explicitly, we find that the amplitude is related to $\epsilon_{\rm rd}$ by

$$\mathcal{A}_{lmn} = \sqrt{\frac{32 Q_{lmn}\epsilon_{\rm rd}}{M f_{lmn}(1+4Q_{lmn}^2)}} \simeq \sqrt{\frac{8\epsilon_{\rm rd}}{M Q_{lmn} f_{lmn}}}\,, \qquad (6.4.26)$$

where the second expression corresponds to the δ-function limit.

Using our general spectrum (6.4.23) we can relate the polarization-phase dependent amplitude to an efficiency per polarization $\epsilon_{\rm rd}^{+,\times}$ by

$$\mathcal{A}_{lmn}^{+,\times} = \sqrt{\frac{64 Q_{lmn}\epsilon_{\rm rd}^{+,\times}}{M f_{lmn}[1+4Q_{lmn}^2 \pm \cos(2\phi_{lmn}^{+,\times})]}} \simeq \sqrt{\frac{16\epsilon_{\rm rd}^{+,\times}}{M Q_{lmn} f_{lmn}}}\,, \qquad (6.4.27)$$

where the upper and lower signs refer to the + and × polarizations, respectively, and where the last step again corresponds to the δ-function limit.

The expressions used in this Section are valid for any interferometric detector. In all of our *LISA* calculations we take into account the fact that the LISA arms form an angle of 60 degrees; as a result, when integrating our results with the LISA noise curve, we must multiply all amplitudes by a geometrical correction factor $\sqrt{3}/2$, so that $\mathcal{A}_{+,\times}^{LISA} = \sqrt{3}/2 \times \mathcal{A}_{+,\times}$.

We now combine the expression (6.4.24) with an analytic approximation for the LISA noise curve of the form

$$S_h^{\rm NSA}(f) = \left[9.18\times10^{-52}\left(\frac{f}{1\ {\rm Hz}}\right)^{-4} + 1.59\times10^{-41} + 9.18\times10^{-38}\left(\frac{f}{1\ {\rm Hz}}\right)^{2}\right]\ {\rm Hz}^{-1}\,. \qquad (6.4.28)$$

Rescaling frequencies in terms of the dimensionless frequency $\mathcal{F}_{lmn} = M\omega_{lmn}$, and inserting redshift factors suitably, we obtain

$$\rho_{\rm FH} = \frac{5.1\times10^3}{\mathcal{F}_{lmn}}\left(\frac{\epsilon_{\rm rd}}{0.03}\right)^{1/2}\left(\frac{(1+z)M}{10^6\,M_\odot}\right)^{3/2}\left(\frac{1\,{\rm Gpc}}{D_L(z)}\right)\left(\frac{S_0}{S_h(f_{lmn})}\right)^{1/2}\frac{2Q_{lmn}}{\sqrt{1+4Q_{lmn}^2}}\,, \qquad (6.4.29)$$

where

$$\frac{S_h(f_{lmn})}{S_0} = \frac{5.4\times10^{-5}}{\mathcal{F}_{lmn}^4}\left(\frac{(1+z)M}{10^6 M_\odot}\right)^4 + 1 + 6.0\,\mathcal{F}_{lmn}^2\left(\frac{10^6 M_\odot}{(1+z)M}\right)^2\,. \qquad (6.4.30)$$

The dimensionless, mode-dependent quantities $\mathcal{F}_{lmn}$ and Q_{lmn} are of order unity and vary relatively weakly from mode to mode; for low order modes they can be determined from analytic fits [45].

So far we have confined attention to the FH convention. If we follow the alternative EF convention of keeping the waveform only for $t > 0$, and use the δ-function limit, we get the SNR

$$\rho_{\rm EF}^2 = \frac{Q_{lmn}}{40\pi^2 f_{lmn}(1+4Q_{lmn}^2)S}$$

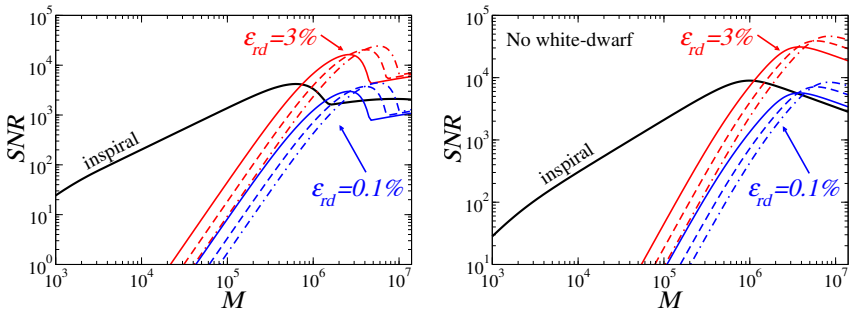

Figure 6.3: Comparison of the SNR for inspiral and ringdown waveforms. In the left panel we use the Barack-Cutler noise-curve; in the right panel we use the same noise curve, but we do not include white-dwarf confusion noise. The thick (black) line marked by "inspiral" is the (angle-averaged) SNR for the inspiral of two equal-mass black holes at $D_L = 3$ Gpc. The other sets of lines (red and blue in color versions) show the SNR for the $l = m = 2$ mode using the δ-function approximation, assuming a ringdown efficiency $\epsilon_{\rm rd} = 3\%$ and 0.1% respectively. Solid, dashed and dot-dashed lines correspond to $j = 0$ (Schwarzschild), $j = 0.8$ and $j = 0.98$ respectively.

$$\times \quad \left\{ \left(\frac{M\mathcal{A}^{+}_{lmn}}{r} \right)^2 \left[1 + \cos(2\phi^{+}_{lmn}) - 2Q_{lmn} \sin(2\phi^{+}_{lmn}) + 4Q^2_{lmn} \right] \right.$$
$$+ \quad \left. \left(\frac{M\mathcal{A}^{\times}_{lmn}}{r} \right)^2 \left[1 - \cos(2\phi^{\times}_{lmn}) + 2Q_{lmn} \sin(2\phi^{\times}_{lmn}) + 4Q^2_{lmn} \right] \right\} , \tag{6.4.31}$$

where the additional phase-dependent term comes from the lack of time symmetry imposed on the waveform. The rest of the formulae in this section can be recast simply using this convention.

6.4.2 Numerical Results

We first compute SNRs for both inspiral and ringdown for events at $D_L = 3$ Gpc, corresponding to a redshift $z \simeq 0.54$. To compute the inspiral SNR we adopt the method discussed in Ref. [35]. We perform an angle-average over pattern functions, assuming that we observe the last year of inspiral and that we can extrapolate the LISA noise curve down to a frequency $f \simeq 10^{-5}$ Hz. Following the common practice, we truncate the signal-to-noise ratio integral, Eq. (6.4.13), using an upper cutoff frequency determined by the conventional Schwarzschild ISCO for a black hole of mass M.

We compute the ringdown SNR for the fundamental mode with $l = m = 2$; calculations for different values of l and m yield similar results, the SNR depending mainly on the ringdown efficiency in a given mode. We use the FH SNR (6.4.21) and adopt the δ-function approximation (6.4.21b). Performing the "full" integral over the Breit-Wigner distribution (6.4.21a) we obtain essentially indistinguishable results, except for a small ($\lesssim$ 10%) disagreement in the mass/frequency region dominated by the white-dwarf confusion noise.

The results are shown in Fig. 6.3. These plots can be viewed as an updated version of Fig. 6 in FH. Compared to FH we use a better model of the LISA noise curve. In particular, a comparison of the left and right panels illustrates the effect of white-dwarf confusion noise on the expected SNR. In both panels of Fig. 6.3, the thick curve marked by "inspiral" represents the inspiral SNR for two equal-mass black holes with total mass M equal to the mass of the final black hole.

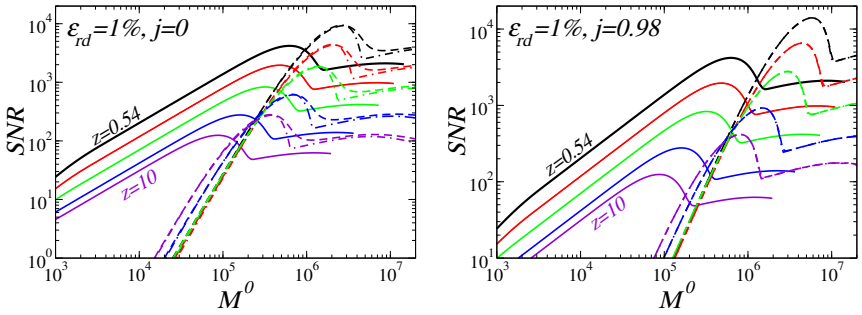

Figure 6.4: Dependence of the SNR on redshift, for both inspiral (continuous lines) and ringdown (dashed and dot-dashed lines). We choose a ringdown efficiency $\epsilon_{\rm rd} = 1\%$ and consider the cases $j = 0$, $j = 0.8$ and $j = 0.98$. From top to bottom the lines in each panel correspond to $z = 0.54$ (black in color versions; $D_L = 3$ Gpc), $z = 1$ (red), $z = 2$ (green), $z = 5$ (blue) and $z = 10$ (purple). The dashed lines are obtained from the full integral, the dot-dashed lines use the δ-function approximation.

The ringdown SNR in Fig. 6.3 is shown as sets of solid, dashed and dot-dashed lines, corresponding to the limiting case of a Schwarzschild black hole with $j = 0$, an intermediate rotation rate $j = 0.8$, and a near extremal rate $j = 0.98$, respectively. For the ringdown efficiency we show the value $\epsilon_{\rm rd} = 3$ % considered by FH, as well as a pessimistic value $\epsilon_{\rm rd} = 0.1$ %. The latter value corresponds to estimates for the energy emitted in a maximally symmetric merger, i.e. in the head-on collision of equal-mass black holes [193]. For unequal-mass mergers, FH suggest (interpolating between numerical and perturbative results) an energy scaling of the form $(4\mu/M)^2$, where μ is the reduced mass. [EB: Update...]

The general features of the SNR curves are easy to understand. The SNR is basically proportional to the inverse of the noise power spectral density $S_h(f)$. It has a maximum in the mass range $M \sim 10^6 M_\odot$ corresponding to the frequency $f \sim 10^{-2}$ Hz at which LISA is most sensitive. If we include white-dwarf confusion noise (left panel) we observe the appearance of a dip in the SNR at masses M of the order of a few times $10^6 M_\odot$. The black hole at our Galactic Center has an estimated mass $M \simeq 4 \times 10^6\ M_\odot$, so an accurate modelling of the white-dwarf confusion noise might be very important for detection of black hole ringdown from galactic centers. Unless otherwise stated, we will include white-dwarf confusion noise in all of our numerical calculations.

Fig. 6.3 illustrates that, even under pessimistic assumptions, the ringdown SNR is generally comparable to the inspiral SNR. Reducing the rotation rate does not have a dramatic effect, degrading the SNR of corotating modes by factors of order unity. The crucial element for detectability is the fraction of mass-energy $\epsilon_{\rm rd}$ going into each mode. Note that Eq. (6.4.24) implies that $\rho \sim \sqrt{\epsilon_{\rm rd}}$.

FH and Ref. [174] pointed out that, depending on the ringdown efficiency, there might be a "critical mass" at which black hole ringdown becomes dominant over inspiral. Assuming an efficiency $\epsilon_{\rm rd} = 1\%$ and a final black hole angular momentum $j = 0.997$, Ref. [174] found that the SNR is greater in the ringdown signal for $M \gtrsim 10^6 M_\odot$ when $z = 1$. Their result is consistent with our Fig. 6.3; in addition, we find that this "critical mass" for the transition from inspiral to ringdown dominance depends only weakly on j, being more sensitive to the efficiency $\epsilon_{\rm rd}$. Numerical relativity simulations provide us with reasonable estimates of $\epsilon_{\rm rd}$, as discussed in Section 6.6 below.

The cosmological redshift affects the detectability window and the SNR both for inspiral and for ringdown waves, both through the decreasing signal strength with

distance and through shifting the relevant frequencies to different parts of the LISA noise spectrum. Fig. 6.4 shows the results of numerical calculations of the SNR. For the ringdown signal, we pick a "best guess" for the efficiency $\epsilon_{\rm rd}$ of 1%, intermediate between the 3% of FH and the 0.1% from head-on collisions. Each plot gives the SNR as a function of M^0 (mass in the source frame) for a different value of j (left to right, $j = 0$, $j = 0.8$ and $j = 0.98$). From top to bottom, the curves show sources at redshifts $z = 0.54$, 1, 2, 5 and 10. The continuous lines are the inspiral SNR, the dashed lines are obtained from the full integral, the dot-dashed lines use the δ-function approximation. The inspiral SNR is (somewhat arbitrarily) truncated at the (large) value of the mass for which the starting frequency (which we pick to be one year before the ISCO, as in [35]) becomes lower than 10^{-5} Hz.

6.5 Parameter Estimation by Detection of a Single Mode

6.5.1 Analytic Results

In this Section we will go beyond the issue of detectability and try to answer a different question: given the detection of a single QNM, what can we learn about the black hole parameters? To estimate the black hole parameters from ringdown waveforms, we use the standard technique of parameter estimation in matched filtering. By maximizing the correlation between a template gravitational waveform that depends on a set of parameters θ^a (for example, the black hole mass and angular momentum) and a measured signal, matched filtering provides a natural way to estimate the parameters of the signal and their errors. With a given noise spectral density for the detector, $S_h(f)$, one defines the inner product between two signals $h_1(t)$ and $h_2(t)$ by

$$(h_1|h_2) \equiv 2\int_0^\infty \frac{\tilde{h}_1^* \tilde{h}_2 + \tilde{h}_2^* \tilde{h}_1}{S_h(f)} df\,, \tag{6.5.32}$$

where $\tilde{h}_1(f)$ and $\tilde{h}_2(f)$ are the Fourier transforms of the respective gravitational waveforms $h(t)$. The components of the "Fisher matrix" Γ_{ab} are then given by

$$\Gamma_{ab} \equiv \left(\frac{\partial h}{\partial \theta^a} \mid \frac{\partial h}{\partial \theta^b} \right)\,, \tag{6.5.33}$$

In the limit of large SNR, if the noise is stationary and Gaussian, the probability that the gravitational-wave signal $s(t)$ is characterized by a given set of values of the source parameters θ^a is

$$p(\boldsymbol{\theta}|s) = p^{(0)}(\boldsymbol{\theta}) \exp\left[-\frac{1}{2}\Gamma_{ab}\delta\theta^a\delta\theta^b \right]\,. \tag{6.5.34}$$

where $\delta\theta^a = \theta^a - \hat{\theta}^a$, and $p^{(0)}(\boldsymbol{\theta})$ represents the distribution of prior information. An estimate of the rms error, $\Delta\theta^a = (\langle(\delta\theta^a)^2\rangle)^{1/2}$, in measuring the parameter θ^a can then be calculated, in the limit of large SNR, by taking the square root of the diagonal elements of the inverse of the Fisher matrix,

$$\Delta\theta^a = \sqrt{\Sigma^{aa}}\,, \qquad \Sigma = \Gamma^{-1}\,. \tag{6.5.35}$$

The correlation coefficients between two parameters θ^a and θ^b are given by

$$c_{ab} = \Sigma^{ab}/\sqrt{\Sigma^{aa}\Sigma^{bb}}\,. \tag{6.5.36}$$

We consider a waveform given by Eq. (6.4.10), with the S_{lmn} assumed to be real,

$$h_+ = \frac{M}{r}\mathcal{A}^+_{lmn} e^{-\pi f_{lmn} t/Q_{lmn}} \cos\left[2\pi f_{lmn} t + \phi^+_{lmn}\right] S_{lmn}(\iota,\beta)\,, \quad (6.5.37a)$$

$$h_\times = \frac{M}{r}\mathcal{A}^\times_{lmn} e^{-\pi f_{lmn} t/Q_{lmn}} \sin\left[2\pi f_{lmn} t + \phi^\times_{lmn}\right] S_{lmn}(\iota,\beta)\,. \quad (6.5.37b)$$

We also define

$$\frac{M}{r}\mathcal{A}^+_{lmn_1} \equiv A^+\,, \qquad \frac{M}{r}\mathcal{A}^\times_{lmn_1} \equiv A^\times \equiv A^+ \mathrm{N}_\times\,, \quad (6.5.38)$$

where $N_\times$ is some numerical factor, and

$$\phi^\times_{lmn} = \phi^+_{lmn} + \phi^0_{lmn}\,. \quad (6.5.39)$$

Assuming that we know $N_\times$ and ϕ^0_{lmn}, this waveform is dependent on four parameters (A^+, ϕ^+_{lmn}, M, j); otherwise it depends on six parameters (A^+, $A^\times$, ϕ^+_{lmn}, $\phi^\times_{lmn}$, M, j). A popular choice for $N_\times$ [96] is to assume that the distribution of the strain in the two polarizations mimics that of the inspiral phase: $N_\times = -2(\hat{\mathbf{L}}\cdot\hat{\mathbf{n}})/[1+(\hat{\mathbf{L}}\cdot\hat{\mathbf{n}})^2]$, where $\hat{\mathbf{L}}$ is the orientation of the binary's angular momentum and $\hat{\mathbf{n}}$ is a unit vector describing the binary's position in the sky. Fortunately, we will see that the errors have a very weak dependence on the number of parameters and on the (uncertain) value of the parameters $N_\times$ and ϕ^0_{lmn}.

Assuming constant noise over the bandwidth of the signal, or taking the δ-function approximation, and using the FH doubling convention, we get the SNR (6.4.20). In this approximation, errors and correlation coefficients can be computed analytically using Mathematica or Maple. The full expressions are lengthy and unenlightening, and we have implemented them numerically in a Fortran code.

We first calculate the Fisher matrix in the parameter basis of (A^+, ϕ^+_{lmn}, f_{lmn}, Q_{lmn}), where it takes on a simpler form:

$$\Gamma_{A^+A^+} = \frac{\gamma}{(A^+)^2}\left(1+4Q^2_{lmn}-\beta\right)\,, \quad (6.5.40a)$$

$$\Gamma_{A^+\phi^+_{lmn}} = \frac{\gamma}{A^+}\alpha\,, \quad (6.5.40b)$$

$$\Gamma_{A^+f_{lmn}} = -\frac{\gamma}{2A^+ f_{lmn}}\left(1+4Q^2_{lmn}-\beta\right)\,, \quad (6.5.40c)$$

$$\Gamma_{A^+Q_{lmn}} = \frac{\gamma}{2A^+Q_{lmn}}\frac{1}{1+4Q^2_{lmn}}\left[(1+4Q^2_{lmn})^2-(1-4Q^2_{lmn})\beta\right] \quad (6.5.40d)$$

$$\Gamma_{\phi^+_{lmn}\phi^+_{lmn}} = \gamma\left(1+4Q^2_{lmn}+\beta\right)\,, \quad (6.5.40e)$$

$$\Gamma_{\phi^+_{lmn}f_{lmn}} = -\frac{\gamma}{2f_{lmn}}\alpha\,, \quad (6.5.40f)$$

$$\Gamma_{\phi^+_{lmn}Q_{lmn}} = \frac{\gamma}{2Q_{lmn}}\left(\frac{1-4Q^2_{lmn}}{1+4Q^2_{lmn}}\right)\alpha\,, \quad (6.5.40g)$$

$$\Gamma_{f_{lmn}f_{lmn}} = \frac{\gamma}{2f^2_{lmn}}\left[(1+4Q^2_{lmn})^2-\beta\right]\,, \quad (6.5.40h)$$

$$\Gamma_{f_{lmn}Q_{lmn}} = -\frac{\gamma}{2f_{lmn}Q_{lmn}}\frac{1}{1+4Q^2_{lmn}}\left[(1+4Q^2_{lmn})^2-(1-4Q^2_{lmn})\beta\right]\,, \quad (6.5.40i)$$

$$\Gamma_{Q_{lmn}Q_{lmn}} = \frac{\gamma}{2Q^2_{lmn}}\frac{1}{(1+4Q^2_{lmn})^2}\left[(1+4Q^2_{lmn})^3-(1-12Q^2_{lmn})\beta\right]\,, \quad (6.5.40j)$$

where

$$\alpha = \sin^2\psi \sin 2\phi^{\times}_{lmn} - \cos^2\psi \sin 2\phi^{+}_{lmn}\,, \tag{6.5.41a}$$
$$\beta = \sin^2\psi \cos 2\phi^{\times}_{lmn} - \cos^2\psi \cos 2\phi^{+}_{lmn}\,, \tag{6.5.41b}$$
$$\gamma = \frac{A^2 Q_{lmn}}{40\pi^2 f_{lmn}(1+4Q^2_{lmn})}\,, \tag{6.5.41c}$$

with $\cos\psi \equiv 1/\sqrt{1+N^2_{\times}}$, $\sin\psi \equiv N_{\times}/\sqrt{1+N^2_{\times}}$ and $A^2 = (A^{+})^2(1+N^2_{\times}) = (A^{+})^2 + (A^{\times})^2$. Note that, in this notation, $\rho^2_{FH} = \gamma(1+4Q^2_{lmn}-\beta)$.

We note that the Fisher matrix written in terms of the frequency and damping time is usually simpler [92,130] than that in terms of mass and angular momentum; however we prefer to deal directly with measurements of j and M.

The transformation from the (A^{+}, ϕ^{+}_{lmn}, f_{lmn}, Q_{lmn}) basis to the (A^{+}, ϕ^{+}_{lmn}, M, j) basis is straightforward, namely, for any index k,

$$\begin{aligned}\Gamma_{k\,M} &= -(f_{lmn}/M)\Gamma_{k\,f_{lmn}}\,,\\ \Gamma_{k\,j} &= f'_{lmn}\Gamma_{k\,f_{lmn}} + Q'_{lmn}\Gamma_{k\,Q_{lmn}}\,,\end{aligned} \tag{6.5.42}$$

where $f'_{lmn} \equiv df_{lmn}/dj$ and $Q'_{lmn} \equiv dQ_{lmn}/dj$.

Converting to this basis and inverting the Fisher matrix, we find, to leading order in Q^{-1}_{lmn}, the errors

$$\sigma_j = \frac{1}{\rho_{\rm FH}}\left|2\frac{Q_{lmn}}{Q'_{lmn}}\left(1+\frac{1+4\beta}{16Q^2_{lmn}}\right)\right|\,, \tag{6.5.43a}$$
$$\sigma_M = \frac{1}{\rho_{\rm FH}}\left|2\frac{MQ_{lmn}f'_{lmn}}{f_{lmn}Q'_{lmn}}\left(1+\frac{1+4\beta}{16Q^2_{lmn}}\right)\right|\,, \tag{6.5.43b}$$
$$\sigma_{A^{+}} = \frac{\sqrt{2}A^{+}}{\rho_{\rm FH}}\left|1+\frac{3\beta}{8Q^2_{lmn}}\right|\,, \tag{6.5.43c}$$
$$\sigma_{\phi^{+}_{lmn}} = \frac{1}{\rho_{\rm FH}}\left|1-\frac{\beta}{4Q^2_{lmn}}\right|\,, \tag{6.5.43d}$$

and the correlation coefficients

$$r_{jM} = {\rm sgn}(f'_{lmn}) \times \left(1-\frac{f^2_{lmn}Q'^2_{lmn}}{16Q^4_{lmn}f'^2_{lmn}}\right) + \mathcal{O}(1/Q^6)\,, \tag{6.5.44a}$$
$$r_{jA^{+}} = -\frac{1}{\sqrt{2}}\left(1-\frac{1-6\beta}{16Q^2_{lmn}}\right) + \mathcal{O}(1/Q^4)\,, \tag{6.5.44b}$$
$$r_{MA^{+}} = -\frac{1}{\sqrt{2}}\left(1-\frac{1-6\beta}{16Q^2_{lmn}}\right) + \mathcal{O}(1/Q^3)\,, \tag{6.5.44c}$$
$$r_{j\phi^{+}_{lmn}} = \frac{\alpha}{2Q^2_{lmn}} - \frac{7-8\beta}{32Q^4_{lmn}} + \mathcal{O}(1/Q^6)\,, \tag{6.5.44d}$$
$$r_{M\phi^{+}_{lmn}} = \frac{\alpha}{2Q^2_{lmn}} - \frac{7-8\beta}{32Q^4_{lmn}} + \mathcal{O}(1/Q^6)\,, \tag{6.5.44e}$$
$$r_{A^{+}\phi^{+}_{lmn}} = -\frac{3\alpha}{4\sqrt{2}Q^2_{lmn}} + \frac{\alpha(10-11\beta)}{32\sqrt{2}Q^4_{lmn}} + \mathcal{O}(1/Q^6)\,. \tag{6.5.44f}$$

In calculating derivatives of the waveforms (6.5.37) with respect to M and j (or with respect to f_{lmn} and Q_{lmn}), we have ignored derivatives of the spheroidal harmonics themselves. The S_{lmn} are functions of $a\omega_{lmn} = j\mathcal{F}_{lmn}$ which is a function of j only. However, the S_{lmn} may be expanded in powers of $j\mathcal{F}_{lmn}$, in the form

$$S_{lmn} = Y_{lm} + (j\mathcal{F}_{lmn})\sum_{l'\neq l} c_{l'lm}Y_{l'm} + O(j\mathcal{F}_{lmn})^2\,, \tag{6.5.45}$$

where Y_{lm} denotes a *spin-weighted* spherical harmonic, and $c_{l'lm}$ are related to Clebsch-Gordan coefficients. As a result, derivatives of the S_{lmn} with respect to j will be linear in derivatives of $j\mathcal{F}_{lmn}$, and because of the orthogonality of the spin-weighted spherical harmonics, inner products of S_{lmn} with S'_{lmn} and of S'_{lmn} with itself will be at least quadratic in $j\mathcal{F}_{lmn}$ and its derivatives. At least for small $j\mathcal{F}_{lmn}$, we may expect these contributions to be small relative to the main contribution obtained by ignoring these derivatives. Nevertheless, the effect of this approximation should be explored further.

The diagonal elements of the correlation matrix $r_{ii} = 1$ for all i. The $\mathrm{sgn}(f'_{lmn})$ in r_{jM} comes from a $\sqrt{f'^2_{lmn}}/f'_{lmn} = |f'_{lmn}|/f'_{lmn}$. It implies that j and M have a positive correlation for corotating and axisymmetric modes ($m \geq 0$), but they are anticorrelated for counterrotating modes ($m < 0$): this is basically determined by the different sign of f'_{lmn} for the two classes of modes (see eg. Fig. 6.1).

The large-Q_{lmn} expansions are typically accurate as long as Q'_{lmn}/Q_{lmn} is not very large (see Fig. 6.6 below, where this statement is made more quantitative). An analytic parametrization for σ can be obtained by combining the SNR formula (6.4.29) and (6.4.30) with the QNM fits, whose coefficients are provided in [45].

Some general comments on Eqs. (6.5.43) and (6.5.44) are in order. First, by combining Eqs. (6.5.43a) and (6.5.43b) with Eq. (6.4.29), we see that the accuracy in measuring M and j can be very high under the right circumstances, namely,

$$\frac{\sigma_M}{M} \simeq 6.8\times 10^{-3}\times h_{lmn}(j)\mathcal{F}_{lmn}\times\left(\frac{10^{-4}}{\epsilon_{\rm rd}}\right)^{1/2}\left(\frac{S_h(f_{lmn})}{S_0}\right)^{1/2}\left(\frac{D_L(z)}{1\ \mathrm{Gpc}}\right)\left(\frac{10^6 M_\odot}{(1+z)M}\right)^{3/2}, \tag{6.5.46a}$$

$$\sigma_j \simeq 6.8\times 10^{-3}\times g_{lmn}(j)\mathcal{F}_{lmn}\times\left(\frac{10^{-4}}{\epsilon_{\rm rd}}\right)^{1/2}\left(\frac{S_h(f_{lmn})}{S_0}\right)^{1/2}\left(\frac{D_L(z)}{1\ \mathrm{Gpc}}\right)\left(\frac{10^6 M_\odot}{(1+z)M}\right)^{3/2}. \tag{6.5.46b}$$

Notice that the measurement error is small (less than a percent), even under the very pessimistic assumption that a SMBH with $M \sim 10^6\ M_\odot$ radiates only a modest fraction $E_{\rm GW} \sim 10^{-4}M$ of its mass. The functions $g_{lmn}(j) = Q_{lmn}/Q'_{lmn}$ and $h_{lmn}(j) = (Q_{lmn}f'_{lmn})/(Q'_{lmn}f_{lmn})$ depend on the particular mode we consider and on the black hole's angular momentum; they are typically of order unity. For example, using the fitting relations in [45], we find that, for the fundamental mode with $l = m = 2$ of a Schwarzschild black hole, these factors take the values $g_{lmn}(0) = 2.992$, $h_{lmn}(0) = 1.214$. So, for a non-rotating black hole the error in angular momentum is slightly larger than the error on the mass. For a near-extremal black hole we have $g_{lmn}(0.98) = 0.043$, $h_{lmn}(0.98) = 0.234$, and the error in angular momentum is now smaller than the error in the mass.

To leading order in a large-Q_{lmn} expansion the errors on angular momentum and mass, Eqs. (6.5.43a) and (6.5.43b), are proportional to Q_{lmn}/Q'_{lmn}. In Fig. 6.5 we plot this quantity as a function of j for different modes. From the plot we can anticipate a few salient features. First of all, errors should decrease with rotation for corotating modes ($m > 0$). This was already pointed out in Refs. [88,92]. However, errors should *increase* with rotation for counterrotating modes ($m < 0$); even worse, at those "critical values" of j for which $Q'_{lmn} = 0$ the errors for counterrotating modes blow up. Fig. 6.5 shows that, typically, this phenomenon is present for counterrotating modes with $|m| \leq l/2$. Finally, we can anticipate that Q_{lmn}/Q'_{lmn} (hence the error) will blow up as $j \to 0$ for modes with $m = 0$.

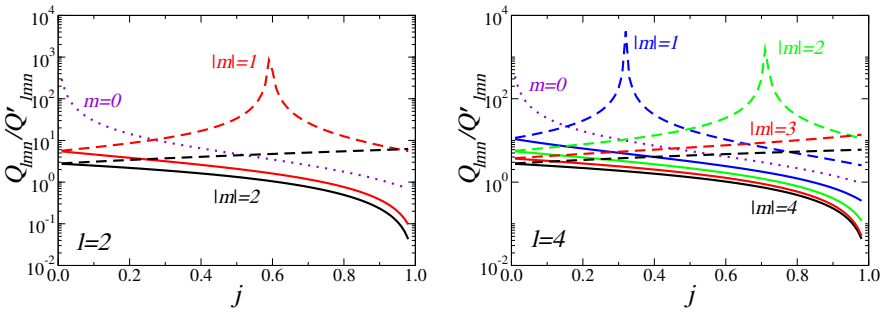

Figure 6.5: Q_{lmn}/Q'_{lmn} for the fundamental mode with $l = 2$ (left) and $l = 4$. Solid lines refer to $m > 0$, dotted lines to $m = 0$, dashed lines to $m < 0$, and different shades (colors) denote different values of m, as indicated. Notice that this factor increases with j when $m > 0$ and decreases with j when $m = -2$. The factor blows up as $j \to 0$ for $m = 0$, and as $j \to j_{\rm crit}$ for certain values of $m < 0$. This explains most qualitative features of the error plots.

6.6 Quasinormal Mode Excitation in Binary Mergers

Black hole QNMs do not form a complete set, and for this reason it is not possible to define unambiguously the beginning of the ringdown phase. In Section 6.7 we consider three different definitions of the ringdown starting time. The first definition is based on looking for the time at which a QNM expansion provides the best fit to the actual numerical waveform, in the sense of a suitably defined norm [85]. Unfortunately, when applied to binary black hole numerical waveforms, this method is not particularly useful. The reason is that the norm is quite flat (and even worse, has some oscillations) over a wide range of starting times around the minimum. A second, more useful definition looks for the time maximizing the *energy content* of the QNM component of the waveform. For this reason, following Nollert [161], we call it the Energy Maximized Orthogonal Projection, or EMOP. We find that the "EMOP time" $t_{\rm EMOP}$ and the maximum fraction of energy carried by ringdown ($\simeq 42\%$) are remarkably independent of the mass ratio q. This is an indication that the ringdown waveform is in some sense "universal": it does not depend too much on the details of the pre-merger phase. To our knowledge, the third definition of the ringdown starting time has not been introduced before. It uses a detection-based criterion, maximizing the "effective energy" deposited in a matched filter.

Table 6.1: Energy and angular momentum radiated in the merger and ringdown.

q	$j_{\rm fin}$	$j_{\rm QNM}$	$\frac{E_{\rm tot}}{M}$	$(\%l=2,3)$	$\frac{J_{\rm tot}}{M^2}$	$\frac{E_{\rm EMOP}}{M}$	$(\%l=2,3)$	$\frac{J_{\rm EMOP}}{M^2}$	$\frac{E_{\rm filter}}{M}$
1.0	0.689	0.684	0.0372	(96.3,0.4)	0.246	0.0185	(97.3,0.7)	0.0700	0.028
1.5	0.665	0.664	0.0340	(94.8,2.0)	0.229	0.0174	(91.9,2.1)	0.0676	0.026
2.0	0.626	0.626	0.0286	(91.8,4.6)	0.196	0.0142	(91.5,5.1)	0.0565	0.021
2.5	0.584	0.581	0.0238	(89.2,6.8)	0.167	0.0119	(92.4,7.6)	0.0480	0.018
3.0	0.543	0.544	0.0200	(86.8,8.7)	0.143	0.0103	(85.4,9.3)	0.0438	0.015
3.5	0.506	0.509	0.0170	(84.6,10.1)	0.124	0.0089	(84.2,9.6)	0.0387	0.012
4.0	0.474	0.478	0.0145	(83.2,11.3)	0.108	0.0078	(82.1,10.4)	0.0345	0.011

For reference, we find it useful to summarize some of our main results in Table 6.1. There we list, for each mass ratio:

(1) the dimensionless angular momentum of the final black hole $J_{\rm fin}/M_{\rm fin}^2$ as estimated from wave extraction methods ($j_{\rm fin}$) and from QNM fits ($j_{\rm QNM}$);

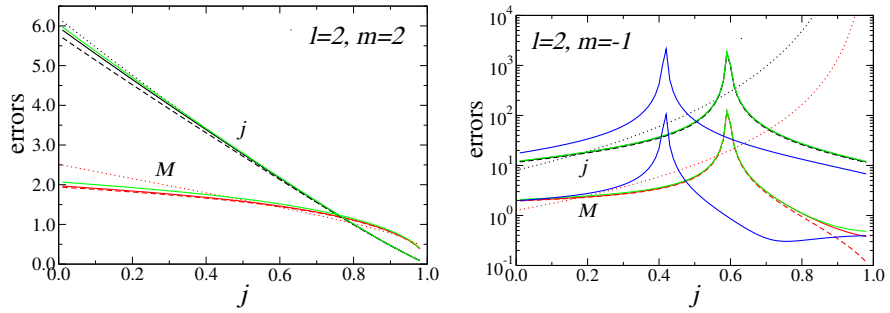

Figure 6.6: Comparison between different approaches to compute the error (multiplied by the SNR) for the fundamental mode for $(l, m) = (2, 2)$ and $(2, -1)$. Solid lines use the numerical implementation of the full expressions obtained by Mathematica, and a numerical calculation of the derivatives of Q_{lmn} and f_{lmn}. Dashed and dotted lines use expressions for the Fisher matrix to leading order in $1/Q_{lmn}$; derivatives of Q_{lmn} and f_{lmn} are evaluated numerically for the former, and using the fitting functions given in [45] for the latter. Black (red) lines refer to calculations of the error in j (M) using the FH "doubling prescription". The plot shows that all these different calculations are in excellent agreement with each other. However, sometimes using the fits can produce only order-of-magnitude estimates of the errors: this happens for counterrotating modes, where an accurate calculation of the derivatives of Q_{lmn} and f_{lmn} is more important (dotted lines in the right panel deviate significantly from the "true" answer obtained by taking numerical derivatives of the QNM tables). Finally (and only in the right panel) we plot, in blue, results obtained using Eqs. (4.20a), (4.20b) in Finn's paper [92], a numerical implementation of the full expressions obtained by Mathematica, and a numerical calculation of the derivatives of Q_{lmn} and f_{lmn}. Finn's formula would lie on top of the other lines in the left plot (for $l = m = 2$), but it gives a slightly different prediction for the errors on the counterrotating mode with $l = 2$, $m = -1$.

(2) the total energy and angular momentum radiated in each simulation ($E_{\rm tot}/M$, $J_{\rm tot}/M^2$);

(3) the energy, angular momentum and linear momentum radiated in ringdown, where the ringdown starting time is chosen according to the EMOP criterion ($E_{\rm EMOP}/M$, $J_{\rm EMOP}/M^2$, $P_{\rm EMOP}/M$);

(4) the effective fraction of energy detected by a ringdown filter ($E_{\rm filter}/M$).

The Table also shows the fraction of energy being radiated in the two dominant multipoles ($l = 2,\ 3$).

6.7 The Merger-Ringdown Transition

The goal of this Section is to study the ringdown phase, and to explore the properties of the final black hole formed after merger. We will compare different fitting methods to extract information from the ringdown waveforms. As discussed in [39], such a comparison can help us resolve real physical effects (such as, for example, time variations of the ringdown frequencies) from systematic parameter estimation errors due to the variance and bias of each particular fitting algorithm. In particular, here we consider two classes of fitting algorithms: the matrix pencil (MP) and Kumaresan-Tufts (KT) methods, which are modern variants of the so-called Prony linear-estimation algorithms for damped exponentials in noise; and a standard non-linear least-squares technique, the Levenberg-Marquardt (LM) algorithm (see [39] for details).

In [39] we pointed out that Prony methods have a number of advantages with respect to standard non-linear least-squares techniques: (i) They do not require an *initial guess* of the fitting parameters; (ii) They provide us with a simple, efficient way to estimate QNM frequencies for the *overtones*, and even to estimate how many overtones are present in the signal; (iii) Statistical properties of Prony-based methods in the presence of noise (such as their variance and bias) are well studied and under control. When compared with the LM algorithm, Prony methods seems to have comparable variance but slightly smaller bias.

In work by Buonanno, Cook and Pretorius ([55]; henceforth BCP), the real and imaginary parts of $\psi_{l\,,m}$ were fitted *separately* using standard non-linear least-squares methods. Prony-like methods allow us to fit the "full", complex signal by a function of the form

$$\psi^{\rm fit}_{l\,,m} = \sum_{l'm'n} \mathcal{A}_{l'm'n} e^{-i[\hat{\omega}_{l'm'n}(j,\ M_{\rm fin})(t-t_{\rm peak})+\phi_{l'm'n}]}\,, \qquad (6.7.47)$$

where $\hat{\omega}_{l'm'n}(j,\ M_{\rm fin})$ denotes a complex QNM frequency. In BCP the final black hole's mass and spin $(j\,, M_{\rm fin})$ are taken as the independent fitting parameters, and the different QNM frequencies $\hat{\omega}_{lmn}$ are obtained, for given $(j,\ M_{\rm fin})$, either by using fitting relations or by interpolating numerical tables [45].

BCP allow for general mode-mixing due to the expansion of *spherical* harmonics in terms of *spheroidal* harmonics. We will assume that each spherical $(l\,, m)$ mode is well described by a single $(l\,, m)$ ringdown mode. Another difference is that BCP include overtones in the QNM expansion. Adding overtones provides a good fit of the strong-field phase by effectively *increasing* the number of fitting parameters (mode amplitudes $\mathcal{A}_{lmn}$ and phases ϕ_{lmn} of the overtones). This idea is perfectly consistent with QNM expansions in the context of linear black hole perturbation theory. An obvious drawback of the idea is that it *assumes* the validity of linear perturbation theory to extend the QNM fit before the peak of the radiation. Another potential problem is that, by using many fitting parameters, we can always get very good agreement with the numerical waveforms, but we do not necessarily get a better physical description of QNM excitation. For simplicity we do not attempt to include overtones in the fit, but we only assess the accuracy of fits of the fundamental QNM. In [39] we have shown that the QNM frequency and damping time evolve quite rapidly right after merger. This evolution could be interpreted as a bias in the fitted frequencies induced by the omission of higher overtones; or, alternatively, it could mean that the mass and angular momentum of the newly formed, dynamical black hole spacetime really are *evolving* on timescales much smaller than the QNM timescales, producing an effective redshift in the QNM frequencies [165,207]. Issues such as the inclusion of overtones and the detailed study of nonlinearities will be addressed in the future.

There are important motivations to try and define the ringdown starting time and to isolate, in a non-ambiguous way, the energy radiated in the ringdown phase. For instance, from a detection-based point of view, the SNR of a ringdown signal scales with the square root of the energy in the signal [45,94]. To define the energy in ringdown waves we must somehow define the ringdown starting time. Being able to define the ringdown starting time is also important when comparing numerical simulations with PN estimates of the energy, angular and linear momentum. In fact, it has been suggested that the discrepancy between PN estimates and numerical results for black hole recoil is due to neglecting the ringdown in the former [106]. To check the validity of this statement we must, again, define the starting time of the ringdown phase.

Unfortunately, early studies in quasinormal ringing have established that there is no such thing as "the" ringdown starting time (see eg. [37] and references therein). In fact, the waveform can *never* be exactly described as a pure superposition of

damped sinusoids: it is always contaminated by noise or by other contributions (such as prompt response or tails). This is essentially a consequence of the incompleteness of QNMs. However, from a practical viewpoint the signal *is* indeed dominated by ringdown at some stage, and this is the reason why we can use ringdown waves to estimate black hole parameters [45]. The time span of the ringdown phase can be defined in different ways, depending on context. In the following we will discuss and implement three possible alternatives, two of which have already been proposed in the past [85, 161].

6.7.1 A Least-squares Approach

A natural way to determine the QNM content of a given signal would be to perform a non-linear fit of the data to an exponentially decaying sinusoid. Here the unknown parameters are usually found in a least-squares sense, by minimizing some functional of the form $\sum_{t=t_i}\left[h(t)-h^{\rm QNM}(t,\{\lambda\})\right]^2$. In our specific case h would be the numerical data, sampled at instants $t=t_i$, and $h^{\rm QNM}(t,\{\lambda\})$ is the model waveform (an exponentially damped sinusoid).

The model depends on a set of unknown parameters $\{\lambda\}$ over which the functional should be minimized. It is of course very tempting to treat the starting time as one of those parameters. This is a possible way to determine the ringdown starting time, and it served as the basis for the proposal in [85]. There it was shown that the quality of a QNM fit can be monitored by using some suitably defined norm. In particular, Ref. [85] proposed to use

$$||N||(\tau_0)=\frac{\int_{\tau_0}^{t_f}|\psi_{l\,,m}(t)-\psi^{l\,,m}_{\rm fit}|dt}{\int_{\tau_0}^{t_f}|\psi_{l\,,m}(t)|dt}\,, \tag{6.7.48}$$

where $\psi^{l\,,m}_{\rm fit}$ has been defined in Eq. (6.7.47). Clearly $||N||\to 0$ when the fit is very close to the numerical waveform. The idea is that the norm should have a local minimum when the "trial" starting time τ_0 tends to the "true" starting time, $\tau_0\to t_0$.

This idea works well for the classical perturbation theory problem of Gaussian pulses scattered off a Kerr background [85], but unfortunately it does not provide a very clear answer when tested on binary black hole merger waveforms. The norm $||N||(\tau_0)$ for a binary with $q=2.0$ is shown in Fig. 6.7, where it is computed in two slightly different ways. The simplest way treats the QNM frequencies as known: their values can be obtained once and for all by using Prony methods or non-linear fits [39], and kept fixed as we change τ_0. The second method achieves a marginal reduction of the norm by fitting for the QNM frequency at each starting time τ_0.

¿From Fig. 6.7 we see that the norm has some of the desired properties. First of all, it grows as the quality of the QNM fit degrades: for example, it is larger for the subdominant $(l,\ m)$ components. In addition the norm grows, as it should, when we try to extend the fit to encompass the merger region, i.e. when $(\tau_0-t_{\rm peak})\lesssim 10$.

We find that the functional (6.7.48) has a minimum for most, but not all of the waveforms. Even when it does have a minimum (as in the case of Fig. 6.7) this minimum is very broad. In addition the norm oscillates with a period which is basically the QNM period, and it has a series of local minima and maxima. The broad minimum and the oscillations make it very hard to locate the starting time. Of course, the functional (6.7.48) is by no means the only possibility.

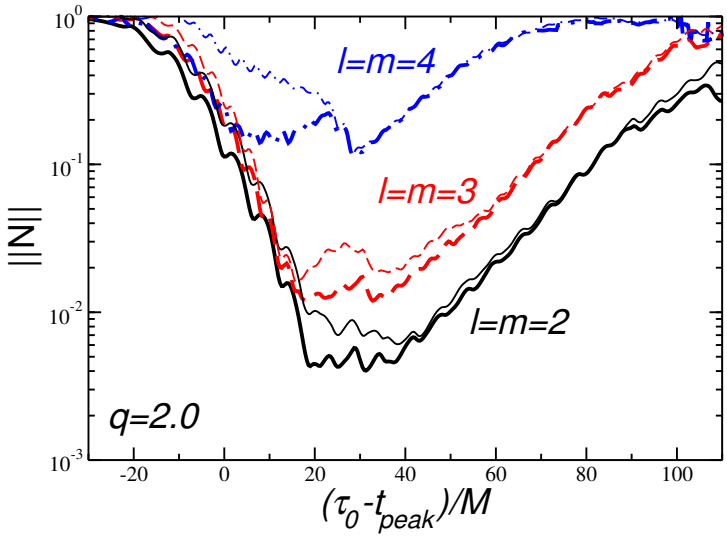

Figure 6.7: Norm (6.7.48) as a function of the trial starting time for the dominant components $(l,\ m) = (2,\ 2),\ (3,\ 3),\ (4,\ 4)$ in a merger with $q = 2.0$ (we consider a D7 run here). Thick lines are obtained by fitting the frequency each time we change τ_0. Thin lines use the following fixed values for the QNM frequency: $M\omega_R = 0.51677$, $M\omega_I = 0.08586$ for $l = m = 2$, $M\omega_R = 0.82210$, $M\omega_I = 0.08571$ for $l = m = 3$, $M\omega_R = 1.12152$, $M\omega_I = 0.08577$ for $l = m = 4$.

6.7.2 Nollert's Energy Maximized Orthogonal Projection (EMOP)

A physically motivated notion of ringdown starting time time was introduced by Nollert [161]. He realized that the problems with defining the starting time arise immediately at the onset: QNMs are not complete and not orthogonal with respect to any inner product, so a quantification of the energy (and therefore of the starting time) going into each mode, using standard "basis expansion" methods, is difficult (if not impossible). The lack of orthogonality can be circumvented by formally defining an orthogonal decomposition of the waveform into the contribution of one (or more) QNMs, and some orthogonal remainder [161]:

$$h = h_{\parallel} + h_{\perp}\,. \tag{6.7.49}$$

Here, $h_{\parallel}$ and $h_{\perp}$ are the part of h parallel and perpendicular, respectively, to a given QNM or a finite number p of QNMs. We therefore write

$$h_{\parallel} = \sum_{i=1}^{p} a_{\parallel}^{(i)} h_{\rm QNM}^{(i)}\,, \tag{6.7.50}$$

where

$$h_{\rm QNM}^{(i)} = \begin{cases} 0 & \text{if } t < t_0 \\ e^{-\omega_i t}\sin\left(\omega_r t + \phi\right) & \text{if } t > t_0\,. \end{cases} \tag{6.7.51}$$

is the QNM, assumed to start at some time t_0. The decomposition is achieved using a standard orthogonal projection

$$\langle h_{\parallel}, h_{\perp}\rangle = 0\,, \tag{6.7.52}$$

where the inner product, following arguments by Nollert [161], is defined in an energy-oriented way:

$$\langle \Psi, \Phi\rangle = \int \dot{\Psi}^{*}\dot{\Phi} dt\,. \tag{6.7.53}$$

One can show that the energy "parallel to the QNM component of the signal" is given by

$$E_{\parallel} = \left| \int \dot{h}^{(i)*}_{\rm QNM} \dot{h} dt \right|^2 \left[\int \dot{h}^{(i)*}_{\rm QNM} \dot{h}^{(i)}_{\rm QNM} dt \right]^{-1} . \tag{6.7.54}$$

It is now meaningful to talk about (say) "the fraction of energy going into the first QNM". This fraction obviously depends on the starting time t_0 in Eq. (6.7.51). Nollert observes that the ratio of the energy "parallel to the QNM component" to the total energy in the signal, $E_{\parallel}/E_{\rm tot}$, has a maximum as a function of t_0. We can define the ringdown starting time as the time t_0 corresponding to this *Energy Maximized Orthogonal Projection* (EMOP). In other words, according to Nollert's criterion, the ringdown starting time $t_0 = t_{\rm EMOP}$ is chosen by looking for[1]

$$\max_{t_0\,,\phi} \frac{E_{\parallel}}{E_{\rm tot}} = \max_{t_0\,,\phi} \left(\left| \int \dot{h}^{(i)*}_{\rm QNM} \dot{h} dt \right|^2 \left[\int \dot{h}^{(i)*}_{\rm QNM} \dot{h}^{(i)}_{\rm QNM} dt \right]^{-1} \times \left[\int \dot{h}^{*} \dot{h} dt \right]^{-1} \right) \tag{6.7.55}$$

The previous integral is evaluated separately for each polarization component. To avoid memory effects, when we integrate Ψ_4 we fix the integration constant so that $\dot{h} = 0$ at the end of the simulation. We denote by $E_{\rm EMOP}$ the maximized energy parallel to the QNM component of the signal:

$$E_{\rm EMOP} \equiv E_{\parallel}(t_0 = t_{\rm EMOP}) \, . \tag{6.7.56}$$

Using Prony methods or non-linear fits [39] we first determine the QNM frequency and the damping time (for simplicity we consider a single QNM). Then we compute $t_{\rm EMOP}$ and $E_{\rm EMOP}$ by maximizing (6.7.55) over both t_0 and ϕ.

Table 6.2: EMOP data for $l = 2$. Numbers separated by a comma correspond to the $+$ and $\times$ polarizations, respectively. The fraction of the total energy in the $l = 2$ mode is about 42% for all mass ratios. We find that, independently of mass ratio, the value of $t_{\rm EMOP}$ for a given polarization is generally at a fixed position relative to the maximum of the waveform's amplitude $t_{\rm peak}$. We measure this relative difference by $\Delta t_{\rm EMOP} \equiv t_{\rm peak} - t_{\rm EMOP}$, which turns out to be roughly independent of q.

q	run	$\frac{E_{\rm EMOP}}{E_{\rm tot}}$	$\frac{\langle t_{\rm EMOP}\rangle}{M}$	$\frac{\Delta t_{\rm EMOP}}{M}$	$\frac{\langle \Delta t_{\rm EMOP}\rangle}{M}$	$\frac{10^2 E_{\rm EMOP}}{M}$	$\frac{\langle 10^2 E_{\rm EMOP}\rangle}{M}$
1.0	D7	0.41, 0.42	225.5	10.0, 7.0	8.5	1.9, 1.7	1.8
1.5	D7	0.41, 0.43	227.2	10.8, 7.4	9.1	1.8, 1.5	1.6
2.0	D7	0.42, 0.42	227.0	9.9, 6.9	8.4	1.4, 1.2	1.3
2.5	D7	0.41, 0.43	229.2	10.6, 7.1	8.8	1.2, 0.98	1.1
3.0	D7	0.41, 0.43	230.2	11.2, 7.8	9.5	0.95, 0.82	0.88
3.5	D7	0.40, 0.43	232.0	12.5, 8.5	10.5	0.80, 0.69	0.75
4.0	D7	0.39, 0.42	233.5	13.3, 9.3	11.3	0.68, 0.59	0.64
2.0	D8	0.40, 0.41	453.0	10.6, 6.6	8.6	1.4, 1.2	1.3
3.0	D8	0.40, 0.41	408.8	11.0, 7.6	9.3	0.95, 0.81	0.88

Our results for $l = m = 2$ and run D7 are presented in Table 6.2 and Fig. 6.8. In the plots, $\epsilon_{+,\times}$ is the fraction of energy radiated at $t > t_0$ in each of the two polarization components, normalized to the total energy radiated in the simulation, and computed for the value of the phase maximizing the EMOP. The first thing to notice is that there is a sharp maximum of the fractional energy going into

[1] Another conceivable definition would not use the total energy in the waveform $E_{\rm tot}$, but the energy in the waveform for $t > t_0$. It turns out that this quantity does not have a well-defined maximum. It is also possible to use a variable frequency in (6.7.55), in which case one could possibly obtain a larger maximum. This method would be equivalent to matched filtering, which is discussed below.

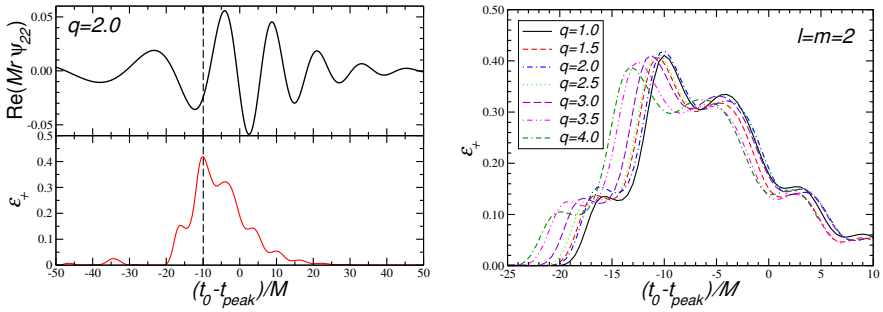

Figure 6.8: EMOP for $l = 2$ computed using run D7 (and high resolution). In the left panel we overplot ϵ_+ and the actual waveform, marking $t_{\rm EMOP}$ by a vertical dashed line. In the right panel we show that results are quite insensitive to q: each line corresponds to a different mass ratio, and linestyles are the same as in Fig. **??**.

ringdown. As seen from Fig. 6.8, $\sim 42\%$ of the total energy in the $l = 2$ merger waveform goes into ringdown. The results differ (very) slightly depending on the chosen polarization state.

In Table 6.2 we measure the ringdown starting time $t_{\rm EMOP}$ relative to the peak in $|Mr\,\psi_{22}|$, i.e., we compute $\Delta t_{\rm EMOP} \equiv t_{\rm peak} - t_{\rm EMOP}$. We see that $\Delta t_{\rm EMOP}$ is basically constant for all mass ratios *and for all runs*, corresponding to different initial separation of the binary. This is an important consistency test on the results. Notice also that $t_{\rm EMOP}$ is located *before* the peak location.

EMOP times for the two polarizations are displaced by about $3M$ for run D7. To define a unique ringdown starting time we take the average of both polarizations (in Table 6.2, an average over the two polarizations is denoted by angular brackets). Using this average starting time we can define an energy radiated in ringdown, also shown in Table 6.2. We find the following formula to be a good fit for the energy in the $l = 2$ mode:

$$\frac{E_{\rm EMOP}}{M} = 0.271\frac{q^2}{(1+q)^4}\,, \quad l = 2\,. \tag{6.7.57}$$

Table 6.3: EMOP data for $l = 3$. In this Table, by "peak" we mean the peak in the amplitude of the $l = 3$ mode. Numbers separated by a comma correspond to the $+$ and $\times$ polarizations, respectively. The fraction of the total energy in the $l = 3$ mode is about 44% for all mass ratios.

q	run	$\frac{E_{\rm EMOP}}{E_{\rm tot}}$	$\frac{\langle t_{\rm EMOP}\rangle}{M}$	$\frac{\Delta t_{\rm EMOP}}{M}$	$\frac{\langle \Delta t_{\rm EMOP}\rangle}{M}$	$\frac{10^4 E_{\rm EMOP}}{M}$	$\frac{\langle 10^4 E_{\rm EMOP}\rangle}{M}$
1.5	D7	0.44, 0.45	233.0	4.4, 6.4	5.4	3.5, 3.9	3.7
2.0	D7	0.45, 0.45	230.5	7.4, 5.4	6.4	7.7, 6.9	7.3
2.5	D7	0.44, 0.45	232.5	8.2, 6.2	7.2	9.6, 8.6	9.1
3.0	D7	0.44, 0.45	234.0	8.4, 6.4	7.4	10, 9.1	9.6
3.5	D7	0.43, 0.45	238.2	4.8, 7.3	6.0	7.8, 9.2	8.5
4.0	D7	0.43, 0.45	240.2	4.8, 7.3	6.0	7.5, 8.8	8.1
2.0	D8	0.44, 0.45	456.5	7.1, 5.1	6.1	7.6, 6.8	7.2
3.0	D8	0.45, 0.44	412.7	4.8, 7.3	6.1	8.8, 10	9.4

Results for $l = 3$ follow the same pattern (see Table 6.3). The average $\langle t_{\rm EMOP}\rangle$ for $l = 3$ is located about $6M - 7M$ after the average $\langle t_{\rm EMOP}\rangle$ for $l = 2$. The following formula provides a good fit for the energy in the $l = 3$ mode:

$$\frac{E_{\rm EMOP}}{M} = 0.104\frac{q^2(q-1)^2}{(1+q)^6}\,, \quad l = 3\,. \tag{6.7.58}$$

If we take $t_{\rm EMOP}$ for $l = 2$ as the fiducial ringdown starting time, we can compute the energy, angular and linear momentum radiated during the ringdown phase (as described by the EMOP). The results of this calculation are listed in Table 6.1.

6.7.3 A Detection-based Approach: Matched Filtering

As we already stated QNMs do not form a complete set, so the signal will always comprise quasinormal ringing plus some other component (such as prompt response or tails). However, in most practical applications we are only interested in some "fairly good approximation" to the ringdown waveform. The notion of "fairly good" must be defined according to the specific context.

A possible definition, based on theoretical considerations, was introduced in the previous Section. Here we propose an alternative, practical definition of the ringdown phase from a detection perspective. Detection of ringdown waves is likely to be achieved through matched filtering [45, 94]. The technique works by cross-correlating the detector's output against a set of theoretical templates. It can be shown that the maximum SNR is achieved when the template is equal in form to the detector's output (hence the name matched filtering). Matched filtering is the method of choice to search for ringdown waves: it is quasi-optimal and inexpensive, in the sense that it achieves the maximum SNR with a relatively small number of templates or filters.

Now, for the purpose of a matched filtering detection, the ringdown definition *must* be related to the use of ringdown templates. The relevant question is therefore: what is the maximum SNR attainable through the use of a filter which is a pure damped sinusoid? By definition, given the numerical waveform $h(t)$, the SNR ρ is

$$\rho = \max_{\{\lambda\},t_0} \frac{(T(\{\lambda\},t_0)|h)}{\sqrt{(T(\{\lambda\},t_0)|T(\{\lambda\},t_0)}}\,, \quad (h_1|h_2) \equiv 2\int_0^\infty \frac{h_1^*(f)h_2(f)+h_1(f)h_2^*(f)}{S_h(f)}\,, \tag{6.7.59}$$

where the template $T(\{\lambda\},t_0)$ is

$$T(\{\lambda\},t_0) = \begin{cases} e^{-\omega_i^T(t-t_0)}\sin(\omega_r^T t+\phi^T)\,, & \text{if } t \geq t_0\,, \\ 0 & \text{if } t < t_0\,. \end{cases} \tag{6.7.60}$$

$S_h(f)$ is the noise spectral density of the detector and $\{\lambda\}$ is a set of parameters characterizing the templates. The procedure is now simple: we "slide" this template backwards (starting at large t_0 and decreasing it progressively) across the numerical waveforms, and determine the maximum of the convolution (6.7.59). A good initial guess for the template parameters $\{\lambda\} = (\omega_i^T, \omega_r^T, \phi^T)$ can be obtained with Prony methods [39].

As expected t_0 will depend on the observer, i.e., on the detector being used, through the noise spectral density $S_h(f)$. In practice, however, the dependence on the detector is usually very weak, since in general the largest contribution to the convolution integral is near the resonant frequency ω_r. Thus, for all practical purposes, the detectors behave as if the noise were white: the spectral density $S_h(f)$ can be approximated as constant and moved out of the integral. This assumption also allows one to sidestep the computation of the Fourier transform of the waveforms: by Parseval's theorem, the frequency integral can be turned into a time integral. A more complete analysis, taking into account the full structure of the detector's noise, is in preparation.

A possible notion of effective ringdown starting time $t_{\rm MF}$ according to a matched filter, which is useful to make contact with previous SNR calculations [45], can be given simply as follows[2]. Define the effective starting time $t_{\rm MF}$ as the instant for

[2]Nollert's "theoretical" definition, explained in the previous Section, is not too dissimilar from

which

$$\rho = \sqrt{(h_{t_{\rm MF}}|h_{t_{\rm MF}})}\,, \qquad h_{t_{\rm MF}} \equiv \begin{cases} T(\{\lambda\}, t_{\rm MF}) & \text{if } t \geq t_{\rm MF}\,, \\ 0 & \text{if } t < t_{\rm MF}\,, \end{cases} \tag{6.7.61}$$

where ρ is computed from Eq. (6.7.59). Notice that, in general, $t_{\rm MF}$ does *not* coincide with the instant at which the convolution between the signal and the template has a maximum. By using Eq. (6.7.61) the SNR can be expressed in terms of energy in the actual signal. This is a common approach in engineering, introduced in the context of gravitational wave detection by Flanagan and Hughes [94] (see also [45]).

Table 6.4: Estimated, polarization-averaged effective starting times t_{MF} and energy radiated in ringdown from a matched-filter detection perspective, as functions of mass ratio. The listed energies should be taken as rough estimates, depending on the number of filters one is willing (and able) to use. We list also $\Delta t_{\rm MF}$, which is the "effective" starting time as measure from the peak of the $l = m = 2$ waveform: $\Delta t_{\rm MF} \equiv t_{\rm peak} - t_{\rm MF}$.

q	$\langle t_{\rm MF}/M\rangle$	$\langle \Delta t_{\rm MF}/M\rangle$	$\langle E_{\rm MF}/M\rangle$
1.0	207	27.0	0.028
1.5	208	28.4	0.026
2.0	209	26.4	0.021
2.5	209	29.1	0.018
3.0	210	29.8	0.015
3.5	211	31.5	0.012
4.0	212	32.8	0.011

The detection-based criterion, when applied to the merger waveforms considered here, yields the results shown in Table 6.4. From the above discussion, it is clear that the values we list for the energy radiated during ringdown are effective energies measured by the detector. These correspond to the values used in data analysis (see for instance [45]). From the Table we see that the effective energy radiated in ringdown for an equal mass merger is $\sim 3\%$, in very good agreement with the "guesstimate" by Flanagan and Hughes [94], which has often been used in the literature to compute SNRs and measurement errors. We also note that this value is much larger than the energy estimated by the EMOP, typically twice as large. This happens because the filter is looking for the maximum correlation, usually implying that the best-match parameters (ω_r and ω_i) will differ significantly from the true signal parameters.

Also notice that different polarizations yield slightly different energies and starting times. For instance, for equal mass mergers, we get $t_{\rm MF} \sim 205$ and $t_{\rm MF} \sim 208$ for the plus and cross polarizations, respectively. If we average over polarization states, this yields an effective radiated energy of $\sim 2.8\%$.

We also point out that the amount of energy depends on the parameter space to be searched. In principle, the correlation (6.7.59) is to be maximized over all possible values of $\omega_r\,, \omega_i$. In practice this would lead to a very large number of filters, so we must choose reasonable cutoffs on the parameters. For instance, in black hole ringdown searches one looks for modes with a quality factor typically smaller than ~ 20. It may be possible to increase the SNR and the amount of effective energy in ringdown by enlarging the parameter search (this would also allow us to search for ringdown modes of other objects, such as neutron stars or boson stars). A discussion of these issues will be presented elsewhere.

a "detection-oriented" definition. Indeed, expression (139) in [161] can be interpreted as the fitting factor between actual waveforms and ringdown templates (for white noise). If we take the ringdown frequencies as unknown parameters and choose them to maximize the EMOP (6.7.55), the results we get are very close to the present matched-filtering criterion.

To conclude this Section, we point out that a fit of the total effective energy radiated in ringdown, according to a matched filtering criterion, is:

$$\frac{E_{\rm MF}}{M} \approx 0.44 \frac{q^2}{(1+q)^4} \,. \tag{6.7.62}$$

6.8 Ringdown Event Rates and Black Hole Spectroscopy

The first binary black hole (BH) merger signal detected by the LIGO Scientific Collaboration, GW150914 [7], had a surprisingly high combined signal-to-noise ratio (SNR) of 24 in the Hanford and Livingston detectors. The quasinormal mode signal ("ringdown") from the merger remnant is consistent with the predictions of general relativity (GR) for a Kerr BH, but it was observed with a relatively low SNR $\rho \sim 7$ [9]. The large masses of the binary components [8] have interesting implications for the astrophysics of binary BH formation [4]. This detection, together with a second detected BH merger [6], placed interesting constraints on the merger rates of BH binaries in the Universe [5, 10, 29, 30, 84].

LISA Pathfinder was successfully launched in December 2015, paving the way for a space-based detector such as eLISA [14,15], which will observe mergers of massive BHs throughout the Universe with very large SNRs and test the Kerr nature of the merger remnants. As we saw earlier, the basic idea is that the dominant $\ell = m = 2$ resonant frequency and damping time can be used to determine the remnant's mass M and dimensionless spin $j = J/M^2$. In GR, all subdominant mode frequencies (e.g. the modes with $\ell = m = 3$ and $\ell = m = 4$ [40]) are then uniquely determined by M and j. The detection of subdominant modes requires high SNR, but each mode will provide one (or more) tests of the Kerr nature of the remnant [44]. As first pointed out by Detweiler in 1980, gravitational waves allow us to do BH spectroscopy: "After the advent of gravitational wave astronomy, the observation of these resonant frequencies might finally provide direct evidence of BHs with the same certainty as, say, the 21 cm line identifies interstellar hydrogen" [80].

Such high SNRs are known to be achievable with an eLISA-like detector [45]. The surprisingly high SNR of GW150914 raised the question whether current detectors at design sensitivity should routinely observe ringdown signals loud enough to perform gravitational spectroscopy. Leaving aside conceptual issues about ruling out exotic alternatives [24,61,74], here we use our current best understanding of the astrophysics of stellar-mass and supermassive BHs to compute the rates of events that would allow us to carry out spectroscopical tests.

Below we provide the details of our analysis, but the main conclusions can be understood relying on the noise power spectral densities (PSDs) $S_n(f)$ of present and future detectors, as shown and briefly reviewed in Fig. 6.9, and simple back-of-the-envelope estimates.

6.8.1 Ringdown Signal-to-Noise Ratio

Consider the merger of two BHs with source-frame masses (m_1, m_2), spins $(\mathbf{j}_1, \mathbf{j}_2)$, total mass $M_{\rm tot} = m_1 + m_2$, mass ratio $q \equiv m_1/m_2 \geq 1$ and symmetric mass ratio $\eta = m_1 m_2 / M_{\rm tot}^2$. The remnant mass and dimensionless spin, M and $j = J/M^2$, can be computed using the fitting formulas in [25] and [117], respectively (see also [26, 173]). The ringdown SNR ρ can be estimated as described in Section 6.4. Including redshift factors and substituting the Euclidean distance r by the luminosity distance

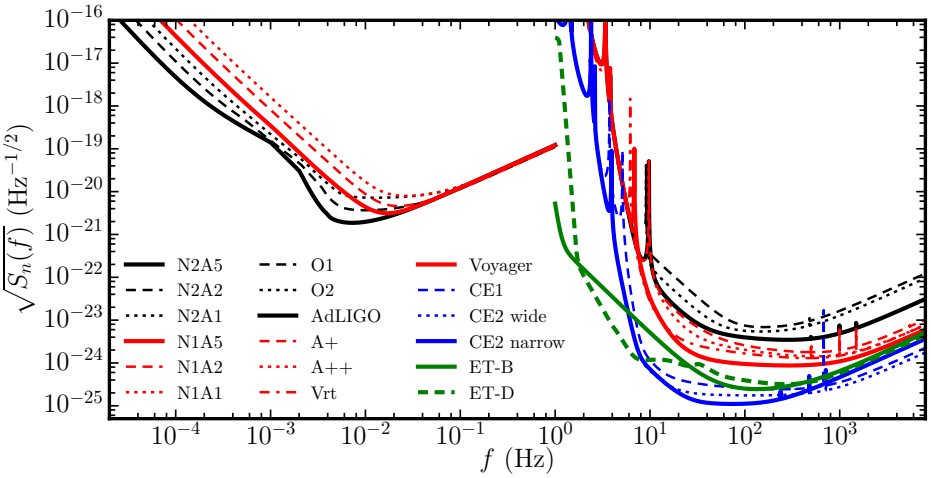

Figure 6.9: Noise PSDs for various space-based and advanced Earth-based detector designs. "NiAk" refers to non sky-averaged eLISA PSDs with pessimistic (N1) and optimistic (N2) acceleration noise and armlength $L = k$ Gm (cf. [125]). In the high-frequency regime, we show noise PSDs for (top to bottom): the first AdLIGO observing run (O1); the expected sensitivity for the second observing run (O2) and the Advanced LIGO design sensitivity (AdLIGO) [3]; the pessimistic and optimistic ranges of AdLIGO designs with squeezing (A+, A++) [151] ; Vrt and Voyager [1,12]; Cosmic Explorer (CE1), basically A+ in a 40-km facility [87]; CE2 wide and CE2 narrow, i.e. 40-km detectors with Voyager-type technology but different signal extraction tuning [1, 86]; and two possible Einstein Telescope designs, namely ET-B [2] and ET-D in the "xylophone" configuration [113].

D_L as appropriate, Eq. (6.4.24) implies that ρ is well approximated by

$$\rho = \frac{\delta_{\rm eq}}{D_{\rm L}\mathcal{F}_{lmn}}\left[\frac{8}{5}\frac{M_z^3\epsilon_{\rm rd}}{S_n(f_{lmn})}\right]^{1/2}, \tag{6.8.63}$$

where $M_z = M(1+z)$. Fits of the mass-independent dimensionless frequencies $\mathcal{F}_{lmn}(j) \equiv 2\pi M_z f_{lmn}$ are given in Eq. (E1) of [45]. The geometrical factor $\delta_{\rm eq} = 1$ for Michelson interferometers with orthogonal arms. For eLISA-like detectors the angle between the arms is 60°, so $\delta_{\rm eq} = \sqrt{3}/2$, and we use the *non sky-averaged* noise PSD $S_n(f)$ [34, 125]. The ringdown efficiency for nonspinning binaries is well approximated by the matched-filtering estimate of Eq. (6.7.62): $\epsilon_{\rm rd} = 0.44\eta^2$. When using the best-fit parameters inferred for GW150914 [8], Eq. (6.8.63) yields a ringdown SNR $\rho \simeq 7.7$ in O1 (in agreement with [9]) and $\rho \simeq 16.2$ in AdLIGO.

Due to the orbital hang-up effect [57], spinning binaries with aligned (antialigned) spins radiate more (less) than their nonspinning counterparts. The dominant spin-induced correction to the radiated energy is proportional to the sum of the components of the binary spins along the orbital angular momentum [25, 50, 51]. We estimate this correction by rescaling the radiated energy by the factor

$$\frac{E_{\rm rad}(m_1,\, m_2,\, \mathbf{j}_1,\, \mathbf{j}_2)}{E_{\rm rad}(m_1,\, m_2,\, \mathbf{0},\, \mathbf{0})}\,, \tag{6.8.64}$$

where the total energy radiated in the merger $E_{\rm rad}$ is computed using Eq. (18) of [25]. We find that spin-dependent corrections change ρ by at most 50%.

It is now easy to understand why Einstein Telescope-class detectors are needed to match the SNR of eLISA-like detectors and to perform BH spectroscopy. The quantity $\mathcal{F}_{lmn}(j)$ is a number of order unity [44, 45]. The physical frequency is $f_{lmn} \propto 1/M_z$: for example, an equal-mass merger of nonspinning BHs produces a remnant with $j \simeq 0.6864$ and fundamental ringdown frequency $f_{220} \simeq$

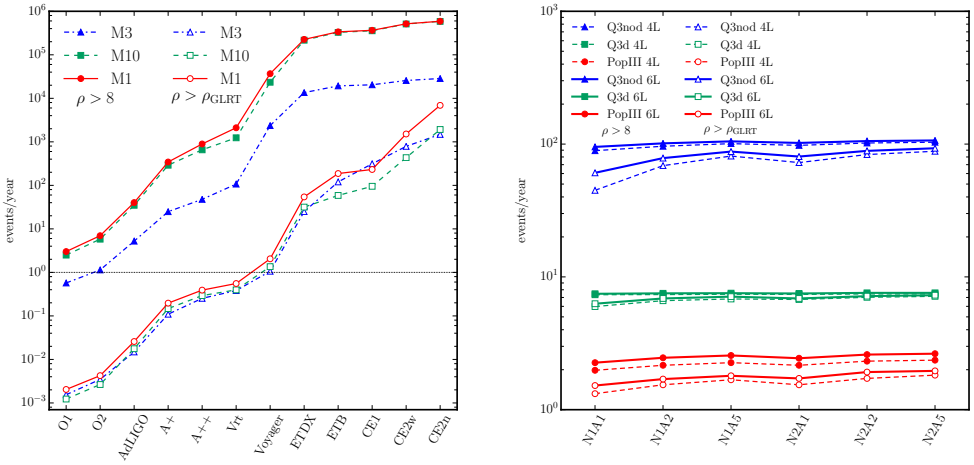

Figure 6.10: Rates of binary BH mergers that yield detectable ringdown signals (filled symbols) and allow for spectroscopical tests (hollow symbols). Left panel: rates per year for Earth-based detectors of increasing sensitivity. Right panel: rates per year for 6-link (solid) and 4-link (dashed) eLISA configurations with varying armlength and acceleration noise.

$170.2(10^2\,M_\odot/M_z)$ Hz. So Earth-based detectors are most sensitive to the ringdown of BHs with $M_z \sim 10^2 M_\odot$, while space-based detectors are most sensitive to the ringdown of BHs with $M_z \sim 10^6 M_\odot$. The crucial point is that, according to Eq. (6.8.63), $\rho \sim M^{3/2}$ at fixed redshift and noise PSD. As shown in Fig. 6.9, the "bucket" of the N2A5 eLISA detector is at $S^{1/2}_{\rm N2A5} \sim 10^{-21}$ Hz$^{-1/2}$. This noise level is $\sim 10^2$ (10^3, 10^4) times larger than the best sensitivity of AdLIGO (Voyager, Einstein Telescope), respectively. However eLISA BHs are $\sim 10^4$ times more massive, yielding signal amplitudes that are larger by a factor $\sim 10^6$. Astrophysical rate calculations are very different in the two frequency regimes, but these qualitative arguments explain why only Einstein Telescope-class detectors will achieve SNRs nearly comparable to eLISA.

6.8.2 Astrophysical Models

We estimate *ringdown* detection rates for Earth-based interferometers (detection rates for the full inspiral-merger-ringdown signal are higher) using three population synthesis models computed with the `Startrack` code: models M1, M3 and M10. Models M1 and M3 are the "standard" and "pessimistic" models described in [29]. The "standard model" M1 and model M10 predict very similar rates for AdLIGO at design sensitivity. In both of these models, compact objects receive natal kicks that decrease with the compact object mass, with the most massive BHs receiving no natal kicks. This decreases the probability of massive BHs being ejected from the binary, increasing merger rates. Model M1 allows for BH masses as high as $\sim$ 100 $M_\odot$. On the contrary, model M10 includes the effect of pair-instability mass loss, which sets an upper limit of $\sim 50 M_\odot$ on the mass of stellar origin BHs [28]. In model M3, all compact objects (including BHs) experience high natal kicks drawn from a Maxwellian with $\sigma = 265$km s^{-1} based on the natal kick distribution measured for single pulsars in our Galaxy [115]. The assumption of large natal kicks leads to a severe reduction of BH-BH merger rates, and therefore model M3 should be regarded as pessimistic [29]. In all of these models we set the BH spins to zero, an assumption consistent with estimates from GW150914 [4]. Even in the unrealistic scenario where all BHs in the Universe were maximally

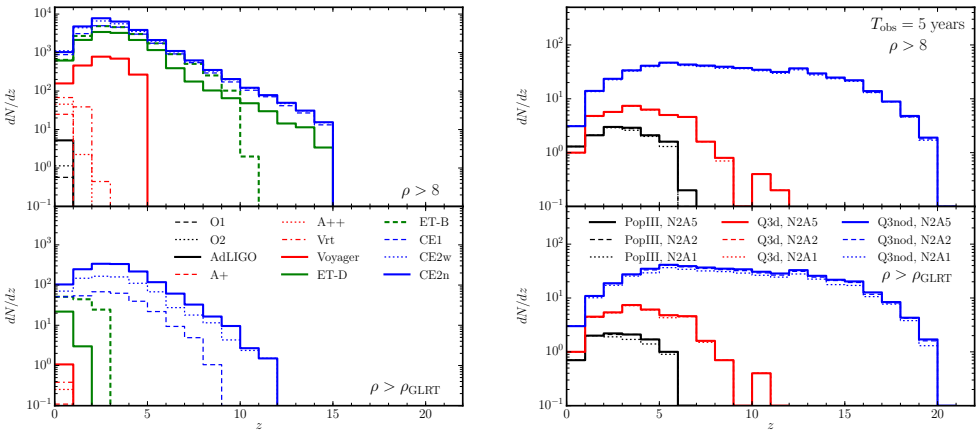

Figure 6.11: Left: redshift distribution of events with $\rho > 8$ (top) and $\rho > \rho_{\rm GLRT}$ (bottom) for model M1 and Earth-based detectors. In the bottom-left panel, the estimated AdLIGO rate ($\approx 2.6 \times 10^{-2}$ events/year) is too low to display. Right: same for models Q3nod, Q3d and PopIII. Different eLISA design choices have an almost irrelevant impact on the distributions.

spinning, rates would increase by a factor $\lesssim 3$ (see Table 2 of [84]). Massive binaries with ringdowns detectable by Earth-based interferometers could also be produced by other mechanisms (see e.g. [31, 76, 142, 175]), and therefore our rates should be seen as lower bounds.

To estimate ringdown rates from massive BH mergers detectable by eLISA we consider the same three models (PopIII, Q3nod and Q3d) used in [125] and produced with the semi-analytical approach of [22] (with incremental improvements described in [19,20,187]). These models were chosen to span the major sources of uncertainty affecting eLISA rates, namely (i) the nature of primordial BH seeds (light seeds coming from the collapse of Pop III stars in model PopIII; heavy seeds originating from protogalactic disks in models Q3d and Q3nod), and (ii) the delay between galaxy mergers and the merger of the BHs at galactic centers (model Q3d includes this delay; model Q3nod does not, and therefore yields higher detection rates). In all three models the BH spin evolution is followed self-consistently [22, 187]. For each event in the catalog we compute ρ from Eq. (6.8.63), where $\epsilon_{\rm rd}$ is rescaled by a spin-dependent factor as necessary.

6.8.3 Detection Rates

The ringdown detection rates (events per year with $\rho > 8$ in a single detector) predicted by models M1, M3, M10 (for stellar-mass BH binaries) and PopIII, Q3d, Q3nod (for supermassive BH binaries) are shown in Fig. 6.10 with filled symbols. For example, models M1 (M10, M3) predict 3.0 (2.5, 0.57) events per year with detectable ringdown in O1; 7.0 (5.8, 1.1) in O2; and 40 (35, 5.2) in AdLIGO. Model Q3d (Q3nod, PopIII) predicts 38 (533, 13) events for a 6-link N2A5 eLISA mission lasting 5 years, but in the plot we divided these numbers by 5 to facilitate a more fair comparison in terms of events *per year*.

6.8.4 Black Hole Spectroscopy

Suppose that we know that a signal contains two (or possibly more) ringdown modes. We expect the weaker mode to be hard to resolve if its amplitude is low

and/or if the detector's noise is large. The critical SNR for the second mode to be resolvable can be computed using the generalized likelihood ratio test (GLRT) [36] under the following assumptions: (i) using other criteria, we have already decided in favor of the presence of one ringdown signal; (ii) the ringdown frequencies and damping times, as well as the amplitude of the dominant mode, are known. Then the critical SNR $\rho_{\rm GLRT}$ to resolve a mode with either $\ell = m = 3$ or $\ell = m = 4$ from the dominant mode with $\ell = m = 2$ is well fitted, for nonspinning binary BH mergers, by

$$\rho^{2,3}_{\rm GLRT} = 17.687 + \frac{15.4597}{q-1} - \frac{1.65242}{q}\,, \tag{6.8.65}$$

$$\rho^{2,4}_{\rm GLRT} = 37.9181 + \frac{83.5778}{q} + \frac{44.1125}{q^2} + \frac{50.1316}{q^3}\,. \tag{6.8.66}$$

These fits reproduce the numerical results in Fig. 9 of [36] within 0.3% when $q \in [1.01 - 100]$. Spectroscopical tests of the Kerr metric can be performed whenever either mode is resolvable, i.e. $\rho > \rho_{\rm GLRT} \equiv \min(\rho^{2,3}_{\rm GLRT}, \rho^{2,4}_{\rm GLRT})$. The $\ell = m = 3$ mode is usually easier to resolve than the $\ell = m = 4$ mode, but the situation is reversed in the comparable-mass limit $q \to 1$, where the amplitude of odd-m modes is suppressed [40, 140]. Extreme mass-ratio calculations [23] and a preliminary analysis of numerical waveforms show that the ratio of mode amplitudes is, to a good accuracy, spin-independent, therefore this SNR threshold is adequate for our present purpose.

The rates of events with $\rho > \rho_{\rm GLRT}$ are shown in Fig. 6.10 by curves with hollow symbols. The key observation here is that, although ringdown *detections* should be routine already in AdLIGO, high-SNR events are exceedingly rare: reaching the threshold of $\sim$ 1 event/year requires Voyager-class detectors, while sensitivities comparable to Einstein Telescope are needed to carry out such tests routinely. This is not the case for space-based interferometers: typical ringdown detections have such high SNR that $\approx 50\%$ or more of them can be used to do BH spectroscopy. The total number of eLISA detections and spectroscopic tests depends on the underlying BH formation model, but it is remarkably independent of detector design (although the N1A1 design would sensibly reduce rates in the most optimistic models).

Perhaps the most striking difference between Earth- and space-based detectors is that a very large fraction of the "spectroscopically significant" events will occur at cosmological redshift in eLISA, but not in Einstein telescope. This is shown very clearly in Fig. 6.11, where we plot redshift histograms of detected events (top panel) and of events that allow for spectroscopy (bottom panel). eLISA can do spectroscopy out to $z \approx 5$ (10, or even 20!) for PopIII (Q3d, Q3nod) models, while even the Einstein Telescope is limited to $z \lesssim 3$. Only 40-km detectors with cosmological reach, such as Cosmic Explorer [86,87], would be able to do spectroscopy at $z \approx 10$.

6.8.5 What's Next?

Using our best understanding of the formation of field binaries, we predict that AdLIGO at design sensitivity should observe several ringdown events per year. However routine spectroscopical tests of the dynamics of Kerr BHs will require the construction and operation of detectors such as the Einstein Telescope [108,150,183], and 40-km detectors [86,87] will be necessary to reach cosmological distances. Many of the mergers for which eLISA can do BH spectroscopy will be located at $z \gg 1$. These systems will test GR in qualitatively different regimes than any low-z observation by AdLIGO: BH spectroscopy with eLISA will test whether gravity behaves *locally* like GR even at the very early epochs of our Universe, possibly placing constraints on proposed extensions of Einstein's theory [46, 97, 204, 205].

Given the time lines for the construction and operation of these detectors, it is likely that the first instances of BH spectroscopy will come from a space-based detector. This conclusion is based on the simple GLRT criterion introduced in [36], and it is possible that better data analysis techniques (such as the Bayesian methods advocated in [108, 150]) could improve our prospects for gravitational spectroscopy with Earth-based interferometers. We hope that our work will stimulate the development of these techniques and their use on actual data.

As shown in Fig. 6.10, differences in rates between models M1 and M10 become large enough to be detectable in A+. We estimate 34 (29) ringdown events per year for M1 (M10) in A+, and 89 (66) events per year in A++. Rate differences are even larger when we consider the complete signal. Therefore, while the implementation of squeezing in AdLIGO may not allow for routine BH spectroscopy, it could reveal the nature of the BH mass spectrum in the range $\sim [50 - 100]\ M_{\odot}$.

Bibliography

[1] LIGO Instrument Science White Paper:
`https://dcc.ligo.org/public/0120/T1500290/002/T1500290.pdf` .

[2] Einstein Telescope design study document:
`http://www.et-gw.eu/etdsdocument` .

[3] J. Aasi et al. Prospects for Observing and Localizing Gravitational-Wave Transients with Advanced LIGO and Advanced Virgo. 2013. [Living Rev. Rel.19,1(2016)].

[4] B. P. Abbott et al. Astrophysical Implications of the Binary Black-Hole Merger GW150914. *Astrophys. J.*, 818(2):L22, 2016.

[5] B. P. Abbott et al. Binary Black Hole Mergers in the first Advanced LIGO Observing Run. 2016.

[6] B. P. Abbott et al. GW151226: Observation of Gravitational Waves from a 22-Solar-Mass Binary Black Hole Coalescence. *Phys. Rev. Lett.*, 116(24):241103, 2016.

[7] B. P. Abbott et al. Observation of Gravitational Waves from a Binary Black Hole Merger. *Phys. Rev. Lett.*, 116(6):061102, 2016.

[8] B. P. Abbott et al. Properties of the Binary Black Hole Merger GW150914. *Phys. Rev. Lett.*, 116(24):241102, 2016.

[9] B. P. Abbott et al. Tests of general relativity with GW150914. *Phys. Rev. Lett.*, 116(22):221101, 2016.

[10] B. P. Abbott et al. The Rate of Binary Black Hole Mergers Inferred from Advanced LIGO Observations Surrounding GW150914. 2016.

[11] M. Abramowitz and I. A. Stegun. *Handbook of Mathematical Functions with Formulas, Graphs, and Mathematical Tables*. Dover, New York, 1972.

[12] R. X. Adhikari. Gravitational Radiation Detection with Laser Interferometry. *Rev. Mod. Phys.*, 86:121, 2014.

[13] J. Alsing, E. Berti, C. M. Will, and H. Zaglauer. Gravitational radiation from compact binary systems in the massive Brans-Dicke theory of gravity. *Phys.Rev.*, D85:064041, 2012.

[14] P. Amaro-Seoane et al. Low-frequency gravitational-wave science with eLISA/NGO. *Class. Quant. Grav.*, 29:124016, 2012.

[15] P. Amaro-Seoane et al. eLISA/NGO: Astrophysics and cosmology in the gravitational-wave millihertz regime. *GW Notes*, 6:4–110, 2013.

[16] N. Andersson. Excitation of Schwarzschild black hole quasinormal modes. *Phys. Rev.*, D51:353–363, 1995.

[17] N. Andersson and C. J. Howls. The asymptotic quasinormal mode spectrum of non-rotating black holes. *Class. Quant. Grav.*, 21:1623–1642, 2004.

[18] N. Andersson, P. Laguna, and P. Papadopoulos. Dynamics of scalar fields in the background of rotating black holes. 2. A Note on superradiance. *Phys.Rev.*, D58:087503, 1998.

[19] F. Antonini, E. Barausse, and J. Silk. The Coevolution of Nuclear Star Clusters, Massive Black Holes, and their Host Galaxies. *Astrophys. J.*, 812(1):72, 2015.

[20] F. Antonini, E. Barausse, and J. Silk. The imprint of massive black-hole mergers on the correlation between nuclear star clusters and their host galaxies. *Astrophys. J.*, 806(1):L8, 2015.

[21] A. Arvanitaki and S. Dubovsky. Exploring the String Axiverse with Precision Black Hole Physics. *Phys.Rev.*, D83:044026, 2011.

[22] E. Barausse. The evolution of massive black holes and their spins in their galactic hosts. *Mon. Not. Roy. Astron. Soc.*, 423:2533–2557, 2012.

[23] E. Barausse, A. Buonanno, S. A. Hughes, G. Khanna, S. O'Sullivan, and Y. Pan. Modeling multipolar gravitational-wave emission from small mass-ratio mergers. *Phys. Rev.*, D85:024046, 2012.

[24] E. Barausse, V. Cardoso, and P. Pani. Can environmental effects spoil precision gravitational-wave astrophysics? *Phys. Rev.*, D89(10):104059, 2014.

[25] E. Barausse, V. Morozova, and L. Rezzolla. On the mass radiated by coalescing black-hole binaries. *Astrophys. J.*, 758:63, 2012. [Erratum: Astrophys. J.786,76(2014)].

[26] E. Barausse and L. Rezzolla. Predicting the direction of the final spin from the coalescence of two black holes. *Astrophys. J.*, 704:L40–L44, 2009.

[27] J. M. Bardeen, W. H. Press, and S. A. Teukolsky. Rotating black holes: Locally nonrotating frames, energy extraction, and scalar synchrotron radiation. *Astrophys. J.*, 178:347, 1972.

[28] K. Belczynski et al. 2016. submitted to A&A.

[29] K. Belczynski, D. E. Holz, T. Bulik, and R. O'Shaughnessy. The origin and evolution of LIGO's first gravitational-wave source. 2016.

[30] K. Belczynski, S. Repetto, D. Holz, R. O'Shaughnessy, T. Bulik, E. Berti, C. Fryer, and M. Dominik. Comparison of LIGO/Virgo upper limits with predicted compact binary merger rates. 2015.

[31] M. J. Benacquista and J. M. B. Downing. Relativistic Binaries in Globular Clusters. *Living Rev. Rel.*, 16:4, 2013.

[32] C. M. Bender and S. A. Orszag. *Advanced Mathematical Methods for Scientists and Engineers*. McGraw-Hill, New York, 1978.

[33] E. Berti. Black hole quasinormal modes: Hints of quantum gravity? 2004. gr-qc/0411025.

[34] E. Berti, A. Buonanno, and C. M. Will. Estimating spinning binary parameters and testing alternative theories of gravity with LISA. *Phys. Rev.*, D71:084025, 2005.

[35] E. Berti, A. Buonanno, and C. M. Will. Testing general relativity and probing the merger history of massive black holes with LISA. *Class. Quant. Grav.*, 22:S943–S954, 2005.

[36] E. Berti, J. Cardoso, V. Cardoso, and M. Cavaglia. Matched-filtering and parameter estimation of ringdown waveforms. *Phys. Rev.*, D76:104044, 2007.

[37] E. Berti and V. Cardoso. Quasinormal ringing of Kerr black holes. I: The excitation factors. *Phys. Rev.*, D74:104020, 2006.

[38] E. Berti, V. Cardoso, and M. Casals. Eigenvalues and eigenfunctions of spin-weighted spheroidal harmonics in four and higher dimensions. *Phys. Rev.*, D73:024013, 2006.

[39] E. Berti, V. Cardoso, J. A. Gonzalez, and U. Sperhake. Mining information from binary black hole mergers: A Comparison of estimation methods for complex exponentials in noise. *Phys. Rev.*, D75:124017, 2007.

[40] E. Berti, V. Cardoso, J. A. Gonzalez, U. Sperhake, M. Hannam, S. Husa, and B. Bruegmann. Inspiral, merger and ringdown of unequal mass black hole binaries: A Multipolar analysis. *Phys. Rev.*, D76:064034, 2007.

[41] E. Berti, V. Cardoso, L. Gualtieri, F. Pretorius, and U. Sperhake. Comment on 'Kerr Black Holes as Particle Accelerators to Arbitrarily High Energy'. *Phys. Rev. Lett.*, 103:239001, 2009.

[42] E. Berti, V. Cardoso, T. Hinderer, M. Lemos, F. Pretorius, et al. Semi-analytical estimates of scattering thresholds and gravitational radiation in ultrarelativistic black hole encounters. *Phys.Rev.*, D81:104048, 2010.

[43] E. Berti, V. Cardoso, and B. Kipapa. Up to eleven: radiation from particles with arbitrary energy falling into higher-dimensional black holes. *Phys. Rev.*, D83:084018, 2011.

[44] E. Berti, V. Cardoso, and A. O. Starinets. Quasinormal modes of black holes and black branes. *Class.Quant.Grav.*, 26:163001, 2009.

[45] E. Berti, V. Cardoso, and C. M. Will. On gravitational-wave spectroscopy of massive black holes with the space interferometer LISA. *Phys. Rev.*, D73:064030, 2006.

[46] E. Berti et al. Testing General Relativity with Present and Future Astrophysical Observations. *Class. Quant. Grav.*, 32:243001, 2015.

[47] E. Berti and K. D. Kokkotas. Asymptotic quasinormal modes of Reissner-Nordstroem and Kerr black holes. *Phys. Rev.*, D68:044027, 2003.

[48] E. Berti and K. D. Kokkotas. Quasinormal modes of Kerr-Newman black holes: Coupling of electromagnetic and gravitational perturbations. *Phys. Rev.*, D71:124008, 2005.

[49] N. T. Bishop and L. Rezzolla. Extraction of Gravitational Waves in Numerical Relativity. 2016.

[50] L. Boyle and M. Kesden. The spin expansion for binary black hole merger: new predictions and future directions. *Phys. Rev.*, D78:024017, 2008.

[51] L. Boyle, M. Kesden, and S. Nissanke. Binary black hole merger: Symmetry and the spin expansion. *Phys. Rev. Lett.*, 100:151101, 2008.

[52] L. Brenneman, C. Reynolds, M. Nowak, R. Reis, M. Trippe, et al. The Spin of the Supermassive Black Hole in NGC 3783. *Astrophys.J.*, 736:103, 2011.

[53] D. R. Brill, P. L. Chrzanowski, C. Martin Pereira, E. D. Fackerell, and J. R. Ipser. Solution of the scalar wave equation in a kerr background by separation of variables. *Phys. Rev.*, D5:1913–1915, 1972.

[54] R. Brito, V. Cardoso, and P. Pani. Massive spin-2 fields on black hole spacetimes: Instability of the Schwarzschild and Kerr solutions and bounds on the graviton mass. *Phys.Rev.*, D88(2):023514, 2013.

[55] A. Buonanno, G. B. Cook, and F. Pretorius. Inspiral, merger and ring-down of equal-mass black-hole binaries. *Phys. Rev.*, D75:124018, 2007.

[56] P. G. Camara, L. E. Ibanez, and F. Marchesano. RR photons. *JHEP*, 1109:110, 2011.

[57] M. Campanelli, C. O. Lousto, and Y. Zlochower. Spinning-black-hole binaries: The orbital hang up. *Phys. Rev.*, D74:041501, 2006.

[58] V. Cardoso and M. Cavaglia. Stability of naked singularities and algebraically special modes. *Phys. Rev.*, D74:024027, 2006.

[59] V. Cardoso, S. Chakrabarti, P. Pani, E. Berti, and L. Gualtieri. Floating and sinking: The Imprint of massive scalars around rotating black holes. *Phys.Rev.Lett.*, 107:241101, 2011.

[60] V. Cardoso, O. J. C. Dias, J. P. S. Lemos, and S. Yoshida. The black hole bomb and superradiant instabilities. *Phys. Rev.*, D70:044039, 2004.

[61] V. Cardoso, E. Franzin, and P. Pani. Is the gravitational-wave ringdown a probe of the event horizon? *Phys. Rev. Lett.*, 116(17):171101, 2016.

[62] V. Cardoso, A. S. Miranda, E. Berti, H. Witek, and V. T. Zanchin. Geodesic stability, Lyapunov exponents and quasinormal modes. *Phys. Rev.*, D79:064016, 2009.

[63] S. M. Carroll. *Spacetime and geometry. An introduction to general relativity.* Addison Wesley, San Francisco, CA, USA, 2004.

[64] S. Chandrasekhar. On the equations governing the perturbations of the Schwarzschild black hole. *Proc. R. Soc. Lond.*, A343:289, 1975.

[65] S. Chandrasekhar. *The Mathematical Theory of Black Holes.* Oxford University Press, New York, 1983.

[66] S. Chandrasekhar. On algebraically special perturbations of black hole. *Proc. R. Soc. Lond.*, A392:1, 1984.

[67] S. Chandrasekhar and S. Detweiler. The quasi-normal modes of the Schwarzschild black hole. *Royal Society of London Proceedings Series A*, 344:441–452, Aug. 1975.

[68] E. S. C. Ching, P. T. Leung, A. Maassen van den Brink, W. M. Suen, S. S. Tong, and K. Young. Quasinormal-mode expansion for waves in open systems. *Rev. Mod. Phys.*, 70(4):1545–1554, Oct 1998.

[69] E. S. C. Ching, P. T. Leung, W. M. Suen, and K. Young. Late time tail of wave propagation on curved space-time. *Phys. Rev. Lett.*, 74:2414–2417, 1995.

[70] E. S. C. Ching, P. T. Leung, W. M. Suen, and K. Young. Wave propagation in gravitational systems: Late time behavior. *Phys. Rev.*, D52:2118–2132, 1995.

[71] M. W. Choptuik. Universality and scaling in gravitational collapse of a massless scalar field. *Phys. Rev. Lett.*, 70:9–12, 1993.

[72] N. J. Cornish and J. J. Levin. Lyapunov timescales and black hole binaries. *Class.Quant.Grav.*, 20:1649–1660, 2003.

[73] T. Damour, N. Deruelle, and R. Ruffini. On Quantum Resonances in Stationary Geometries. *Lett.Nuovo Cim.*, 15:257–262, 1976.

[74] T. Damour and S. N. Solodukhin. Wormholes as black hole foils. *Phys. Rev.*, D76:024016, 2007.

[75] M. Davis, R. Ruffini, W. H. Press, and R. H. Price. Gravitational radiation from a particle falling radially into a schwarzschild black hole. *Phys. Rev. Lett.*, 27:1466–1469, 1971.

[76] S. E. de Mink and I. Mandel. The Chemically Homogeneous Evolutionary Channel for Binary Black Hole Mergers: Rates and Properties of Gravitational-Wave Events Detectable by Advanced Ligo. 2016.

[77] C. de Rham. Massive Gravity. *Living Rev.Rel.*, 17:7, 2014.

[78] Y. Decanini and A. Folacci. Regge poles of the Schwarzschild black hole: A WKB approach. *Phys.Rev.*, D81:024031, 2010.

[79] Y. Decanini, A. Folacci, and B. Jensen. Complex angular momentum in black hole physics and the quasi-normal modes. *Phys. Rev.*, D67:124017, 2003.

[80] S. Detweiler. Black holes and gravitational waves. III. The resonant frequencies of rotating holes. *Astrophys. J.*, 239:292–295, 1980.

[81] S. L. Detweiler. Klein-Gordon Equation and Rotating Black Holes. *Phys.Rev.*, D22:2323–2326, 1980.

[82] S. R. Dolan. Instability of the massive Klein-Gordon field on the Kerr spacetime. *Phys.Rev.*, D76:084001, 2007.

[83] S. R. Dolan and A. C. Ottewill. On an Expansion Method for Black Hole Quasinormal Modes and Regge Poles. *Class.Quant.Grav.*, 26:225003, 2009.

[84] M. Dominik, E. Berti, R. O'Shaughnessy, I. Mandel, K. Belczynski, C. Fryer, D. Holz, T. Bulik, and F. Pannarale. Double Compact Objects III: Gravitational Wave Detection Rates. *Astrophys. J.*, 806(2):263, 2015.

[85] E. N. Dorband, E. Berti, P. Diener, E. Schnetter, and M. Tiglio. A numerical study of the quasinormal mode excitation of Kerr black holes. *Phys. Rev.*, D74:084028, 2006.

[86] S. Dwyer and M. Evans. 2016. private communication.

[87] S. Dwyer, D. Sigg, S. W. Ballmer, L. Barsotti, N. Mavalvala, and M. Evans. Gravitational wave detector with cosmological reach. *Phys. Rev.*, D91(8):082001, 2015.

[88] F. Echeverria. Gravitational wave measurements of the mass and angular momentum of a black hole. *Phys. Rev.*, D40:3194–3203, 1989.

[89] L. A. Edelstein and C. V. Vishveshwara. Differential equations for perturbations on the Schwarzschild metric. *Phys. Rev.*, D1:3514–3517, 1970.

[90] V. Ferrari and B. Mashhoon. New approach to the quasinormal modes of a black hole. *Phys.Rev.*, D30:295–304, 1984.

[91] V. Ferrari and R. Ruffini. On the Structure of Gravitational Wave Bursts: Implosion With Finite Kinetic Energy. *Phys. Lett.*, B98:381–384, 1981.

[92] L. S. Finn. Detection, measurement and gravitational radiation. *Phys. Rev.*, D46:5236–5249, 1992.

[93] C. Flammer. *Spheroidal wave functions*. 1957.

[94] E. E. Flanagan and S. A. Hughes. Measuring gravitational waves from binary black hole coalescences: 1. Signal-to-noise for inspiral, merger, and ringdown. *Phys. Rev.*, D57:4535–4565, 1998.

[95] V. P. Frolov and I. D. Novikov. *Black hole physics: Basic concepts and new developments*. Dordrecht, Netherlands: Kluwer Academic (1998) 770 p.

[96] C. L. Fryer, D. E. Holz, and S. A. Hughes. Gravitational wave emission from core-collapse of massive stars. *Astrophys. J.*, 565:430–446, 2002.

[97] J. R. Gair, M. Vallisneri, S. L. Larson, and J. G. Baker. Testing General Relativity with Low-Frequency, Space-Based Gravitational-Wave Detectors. *Living Rev. Rel.*, 16:7, 2013.

[98] U. H. Gerlach and U. K. Sengupta. Even parity junction conditions for perturbations on most general spherically symmetric space-times. *J. Math. Phys.*, 20:2540–2546, 1979.

[99] U. H. Gerlach and U. K. Sengupta. Gauge invariant perturbation on most general spherically symmetric space-times. *Phys. Rev.*, D19:2268–2272, 1979.

[100] U. H. Gerlach and U. K. Sengupta. Gauge invariant coupled gravitational, acoustical, and electromagnetic modes on most general spherical spce-times. *Phys. Rev.*, D22:1300–1312, 1980.

[101] K. Glampedakis and N. Andersson. Late-time dynamics of rapidly rotating black holes. *Phys. Rev.*, D64:104021, 2001.

[102] K. Glampedakis and N. Andersson. Quick and dirty methods for studying black-hole resonances. *Class. Quant. Grav.*, 20:3441–3464, 2003.

[103] E. N. Glass. Newtonian spherical gravitational collapse. *Journal of Physics A Mathematical General*, 13:3097–3104, Sept. 1980.

[104] C. J. Goebel. Comments on the "vibrations" of a black hole. *Astrophys. J.*, L172:95, 1972.

[105] A. S. Goldhaber and M. M. Nieto. Photon and Graviton Mass Limits. *Rev.Mod.Phys.*, 82:939–979, 2010.

[106] J. A. Gonzalez, U. Sperhake, B. Bruegmann, M. Hannam, and S. Husa. Total recoil: the maximum kick from nonspinning black-hole binary inspiral. *Phys. Rev. Lett.*, 98:091101, 2007.

[107] M. Goodsell, J. Jaeckel, J. Redondo, and A. Ringwald. Naturally Light Hidden Photons in LARGE Volume String Compactifications. *JHEP*, 0911:027, 2009.

[108] S. Gossan, J. Veitch, and B. S. Sathyaprakash. Bayesian model selection for testing the no-hair theorem with black hole ringdowns. *Phys. Rev.*, D85:124056, 2012.

[109] C. Gundlach, S. Akcay, L. Barack, and A. Nagar. Critical phenomena at the threshold of immediate merger in binary black hole systems: the extreme mass ratio case. *Phys.Rev.*, D86:084022, 2012.

[110] C. Gundlach and J. M. Martin-Garcia. Gauge invariant and coordinate independent perturbations of stellar collapse. 1. The Interior. *Phys. Rev.*, D61:084024, 2000.

[111] C. Gundlach and J. M. Martin-Garcia. Critical phenomena in gravitational collapse. *Living Rev.Rel.*, 10:5, 2007.

[112] J. B. Hartle. *Gravity : an introduction to Einstein's general relativity*. Addison Wesley, San Francisco, CA, USA, 2003.

[113] S. Hild, S. Chelkowski, A. Freise, J. Franc, N. Morgado, R. Flaminio, and R. DeSalvo. A Xylophone Configuration for a third Generation Gravitational Wave Detector. *Class. Quant. Grav.*, 27:015003, 2010.

[114] K. Hinterbichler. Theoretical Aspects of Massive Gravity. *Rev.Mod.Phys.*, 84:671–710, 2012.

[115] G. Hobbs, D. R. Lorimer, A. G. Lyne, and M. Kramer. A Statistical study of 233 pulsar proper motions. *Mon. Not. Roy. Astron. Soc.*, 360:974–992, 2005.

[116] S. Hod. Bohr's correspondence principle and the area spectrum of quantum black holes. *Phys. Rev. Lett.*, 81:4293, 1998.

[117] F. Hofmann, E. Barausse, and L. Rezzolla. The final spin from binary black holes in quasi-circular orbits. 2016.

[118] S. A. Hughes. Computing radiation from Kerr black holes: Generalization of the Sasaki-Nakamura equation. *Phys. Rev.*, D62:044029, 2000. [Erratum: Phys. Rev.D67,089902(2003)].

[119] A. Ishibashi and H. Kodama. Stability of higher-dimensional Schwarzschild black holes. *Prog. Theor. Phys.*, 110:901–919, 2003.

[120] S. Iyer. Black Hole Normal Modes: A WKB Approach. 2. Schwarzschild Black Holes. *Phys.Rev.*, D35:3632, 1987.

[121] S. Iyer and C. M. Will. Black Hole Normal Modes: A WKB Approach. 1. Foundations and Application of a Higher Order WKB Anaysis of Potential Barrier Scattering. *Phys.Rev.*, D35:3621, 1987.

[122] J. Jaeckel and A. Ringwald. The Low-Energy Frontier of Particle Physics. *Ann.Rev.Nucl.Part.Sci.*, 60:405–437, 2010.

[123] G. Jaffé. *Z. Phys.*, 87:535, 1934.

[124] B. P. Jensen and P. Candelas. The Schwarzschild radial functions. *Phys. Rev.*, D33:1590, 1986.

[125] A. Klein et al. Science with the space-based interferometer eLISA: Supermassive black hole binaries. *Phys. Rev.*, D93(2):024003, 2016.

[126] H. Kodama and A. Ishibashi. A Master equation for gravitational perturbations of maximally symmetric black holes in higher dimensions. *Prog.Theor.Phys.*, 110:701–722, 2003.

[127] H. Kodama and A. Ishibashi. Master equations for perturbations of generalized static black holes with charge in higher dimensions. *Prog.Theor.Phys.*, 111:29–73, 2004.

[128] H. Kodama, A. Ishibashi, and O. Seto. Brane world cosmology: Gauge invariant formalism for perturbation. *Phys. Rev.*, D62:064022, 2000.

[129] H. Kodama and H. Yoshino. Axiverse and Black Hole. *Int.J.Mod.Phys.Conf.Ser.*, 7:84–115, 2012.

[130] K. D. Kokkotas, T. A. Apostolatos, and N. Andersson. The Inverse problem for pulsating neutron stars: A 'Fingerprint analysis' for the supranuclear equation of state. *Mon. Not. Roy. Astron. Soc.*, 320:307–315, 2001.

[131] K. D. Kokkotas and B. G. Schmidt. Quasi-normal modes of stars and black holes. *Living Rev. Rel.*, 2:2, 1999.

[132] R. Konoplya and A. Zhidenko. Quasinormal modes of black holes: From astrophysics to string theory. *Rev.Mod.Phys.*, 83:793–836, 2011.

[133] R. A. Konoplya. Quasinormal behavior of the d-dimensional Schwarzschild black hole and higher order WKB approach. *Phys. Rev.*, D68:024018, 2003.

[134] W. Krivan, P. Laguna, P. Papadopoulos, and N. Andersson. Dynamics of perturbations of rotating black holes. *Phys. Rev.*, D56:3395–3404, 1997.

[135] E. W. Leaver. An Analytic representation for the quasi normal modes of Kerr black holes. *Proc. Roy. Soc. Lond.*, A402:285–298, 1985.

[136] E. W. Leaver. Solutions to a generalized spheroidal wave equation: Teukolsky's equations in general relativity, and the two-center problem in molecular quantum mechanics. *J. Math. Phys.*, 27:1238, 1986.

[137] E. W. Leaver. Spectral decomposition of the perturbation response of the Schwarzschild geometry. *Phys. Rev.*, D34:384–408, 1986.

[138] P. Leung, A. Maassen van den Brink, W. Suen, C. Wong, and K. Young. SUSY transformations for quasinormal and total transmission modes of open systems. 1999. math-ph/9909030.

[139] A. P. Lightman, W. H. Press, R. H. Price, and S. A. Teukolsky. *Problem book in relativity and gravitation.* Princeton Univ. Press, Princeton, NJ, 1975.

[140] L. London, D. Shoemaker, and J. Healy. Modeling ringdown: Beyond the fundamental quasinormal modes. *Phys. Rev.*, D90(12):124032, 2014.

[141] M. Maggiore. *Gravitational Waves. Vol. 1: Theory and Experiments.* Oxford Master Series in Physics. Oxford University Press, 2007.

[142] P. Marchant, N. Langer, P. Podsiadlowski, T. M. Tauris, and T. J. Moriya. A new route towards merging massive black holes. *Astron. Astrophys.*, 588:A50, 2016.

[143] D. Markovic. On the possibility of determining cosmological parameters from measurements of gravitational waves emitted by coalescing, compact binaries. *Phys. Rev.*, D48:4738–4756, 1993.

[144] J. M. Martin-Garcia and C. Gundlach. All nonspherical perturbations of the Choptuik space-time decay. *Phys. Rev.*, D59:064031, 1999.

[145] J. M. Martin-Garcia and C. Gundlach. Gauge invariant and coordinate independent perturbations of stellar collapse. 2. Matching to the exterior. *Phys. Rev.*, D64:024012, 2001.

[146] B. Mashhoon. In H. Ning, editor, *Proceedings of the Third Marcel Grossmann Meeting on Recent Developments of General Relativity*, page 599, Amsterdam, 1983. North-Holland.

[147] B. Mashhoon. Stability of charged rotating black holes in the eikonal approximation. *Phys. Rev.*, D31:290, 1985.

[148] B. Mashhoon and M. Hossein Partovi. On the gravitational motion of a fluid obeying an equation of state. *Annals of Physics*, 130:99–138, Nov. 1980.

[149] J. Mathews. Gravitational multipole radiation. *J. Soc. Ind. Appl. Math.*, 10:768, 1962.

[150] J. Meidam, M. Agathos, C. Van Den Broeck, J. Veitch, and B. S. Sathyaprakash. Testing the no-hair theorem with black hole ringdowns using TIGER. *Phys. Rev.*, D90(6):064009, 2014.

[151] J. Miller, L. Barsotti, S. Vitale, P. Fritschel, M. Evans, and D. Sigg. Prospects for doubling the range of Advanced LIGO. *Phys. Rev.*, D91:062005, 2015.

[152] C. W. Misner, R. Breuer, D. Brill, P. Chrzanowski, H. Hughes, et al. Gravitational synchrotron radiation in the schwarzschild geometry. *Phys.Rev.Lett.*, 28:998–1001, 1972.

[153] C. W. Misner, K. S. Thorne, and J. A. Wheeler. *Gravitation*. W. H. Freeman, 1973.

[154] G. Mocanu and D. Grumiller. Self-organized criticality in boson clouds around black holes. *Phys.Rev.*, D85:105022, 2012.

[155] P. M. Morse and H. Feshbach. *Methods of Theoretical Physics*. McGraw-Hill, New York, 1953.

[156] L. Motl. An analytical computation of asymptotic Schwarzschild quasinormal frequencies. *Adv. Theor. Math. Phys.*, 6:1135–1162, 2003.

[157] L. Motl and A. Neitzke. Asymptotic black hole quasinormal frequencies. *Adv. Theor. Math. Phys.*, 7:307–330, 2003.

[158] A. Nagar and L. Rezzolla. Gauge-invariant non-spherical metric perturbations of schwarzschild black-hole spacetimes. *Class. Quant. Grav.*, 22:R167, 2005.

[159] H.-P. Nollert. Quasinormal modes of Schwarzschild black holes: The determination of quasinormal frequencies with very large imaginary parts. *Phys.Rev.*, D47:5253–5258, 1993.

[160] H.-P. Nollert. Quasinormal modes: the characteristic 'sound' of black holes and neutron stars. *Class. Quant. Grav.*, 16:R159–R216, 1999.

[161] H.-P. Nollert. *Characteristic Oscillations of Black Holes and Neutron Stars: From Mathematical Background to Astrophysical Applications*. Tubingen, 2000. Habilitationsschrift Der Fakultat fur Physik der Eberhard-Karls-Universitat Tubingen.

[162] H.-P. Nollert and R. H. Price. Quantifying excitations of quasinormal mode systems. *J. Math. Phys.*, 40:980–1010, 1999.

[163] P. Pani, V. Cardoso, L. Gualtieri, E. Berti, and A. Ishibashi. Black hole bombs and photon mass bounds. *Phys.Rev.Lett.*, 109:131102, 2012.

[164] P. Pani, V. Cardoso, L. Gualtieri, E. Berti, and A. Ishibashi. Perturbations of slowly rotating black holes: massive vector fields in the Kerr metric. *Phys.Rev.*, D86:104017, 2012.

[165] P. Papadopoulos. Nonlinear harmonic generation in finite amplitude black hole oscillations. *Phys. Rev.*, D65:084016, 2002.

[166] E. Poisson and C. G. Gray. When action is not least for orbits in general relativity. *Am.J.Phys.*, 79:43, 2011.

[167] E. Poisson and C. M. Will. *Gravity: Newtonian, Post-Newtonian, Relativistic*. Cambridge University Press, Cambridge, July 2014.

[168] W. H. Press. Long wave trains of gravitational waves from a vibrating black hole. *Astrophys. J.*, L170:105, 1971.

[169] W. H. Press and S. A. Teukolsky. Floating Orbits, Superradiant Scattering and the Black-hole Bomb. *Nature*, 238:211–212, 1972.

[170] F. Pretorius and D. Khurana. Black hole mergers and unstable circular orbits. *Class.Quant.Grav.*, 24:S83–S108, 2007.

[171] R. H. Price. Nonspherical Perturbations of Relativistic Gravitational Collapse. I. Scalar and Gravitational Perturbations. *Phys. Rev.*, D5:2419–2438, 1972.

[172] T. Regge and J. A. Wheeler. Stability of a schwarzschild singularity. *Phys. Rev.*, 108:1063–1069, Nov. 1957.

[173] L. Rezzolla, E. Barausse, E. N. Dorband, D. Pollney, C. Reisswig, J. Seiler, and S. Husa. On the final spin from the coalescence of two black holes. *Phys. Rev.*, D78:044002, 2008.

[174] K. J. Rhook and J. S. B. Wyithe. Realistic Event Rates for Detection of Supermassive Black Hole Coalescence by LISA. *Mon. Not. Roy. Astron. Soc.*, 361:1145–1152, 2005.

[175] C. L. Rodriguez, S. Chatterjee, and F. A. Rasio. Binary Black Hole Mergers from Globular Clusters: Masses, Merger Rates, and the Impact of Stellar Evolution. *Phys. Rev.*, D93(8):084029, 2016.

[176] J. G. Rosa. The Extremal black hole bomb. *JHEP*, 1006:015, 2010.

[177] R. Ruffini. *Black Holes: les Astres Occlus*. Gordon and Breach Science Publishers, New York, 1973.

[178] N. Sago, H. Nakano, and M. Sasaki. Gauge problem in the gravitational self-force. I: Harmonic gauge approach in the Schwarzschild background. *Phys. Rev.*, D67:104017, 2003.

[179] E. Salpeter. Accretion of Interstellar Matter by Massive Objects. *Astrophys.J.*, 140:796–800, 1964.

[180] M. Sasaki and T. Nakamura. A Class of New Perturbation Equations for the Kerr Geometry. *Phys. Lett.*, A89:68–70, 1982.

[181] M. Sasaki and T. Nakamura. Gravitational Radiation From a Kerr Black Hole. 1. Formulation and a Method for Numerical Analysis. *Prog. Theor. Phys.*, 67:1788, 1982.

[182] M. Sasaki and H. Tagoshi. Analytic black hole perturbation approach to gravitational radiation. *Living Rev. Rel.*, 6:6, 2003.

[183] B. Sathyaprakash et al. Scientific Objectives of Einstein Telescope. *Class. Quant. Grav.*, 29:124013, 2012. [Erratum: Class. Quant. Grav.30,079501(2013)].

[184] S. Schmoll, J. Miller, M. Volonteri, E. Cackett, C. Reynolds, et al. Constraining the Spin of the Black Hole in Fairall 9 with Suzaku. *Astrophys.J.*, 703:2171–2176, 2009.

[185] B. Schutz. *A First Course in General Relativity.* Cambridge University Press, Cambridge, May 2009.

[186] B. F. Schutz and C. M. Will. Black hole normal modes: A semianalytic approach. *Astrophys. J.*, L291:33–36, 1985.

[187] A. Sesana, E. Barausse, M. Dotti, and E. M. Rossi. Linking the spin evolution of massive black holes to galaxy kinematics. *Astrophys. J.*, 794:104, 2014.

[188] S. L. Shapiro and S. A. Teukolsky. Black holes, white dwarfs, and neutron stars: The physics of compact objects. 1983.

[189] Y. Shlapentokh-Rothman. Exponentially growing finite energy solutions for the Klein-Gordon equation on sub-extremal Kerr spacetimes. *Commun.Math.Phys.*, 329:859–891, 2014.

[190] U. Sperhake, E. Berti, V. Cardoso, and F. Pretorius. Universality, maximum radiation and absorption in high-energy collisions of black holes with spin. *Phys.Rev.Lett.*, 111(4):041101, 2013.

[191] U. Sperhake, V. Cardoso, F. Pretorius, E. Berti, and J. A. Gonzalez. The high-energy collision of two black holes. *Phys. Rev. Lett.*, 101:161101, 2008.

[192] U. Sperhake et al. Cross section, final spin and zoom-whirl behavior in high-energy black hole collisions. *Phys. Rev. Lett.*, 103:131102, 2009.

[193] U. Sperhake, B. J. Kelly, P. Laguna, K. L. Smith, and E. Schnetter. Black hole head-on collisions and gravitational waves with fixed mesh-refinement and dynamic singularity excision. *Phys. Rev.*, D71:124042, 2005.

[194] J. M. Stewart. Solutions of the wave equation on a Schwarzschild space-time with localized energy. *Proc. R. Soc. London*, A424:239–244, 1989.

[195] Y. Sun and R. H. Price. Excitation of quasinormal ringing of a Schwarzschild black hole. *Phys. Rev.*, D38:1040–1052, 1988.

[196] S. A. Teukolsky. Perturbations of a Rotating Black Hole. I. Fundamental Equations for Gravitational, Electromagnetic, and Neutrino-Field Perturbations. *Astrophys. J.*, 185:635–648, Oct. 1973.

[197] S. A. Teukolsky. The Kerr Metric. 2014. arXiv:1410.2130 [gr-qc].

[198] K. S. Thorne. Multipole Expansions of Gravitational Radiation. *Rev. Mod. Phys.*, 52:299–339, 1980.

[199] C. V. Vishveshwara. Stability of the schwarzschild metric. *Phys. Rev.*, D1:2870–2879, 1970.

[200] M. Visser. The Kerr spacetime: A Brief introduction. In *Kerr Fest: Black Holes in Astrophysics, General Relativity and Quantum Gravity Christchurch, New Zealand, August 26-28, 2004*, 2007.

[201] H. Witek, V. Cardoso, A. Ishibashi, and U. Sperhake. Superradiant instabilities in astrophysical systems. *Phys.Rev.*, D87:043513, 2013.

[202] H. Yoshino and H. Kodama. Bosenova collapse of axion cloud around a rotating black hole. *Prog.Theor.Phys.*, 128:153–190, 2012.

[203] N. Yunes, P. Pani, and V. Cardoso. Gravitational Waves from Quasicircular Extreme Mass-Ratio Inspirals as Probes of Scalar-Tensor Theories. *Phys.Rev.*, D85:102003, 2012.

[204] N. Yunes and X. Siemens. Gravitational-Wave Tests of General Relativity with Ground-Based Detectors and Pulsar Timing-Arrays. *Living Rev. Rel.*, 16:9, 2013.

[205] N. Yunes, K. Yagi, and F. Pretorius. Theoretical Physics Implications of the Binary Black-Hole Merger GW150914. 2016.

[206] F. J. Zerilli. Gravitational field of a particle falling in a schwarzschild geometry analyzed in tensor harmonics. *Phys. Rev.*, D2:2141–2160, 1970.

[207] Y. Zlochower, R. Gomez, S. Husa, L. Lehner, and J. Winicour. Mode coupling in the nonlinear response of black holes. *Phys. Rev.*, D68:084014, 2003.

[208] T. Zouros and D. Eardley. Instabilities of Massive Scalar Perturbations of a Rotating Black Hole. *Annals Phys.*, 118:139–155, 1979.